

**STUDY OF ELECTRICAL RELAXATION OF SOME
TRANSITION METAL ION DOPED CHALCOGENIDE
GLASS-NANOCOMPOSITES**

Thesis submitted by

SWARUPA OJHA

Doctor of Philosophy in Engineering

Electrical Engineering Department
Faculty Council of Engineering & Technology
Jadavpur University
Kolkata, India

2021

Jadavpur University

Faculty of Engineering and Technology

INDEX NO. - 175/17/E

1. **Title of the Thesis:** Study of Electrical Relaxation of some Transition Metal Ion doped Chalcogenide Glass-Nanocomposites

2. **Name, Designation & Institution of the Supervisors:**

i. **DR. MADHAB ROY**

Associate Professor
Electrical Engineering Department
Jadavpur University

ii. **DR. SANJIB BHATTACHARYA**

Associate Professor-Deputy Director
HRDC & Physics Department
University of North Bengal

3. **List of Publications:**

Journal Papers:

- i. Title of the Paper: Hopping frequency and conductivity relaxation of promising chalcogenides: AC conductivity and dielectric relaxation approaches
Journal of Publication: Materials Research Express
Year: 2021
Role: Swarupa Ojha, Mir Sahidul Ali, Madhab Roy and Sanjib Bhattacharya
Volume: 8
Page numbers: 085203
DOI: <https://doi.org/10.1088/2053-1591/ac1d17>
- ii. Title of the Paper: Transport phenomena of Cu–S–Te chalcogenide nanocomposites: frequency response and AC conductivity
Journal of Publication: Physical Chemistry Chemical Physics
Year: 2020
Role: Swarupa Ojha, Madhab Roy, Anil Chamuah, Koyel Bhattacharya and Sanjib Bhattacharya
Volume: 22 (42)
Page numbers: 24600-24613
DOI: <https://doi.org/10.1016/j.matlet.2019.126792>
- iii. Title of the Paper: Electrical transport of chalcogenide glassy system: interpretation by Hunt's model and microstructure

Journal of Publication: SN Applied Sciences

Year: 2020

Role: Swarupa Ojha, Madhab Roy, Anil Chamuah, Koyel Bhattacharya and Sanjib Bhattacharya

Volume: 2 (838)

DOI: <https://doi.org/10.1007/s42452-020-2518-5>

- iv. Title of the Paper: Electrical Relaxation Studies of Chalcogenide $x\text{Ag}_2\text{S}-(1-x)(0.5\text{S}-0.5\text{Te})$ Glassy System
Journal of Publication: International Journal of Advanced Science and Engineering
Year: 2020
Role: Swarupa Ojha, Madhab Roy, Anil Chamuah, Koyel Bhattacharya and Sanjib Bhattacharya
Volume: 6 (S2)
Page numbers: 28-34
DOI: <https://doi.org/10.29294/IJASE.6.S2.2020.28-34>
- v. Title of the Paper: AC conductivity and dielectric behavior of Cu-S-Te chalcogenide glassy system
Journal of Publication: Materials Letters
Year: 2020
Role: Swarupa Ojha, Madhab Roy, Anil Chamuah, Koyel Bhattacharya and Sanjib Bhattacharya
Volume: 258
Page numbers: 126792
DOI: <https://doi.org/10.1016/j.matlet.2019.126792>
- vi. Title of the Paper: Temperature and Frequency Response of Conductivity in Ag_2S Doped Chalcogenide Glassy Semiconductor
Journal of Publication: Physica B: Condensed Matter
Year: 2018
Role: Swarupa Ojha, Anindya Sundar Das, Madhab Roy and Sanjib Bhattacharya
Volume: 538
Page numbers: 191–198
DOI: <https://doi.org/10.1016/j.physb.2018.03.043>

Conference Papers:

- i. Title of the Paper: Study of Electrical Relaxation of Some Transition Metal Ion Doped Chalcogenide Glass Nanocomposites
Conference: 2nd Indian Materials Conclave & 31st Annual General Meeting of Materials Research Society of India (MRSI) at CSIR – Central Glass & Ceramic Research Institute, Kolkata during 11th-14th February, 2020
Year: 2020
Role: Swarupa Ojha, Madhab Roy and Sajib Bhattacharya
- ii. Title of the Paper: Electrical Relaxation Studies of Chalcogenide $x\text{Ag}_2\text{S} - (1-x)(0.5\text{S} - 0.5\text{Te})$ Glassy System

Conference: International Conference on Current Trends in Materials Science and Engineering (CTMSE 2019) organized by S. N. Bose National Centre for Basic Sciences, Kolkata and Institute of Engineering & Management, Kolkata at S. N. Bose National Centre for Basic Sciences, Kolkata, 18th-20th July, 2019

Year: 2019

Role: Swarupa Ojha, Madhab Roy, Anil Chamuah, Koyel Bhattacharya and Sanjib Bhattacharya

- iii. Title of the Paper: Chalcogenide Glassy Semiconductor: Electrical Properties and Future Aspects

Conference: 26th West Bengal State Science & Technology Congress, organised by Dept of Science & Technology and Biotechnology, Govt of West Bengal at Science City Kolkata, 28th Feb & 1st March 2019

Year: 2019

Role: Swarupa Ojha, Madhab Roy and Sanjib Bhattacharya

- iv. Title of the Paper: Chalcogenide Glassy Semiconductor: Structure and Electrical Transport

Conference: 1st Indian Materials Conclave & 30th Annual General Meeting of Materials Research Society of India (MRSI) at IISc Bangalore, 12th-15th February, 2019

Year: 2019

Role: Swarupa Ojha, Madhab Roy and Sanjib Bhattacharya

- v. Title of the Paper: Ag₂S Doped Chalcogenide Glassy Semiconductor: Electrical Properties and Future Aspects

Conference: 3rd Regional Science Congress organised by Dept. of Science & Technology and Biotechnology, Govt of West Bengal, 20-21st Dec, 2018

Year: 2018

Role: Swarupa Ojha, Madhab Roy and Sanjib Bhattacharya

- vi. Title of the Paper: Temperature and Frequency Response of Conductivity in Ag₂S Doped Chalcogenide Glassy Semiconductor.

Conference: International Conference on Advancement in Science and Technology at Visva-Bharati University, Santiniketan, organized by Indian Japan Society for the Promotion of Science (JSPS) Alumni Association during 3rd-4th September, 2018

Year: 2018

Role: Swarupa Ojha, Madhab Roy and Sanjib Bhattacharya

4. List of Patents: None

5. List of Presentations in National / International Conferences

- i. "Study of Electrical Relaxation of Some Transition Metal Ion Doped Chalcogenide Glass Nanocomposites", 2nd Indian Materials Conclave & 31st Annual General Meeting of Materials Research Society of India (MRSI) at CSIR

- Central Glass & Ceramic Research Institute, Kolkata during 11th-14th February, 2020
- ii. “Electrical Relaxation Studies of Chalcogenide $x\text{Ag}_2\text{S} - (1-x)(0.5\text{S} - 0.5\text{Te})$ Glassy System”, International Conference on Current Trends in Materials Science and Engineering (CTMSE 2019) organized by S. N. Bose National Centre for Basic Sciences, Kolkata and Institute of Engineering & Management, Kolkata at S. N. Bose National Centre for Basic Sciences, Kolkata, 18th-20th July, 2019
 - iii. “Chalcogenide Glassy Semiconductor: Electrical Properties and Future Aspects”, 26th West Bengal State Science & Technology Congress, organised by Dept of Science & Technology and Biotechnology, Govt of West Bengal at Science City Kolkata, 28th Feb & 1st March 2019
 - iv. “Chalcogenide Glassy Semiconductor: Structure and Electrical Transport”, 1st Indian Materials Conclave & 30th Annual General Meeting of Materials Research Society of India (MRSI) at IISc Bangalore, 12th-15th February, 2019
 - v. “Ag₂S Doped Chalcogenide Glassy Semiconductor: Electrical Properties and Future Aspects”, 3rd Regional Science Congress organised by Dept. of Science & Technology and Biotechnology, Govt of West Bengal, 20-21st Dec, 2018
 - vi. “Temperature and Frequency Response of Conductivity in Ag₂S Doped Chalcogenide Glassy Semiconductor”, International Conference on Advancement in Science and Technology organized by Indian Japan Society for the Promotion of Science (JSPS) Alumni Association at Visva-Bharati University, Santiniketan, 3rd-4th September, 2018

Jadavpur University
Faculty of Engineering and Technology

INDEX NO. - 175/17/E

STATEMENT OF ORIGINALITY

I **Swarupa Ojha** registered on **19.07.2017** do hereby declare that this thesis entitled “**Study of Electrical Relaxation of some Transition Metal-Ions doped Chalcogenide Glass-Nanocomposites**” contains literature survey and original research work done by the undersigned candidate as part of Doctoral studies.

All information in this thesis have been obtained and presented in accordance with existing academic rules and ethical conduct. I declare that, as required by these rules and conduct, I have fully cited and referred all materials and results that are not original to this work.

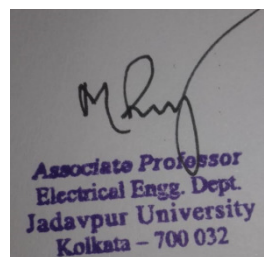
I also declare that I have checked this thesis as per the “Policy on Anti Plagiarism, Jadavpur University, 2019”, and the level of similarity as checked by iThenticate software is 8 %.

Signature of Candidate:
Date: 29/10/2021

Swarupa Ojha

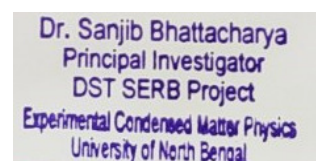
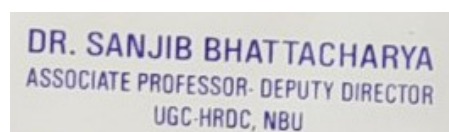
Certified by Supervisor(s):

1. **Dr. Madhab Roy:**
Date: 29/10/2021



2. **Dr. Sanjib Bhattacharya:**
Date: 29/10/2021

Sanjib Bhattacharya

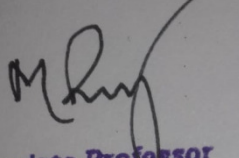


Jadavpur University
Faculty of Engineering and Technology

INDEX NO. - 175/17/E

CERTIFICATE FROM THE SUPERVISORS

This is to certify that the thesis entitled “**Study of Electrical Relaxation of some Transition Metal-Ions doped Chalcogenide Glass-Nanocomposites**” Submitted By **Ms. Swarupa Ojha**, who got her name registered on **19.07.2017** for the award of Ph.D. (Engineering) degree of Jadavpur University is absolutely based upon her own work under the supervision of **Dr. Madhab Roy and Dr. Sanjib Bhattacharya** and that neither her thesis nor any part of the thesis has been submitted for any degree/diploma or any other academic award anywhere before.




Associate Professor
Electrical Engg. Dept.
Jadavpur University
Kolkata - 700 032

1. Dr. Madhab Roy

Signature of the Supervisor
and date with Office Seal

Date: 29/10/2021



DR. SANJIB BHATTACHARYA
ASSOCIATE PROFESSOR- DEPUTY DIRECTOR
UGC-HRDC, NBU

2. Dr. Sanjib Bhattacharya

Signature of the Supervisor
and date with Office Seal

Date: 29/10/2021



Dr. Sanjib Bhattacharya
Principal Investigator
DST SERB Project
Experimental Condensed Matter Physics
University of North Bengal

Jadavpur University
Faculty of Engineering and Technology

INDEX NO. - 175/17/E

ACKNOWLEDGEMENT

The work presented in this thesis would not have been possible without my close association with many people. I take this opportunity to extend my sincere gratitude and appreciation to all those who have been instrumental in the successful completion of this thesis.

First and foremost, I would like to extend my sincere gratitude to my research guide Dr. Madhab Roy, Associate Professor, Electrical Engineering Department, Jadavpur University, for his dedicated help, advice, inspiration, encouragement and continuous support throughout my course work. His enthusiasm, integral view on research and his mission for providing high-quality work have made a deep impression on me.

My special words of thanks go to my research co-guide Dr. Sanjib Bhattacharya, Associate Professor-Deputy Director, HRDC & Physics Department, University of North Bengal, for continuous support, supervision, cooperation and encouragement. His constant guidance, cooperation, motivation and support have always kept me going ahead. This research work would not have been possible without his direction and I will forever be grateful for it.

I would like to pay my special thanks to the HOD, Electrical Engineering Department, Jadavpur University for the cooperation during the research. I am grateful for her constant support and help. I would also like to thank all the members of my thesis committee for their encouragement and insightful comments. I gratefully acknowledge all the faculty members of Electrical Engineering Department of Jadavpur University.

My special thanks are extended to Prof. Dipankar Chattopadhyay, Polymer Science & Technology Department - Calcutta University, for providing X-Ray Diffraction and FT-IR Spectroscopy facilities. I am grateful to Prof. Joydeep Choudhury, Physics Department -

Jadavpur University, for giving me opportunities to conduct research in his laboratory and providing permission to use XRD and UV-Vis Spectroscopy facilities there.

I would like to express my gratitude to Mr. Arunim Paul, Department of Central Scientific Service - Indian Association for the Cultivation of Science, for providing HRTEM facility. I extend my sincere thanks to Mr. A Saha of REMCO India for providing quartz tube vacuum sealing facility.

My heartfelt thanks also go to my fellow research scholars Mr. Anil Chamuah, Mr. Amartya Acharya and Ms. Ashmita Poddar for their help and moral support. They always helped me out when I got any difficulties or queries regarding experiments. I thankfully acknowledge Siliguri Institute of Technology for my experimental work at Composite Materials Research Laboratory during the early stage of my research. I would also like to acknowledge all the faculty members of Department of Engineering Sciences and Humanities, Siliguri Institute of Technology for their excellent cooperation. I am forever thankful to my colleagues at OmDayal Group of Institutions for their friendship and support, and for creating a cordial working environment.

Finally, my sincere gratitude to my father, mother and sister for their continuous and unparalleled love, help and support through the years. I am forever indebted to my father for giving me opportunities and experiences that have made me who I am. My mother selflessly encouraged me to explore new directions in life and seek my own destiny. I am thankful to my sister for always being there for me as a friend.

I offer my regards and blessings to all those who supported me in any respect during the completion of my research.

SWARUPA OJHA

PREFACE

In recent days, studies on Chalcogenide glassy systems paid much attention because of their higher electrical conductivity at room temperature and large composition flexibility, which made them suitable candidates for rechargeable batteries.

Transition Metal Ions doped Chalcogenide glassy systems showed that the electrical conduction mechanism predominated by hopping of small polarons. To explore the conduction mechanism in Chalcogenide semiconductors, the study of frequency dependent electrical conductivity is very much essential not only for practical applications but also for academic interest. A complete description on electrical transport phenomenon and dielectric relaxation of such glassy system is still pending till date because of lack of their micro-structural information and approximation in data analysis.

The motivation of this work is to study composition dependent electrical and dielectric properties of the Chalcogenide glassy systems: $x\text{Ag}_2\text{S} - (1-x) (0.5\text{S} - 0.\text{Te})$ where $x = 0.35$ and 0.45 ; $x\text{Cu} - (1-x) (0.5\text{S} - 0.\text{Te})$ where $x = 0.0, 0.1, 0.2$ and 0.3 ; $x\text{Ag}_2\text{S} - (1-x) (0.5\text{Se} - 0.\text{Ge})$ where $x = 0.1$ and 0.2 ; and $x\text{Ag}_2\text{S} - (1-x) (0.5\text{Se} - 0.\text{Te})$ where $x = 0.05, 0.1$ and 0.2 . The results may open the way to the preparation, application and investigation of significant electrical and dielectric properties of the Chalcogenide glassy systems.

The proposed thesis to be submitted will have six chapters.

Chapter 1 is an introduction to Chalcogenide Glass Nanocomposites and its comparison with oxide glasses. Different work carried out by many researchers on Chalcogenide glassy systems is also discussed. The chapter focuses on electrical relaxation process in Chalcogenide glassy system and study of their electrical properties by many researchers. Possible and existing applications of these systems, due to their peerless properties, is reported followed by a discussion on Transition Metal Ion doped Chalcogenide systems and the main objectives of the research work.

Chapter 2 focuses on the description of different methods which are used for preparing Chalcogenide glassy systems. It also deals with the various characterization techniques used in the present work for analyzing structure and electrical properties of the prepared systems. In the first part of the chapter, there is a brief discussion on different preparation techniques of glasses with special attention on melt quenching method, in which rapid cooling is

required for avoiding crystallization in glasses. Structural characterization techniques like density and molar volume measurements, XRD, FT-IR, TEM and UV-Vis are discussed in detail. In the later part of the chapter, there is a discussion on the analysis of DC conductivity and AC conductivity data for studying electrical properties of systems.

Chapter 3 focuses on the study of electrical characterization and microstructure of Ag₂S doped S-Te Chalcogenide system. The addition of Ag₂S to the system changes its structure and hence its electrical properties. Structural characterization of the system with the help of XRD, TEM, FT-IR spectroscopy, density and molar volume is reported. Use of Mott's model and Greaves's model for DC conductivity analysis is discussed. For analyzing AC conductivity of the system, use of methods like Almond West formalism, MN Rule, AC conductivity scaling, dielectric relaxation studies etc is reported in the chapter. To know the conduction mechanism in the system, use of CBH and NSPT (modified) models in the analysis of AC conductivity data is discussed. To find the dependency of electrical relaxation of the system on composition and temperature, AC conductivity and electric modulus scaling methods are discussed in the chapter.

Chapter 4 deals with the study of structural behaviour and electrical conductivity of Cu doped S-Te glassy system. There is a brief discussion on advantages of adding Cu in the system. The preparation of the system using melt quenching method is discussed in the first part of the chapter followed by its structural characterization with the help of various techniques like XRD, TEM, FT-IR spectroscopy, molar volume and density calculations etc. In the later part of the chapter, temperature, composition and frequency dependent electrical conductivity measurements and analysis of data with the help of Mott's model, Greaves's model, Power law, MN Rule, Almond West formalism, CBH model and NSPT model are reported.

Chapter 5 focuses on study of electrical conductivity and dielectric relaxation of Ag₂S-Se-Ge glassy system. The chapter begins with discussion on attractive properties of Ag₂S, Se and Ge followed by the method of preparation of the glassy system. Then, the use of XRD, UV-Vis, FT-IR, molar volume and density calculations are discussed for structural characterization. Analysis of DC conductivity with the help of Mott's model and Greaves's model is reported. AC conductivity data is analysed with Power law, MN Rule, Almond West formalism, CBH model and NSPT model. Study of dielectric relaxation properties with the help of permittivity and electric modulus studies is also discussed in the chapter.

Chapter 6 mainly deals with study of electrical spectra of $\text{Ag}_2\text{S} - \text{Se} - \text{Te}$ Chalcogenide glassy system. In this chapter the use of melt quenching method is reported for the preparation of the system. For structural characterization use of XRD and FT-IR techniques is discussed. DC conductivity and AC conductivity measurements and their analysis using Power law, MN Rule, Almond West formalism, CBH model and dielectric relaxation studies are also reported. For finding the composition and temperature dependency of relaxation process in the system, AC conductivity and electric modulus scaling are reported. Calculation of carrier mobility and density in the present system is also discussed in the chapter.

CONTENTS

Chapter 1 - Introduction	1-25
1.1. Glass	3
1.2. Nanocomposites	4
1.2.1. Classification of nanocomposites	5
1.3. Classification of Semiconducting Glasses	5
1.3.1. Oxide glasses	6
1.3.2. Non oxide glasses	6
1.3.2.1. Heavy-Metal Fluoride Glasses (HMFGs)	6
1.3.2.2. Glassy metals	6
1.3.2.3. Chalcogenide Glasses	6
1.3.2.4. Glass ceramics	7
1.3.2.5. Glass composites	7
1.3.2.6. Natural glasses	7
1.4. Chalcogenide Glasses	7
1.4.1. Comparison between Oxide and Chalcogenide glasses	8
1.4.2. Some previous works on various Chalcogenide glasses	9
1.4.3. Electrical relaxation process in Chalcogenide glassy system	14
1.4.4. Applications of Chalcogenide glasses	17
1.5. Transition Metal Ion doped Chalcogenide Glasses	18
1.6. Objective of the Research Work	19
References	20
Chapter 2 - Experimental Methods	26-48
2.1. Introduction	26
2.2. Preparation of Glassy Systems	27
2.2.1. Mechanical Milling technique	27
2.2.2. Sol-gel process	28
2.2.3. Chemical Vapour Deposition technique	28
2.2.4. Chemical Bath deposition technique	28
2.2.5. Melt Quenching method	29
2.2.5.1. Composition of the glassy systems prepared in the present work using melt quenching method	31
2.3. Structural and Physical Characterization	31
2.3.1. Measurement of density and molar volume	31
2.3.2. XRD	32
2.3.3. FTIR	34
2.3.4. UV-Vis	34
2.3.5. TEM	35
2.4. Analytical Techniques	37
2.4.1. DC Conductivity	37
2.4.2. AC Conductivity	39
2.4.2.1. Meyer-Neldel (MN) Rule	40
2.4.2.2. Power Law and Almond West Formalism	41
2.4.3. Dielectric Properties	42

2.4.3.1. Permittivity	42
2.4.3.2. Electric Modulus	43
2.5. Observations	44
2.6. Conclusion	45
References	46

Chapter 3 - Study of Electrical Characterization and Microstructure of Ag₂S doped S-Te Chalcogenide System **49-82**

3.1. Introduction	49
3.2. Preparation of the Glassy System	50
3.3. Results and Analysis	51
3.3.1. XRD	51
3.3.1.1. Crystalline size, dislocation density and lattice strain	51
3.3.1.2. Crystalline Volume Fraction	52
3.3.2. TEM	53
3.3.3. FTIR	55
3.3.4. Density and molar volume	56
3.3.5. DC Conductivity	57
3.3.6. AC Conductivity	60
3.3.6.1. Power Law	60
3.3.6.2. Almond West Formalism	64
3.3.6.3. Scaling of AC Conductivity	67
3.3.6.4. Meyer–Neldel (MN) rule	68
3.3.6.5. Mobility and Carrier Density	69
3.3.7. Dielectric Properties	70
3.3.7.1. Permittivity	70
3.3.7.2. Electric modulus	73
3.3.7.3. Electric Modulus Scaling	76
3.4. Conclusion	78
References	80

Chapter 4 - Study of Structural Behaviour and Electrical Conductivity of Cu Doped S-Te Glassy System **83-114**

4.1. Introduction	83
4.2. Preparation of the Glassy System	84
4.3. Results and Analysis	85
4.3.1. XRD	85
4.3.1.1. Crystallite size, dislocation density and lattice strain	85
4.3.1.2. Crystalline Volume Fraction	88
4.3.2. TEM	89
4.3.3. FT-IR	91
4.3.4. Density and molar volume	92
4.3.5. Analysis of DC Conductivity	93
4.3.6. AC Conductivity Analysis	95
4.3.6.1. Power Law	95
4.3.6.2. Almond West Formalism	98

4.3.6.3. AC Conductivity Scaling	101
4.3.6.4. Meyer–Neldel Rule	102
4.3.6.5. Mobility and Carrier Density	104
4.3.7. Dielectric Properties Analysis	105
4.3.7.1. Permittivity	105
4.3.7.2. Electric modulus	107
4.3.7.3. Electric Modulus Scaling	110
4.4. Conclusion	111
References	113

Chapter 5 - Study of Electrical Conductivity and Dielectric Relaxation of Ag₂S – Se – Ge Glassy System **115-141**

5.1. Introduction	115
5.2. Preparation of the glassy system	116
5.3. Results and Analysis	117
5.3.1. XRD	117
5.3.1.1. Crystalline size, dislocation density and lattice strain	117
5.3.1.2. Crystalline Volume Fraction	119
5.3.2. UV-Vis Spectroscopy	120
5.3.3. FTIR	120
5.3.4. Density and Molar volume	121
5.3.5. DC Conductivity	122
5.3.6. AC Conductivity	125
5.3.6.1. Power Law	125
5.3.6.2. Almond West Formalism	127
5.3.6.3. AC Conductivity Scaling	129
5.3.6.4. Meyer–Neldel (MN) rule	131
5.3.6.5. Mobility and Carrier Density	132
5.3.7. Dielectric Properties Analysis	133
5.3.7.1. Permittivity	133
5.3.7.2. Electric Modulus	135
5.3.7.3. Electric Modulus Scaling	138
5.4. Conclusion	139
References	141

Chapter 6 - Study of Electrical Spectra of Ag₂S – Se –Te Chalcogenide Glassy System **142-167**

6.1. Introduction	142
6.2. Preparation of the Glassy System	143
6.3. Results and Analysis	144
6.3.1. XRD	144
6.3.1.1. Crystalline size, dislocation density and lattice strain	144
6.3.1.2. Crystalline Volume Fraction	146
6.3.2. FTIR	147
6.3.3. DC Conductivity	148
6.3.4. AC Conductivity	149

6.3.4.1. Power Law	149
6.3.4.2. Almond West Formalism	152
6.3.4.3. AC Conductivity Scaling	155
6.3.4.4. Mobility and Carrier Density	157
6.3.5. Study of Dielectric Properties	158
6.3.5.1. Permittivity	158
6.3.5.2. Electric modulus	160
6.3.5.3. Electric Modulus Scaling	163
6.4. Conclusion	165
References	167
Chapter 7 - Conclusions and Future Prospects	168-170
References	170

Chapter 1

INTRODUCTION

Chalcogenide glasses, a class of amorphous semiconductors, have been accentuating researchers in the recent years, especially in the solid state science they are being considered as a very active area [1]. Amorphous solids, also known as non crystalline solids, do not have their atomic arrangements in periodic order of long range, although they conserve high degree periodic order of short range [2]. Usually disorder arrangement of atoms in liquid state is quickly arrested into solid state to obtain an amorphous solid [3]. Glass is a unique category of amorphous materials and when it is heated it shows glass transition phenomenon [4]. Many advantages of glasses like easy manufacturing method, composition flexibility, low-priced raw materials, transparent at high temperatures etc, make these amorphous solids different from crystalline solids.

In amorphous solids the electronic configuration of atoms and the type of bonding among their nearby atoms determine their properties and accordingly they can be insulating, conducting or semiconducting in nature. In the year of 1954 the semiconducting property of amorphous solids was first discovered by Kolomiets and Goryunova [5, 6].

According to the types of the chemical bonding in their constituent atoms the amorphous semiconductors are usually categorized into following groups:

- Ionic bonded – in these amorphous semiconductors compositional variation is not possible over wide range due to ionic nature and the atoms in these pure materials are in disordered positions. Oxides and halides glasses are examples of this type of amorphous semiconductors.
- Covalently bonded – these amorphous semiconductors are classified into two types [7]:
 - Tetrahedral bonded amorphous semiconductors – examples of such materials are amorphous silicon, amorphous germanium etc. Solar cells, image scanners, temperature sensors, gas sensors, thin film transistors etc are some of the applications of these materials [8, 9].

- Chalcogenide glasses – glasses which contain group 16 elements of periodic table i.e. chalcogens (sulphur, selenium and/or tellurium) in conjunction with one or more other suitable elements of the periodic table. Applications of these materials are xerography, inexpensive solar cells, optical fibres, phase change memories (PCM), fiber optics, X-ray imaging plates, etc [10].

In the energy band of amorphous semiconductors the density of electronic states (tails) is present which pierce the energy gap. Due to this reason the energy band of these semiconductors are different from that of crystalline semiconductors. One can consider amorphous semiconductors as heavily doped semiconductors in which the top of valence band and bottom of conduction band may vary on large scale more or less its energy gap width. Electrons and holes are located in potential wells in conduction band and valence band respectively, which are separated by high potential barriers. In these semiconductors the electrical conductivity at low temperatures occurs due to tunnelling of electrons through the potential barrier between wells. Charge carriers are thermally excited into higher energy levels which cause conduction at higher temperatures.

The unique and intriguing properties of amorphous semiconductors made these materials attractive to researchers [11, 12]. Because of the possibility of their applicability in numerous areas, these materials can be considered as more advantageous than crystalline semiconductors. Preparations of these materials, in thin films form (for solar cell applications) as well as in bulk forms, are very easy. Melt quenching method is generally used for preparation of bulk samples of amorphous semiconductors. These materials have pervasive applications in many fields of modern technology like optical, electrical, electronics, mechanical, electrochemical etc. They can be used in many electronic devices as active and passive elements [13, 14]. Some of their applications in electronics field are: solar cells, thin film transistors, electrophotography, electrochemical sensors, solid state batteries, temperature sensors etc [15, 16]. These materials have also found many applications in communication systems. They have also been shown their ability to be used in the optical fibres fabrications, making of prisms and optical windows, as Laser materials and LEDs. Manufacturing of transformer cores is another possible application of amorphous semiconductors.

1.1. GLASS

Structure of a glass is like a super cooled liquid but its mechanical properties are similar to that of a solid [17, 18]. A glass is generally made by quick melt quenching of its constituent elements [19-23]. The name 'glass' is applied only to those amorphous solids which display glass transition temperature, T_g . In the melt quenching method the cooling process should be very quick to freeze the atoms of the liquid, which are in disordered form, preventing them from being crystallized at glass transition temperature. The affinity of a material to form glass on quenching is known as its glass forming ability.

The imperative factor in the preparation of glasses is speed. In Fig-1.1 two paths are shown which may be used by a material to get solidify. Crystallization is a time taking process. In this process the temperature of a melted material is lowered to T_f to crystallise the material to the solid state. In Fig-1.1, Path 1 indicates this process. When the temperature of the melted material lies between T_f and T_g the material is called super-cooled liquid. If material's temperature is abruptly decreased to T_g without giving any time to the material to get crystallised, the super-cooled liquid becomes glass and remain in that form forever. Therefore, the preparation of amorphous solid or glass is the process of avoiding crystallization which can be achieved by cooling the liquid material very speedy.

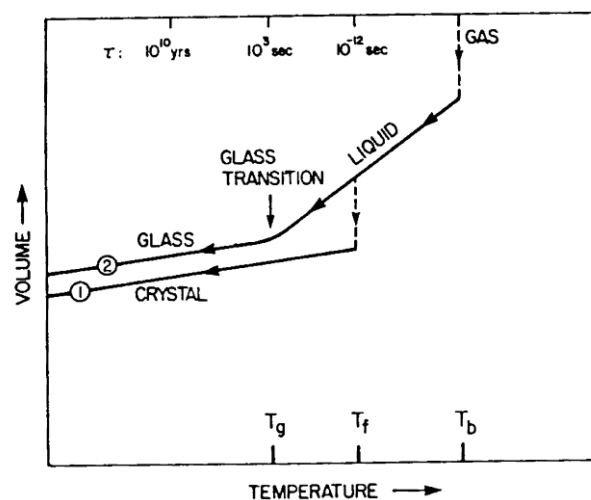


Fig-1.1: Cooling Paths used by a material to get solidify – 1: Path to crystalline state
2: Path to amorphous state

Glass has been enchanting people from so many decades due to its numerous favourable properties which help it to become an attractive material [24, 25]. However, it exhibits some undesirable properties such as low tensile strength, less hardness etc which makes its usage

limited. Many researchers have reported the overcoming of the drawbacks of glass by amalgamation of some nanoparticles of metals in its matrix forming nanocomposite materials. These nanocomposite materials possess unique electrical, optical, thermal, mechanical properties which makes the glass suitable to be used in different applications in nanotechnology [26-31]. The desirable properties of the nanocomposites for a particular application are dependent on amount, shape and size of the incorporated nano particles [32, 33].

1.2. NANOCOMPOSITES

Nanocomposites are those materials which contain more than one constituent elements and its constituent elements must have at least one dimension in the 1-100nm range. Fig-1.2 shows different types of nanocomposites – (a) Nanoparticles - which contain three nano-scale dimensions, (b) Nanofibres - which contain two nano-scale dimensions and (c) Nanoclays - which contain one nano-scale dimension.

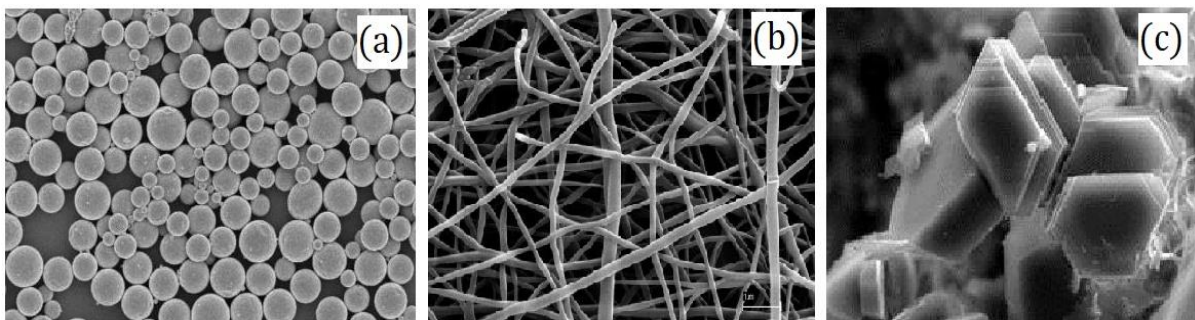


Fig-1.2: Different types of nanocomposites – (a) Nanoparticles, (b) Nanofibres and (c) Nanoclays

To produce a nanocomposite, nano materials (usually called fillers) are incorporated into the sample material (usually called matrix) which is in macroscale regime [34-36]. The incorporation of nano materials or the fillers in the matrix material intensifies its electrical conductivities and improves its optical, thermal, dielectric, mechanical and many other properties. Nanocomposite materials are rising as a promising material which can be used for overcoming the drawbacks of microcomposite materials. Because of exhibiting unique properties, which are impossible to be found in a usual composite, the nanocomposites are treated as the materials of the present and future centuries.

1.2.1. Classification of Nanocomposites

Based on the matrix materials, the nanocomposites are categorized into three classes: (a) metal matrix, (b) ceramic matrix and (c) polymer matrix nanocomposites. Nanocomposites containing matrix which is insulating in nature, like glass, ceramic or polymer, in which metal nanoparticles are incorporated have become an interesting topic of research because of their attractive properties. Among these nanocomposites, metal glass nanocomposites possesses exciting unique properties such as enhanced mechanical strength, refractive index, electrical resistivity etc. These nanocomposites are formed by incorporation of metal nanoparticles into glass matrices. One of the important applications of these materials is in communication systems as formation of low power high speed optical device [37, 38].

1.3. CLASSIFICATION OF SEMICONDUCTING GLASSES

Semiconducting glasses are amorphous semiconductors which exhibit electrical properties that are dissimilar to the properties of existing crystalline semiconductors. Germanium, Silicon, Gallium Arsenide etc are some examples of crystalline semiconductors. Amorphous semiconductors are those kinds of materials which are having negative temperature coefficient of resistivity. The amorphous and crystalline structures of Silicon are shown in Fig-1.3(a) and (b) respectively.

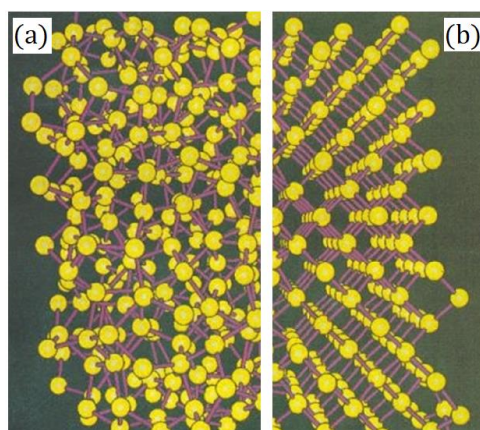


Fig-1.3: (a) Amorphous Structure and (b) Crystalline structure of Si

Based on the occurrence of these glasses they can be categorized into two classes: (a) natural and (b) artificial glasses. The artificial or manmade glasses are further categorized into two

classes depending on their constituent elements: (a) oxide and (b) non-oxide. Explanations of these types are given in the following sections:

1.3.1. Oxide Glasses

The glass which contains oxygen as one of its constituent elements is known as oxide glass. Most of the commercially available glasses are based on SiO_2 or silica. Silica is a mineral which is abundantly available in nature in form of sands. The glasses which are made up of silica only are known as vitreous silica or silica glasses. Sometimes these are referred as fused quartz when quartz crystals are melted to prepare them. Use of silica glasses have been found mainly in those applications in which low electrical conductance, high thermal shock resistance, superior chemical durability and ultraviolet transparency are required. Soda lime silica glasses are found to be best fitted in preparation of most of the daily use glass products like glass containers, flower vase, windows, bulbs etc where the major requirements are fine durability and low price.

1.3.2. Non Oxide Glasses

The glasses which do not contain oxygen as one of the constituent elements are called non oxide glasses. Non oxide glasses are classified into the following categories:

1.3.2.1. Heavy-Metal Fluoride Glasses (HMFGs): These non-oxide glasses are usually made up of elements like Barium, Lanthanum, Aluminium Sodium etc. Suitable applications of these glasses are in telecommunication fibres because of quite less optical losses. But the preparation of these glasses is very complicated and their chemical durability is not good.

1.3.2.2. Glassy metals: To prepare these non-oxide glasses, metals in melted form are quenched very rapidly. These glasses are generally composed of Iron, Phosphorous, Nickel and Boron and existing in the commercial sector as METGLAS. Applications of these glasses are found in magnetic shielding and power transformers.

1.3.2.3. Chalcogenide Glasses: These non oxide glasses are amorphous semiconductors which contain chalcogens (Sulphur, Selenium and/or Tellurium) in addition with some other suitable elements of the periodic table. Due to the semiconducting nature of these glasses their usage have been found in many applications like

memory switching devices, xerography etc. They have shown their potential to be used in photovoltaic applications like solar cells.

1.3.2.4. Glass ceramics: These are the glasses in which the possibility of bringing crystallization in the normal disordered atomic structures to some extent is strong. In the glass ceramics, which are commercially available, evenly sized high density non oriented crystals are attained throughout the bulk samples of the glasses instead of at surface or in distinct areas of the glasses. Some applications of these glasses are found in cooking vessels, dental implants etc.

1.3.2.5. Glass composites: To prepare functional glass products ceramic, polymer and metal powders are mixed together to form glass composites. The products made from such composites possess unique properties which can only be achieved from the combined effects of the constituent elements. Applications of these glasses are thick film conductors, resistors, dielectrics in which the tailoring of electrical properties is required in the field of microelectronics and glass fibre reinforced plastics.

1.3.2.6. Natural glasses: These are those glasses which are available in nature. Some of the examples of these glasses are fulgurites (produced on hitting of lightning on ground), obsidians or volcanic glass, tektites (produces from terrestrial debris evicted through meteorite collisions), microtektites (usually found in deep ocean), moldavites (produced due to collisions of meteorite generally found in central Europe) etc. Microtektites exhibit high chemical stability under sea which makes them useful in hazardous waste control applications.

1.4. CHALCOGENIDE GLASSES

Chalcogenide glasses are non oxide glasses which are comprised of Chalcogens i.e. group 16 elements (Sulphur, Selenium or/and tellurium) of periodic table with other suitable elements for a particular application. These glasses belong to the category of amorphous materials which are semiconducting by nature. They have become an interesting area of research for scientists and researchers in the material science and nanotechnology. This is mainly due to their unique and attractive properties which can be achieved only from the combined effects of the properties of different constituent elements. For this reason their uses are being

observed in many technological applications [1, 39]. These amorphous semiconductors exhibit band gap energy range of which is generally 1 to 3 electron volts [40]. For studying physical properties of a material, proper knowledge regarding its structure is very necessary. The variation in its different properties like optical and electrical is mostly related to its structural behaviour. Therefore, the detailed study of structure of a Chalcogenide glass is very necessary for exploring the relation between the properties with its structure [41].

Different incorporated impurities in a glassy system show obvious effect in its structure and hence on the change in its conduction mechanisms. For different incorporated impurities the effects are extensively different. Many reports are available in which the study on incorporated impurity effects on Chalcogenide glasses have been reported [42-44]. Due to ease of fabrication and processing, these glasses can be used in optical fibres particularly when there is a need of short length and flexibility [45, 46].

Vibhav K. Saraswat et al. [47] studied the effects of addition of Lead on band gap and conductivity in Se-Te glasses. V-I characteristics of the glasses at various temperatures was recorded and based on the analysis of these characteristics, the variation of conductivity in these glasses were explained. In these glasses Poole-Frenkel conduction mechanism was found good for conduction in the given range of temperature. Recording of absorption spectra and its analysis was done from which the direct band gap semiconducting nature of the glasses has been observed. Some more Chalcogenide systems reported by many researchers are briefly explained in the next section.

1.4.1. Comparison between Oxide and Chalcogenide Glasses

Oxide glasses are most recognizable glasses. These glasses possess many striking features such as: these can be acts as good dielectrics, optical transmitters, thermal insulators etc. These glasses are basically belonging to amorphous solids which contain ionic bonding [6]. These glasses are having extraordinary capability to decant, cast, roll, press and float glasses of windows. The electrical conductivity of most of these glasses is generally less than $10^{-8} \Omega^{-1} \text{cm}^{-1}$, which makes them insulating in nature. Due to the natural oxidizing tendency of metals and their insulating properties, metal oxide nanocomposite glasses have become very valuable in many applications [48].

Chalcogenide glasses belong to the class of non-oxide glasses. Their electrical conductivity is around $10^{-13} - 10^{-3} \Omega^{-1} \text{cm}^{-1}$, which is higher than that of oxide glasses, which makes them

semiconducting in nature. The conductivity in Chalcogenide glasses is usually electronic instead of ionic, unlike oxide glasses. Mostly covalent bonding is present in these glasses in addition to a very little contribution of ionic bonding. But some of these glasses (like Selenium based glasses) contain covalent as well as Van Der Waals bonding [48]. The formation of valence bonds of Chalcogenide glasses are mainly due to lone pair electrons. The exhibition of quite a lot of oxidation states is the most vital property of these glasses. The most familiar oxidation state of these glasses is -2. In addition to this, Sulphur exhibits +4 and +6 states. +2, +4 and +6 oxidation states are exhibited by Selenium, Tellurium and Polonium.

Chalcogenide and oxide glasses exhibit different mechanical, optical, thermal, electrical and other properties. The band gap energy of these two types of glasses is one of the major differences between them. Oxide glasses are having large band gap energies (about 10eV), while band gap energies of glasses based on Chalcogens are generally lie in the range of 1eV to 3eV [40].

1.4.2. Some previous work on various Chalcogenide Glasses

Kedar Singh, et al. reported the analysis on reflection spectra to obtain the optical energy band gap of Se-In based glasses [49] which was found to lie between 2eV to 2.23eV. The glass with value $x=10$ is found to have least optical band gap energy which can be due to the localized states in high density at the mobility edge of the glass .

Vibhav K. Saraswat et al. studied the electrical conductivity and I-V characteristics of Se-In based glassy systems [50]. Based on bond strengths and bond lengths of different bonds present, the glassy system bearing the composition $Se_{90}In_{10}$ was found most conducting in nature as compared with other compositions of the system.

R. Shukla et al. reported the use of differential scanning calorimeter to study the crystallization kinetics of $Se_{100-x}In_x$ glasses [51]. Kissinger's relation and Friedman method have been used to find the crystallization's activation energy which was found to decrease on increase of crystallization degree. The dependency of activation energy on composition of the glass was also reported.

Spoorti Shrivastav et al. reported the investigations on kinetics of glass transition for the system $Se_{100-x}Bi_x$ using DSC [52]. Relations of Moynihan and Kissinger were used to find the glass transition activation energy E_g . The values of E_g as well as their compositional

dependency measured from both the relations were found very similar. E_g was found to vary with the concentration of bismuth in the system. Low thermal stability of the system for higher concentrations of Bismuth was found.

S. K. Dwivedi et al. reported the effects of photo crystallization in Chalcogenide glassy thin films of $Se_{1-x}Sb_x$ [53]. Crystallizations in the films were confirmed from XRD and electron microscopy methods. There was an indication of increasing DC conductivity in the films on crystallization. On increasing the concentration of Antimony in the system the photo crystallization effect was found to be decreased.

S. Yadav et al. reported the decrease of activation energy on increase of Bismuth concentrations in the glassy alloys of $Se_{100-x}Bi_x$ [54]. Dependency of conductivity on composition of the glass is also reported. The conductivity was found to decrease first and then increase on the increase of Bismuth concentration in the system. Variation of DC conductivity with temperature plot has been fitted with Mott's model in the lower temperature region from which density of localized states were calculated.

N. Mehta et al. reported the use of non isothermal DSC to study thermal crystallization of $Se_{80}Te_{20}$ and $Se_{80}In_{20}$ Chalcogenide glassy samples [55]. Decrease of Avrami index with the rise of temperature was observed and exhibiting of higher crystallization activation energy by $Se_{80}Te_{20}$ glassy samples than $Se_{80}In_{20}$ Chalcogenide samples, which is due to the higher mean bond energy of $Se_{80}Te_{20}$ samples, is reported.

J. Sharma et al. studied the dielectric properties of Chalcogenide $Ge_{100-x}Se_x$ glassy alloys which are covalently bonded in nature [56]. Glasses formed by amalgamation of Germanium into amorphous Selenium exhibit good chemical stability. The increase of both dielectric loss and dielectric constant on incorporation of Germanium into pure a-Selenium had been observed.

S. S. Fouad et al. studied the frequency and temperature dependent electrical properties (dielectric constant, dielectric loss, and electrical conduction) of Ge_xSe_{100-x} Chalcogenide glassy alloys [57]. Conduction mechanisms of the glasses were studied using CBH model. The comparison of hopping conductivity of this glassy system with theoretical data is also reported.

N. A. Bakr et al. reported the studies on structural properties of Ge_xSe_{1-x} Chalcogenide thin films prepared using thermal evaporation method [58]. XRF method was used to check the

compositions of the prepared thin films. The polycrystalline nature of the amorphous films has been confirmed through XRD data analysis. The glass transition temperature value was found utmost for range of x from 0.25 to 0.32. Bandgap energy of the glass with respect to Germanium content was found maximum for $x=0.28$ and for the values $0.2 < x < 0.32$ the width of band tail was largest. The strong dependency of transparency and refractive index on composition of the glass had been observed.

K. Singh et al. reported the study on heating rate and compositional effects on glass transition temperature T_g of Ge-Se-As based Chalcogenide glassy system by means of DSC [59]. The dependency of T_g on the heating rate as well as composition was found. The maximum glass transition activation energy was found in the system with the composition $Ge_{20}Se_{65}As_{15}$ on comparing with other compositions of the system.

S. A. Fayek et al. reported the use of DTA for calorimetric measurements for thermal characterization of Chalcogenide $Ge_{2.5-x}Se_{7.5}Sb_x$ glassy alloys [60]. The DTA result shows an indication of the decrease of glass transition temperature for these glassy alloys with heating rate.

Investigation of crystallization kinetics of Chalcogenide glassy system $Si_{20}Te_{80-x}Bi_x$ using DSC method to study the variation of its glass transition and crystallization temperatures with composition is reported by B. J. Fernandes et al. [61]. Calculations of activation energy, deduction of specific heat, fragility index, thermal stability, entropy and enthalpy have also been reported there.

Preparations and thermal diffusivity measurements using photoacoustic technique of bulky samples of $Pb_xGe_{42-x}Se_{58}$ and $Pb_{20}Ge_ySe_{80-y}$ systems for different values of x and y were reported by R. Ganesan et al. [62]. The composition dependency of thermal diffusivity of these glasses is also reported. The reversal of conductivity takes place in $Pb_xGe_{42-x}Se_{58}$ glass at $x = 9$ and $Pb_{20}Ge_ySe_{80-y}$ glass at $y = 21$. Fermi level shifting is the cause of the reversal of conduction. Kolobov Model was used to describe the results which were mainly based on the defect states occurred because of the metallic elements added to the system

Crystallization kinetics of $Se_{68}Ge_{22}Pb_{10}$ glass using DSC technique has been studied by N. Mehta et al. [63]. Crystallization activation energy (E_C) has been calculated using four methods: Kissinger, Matusita-Sakka, Augis-Bennett Approximation and Ozawa-Chen methods and the obtained average activation energy is 1.477eV. There is an indication of

simultaneous working of two crystallization mechanisms during the transformation from amorphous state to crystalline state. The rate constant K is found to be increased on increasing temperature and heating rate.

N. S. Saxena reported the thermodynamics in glass to crystal phase transition in Se-Ge-Pb based Chalcogenide glasses [64]. To determine different thermodynamics quantities like entropy, enthalpy etc DSC method has been used. The increase of system's stability on increasing the amount of Pb has also been reported.

A. Ganjoo et al. investigated effects of Sb addition on structure of amorphous film of Se-Ge using EXAFS measurements [65]. EXAFS shows the existence of different bonds like Ge-Ge and Ge-Se in the film. The disappearance of these bonds takes place on increasing Se content in the film. In Ge Sb-Ge based glasses, the structural network was found stronger and stable.

Investigations on structural and thermal properties of Chalcogenide Ge Sb-Ge based system have been reported by J. B. Ko and Tea-Sik Myung [66]. From DSC result analysis an irregularity in crystallization has been observed. Use of Ozawa model to calculate activation energy has been reported. The obtained activation energy reported from this model is 3.2eV.

Preparation and optical characterization of Chalcogenide $\text{Ge}_{28}\text{Se}_{60}\text{Sb}_{12}$ glassy thin films has been reported by R. Tintu et al [67]. The optical bandgap energy was increased from 2.51eV to 3.56eV on decrease of content of $\text{Ge}_{28}\text{Se}_{60}\text{Sb}_{12}$. The Wemple – DiDomenico single oscillator model has been used for analyzing the dispersion in refractive index. For the characterization of these films different parameters like extinction coefficient, static refractive index, static dielectric constant, refractive index, etc have been measured.

Study of photoconductivity dependent on temperature and intensity of thin films of Chalcogenide $\text{Se}_{90}\text{Ge}_{10-x}\text{In}_x$ glasses has been reported by S. Singh et al. [68]. The minimum value of photoconductivity and photosensitivity was found at 4 atomic percentage of Indium. Their DC conductivity measurement is also reported there. There is an indication of compositional dependency of space charge up to 4 atomic percentage of Indium and dominance of heating effect after that amount.

M. A. Abdel-Rahim et al. reported the analysis of DSC results of Ge-Se-In system under non isothermal conditions [69]. Dependency of glass transition and crystallization temperatures on heating rate as well as composition of the glass has been found. The composition dependent glass transition and crystallization activation energies have been discussed. XRD

and SEM techniques have been used to identify the crystallization phases obtained from DSC.

Preparations of thin films of $\text{Ge}_{20}\text{Se}_{80-x}\text{Te}_x$ Chalcogenide glasses on the surfaces of glass and silicon wafers have been reported by F.A. Al-Agel [70]. The amorphous nature of these films has been determined by XRD diffractograms. Optical band gap was found to decrease from 2.06eV to 1.79eV and increase of absorption coefficient and refractive index with increase of Te in the composition has been observed. Their DC electrical conductivity has been measured at various temperatures (292K - 393K). The activation energy, measured from the analysis of DC conductivity results, has been observed to be decreased from 0.91eV to 0.55eV when amount of Te increases. The occurrence of conduction due to thermal supported charge carriers' tunneling among different localized states near Fermi level has been reported for these glasses.

S. K. Pal et al. [71] reported the preparation of Se-Te-Sn-Ge Chalcogenide system as dielectric materials with high dielectric constant and low dielectric loss. Ge was found to play a very important role to improve dielectric properties of system. Incorporation of Germanium in the glassy system helps in the optimization of dielectric properties in $\text{Se}_{74}\text{Te}_{20}\text{Sn}_2\text{Ge}_4$ and $\text{Se}_{72}\text{Te}_{20}\text{Sn}_2\text{Ge}_6$ systems.

B. S. Patial et al. [72] reported the use of DSC for calorimetric study of $\text{Se}_{85-x}\text{Te}_{15}\text{Sn}_x$ system for different values of x under non isothermal conditions. There is an enhancement of glass transition and crystallization temperatures with rise of heating. The glass transition and crystallization activation energies and Avrami exponent (n) are found to be dependent on composition. On increasing the content of Sn in the system the ability of crystallization has been found to increase. The glass having the composition $\text{Se}_{83}\text{Te}_{15}\text{Sn}_2$ is found to be more thermally stable.

Study of I-V characteristics of $\text{Ge}_{30-x}\text{Se}_{70}\text{Sn}_x$ alloys has been reported by V. Kumari et al. [73]. Ohmic and non ohmic behaviors of this glass have been studied using I-V characteristic analysis. The increase in Sn content in the glass increases the DC conductivity. The glass with composition $\text{Ge}_{10}\text{Se}_{70}\text{Sn}_{20}$ shows the maximum electrical conductivity.

1.4.3. Electrical relaxation process in Chalcogenide glassy system

Electrical relaxation refers to the relaxation response of a dielectric material to an external electric field. It is a brief delay in the dielectric constant of the material. It occurs due to delay in molecular polarization with respect to change in the electric field. Frequency dependent electrical conductivity helps in understanding the conduction mechanism of a Chalcogenide glassy system. Hence, study of electrical behaviour of these systems are very important through which information regarding the transport process in localized states and the type of polarization can be obtained. By adding impurities to the disordered structure of these systems, their structures can be changed. This results in the change in their conduction mechanisms which is different for different impurities.

With the help of dielectric relaxation studies we can determine the frequency dependent electrical properties of materials. It helps to find two basic electrical characteristics of a material: capacitive nature (charge storage capability) and conduction nature (charge transfer capability). The dielectric behaviour of a Chalcogenide glassy system mainly depends upon charged defect states D^+ and D^- which form dipoles [74]. These dipoles contribute to dielectric relaxation when an alternating electric field is applied. On the application of this alternating electric field to a dipole in the system, dipole starts rotating for aligning itself in the direction of the field. After sometime the electric field reverses its direction. The dipole must start rotating again to remain aligned in the field's direction. When the dipoles rotate, some energy is lost due to generation of heat and acceleration - deceleration of dipole's rotational motion. This produces dielectric loss which is a function of structure, frequency and temperature. Therefore, to investigate a Chalcogenide glassy system, study of its frequency and temperature dependent electrical relaxation becomes very important which results in dielectric dispersion in the system. For studying electrical properties of a glassy system, analysis of its DC and AC conductivity data is very essential.

DC conductivity of sample of a glassy system can be obtained by the equation:

$$\sigma_{DC} = \frac{L}{R \times A} \quad (1.1)$$

where, R is resistance, L represents thickness and A denotes cross sectional area of glass sample.

DC conductivity of a semiconductor generally obeys the Arrhenius equation which is:

$$\sigma_{DC} = \sigma_0 \exp\left(-\frac{\Delta E}{K_B T}\right) \quad (1.2)$$

where, ΔE represents activation energy for conduction, K_B is Boltzmann constant, σ_0 is pre-exponential factor and T is absolute temperature. Taking log on both sides of Eqn. (1.2) becomes:

$$\log \sigma_{DC} = \log \sigma_0 - \Delta E/KT$$

$$\text{or, } \log \sigma_{DC} = - [(\Delta E/1000K) \times (1000/T)] + \log \sigma_0$$

When $\log \sigma_{DC}$ versus $1000/T$ is plotted, a straight line can be obtained. Activation energy can be calculated from the slope as:

$$\Delta E = 1000 \times K \times \text{Slope of the line} \quad (1.3)$$

The electrical response area of a system can be defined in four related immittance levels: complex resistivity: $\rho(\omega)$; complex modulus: $M(\omega) = i\omega\epsilon_1/\rho(\omega)$; complex dielectric constant: $\epsilon(\omega) = [M(\omega)]^{-1}$; and complex conductivity, $\sigma(\omega) = i\omega\epsilon_1/\epsilon(\omega)$, where, ϵ_1 is permittivity of vacuum and ϵ_1/ϵ is permittivity related to a dielectric constant ϵ . Many researchers have reported the studies of electrical properties of various Chalcogenide glassy systems, some of which are mentioned below:

Electrical properties study of bulk $Cd_{50}S_{50-x}Se_x$ ($30\% \leq x \leq 50\%$) Chalcogenide glass prepared by mechanical milling method has been reported by A.S. Hassanien et al. [75]. The increase of DC conductivity and decrease of activation energies on increasing Se in system was observed. The composition and temperature dependent conductivity mechanism in the glass has been found. The transition temperature of the glass has been found at around 370K. Below 370K the DC conductivity data was analyzed by Mott's model and above this temperature the activated thermoionic emission causes the hopping conduction in different localized states

R. Belin et al. [76] reported the study of electrical conductivity of $0.5Ag_2S - 0.5GeS_2$ Chalcogenide glasses at different temperatures (123K - 473K) and frequencies (10Hz - 6THz). For analyzing AC conductivity spectra of this system, the power law method and the master curve procedure have been used.

Study of DC conductivity of fast ionic of $0.5\text{Ag}_2\text{S} - 0.5\text{GeS}_2$ glasses and the use of empirical Vogel-Fulcher-Tammann law to describe the conductors having conductivity at room temperature with little activation energy was reported by M. Ribes et al. [77].

A. Kumar et al. [78] reported the measurements of capacitance and conductance for studying the dependency of dielectric parameters on temperature (223K-293K) and frequency (2KHz-50KHz) of Chalcogenide $\text{Se}_{85-x}\text{Te}_{15}\text{In}_x$ ($x = 0, 2, 6, 10$) glasses. Occurrence of dielectric dispersion in these ranges of temperature and frequency and more dispersion of dielectric at lower frequency region has been observed.

Investigations on AC electrical conductivity and dielectric response of silica glasses doped with CdSe in frequency range 1-3MHz at room temperature was reported by P.V. Jyothy et al. [79]. At high frequencies low values of dielectric loss and constant has been observed from the studies. The values of conductivity have been found in the order of 10^{-5} – 10^{-7} S/cm for these glasses.

M. Kubliha et al. [80] reported the study of temperature dependent DC conductivity of Ho doped $\text{Ge}_{20}\text{Se}_{80-x}\text{Te}_x$ system. The reduction of DC conductivity and increase of conduction activation energy on the decrease of Te concentration have been found. Reduction in the activation energy has been observed in these glasses when doped with Ho^{3+} ions in a metallic form.

Anjani Kumar et al. [81] studied effects of electric field on semiconducting parameters of Se-Sb-Ag based Chalcogenide glasses. At low Electric field, the independent nature of activation energy and the pre-exponential factor on field was observed. However, variation of activation energy and pre-exponential factor with the field has been found at higher electric fields. Yelon and Movaghar model has been used to explain the correlation which has been observed in the glass between activation energy and the pre-exponential factor.

Vandana Kumari et al. [82] have reported the electrical conductivity studies of Ge-Se-Sb based glass using I-V characteristics curves at various temperatures. In these glasses Poole-Frenkel conduction mechanism was found good for conduction in the given range of temperature.

The study of electrical conductivity in superionic $(\text{Ag}_3\text{AsS}_3)_x(\text{As}_2\text{S}_3)_{1-x}$ glass in frequencies 10Hz – 3×10^9 Hz and temperature range 300K-400K has been reported by Studenyak et al. [83]. The compositional dependency of electrical conductivity and activation energies has

also been analyzed. The enhancement of electrical conductivity and reduction of activation energy on adding Ag_3AsS_3 to the glass have been observed.

S. Srivastava et al. [84] observed the exponential variation of AC conductivity with temperature in $\text{Se}_{70}\text{Te}_{30-x}\text{Zn}_x$ Chalcogenide glasses at particular frequency. Different activation energies have been obtained at different frequencies. Correlation of pre-exponential factor and activation energy has been found which follows Meyer Neldel (MN) rule.

Study of temperature and frequency dependent dielectric constant and loss in $\text{Se}_{100-x}\text{Te}_x$ ($x=4, 8, 12, 16$) Chalcogenide glassy system at frequencies 1KHz - 1MHz and temperatures 290K – 360K has been reported by Mohsin Ganaie et al. [85]. The dielectric constant and loss were found to increase with of Te concentration, which may be because of increase in the defect state. On increasing amount of Te, increase of DC conductivity and decrease of activation energy are because of increases in the density of defect states.

The narrowing of electrical and optical band gap on adding Copper to As-Se glasses has been reported by V. I. Mikla et al. [86]. The dark conductivity values and activation energy of the glasses have been found to change with the addition of Cu in the system.

1.4.4. Applications of Chalcogenide Glasses

The attractive unique properties of the Chalcogenide glasses enhance the possibilities of being used in a variety of technological applications. One of the important applications is resistance switching [87]. For threshold type switching it can be used as ON/OFF switch and for memory type switching it can be used as memory storage applications. Application of Chalcogenide glasses have also been found in many different areas like military, civil, medical etc [88-90]. Some other applications of these glasses are optical filters, waveguides, optical and temperature sensors, xerography, photovoltaic applications like solar cells etc [91-94].

Temperature monitoring, energy management and night vision are some of the applications of Chalcogenide glasses used in Infrared optics [95]. In some applications like switching and photocopying, these glasses act as active electronics devices. For transmitting telecom signals, they can be used in ultra low loss IR fibres [96, 97]. Chalcogenide fibres are also suitable in some applications where low power transmission are required, like welding operations in industries and microsurgeries in biological and medical areas [98, 99]. Their

suitability has also been found in some applications like optical lenses for IR cameras, scanners, multiplexers, demultiplexers, printer heads etc [100]. These glasses have also been found suitable in optical memory applications like optical recording (rewritable) and programmable non volatile memory. Some other applications of these glasses are [101]:

- Image storage
- Photo-resistors
- Opto-electronics
- Non linear optics
- Photo electrochemical solar cell
- Electroluminescent device
- IR Photodetectors
- Photo-transistors
- Lasers

1.5. TRANSITION METAL ION DOPED CHALCOGENIDE GLASSES

Atoms of Transition Metal Ions (TMI) contain incompletely filled d sub-shell. These elements belong to Group 3 – 12 of periodic table. In Transition Metal Ions or TMI doped glasses there is a quite high propensity of small polarons' generation. Hopping of these polarons among the different valence states of TMI causes electrical conduction [102]. To get the enhanced knowledge regarding the transport mechanisms in amorphous semiconductors, many researchers studied different TMI doped glasses [103-106]. The structural network of a glass gets changed when it is doped with TMIs. As the consequence the glass exhibits some unique properties which enable the possibility of their usage in various applications.

Elalaily and Mahamed [107] and Kumar et al. [108] investigated the electrical conduction in many TMIs doped glasses. It had been observed by them that electrical conduction of these glasses varies with the change in their structural network which arises due to the existence of TMIs. The conductivity of these glasses is also highly dependent on temperature. Variation of activation energy in these glasses depends on ligancy of the involved TMIs. Sayer and Mansingh [109] reported the studies on dielectric properties of many glasses doped with TMIs. They observed the dependence of dielectric relaxation on polarons hopping among pairs of TMIs (pair approximation model). The AC conductivity spectra at different

temperatures had been analysed which helps in finding the pertinent hopping mechanism as to pair approximation [110].

1.6. OBJECTIVE OF THE RESEARCH WORK

The purpose of this research work is to prepare some new types of cheap and reliable semiconducting glassy nanocomposite materials and to identify the possible technological applications of these materials in industry as well as academic purposes.

The main objectives of the PhD work:

- To develop some new glass nanocomposite systems containing Transition Metal Ion doped chalcogens like $\text{Ag}_2\text{S-S-Te}$, Cu-S-Te , $\text{Ag}_2\text{S-Se-Ge}$ and $\text{Ag}_2\text{S-Se-Te}$. It is a very interesting field of research not only for their application point of view but also for academic interest.
- Structural characterization of all the prepared samples to study their physical properties by using different methods like X-Ray Diffraction (XRD), Transmission Electron Microscopy (TEM), Fourier Transform Infrared Spectroscopy (FT-IR), Ultraviolet Visible Spectroscopy or UV-Vis etc.
- To study the electrical conductivity and relaxation mechanism in wide frequency range and at various temperatures and hence to explore electrical transport properties of the prepared TMI doped Chalcogenide glass nanocomposites
- To explore the correlation between electrical conduction parameters (such as conductivity, resistivity etc) and some structural parameters (obtained from XRD, HRTEM etc.).
- To explore the device application of the prepared glassy systems: Chalcogenide glasses can be used in many device applications like solar cells, temperature sensor, gas sensor, light emitting diodes, electro-photography etc because of their unique properties. To find proper electronic device applications of a Chalcogenide glassy system, study of its electrical properties and structural analysis play a very important role. From the studies of temperature dependent electrical conductivity, information regarding structural defects and localized states of the system can be obtained. The

electrical conductivity studies also give information concerning the nature of defect centres which helps in determining the type of conduction in the system. Electrical properties of these systems are controlled by density of defect states - which can be calculated after knowing the conduction mechanism in the system. Therefore, after studying the electrical properties and structural analysis of all the prepared glassy systems, their suitable applications in electronics devices will be explored.

REFERENCES

- [1] V. S. Shiryaev and M. F. Churbanov, *J. Non-Cryst. Solids*, 475, 1 (2019)
- [2] J. M. Ziman, "Models of Disorder", Cambridge University Press, London (1979)
- [3] D. Tumbull, *Contemp. Phys.* 10, 5, 473 (1969)
- [4] Materials Advisory Board, Nat. Acad. Sci. Res. Council, MAB-243 (1968)
- [5] N. A. Goryunova and B. T. Kolomiets, *Zh. Tekhn. Fiz.* 25, 984 (1955)
- [6] N. A. Goryunova and B. T. Kolomiets, *Izv. Akad. Nauk., Ser. Fiz.* 20, 1496 (1956)
- [7] H. Fritzsche, "Amorphous and Liquid Semiconductors", edited by J. Tauc, Plenum, New York (1974)
- [8] J. Singh and K. Shimakawa, "Advances in Amorphous Semiconductors", Taylor & Francis, London and New York (2003)
- [9] D. A. Adler, H. Fritzsche, "Tetraedrally-Bonded Amorphous Semiconductors", Springer (2013)
- [10] P. Boolchand, "Insulating and Semiconducting glasses" Series on Directions in Condensed matter Physics-Volume 17 (2000)
- [11] Y. Hamakawa, "Amorphous Semiconductor Technologies & Devices", Elsevier (1984)
- [12] K. Morigaki and C. Ogihara "Amorphous Semiconductors: Structure, Optical and Electrical Properties", Handbook of Electronic and Photonic Materials, Springer (2017)
- [13] K. Ide, H. Hosono and T. Kamiya, *International Conference on Display Technology*, 52, 97 (2021)
- [14] A. Madan and M. P. Shaw "The physics and applications of amorphous semiconductors" Academic Press (1988)

- [15] K. Morigaki, S. Kugler and K. Shimakawa, “Applications – Amorphous Semiconductors”, J. Wiley and Sons Ltd., 247-264 (2017)
- [16] S. Sagadevan, *Rev. Adv. Mater. Sci.*, 34, 44 (2013)
- [17] M. D. Ediger and P. Harrowell, *J. Chemical Physics*, 137, 080901 (2012)
- [18] P. Gibbs, *Glass Worldwide*, 14–18 (2007)
- [19] W. Bragg, “The Glassy State”, *Structural Chemistry of Glasses*, 13 (2002)
- [20] R. Zallen, “The Physics of Amorphous Solids. New York: John Wiley. ISBN 0-471-01968-2 (1983)
- [21] N. E. Cusack, “The physics of structurally disordered matter: an introduction”, Adam Hilger in association with the University of Sussex press, ISBN 0-85274-829-9 (1987)
- [22] S. R. Elliot, “Physics of Amorphous Materials”. Longman group ltd. (1984)
- [23] Scholze, Horst “Glass – Nature, Structure, and Properties”. Springer. ISBN 0-387-97396-6 (1991)
- [24] J. E. Shelby, “Introduction to Glass Science and Technology”, Royal Society of Chemistry, Cambridge (2005)
- [25] A. K. Varshneya, “Fundamentals of Inorganic Glasses”, Academic Press, Inc., New York (1994)
- [26] N. I. Min’ko and V. M. Nartsev, *Glass and Ceramics*, 65, 12 (2008)
- [27] A. Dan, B. Satpati, P.V. Satyam and D. Chakravortya, *J. Appl. Phys.* 93, 4794 (2003)
- [28] L. A. H. Fleming, S. Wackerow, A. C. Hourd, W. A. Gillespie, G. Seifert and A. Abdolvand, *Opt. Express* 20, 22579 (2012)
- [29] W. G. Drost, H. Hofmeister and A. Berger, *Proceedings 33rd Topical Meeting on Liquid Crystals*, Deutsche Flüssigkristall-Gesellschaft, Frankfurt, Germany P2-1-P2-4 (2005)
- [30] A. L. Stepanov, *Rev. Adv. Mater. Sci.* 27, 115 (2011)
- [31] A. Stalmashonak, A. Abdolvand and G. Seifert, *Appl. Phys. Lett.* 99, 201904 (2011)
- [32] S. Thomas, S. K Nair, E. M. A. Jamal, S. H. Al-Harhi, M. R. Varma and M. R. Anantharaman, *Nanotechnology* 19, 075710 (2008)
- [33] I. Khan, K. Saeed and , I. Khan, *Arabian J. Chemistry*, 22, 908 (2019)
- [34] P. M. Ajayan, L. S. Schadler and P. V. Braun, “Nanocomposite Science and Technology”, Wiley-VCH Verlag (2003)

- [35] J. P. Davim, “Tribology of Nanocomposites”, Springer-Verlag Berlin Heidelberg, New York (2013)
- [36] L. M. Manocha, J. Valand, N. Patel, A. Warriar and S. Manocha, *Indian J. Pure Appl. Phys.* 44, 135 (2006)
- [37] P. H. C. Camargo, K. G. Satyanarayana and F. Wypych, *Mat. Res.* 12, 1 (2009)
- [38] P. H. C. Camargo, K. G. Satyanarayana and F. Wypych, *Material Research*, 12, 1 (2009)
- [39] F. S. Al-Hazmi, *Chalcogenide Letters*, 6, 63 (2009)
- [40] S. El-Sayed, *Chalcogenide Letters*, 6, 241 (2009)
- [41] I. Pethes, A. Piarristeguy, A. Pradel, S. Michalik, R. Nemausat, J. Darpentigny and P. Jovari, *J. Alloys and Compounds*, 834, 155097 (2020)
- [42] K. Sedeek, A. Adam, L. A. Wahab and F. M. Hafez, *Mater. Chem. Phys.*, 85, 20 (2004)
- [43] Y. Yang, O. Ba, S. Dai, F. Chen and G. Boudebs^c, *J. Non-Cryst. Solids*, 554, 120581 (2021)
- [44] J. Zhang, Y. Li, C. Zhang, F. Chen, X. Zhang and W. Ji, *J. Non-Cryst. Solids*, 545, 120240 (2020)
- [45] J. S. Sanghera, L. B. Shaw and I. D. Aggarwal, *Comptes Rendus Chimie* 5, 873 (2002)
- [46] F. Smektala, A. Lemièrre, A. Maldonado, P. Froidevaux, F. Désévéday, and B. Kibler, *Proc. SPIE 11357, Fiber Lasers and Glass Photonics: Materials through Applications II*, 113570Z (2020)
- [47] V. K. Saraswat, V. Kishore, K. Singh, N. S. Saxena, T. P. Sharma, Electrical conductivity of Se-In Chalcogenide glasses, *Chalcogenide letters* 8, 61 (2006)
- [48] “Fundamentals of Amorphous Semiconductors”, NMAB-284, National Academy Press - 2101 Constitution Avenue, NW. Washington, D.C. 20418 (1971)
- [49] K. Singh, N. S. Saxena, O. N. Srivastav, D. Patidar and T. P. Sharma, *Chalcogenide Letters* 3, 33 (2006)
- [50] V. K. Saraswat, V. Kishore, K. Singh, N. S. Saxena and T. P. Sharma, *Chalcogenide letters* 8, 61 (2006)
- [51] R. Shukla, D. Agarwal and A. Kumar, *Chalcogenide Letters* 7, 249 (2010)
- [52] S. Srivastav, M. Zulfear and A. Kumar, *Chalcogenide Letters* 6, 40 (2009)
- [53] S. K. Dwivedi, V. S. Kushwaha and A. Kumar, *Chalcogenide Letters*, 5, 187 (2008)

- [54] S. Yadav, S. K. Sharma, P. K. Dwivedi and A. Kumar, *J. Non-oxide glasses* 3, 17 (2011)
- [55] N. Mehta, V. S. Kushwaha and A. Kumar, *Indian J. of Engg & Mat. Sciences.* 12, 571 (2005)
- [56] J. Sharma and S. Kumar, *J. Non-oxide glasses* 1, 120 (2009)
- [57] S. S. Fauad, M. Fadel, E. Abd. El-Wahabb, *J. Ovonic Research* 4, 51 (2008)
- [58] N. A. Bakr, M. S. Aziz and M. Hannan, *Egypt. J. Sol.* 23, 45 (2000)
- [59] K. Singh and N. S. Saxena, *Bulletin of Material Science* 26, 543 (2003)
- [60] S. A. Fayek and M. Fadel, *J. Non-oxide glasses* 1, 239 (2009)
- [61] B. J. Fernandes, K. Ramesh and N. K. Udayashankar, *Material Science and Engineering B*, 246, 34 (2019)
- [62] R. Ganesan, B. Thangaraju, K. S. Sangunni and E. S. R. Gopal, *J. Opto electr. and Adv. Mat.*, 3, 467 (2001)
- [63] N. Mehta, P. Agarwal and A. Kumar, *Indian J. of Engg. & Mat. Sci.*, 11, 511 (2004)
- [64] Deepika, N. S. Saxena, *J. Phys. Chem. B.* 114, 28 (2010)
- [65] A. Ganjoo, H. Jain, S. Khalid and C. G. Panjano, *Philosophical Magazine Lett.* 85, 503 (2005)
- [66] J. B. Ko and Tea-Sik Myung, *J. Ceramic Processing Research* 12, 132 (2011)
- [67] R. Tintu, K. Saurav, K. Sulakshna, V. P. N. Nampoori, P. Radhakrishnan and S. Jhomas, *J. Non-oxide glasses* 2, 167 (2010)
- [68] S. Singh, R. S. Sharma, R. K. Shukla and A. Kumar, *Chalcogenide Letters* 1, 83 (2004)
- [69] M. A. Abdel-Rahim, M. M. Hafiz and A. M. Shamekh, *Physica B*, 369, 143 (2005)
- [70] F.A. Al-Agel, *Optics & Laser Technology* 43, 781 (2011)
- [71] S. K. Pal, A. Kumar and N. Mehta, *Ceramics International*, 45, 16279 (2019)
- [72] B. S. Patial, N. Thakur and S. K. Tripathi, *J Therm Anal Calorim* 106, 845 (2011)
- [73] V. Kumari, A. Kaswan, D. Patidar, N. Sahai Saxena and K. Sharma, *Processing and Application of Ceramics* 9, 161 (2015)
- [74] S. R. Elliott, *Phil. Mag.* 36, 1291 (1977)
- [75] A. S. Hassanien and A.A. Akl, *J. Non-Cryst. Solids* 432, 471 (2016)
- [76] R. Belin, G. Taillades, A. Pradel and M. Ribes, *Solid State Ionics* 136, 1025 (2000)
- [77] M. Ribes, G. Taillades and A. Pradel, *Solid State Ionics* 105, 159 (1998)
- [78] A. Kumar, M. Lal, K. Sharma and N. Goyal, *J. Non-Oxide Glasses* 5, 4, 47 (2013)

- [79] P. V. Jyothy, K. V. Arun Kumar, S. Karthika, R. Rajesh and N. V. Unnikrishnan, *J. Alloys and Compounds* 493, 223 (2010)
- [80] M. Kubliha, P. Kostka, V. Trnovcova, J. Zavadil, J. Bednarcik, V. Labaš, J. Pedlikova, A.-Ch. Dippel, H.-P.Liermann and J. Psota, *J. Alloys and Compounds* 586, 308 (2014)
- [81] A. Kumar and A. Kumar, *J. Non-Crystalline Solids* 386, 51 (2014)
- [82] V. Kumari, A. Kaswan, D Patidar, K. Sharma and N. S. Saxena, *Bull. Mater. Sci. Indian Academy of Sciences*, 39, 1, 255 (2016)
- [83] I. P. Studenyak, Yu. Yu. Neimet, M. Kranjčec, A. M. Solomon, A. F. Orliukas, A. Ke_zionis, E. Kazakevičius and T.Salkus, *J. Appl. Phys.* 115, 033702 (2014)
- [84] S. Srivastava, S. Yadav, R. K. Shukla and A. Kumar, *J. Non-Oxide Glasses*, 1, 1, 51 (2010)
- [85] M. Ganaie, S. Ahmad and S. Islam M. Zulfequar, *International Journal of Physics and Astronomy*, 2, 2 (2014)
- [86] V. I. Mikla, A. A. Kikineshi, V. V. Mikla and D. G.Semak, *J. Non-Oxide Glasses* 1, 1, 61 (2009)
- [87] S. R. Ovshinsky, *Phys. Rev. Lett.* 21, 713 (1968)
- [88] A. Zakery and S. R. Elliott, *J. Non-Cryst. Solids*, 1, 330 (2003)
- [89] D. Lezal, *J. Optoelectron Adv Mater.* 5, 23 (2003)
- [90] A. B. Seddon, *J. Non-Cryst. Solids.* 184, 44 (1995)
- [91] J. S. Sanghera and I. D. Agarwal, *J. Non-Cryst. Solids.* 256, 6 (1999)
- [92] J. Lucas, P. Lucas, D. Le Coq, M. R. Riley and J. H. Simmons, *J. Non-Cryst. Solids*, 276, 346 (2004)
- [93] T. Ohta, *J. Optoelectron. Adv. Mater.*, 3, 609 (2001)
- [94] A. M. Andriesh, M. S. Iovu and S.D. Shutov, *J. Optoelectron. Adv. Mater.*, 4, 631 (2002)
- [95] R. B. Johnson, *Proc Soc Photo-Optical Instrumentation Engrs, SPIE*, 915, 106 (1998)
- [96] T. Katsuyama & H. Matsumura, *Infrared Optical Fibres* (Adam Hilger, Bristol) 1989
- [97] J. M. Parker & A. B. Seddon, *High Performance Glasses*, edited by M Cable & J M Parker (Blackie, London) 1992

- [98] J. Keirsse, C. Boussard-Pledel, O. Loreal, O. Sire, B. Bureau, P. Leroyer, B. Turlin & J. Lucas, Chalcogenide glass fibers used as biosensors, *J. Non-Cryst Solids*, 326, 430 (2003)
- [99] J. Keirsse, C. Boussard-Pledel, O. Loreal, O. Sire, B. Bureau, P. Leroyer, B. Turlin & J. Lucas, IR optical fiber sensor for biomedical applications, *Vib Spectrosc*, 32, 23 (2003)
- [100] A.M. Andriesh, M. S. Iovu & S. D. Shutov, Chalcogenide noncrystalline semiconductors in optoelectronics, *J. Optoelectron Adv Mater*, 4, 631 (2002)
- [101] A. S. Hassanien and A.A. Akl, *J. Non-Cryst. Solids*, 428, 112 (2015)
- [102] A. Mansingh, J. K. Vaid and R. P. Tondon, *J. Phys. C Solid State Phys.* 10, 4061 (1977)
- [103] N. Nagaraja, T. Sankarappa and M. Prashant Kumar, *J. Non-Cryst. Solids* 354, 1503 (2008)
- [104] B. Dutta, N. A. Fahmy and I. L. Pegg, *J. Non-Cryst. Solids* 351, 1958 (2005)
- [105] B. Dutta, N. A. Fahmy and I. L. Pegg, *J. Non-Cryst. Solids* 351, 2552 (2005)
- [106] B. Dutta, N. A. Fahmy and I. L. Pegg, *J. Non-Cryst. Solids* 352, 2100 (2006)
- [107] N. A. Elalaily and R. M. Mahamed, *J. Nucl. Mater.* 303, 44 (2002)
- [108] B. V. Kumar, T. Sankarappa, S. Kumar, M. P. Kumar, P. J. Sadashivaiah and R. R. Reddy, *Phys. B: Condens. Matter*, 404, 3487 (2009)
- [109] M. Sayer and A. Mansingh, *Phys. Rev. B*, 6, 4629 (1972)
- [110] S. R. Elliott, *Adv. Phys.* 36, 135 (1987)

Chapter 2

EXPERIMENTAL METHODS

2.1. INTRODUCTION

This chapter is mainly focused on the various methods which are used for the preparation of Chalcogenide glassy systems having various compositions and the different characterization techniques which can be used for the analysis of the structure and electrical properties of the systems.

The chapter starts with the discussion on preparation of glassy systems using different methods like mechanical milling technique, sol-gel process, chemical vapour deposition (CVD) technique, chemical bath deposition (CBD) technique, melt-quenching method, etc [1-10] along with their advantages and disadvantages.

For structural and physical characterization of a glassy system, different methods like density and molar volume measurements, XRD, FT-IR, TEM and UV-Vis can be used. For any glassy system density is a vital property which is used to determine its structure. Higher value of density of a glassy system is an indication of closely packed particles in the structure. The variation of molar volume of a system on changing its composition is an indication of change of structure in its network [11].

XRD analysis helps to find the crystallite size of the different phases present in a system with their [h,k,l] values, dislocation density and strain [12-16]. Crystalline volume fraction percentage can also be determined from XRD analysis. FT-IR is an important structural characterization technique [17-18] which is generally used to get some useful information of a system like: unknown material identification, material quality and reliability, amount of component in a mixture etc. UV-Vis spectra analysis helps to obtain the optical band gap energy of a material [19]. From TEM analysis, the distribution of nanoparticles embedded in a system can directly be visualized. Using TEM area of nanoparticles in the system can be calculated. The interplanar spacings (D) between different crystalline phases in the system can be determined from SAED i.e., Selected Area Electron Diffraction pattern obtained from TEM technique [20, 21].

In order to study electrical properties of a system, DC and AC conductivities data analysis is very important. For the analysis of DC conductivity data various analytical models such as Mott's model [22] and Greaves' model [23] are used from which density of states in the system can be calculated at lower and higher temperature regions respectively.

AC conductivity data are analysed with the help of different techniques like: MN rule [24], Power law [25], Almond West formalism [26], etc. Conduction mechanism in a system can be determined with the help of appropriate models like CBH, NSPT, OLPT, etc. Permittivity and electric modulus studies are carried out for dielectric properties analysis of a system.

2.2. PREPARATION OF GLASSY SYSTEMS

Many techniques are available for the preparation of glassy systems or materials in amorphous phase. Some of these techniques are: mechanical milling technique, sol-gel process, chemical vapour deposition (CVD) technique, chemical bath deposition (CBD) technique, metal dielectric co-sputtering deposition etc. Some severe disadvantages of the use of these techniques are: high cost, not suitable for low melting or low softening glass preparations, possibility of sample damaging on exposure to radiation of high intensity, possibility of obtaining only thin glass plates etc. To overcome these disadvantages melt quenching method are used widely for the formation of a glassy system due to its rapid glass forming ability, simplicity and efficiency. The details of some glassy system preparation techniques are given in the sections below:

2.2.1. Mechanical Milling Technique

In this method high purity required elemental powders are weighted as per their percentage of atomic mass in stoichiometry. The powders are mixed and ground using mortar and agitated continuously for ensuring homogeneity. Then the mixture is placed in an electric mill in which it is ball-milled at 400 rpm using a stainless steel ball for at least 12 hours in order to get a high homogeneous solid solution of the system. Diameter of this ball is generally 10mm and the ratio of the steel ball and the mixture is 5:1. This is one of the easiest and inexpensive methods of preparation of glassy systems. But it is a time consuming process and requires safety measures for preventing contamination from the milling medium. A.S. Hassanien et al. [1] have reported the preparation of $Cd_{50}S_{50-x}Se_x$ glassy system using mechanical milling method.

2.2.2. Sol-Gel Process

It is another method to produce glassy systems, like SiO_2 , in which monomers are transformed into colloidal solution, which is called 'sol'. The sol acts as precursor for an integrated network called 'gel' which contains both liquid and solid phase. Usual precursors are metal alkoxides or metal chlorides. The precursor undergoes hydrolysis and polycondensation reactions for forming colloid (solid-liquid or liquid-liquid mixture in which distinct particles of solid or liquid are dispersed in a liquid medium). This method is considered as promising for the formation of ultra fine metallic oxide as well as some non-oxide glassy systems. Some of the advantages of this method are: versatile - due to which incorporation of nanoparticles and organic materials are possible in the systems fabricated from this method, better homogeneity – as the mixing takes place at molecular level better homogeneity can be achieved, less energy consumption, low cost – as expensive equipments are not required. However, this method has some drawbacks like: precursor cost, possibility of shrinkage of gel on drying, residual porosity and OH groups are not easy to avoid etc. P. V. Jyothy et al. [2] have reported the preparation of CdSe doped Silica glassy system by sol-gel process with tetraethyl orthosilicate as precursor.

2.2.3. Chemical Vapour Deposition Technique

It is a vapour deposition technique in which vapour-phased chemical precursors are decomposed on the surface of a heated substrate. This technique is used to produce solid materials having high quality and high performance. In this technique deposition of thin film takes place on the surface of a substrate through chemical reaction from precursor when the substrate is exposed to the volatile precursor. Some advantages of this method are: high throughput, high purity, low cost etc. However, it has some disadvantages also like: requirement of high deposition temperature for some precursors which are unsuitable for substrates, precursors are often hazardous or toxic etc. Therefore to handle precursors, extra steps need to be taken. The preparation of thin films of Si- doped ZnO using CVD technique has been reported by D. B. Potter et al. [3].

2.2.4. Chemical Bath Deposition Technique

It is a method to deposit thin films on substrates. This technique involves two steps: nucleation and particle growth. Basically, a solid state is formed from a solution in this technique. In this process the substrate is immersed in bath (a solution which contains

precursors). The deposition of thin films on the substrate by this method is dependent on various factors like: bath temperature, solution's pH value, time, chemical nature of the substrate etc. No physical damage in the substrate can be caused by this process. The major benefit of this technique is that it requires only substrate mounting devices and containers for solutions. Using this technique, uniform, hard, adherent and stable films can be produced. The most important drawback of this technique is the wastage of solution after each deposition. Many reports are available on preparation of thin films of glassy systems by this technique [4-5].

2.2.5. Melt Quenching Method

In this research work a very well known method – melt-quenching has been used for the preparation of bulk samples of Chalcogenide glassy systems having various compositions. This method is used to produce amorphous solids from the molten states of materials by rapid cooling of the molten materials to avoid the growth of crystal in the solids. Many reports are available on preparation of glassy systems using this method [6-10].

In melt-quenching method weighting and then the mixing of high purity constituent elements take place followed by melting in sealed evacuated quartz ampoules. Sealing of the mixture in the ampoules under a vacuum of $10^{-3} - 10^{-4}$ Torr lowers down the chances of reaction of these glasses with oxygen at higher temperatures. For weighing the constituent elements of each composition, an electrical balance – DHONA 200D (shown in Fig-2.1(a) having accuracy $\pm 10^{-4}$ gm has been used. The sealed quartz tubes containing the mixture are placed into the furnace (manufactured by Jay Crucibles, S. No. 272.9.19), shown in Fig-2.1(b), in which the temperature was raised gradually up to the melting points of the elements. Shaking of the mixture, on certain interval, in the quartz tubes is needed to realize the homogeneity of the mixture. When the mixture in the solid state are found in molten form, the tubes are taken out from the furnace and immediately quenched in crushed ice cubes. Due to rapid quenching of the molten materials, glassy ingots of the materials can be obtained. The immediate cooling process prevents crystallization to take place in the mixture. The glass forming capability of these materials depends upon quenching rate. If the rate of quenching of a molten material is higher, then its capability of glass formation will be more. Fig-2.1(c) shows the pelletizer (manufactured by ALFA India Enterprise) which has been used to form pellets from the powdered form of the as prepared bulk samples.



Fig-2.1: Instruments used for sample preparation: (a) Electric Balance (b) Furnace (c) Pelletizer

2.2.5.1. Composition of glassy systems prepared in the present work

In the present investigation following compositions of Chalcogenide glassy systems have been prepared by means of melt quenching process:

S. No.	Compositions	x values	Raw Materials
1	$x\text{Ag}_2\text{S}-(1-x)(0.5\text{S}-0.5\text{Te})$	0.35 & 0.45	Silver Sulphide, Sulphur, Tellurium (Aldrich 99.9%)
2	$x\text{Cu}-(1-x)(0.5\text{S}-0.5\text{Te})$	0, 0.1, 0.2, 0.3	Copper, Sulphur, Tellurium (Aldrich 99.9%)
3	$x\text{Ag}_2\text{S}-(1-x)(0.5\text{Se}-0.5\text{Ge})$	0.1, 0.2	Silver Sulphide, Selenium, Germanium (Aldrich 99.9%)
4	$x\text{Ag}_2\text{S}-(1-x)(0.5\text{Se}-0.5\text{Te})$	0.05, 0.1, 0.2	Silver Sulphide, Selenium, Tellurium (Aldrich 99.9%)

2.3. STRUCTURAL AND PHYSICAL CHARACTERIZATION

To carry out the structural and physical characterization of the as prepared glassy systems different methods have been used like: density and molar volume measurements, XRD, FT-IR, TEM, UV-Vis etc.

2.3.1. Measurement of Density and Molar Volume

Density of a glassy system is a significant property which is used to determine its structure. To measure density Archimedes principle is generally used, according to which density (ρ) is equal to [27]

$$\rho = W_a \rho_b / (W_a - W_b) \quad (2.1)$$

where, W_a and W_b represent the weight of the glassy system's sample in air and in buoyant liquid respectively, ρ_b is buoyant liquid's density and $W_a - W_b$ indicates the buoyancy. A digital balance has been used to carry out all the measurements. Several reports are available on the consideration that the density of a glass is dependent on its composition [11, 27]

The change in molar volume on altering the composition of system is an indication of change of structure in the glass network [27]. To calculate molar volumes V_M of glassy samples following expression can be used [28]:

$$V_M = \sum \frac{x_i M_i}{\rho} \quad (2.2)$$

where, M_i is sample's molecular weight, ρ indicates density and x_i represents molar fraction. Higher value of density of a glass is the indication of closely packed particles in the structure.

2.3.2. XRD

In material science and engineering field, the usage of XRD technique for characterization is very significant. Using this technique the structure of crystals can be analysed. It can be used for determining the crystallite size and microstrain. It also helps in determining the different phases of the compositions present in the system. It is suitable for analyzing not only crystalline materials, but amorphous materials also.

Basically XRD technique works on the principle of occurrence of diffraction when electromagnetic radiation is interacted with atoms having periodic structure and the interatomic distance is equal to the radiation's wavelength. As X-Ray wavelength and the interatomic distance of a crystalline material is nearly same, which is generally in the order of Armstrong, the diffraction of X-Ray is possible in different directions when X-Ray beam falls on the material. Information related to structure of the material can be revealed from the diffraction patterns. By measuring intensities and angles of the diffracted beams, arrangement of atoms in the material's structure can be obtained. As per Bragg's Law,

$$n\lambda = 2D\sin\theta \quad (2.3)$$

where, D represents distance between atomic layers, θ represents angle of incidence, λ denotes X-Ray wavelength (1.54 Å) and n is an integer. Nonappearance of any peak in the XRD pattern points towards amorphous character of the material. Crystallite size can be measured from FWHM i.e., full width at half maxima of diffraction peaks of the diffractogram with the help of Debye Scherrer equation [12] which is:

$$d = \frac{0.89\lambda}{\beta\cos\theta} \quad (2.4)$$

where, d is the crystallite size, θ represents Bragg's diffraction angle and $\beta = [(\beta_{\text{abs}})^2 - (\beta_{\text{std}})^2]^{1/2}$, where β_{abs} and β_{std} represents FWHM of the same peak obtained from XRD scans of the experimental and reference powder respectively [13].

Using X-Ray diffraction method the dislocation density δ can be determined with the help of equation [14]:

$$\delta = \frac{1}{d^2} \quad (2.5)$$

where, d represents crystallite size. Lattice strain (ϵ) which is connected to the crystal imperfection which causes the broadening of diffraction line, can be calculated from the equation [15, 16]:

$$\epsilon = \frac{B}{4 \tan \theta} \quad (2.6)$$

where, B denotes integral breadth of FWHM intensity of the peak, which is related to FWHM peak width (β) by the following equation [29]:

$$B = 0.5 \beta \frac{\pi}{(\log_e 2)^{1/2}} \quad (2.7)$$

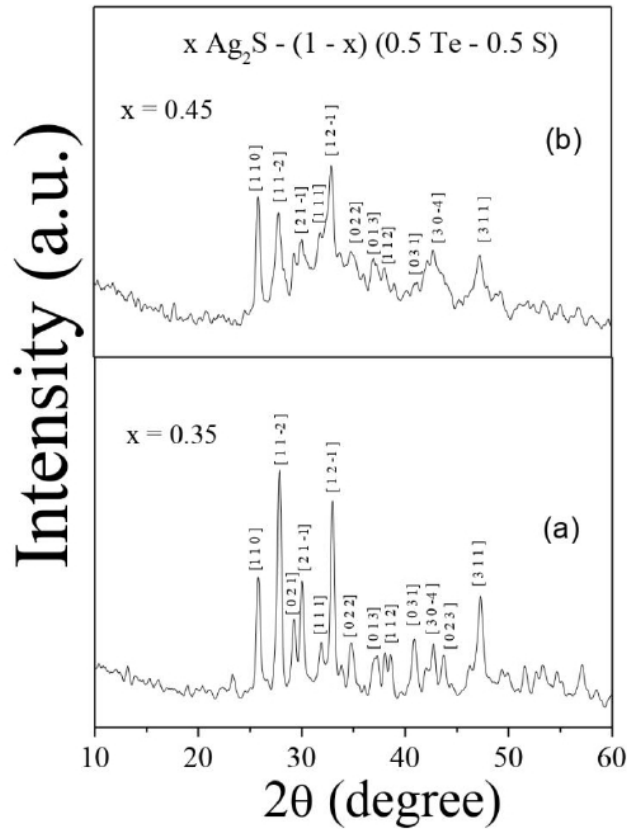


Fig-2.2: XRD Diffractograms of Chalcogenide system $x\text{Ag}_2\text{S} - (1-x) (0.5 \text{ S} - 0.5 \text{ Te})$ where, $x = 0.35$ and 0.45

The XRD diffractogram of Chalcogenide system $x\text{Ag}_2\text{S} - (1-x) (0.5 \text{ S} - 0.5 \text{ Te})$ with $x = 0.35$ and 0.45 is shown in **Fig-2.2**, from which polycrystalline nature of the system can be observed.

2.3.3. FT-IR

FT-IR is an infrared spectroscopy method in which Infrared radiation is made to fall on surface of a system. Some of the radiations are absorbed by the material while the rest is transmitted by it. Infrared Spectrometer is the instrument which is used for detecting the transmitted radiations and converting them into spectrum. This spectrum represents absorption and transmission of radiation by the material and hence it generates molecular finger print of the material. Two different materials can never produce identical IR spectrum. For this reason, FT-IR has become a powerful technique for structural characterization of materials.

The Infrared spectrum represents the infrared light absorbance or transmittance on y axis and frequency or wavelength on x axis. Wave number or cm^{-1} as the unit of frequency and micrometers or μm as the unit of wavelength are generally used in Infrared spectrum.

Infrared spectroscopy works on the fact that molecules absorb electromagnetic radiation if their vibration frequency is matched with the frequency of the radiation. When a beam of infrared light is allowed to fall on a sample, absorption of light by the sample takes place if the vibrational frequency of any bond in the sample is same as the frequency of the infrared light. The information on the absorption of light at each frequency is revealed by observing the transmitted light. FT-IR is an important structural characterization technique used to get much useful information like: unknown material identification, material quality and reliability, amount of component in a mixture etc [17-18].

The range of the infrared spectra in the electromagnetic spectrum is from 12500cm^{-1} – 10cm^{-1} . This spectra is divided into three regions: near -infrared (range: 12500cm^{-1} – 4000cm^{-1}), mid-infrared (range: 4000cm^{-1} – 400cm^{-1}) and far-infrared (range: 400cm^{-1} – 10cm^{-1}). The mid infrared region is abundant in chemical information because of the occurrence of most basic molecular vibrations in this region. In near infrared region the mixtures of fundamental vibrations occur which involve mainly hydrogen atoms and in the far infrared region vibrations which involve heavy atoms occurs.

2.3.4. UV-Vis

UV-Vis or Ultraviolet-visible Spectroscopy is an important technique used for structural analysis of a material. This technique has the ability to detect almost all molecules. In this technique when an UV light is made to strike on matter, the matter absorbs some light and

transmission of electrons in the matter starts taking place from the state of lower energy to that of higher energy while rest of the light get transmitted through it. The absorption occurs when light's energy and the bandgap in the matter are same.

To measure the degree of absorption of light by a material at distinct wavelengths, UV-Vis spectrometer is used. To measure the absorption coefficient $\alpha(\nu)$ at distinct wavelengths the following expression can be used [30]:

$$\alpha(\nu) = \frac{1}{t} \ln \left(\frac{I_i}{I_t} \right) \quad (2.8)$$

where, t represents the sample's thickness, I_i denotes incident light intensity, I_t is the transmitted light intensity and the component $\ln(I_i/I_t)$ represents the absorbance. The absorbance of the light by a compound in the materials, which mainly occurs because of the chemical structure of the compound or molecule, at various wavelengths is shown by an absorbance spectrum. The absorbance spectrum produced by each compound or molecule is distinct which helps in recognizing the compound.

By using the UV-Vis spectra analysis, optical band gap energy E_{opt} of a material can be obtained. For calculating E_{opt} , Tauc equation [31] is used which is expressed as

$$\alpha h\nu = [A(h\nu - E_{opt})]^n \quad (2.9)$$

where, α represents absorption coefficient, A is constant and $h\nu$ is photon energy. Exponent n is a constant. Depending on different transition mechanisms, values of n may be $1/2$ - for allowed direct, 2 - for allowed indirect, $3/2$ - for forbidden direct and 3 - for forbidden indirect [32]. Using Tauc's plot, E_{opt} of an amorphous semiconductor is usually determined, which shows variation of $(\alpha h\nu)^{1/n}$ with the photon energy, $h\nu$ [33].

2.3.5. TEM

TEM is a technique to explore structure of nanomaterials [20, 21]. Many structural information like Topographical – in which features of material's surface like texture etc and their relationship with material properties like hardness, reflectivity etc; Morphological – by which shape and size of the particles in the materials and their relationship with properties like ductility, strength etc; Compositional – amount of different elements and compounds with which the material is comprised of and its relationship with properties of materials like melting point, hardness etc; and Crystallographic – by which arrangement of atoms in the

materials and its relationship with properties like electrical properties conductivity, strength etc can be obtained using this technique.

In this technique an electron beam is allowed to transmit through an ultrathin specimen (thickness is less than 100nm) for forming an image. Instead of being absorbed by the specimen the electrons of the beam interact with the specimen electrons and get scattered. A giant electron gun with very high voltage, typically from 50000 volts to several million volts, is used for the acceleration of electrons at a very high speed.

The basic operating principle of a Transmission Electron Microscope and a light microscope is same; the only difference is the use of electron beam in place of light. Electrons' wavelength is much lower than wavelength of light, due to which the possibility of getting a much better resolution is high in TEM.

Sample preparation for TEM: To support TEM samples a 3 mm grid, generally made up of copper, of different mesh sizes is used. No additional support is needed for the section of materials which is thin to outspread over the grid. But for the other section of materials i.e., for thick materials a thin electron-transparent film, usually made of carbon, is required to be spread over the grid for supporting particles of the materials.

Fig-2.3 shows the TEM images of the Chalcogenide glassy system $x\text{Ag}_2\text{S} - (1-x) (0.5 \text{S} - 0.5 \text{Te})$, where $x = 0.35$ and 0.45 , from which the distribution of nanoparticles embedded in the system can be observed.

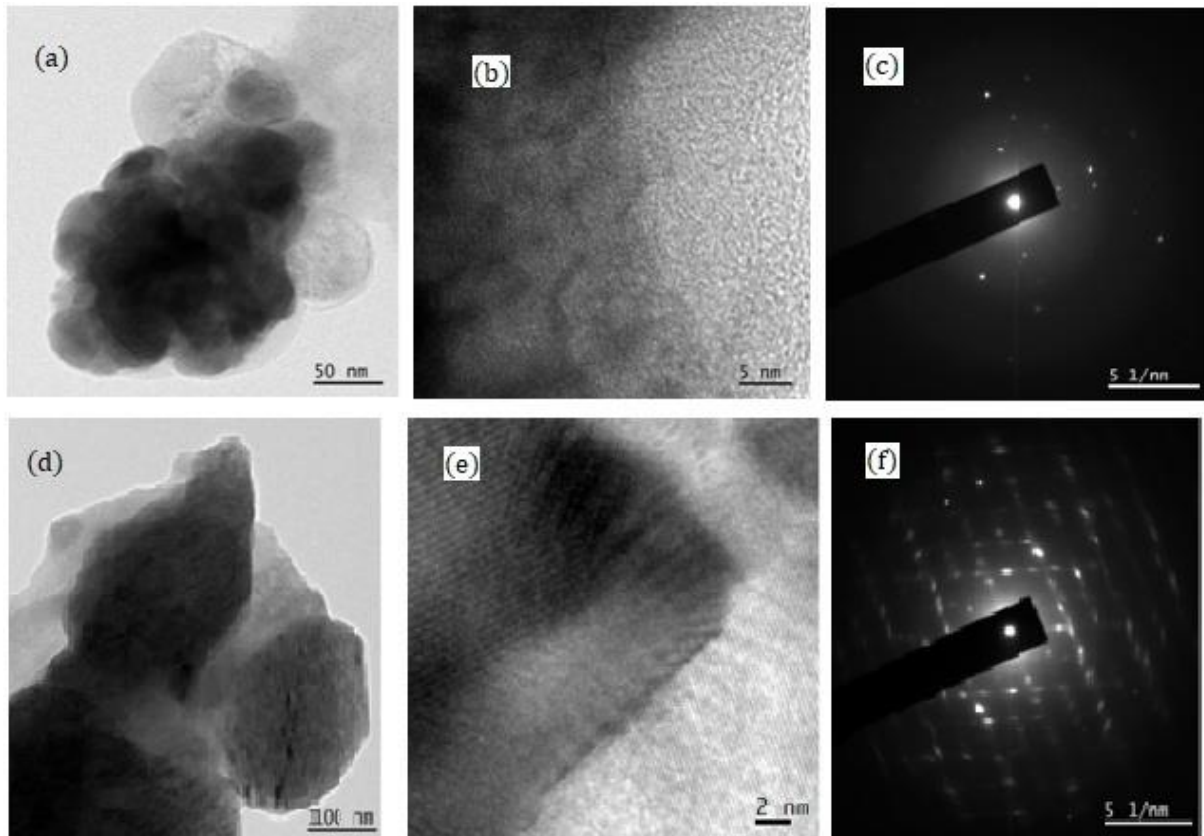


Fig-2.3: TEM images of the Chalcogenide glassy system $x\text{Ag}_2\text{S} - (1-x) (0.5 \text{ S} - 0.5 \text{ Te})$
 (a), (b), (c) - for $x = 0.35$; (d), (e), (f) – for $x = 0.45$

2.4. ANALYTICAL TECHNIQUES

2.4.1. DC Conductivity

Studies of electrical properties of Chalcogenide glassy systems are very helpful to find their possibility to be used in different applications. To carry out DC conductivity measurements, usually two probe or four probe method is used. For a sample to reach thermal equilibrium, enough time should be allowed to perform the measurement at each temperature. The structural defect characteristics such as dangling bonds, interstitials etc produce localized states close to the centre of bandgap of materials of such systems. From the temperature dependent electrical conductivity study, information regarding different parameters like density of localized states $N(E_F)$ in the systems are obtained [34, 35].



Fig-2.4: DC conductivity measurement experimental setup

To measure the DC conductivity of all glassy systems prepared in the present work, two-probe method has been used using ‘Metravi’ Digital Multimeter (model no. 450 DMM). Experimental setup for measuring DC conductivities of all the prepared glassy systems is shown in Fig-2.4.

For analysing the DC conductivity of Chalcogenide glassy systems different models are available like Mott’s and Greaves’s models. At lower temperature region (below the Debye temperature) the measured DC conductivity data at different temperatures can be analysed

using Mott's model [22] according to which conduction is caused by hopping of polarons in the localized states close to the Fermi level.

According to Mott's model [22]

$$\sigma = A \exp \left[-\frac{T_0}{T} \right]^{0.25} \quad (2.10)$$

where, both A and T_0 are constant. T_0 can be expressed by

$$T_0 = \frac{16\alpha^3}{K_B N(E_F)} \quad (2.11)$$

here, $N(E_F)$ represents localized states density near Fermi level, α^{-1} is degree of localization (value of $\alpha^{-1} = 10\text{\AA}$) and K_B denotes Boltzmann constant.

Greaves model [23] can be used for the analysis of system's DC conductivity at higher temperature (above Debye temperature). As per this model the conduction takes place because of thermal assisted tunnelling of polarons in extended states of these systems. This model can be expressed by the equation [23]:

$$\sigma_{DC} T^{1/2} = A' \exp \left[-\frac{T_0'}{T} \right]^{1/4} \quad (2.12)$$

here, A' as well as T_0' is constant. T_0' can be expressed as:

$$T_0' = \frac{19.4\alpha^3}{K_B N(E_F)} \quad (2.13)$$

2.4.2. AC Conductivity

AC conductivity measurement is used to obtain the conductivity data of the amorphous glassy systems with respect to frequency at diverse temperatures. For carrying out AC conductivity measurements of all systems prepared in the present work, Hioki LCR Hi-Tester (3532-50) has been used. In Fig-2.5 the experimental setup of this is shown. To analyze AC conductivity data, Meyer-Neldel (MN) rule, Power Law and Almond-West formalism were used for these systems.



Fig-2.5: AC conductivity measurement experimental setup

2.4.2.1. Meyer-Neldel (MN) Rule

Meyer-Neldel (MN) rule can be applied to many phenomena which are activated thermally in amorphous and crystalline semiconductors. According to this rule, the thermally activated AC conductivity σ_{AC} is related to the activation energy ΔE of the system by obeying following expression [24]:

$$\sigma_{AC} = \sigma_0 \exp\left(-\frac{\Delta E}{K_B T}\right) \quad (2.14)$$

where, σ_0 and T represent pre-exponential factor and absolute temperature respectively. In most semiconductors, σ_0 is independent on ΔE . But, in few cases, like amorphous semiconductors, σ_0 increases with ΔE exponentially by satisfying the relation:

$$\sigma_0 = \sigma_{00} \exp\left(\frac{\Delta E}{\Delta E_{MN}}\right) \quad (2.15)$$

where, σ_{00} denotes MN pre-exponential factor and E_{MN} represents MN characteristics energy. This is called Meyer-Neldel rule. Some researchers have reported the applicability of this rule in many Chalcogenide glassy systems [24, 36-37] in which ΔE is altered by varying the composition of the glassy systems. The change in the composition in a system is responsible for change in defect states' density and their distribution with energy.

2.4.2.2. Power Law and Almond West Formalism

Total conductivity in an amorphous glassy system can be written as [38]:

$$\sigma_{\text{Total}} = \sigma_{\text{DC}} + \sigma_{\text{AC}} \quad (2.16)$$

here, σ_{DC} and σ_{AC} represent DC and AC conductivities respectively. For many materials, which are semiconducting or insulating in nature, the frequency dependent AC conductivity σ_{AC} or $\sigma(\omega)$ is expressed as [25]:

$$\sigma(\omega) = A\omega^S \quad (2.17)$$

here, A is constant and S represents frequency exponent. The values of slopes, which can be calculated from linear fitting of AC conductivity plots at diverse temperatures at higher frequency region, provide S values.

Many theoretical models like QMT, NSPT, CBH, OLPT etc have been used to explain AC conductivity on the basis of S dependency on frequency and temperature for these semiconducting glassy systems. In QMT or quantum mechanical tunnelling model [39] S is dependent on frequency and independent on temperature. NSPT or non-overlapping small polaron tunnelling model [39] can be applied when S increases on rising of temperature. For OLPT or overlapping large polaron tunnelling model [40] to be applied, S must be dependent on temperature as well as frequency and on temperature raising its value decreases from unity. For the systems in which S is found to decrease on rising temperature, CBH or correlated barrier hopping model can be applicable [41].

Almond West formalism [26] can be used for the analysis of AC conductivity spectra, according to which the frequency dependent conductivity is expressed with the equation:

$$\sigma(\omega) = \sigma_{\text{dc}} \left[1 + \left(\frac{\omega}{\omega_{\text{H}}} \right)^n \right] \quad (2.18)$$

where, σ_{DC} represents AC conductivity at low frequencies, ω_{H} represents polarons' hopping frequency, n denotes fractional power law exponent and ω represents frequency of the applied electric field.

2.4.3. Dielectric Properties

2.4.3.1. Permittivity

To check the suitability of these materials in a particular solid state device application the study of dielectric relaxation process plays a vital role. Basically when a dielectric material is kept in an electric field, induced dipole moment or rotation of permanent dipoles in the material causes polarization. In dielectric materials the possible polarizations are: Electronic polarization – which occurs because of the shifting of the negative electrons cloud of atom with respect to nucleus on application of electric field; Ionic polarization – in which displacement of negative and positive ions takes place from their equilibrium positions on the influence of electric field which causes dipole moment; Orientation polarization – which takes place due to orientation of molecular dipoles in the applied electric field's direction; Space charge polarization – which mainly occurs at grain boundary or electrode-material interface, it generally limits the movement of charges which results in alignment of charge dipoles on the application of electric field.

Study of dielectric relaxation helps in understanding origin and nature of dielectric losses and thus is helpful to analysis the structure of a solid. Dielectric permittivity reveals the idea about the maximum energy storage capability of a dielectric material. It also gives the information about the amount of energy loss in the material. The dielectric constant or permittivity, ϵ , of a material can be expressed as:

$$\epsilon = \epsilon' - j \epsilon'' \quad (2.19)$$

where, ϵ' represents real part of ϵ which signifies the maximum amount of energy that can be stored in the dielectric material and ϵ'' represents imaginary part of ϵ which signifies energy loss in the material [42]. ϵ' can be calculated by using the equation:

$$\epsilon' = C_p t / \epsilon_0 A \quad (2.20)$$

where, C_p denotes capacitance of sample in Farad, t represents thickness of sample, A represents area of sample, ϵ_0 is free space permittivity (8.854×10^{-12} F/m). ϵ'' can be obtained by the equation:

$$\epsilon'' = \epsilon' \tan \delta \quad (2.21)$$

where, $\tan\delta$ represents dielectric loss tangent which is proportional to energy loss, dissipated as heat, in the sample. At low frequencies both ϵ' and $j\epsilon''$ are appeared to be dispersed strongly on increasing the temperature which is a feature of charged carrier systems [43].

To analyze the dielectric relaxation process in these glassy systems Hunt's model can be applied. Application of this model in many oxide glassy systems for relaxation analysis has been reported by many researchers [44-46]. According to this model [44-46] the conductivity of these glasses can be defined in two distinct regions depending upon two frequency domains, $\omega < \omega_m$ and $\omega > \omega_m$, where ω_m is the dielectric loss peak frequency. In the frequency domain where $\omega > \omega_m$ the relaxation process is because of the hopping of carriers in pairs between the sites. In the other frequency domain i.e. when $\omega < \omega_m$, the relaxation process cause is the particles transportation over macroscopic distance in clusters [44-46]. Hunt described the frequency dependent conductivity of these glassy systems in the two regions as [44-46]:

$$\sigma_f(\omega) = \sigma_{DC} (1 + A(\omega/\omega_m)^s) \text{ for } s < 1, \omega > \omega_m \quad (2.22)$$

$$\sigma_f(\omega) = \sigma_{DC} (1 + K(d) (\omega/\omega_m)^r) \text{ for } r > 1, \omega < \omega_m \quad (2.23)$$

where, $r = 1 + d - d_f$, d represents dimensionality of space containing pertinent clusters, A and $K(d)$ are constants, ω_m is the peak frequency and d_f represents functional dimensionality of clusters. Hence the dielectric relaxation studies are very useful to get information regarding the conduction mechanism in a glassy system.

2.4.3.2. Electrical Modulus

To invalidate the effects of electrode polarization, study of electrical modulus can be done for investigating the complex electrical response of a material [47]. The complex electrical modulus can be defined as the reciprocal of complex permittivity [47], i.e,

$$M^* = \frac{1}{\epsilon^*} = M' + j M'' = \frac{\epsilon'}{(\epsilon')^2 + (\epsilon'')^2} + j \frac{\epsilon''}{(\epsilon')^2 + (\epsilon'')^2} \quad (2.24)$$

where, M^* is the complex modulus, ϵ^* represents complex dielectric permittivity, M' is real and M'' is imaginary parts of electric modulus.

M^* can also be demonstrated mathematically by means of Fourier Transform of relaxation function $\phi(t)$ as below:

$$M^* = M_\infty \left[1 - \int_0^\infty \exp(-\omega t) \left(\frac{d\phi}{dt} \right) dt \right] \quad (2.25)$$

where, $\phi(t)$ denotes KWW or Kohlrausch-Williams-Watts function [48-50] which represents the electric field's time evolution function inside the material and can be defined as:

$$\phi(t) = \exp \left[- \left(\frac{t}{\tau_m} \right)^\beta \right] \quad (2.26)$$

where, $0 < \beta < 1$, τ_m and β denote conductivity relaxation time and KWW stretched coefficient respectively [48-50].

To interpret the activation energy (E_τ) which is related to relaxation time τ_m , the following relation can be used [48-50]:

$$\tau_m = \tau_0 \exp \left(- \frac{E_\tau}{K_B T} \right) \quad (2.27)$$

where, τ_0 is a pre-exponential factor. The electric modulus formalism on the dielectric data can be used to get an enhanced idea about contribution of conductivity effects. The dielectric modulus, defined by Eqn. (2.24), is used to find information regarding relaxation mechanism when no well defined peak is formed in dielectric loss plots. Relaxation maxima, which can be obtained from the dielectric modulus loss M'' versus frequency plots, are an indication of the contribution of conductivity effects in the system. The use of dielectric modulus formalism also eliminates the electrode screening effect in low frequency spectrum.

2.5. OBSERVATIONS

This chapter is mainly focused on the following points:

- Various preparation methods of Chalcogenide glassy systems with main focus on melt-quenching method
- Different Chalcogenide glassy systems doped with Transition Metal Ions have been prepared during this research work
- Density and molar volume measurement techniques for structural characterization of a glassy system
- X-Ray Diffraction (XRD) for structural characterization from which crystallite size of different phases, dislocation density and strain in a glassy system can be determined

- FT-IR from which presence of different functional groups and molecules in a glassy system can be determined
- UV-Vis Spectroscopy from which optical bandgap energy of glassy system can be determined
- Transmission Electron Microscopy (TEM) which can be for observing distribution of nanoparticles embedded in a system
- Study of the electrical properties of a glassy system
 - DC conductivity data analysis using different models like Mott's model and Greaves' model which can be used to find density of states in the system at lower and higher temperature regions respectively.
 - AC conductivity data analysis with the help of different techniques like: MN rule, Power law, Almond West formalism, etc. Conduction mechanism in a system can be determined with the help of appropriate models like CBH, NSPT, OLPT, etc.
 - Dielectric relaxation studies reveal the idea about the maximum energy storage capability and the amount of energy loss in a dielectric material. The use of electric modulus formalism on the dielectric data helps to get an enhanced idea about contribution of conductivity effects on a glassy system.

2.6. CONCLUSION

In this chapter, different glass preparation techniques like mechanical milling technique, sol-gel process, chemical vapour deposition (CVD) technique, chemical bath deposition (CBD) technique, melt-quenching method along with their advantages and disadvantages have been discussed with main focus on melt-quenching method. The different glass compositions which have been prepared during this research work using melt-quenching method have also been discussed here.

After that, different structural and physical characterization techniques have been explained. From the measurements of density and molar volume of a system, its structure can be determined. High density indicates the closely packed particles in the system. XRD technique is used to determine crystallite size of different phases present in a system, dislocation density and strain. Fourier Transform Infrared (FT-IR) Spectra helps to get much useful information of a system like: unknown material identification, material quality and reliability,

amount of component in a mixture etc. Optical bandgap energy of glassy system can be calculated from UV-Vis spectra analysis. From TEM, area of nanoparticles in the system can be calculated. The interplanar spacing between different crystalline phases in the system can also be determined with this technique.

In the later sections of the chapter a brief discussion on analytical techniques to study the electrical properties of a glassy system have been discussed. DC conductivity data of a glassy system can be analysed using different models such as Mott's and Greaves's models from which density of states in the system can be calculated at lower and higher temperature regions respectively. To analyse AC conductivity data, different techniques like: Power law, Almond West formalism, MN rule etc can be used. Conduction mechanism of a system can be determined with the help of application of appropriate models like CBH, NSPT, OLPT etc. Dielectric relaxation properties of a system can be studied with the help of its permittivity and electric modulus studies.

So, in this chapter various methods for studying structural and electrical properties of a glassy system have been mentioned. This study is very helpful in determining the correlation between structural and electrical properties which helps in understanding the actual conduction mechanism in a glassy system.

REFERENCES

- [1] A. S. Hassanien, Alaa A. Akl, *J. Non-Cryst. Solids*, 428, 112 (2015)
- [2] P. V. Jyothy, K. V. Arun Kumar, S. Karthika, R. Rajesh, N. V. Unnikrishnan, *J. Alloys and Compounds* 493, 223 (2010)
- [3] D. B. Potter, M. J. Powell, J. A. Darr, I. P. Parkin and C. J. Carmalt, *Royal Society of Chemistry*, 7, 10806 (2017)
- [4] S. Suresh, *J. Non-Oxide Glasses* 6,47 (2014)
- [5] J. C. Osuwa and C. I. Oriaku, *J. Non-Oxide Glasses* 2, 1 (2010)
- [6] V. Kumari, A. Kaswan, D. Patidar, K. Sharma and N. S. Saxena, *Bull. Mater. Sci. Indian Academy of Sciences*, 39, 1, 255 (2016)
- [7] B. J. Fernandes, K. Ramesh and N. K. Udayashankar, *Mat. Sci. and Engineering B*, 246, 34 (2019)
- [8] S. K. Pal, A. Kumar and N. Mehta, *Ceramics International*, 45, 16279 (2019)

- [9] A. Ravagli, M. Naftaly, C. Craig, E. Weatherby and D. W. Hewak, *Optical Materials*, 69, 339 (2017)
- [10] E. Zhu, Y. Liu, X. Sun, G. Yin, Q. Jiao, A. Dai and C. Lin, *J. Non-Cryst. Solids: X*, 1, 100015 (2019)
- [11] U B. Chanshetti, V. A. Shelke, S. M. Jadav, S. G. Shankarwar, T. K. Chondhekar, A. G. Shankarwar, V. Sudarsan and M. S. Jogad, *Physics, Chemistry and Technology*, 9, 29 (2011)
- [12] S. Singhal, J. Kaur, T. Namgyal and R. Sharma, *Physica, B* 407, 1223 (2012)
- [13] X. Mathew, J. P. Enriquez, P. Sebastian, M. Pattabi, A. Sanchez-Juarez, J. Campos, J. C. McClure and V. P. Singh, *Sol. Energy Mater. Sol. Cells*, 63, 355 (2000)
- [14] G. Frederick Harrington, A. Cavallaro, D. W. McComb, S. Skinner, J. A. Kilner, *Phys Chem Chem Phys*, 19, 14319 (2017)
- [15] A. Janosi, *Acta Crystallogr*, 17, 311 (1964)
- [16] E. J. Mittemeijer, R. H. J. Fastenau and R. P. Van Ingen, *J. Appl. Phys.*, 76, 1871 (1994)
- [17] Sanjay, N. Kishore, R. S. Kundu and S. Dhankhar, *Mat Sci. and Engg.* 73, 012150 (2015)
- [18] A. K. Singh, N. Mehta and K. Singh, *Physica B: Condensed Matter*, 404, 3470 (2009)
- [19] S. Ahmadpour, M. Rezvani and P. Bavafa, *Spectrochimica Acta Part A: Molecular and Biomolecular Spectroscopy*, 205, 258 (2018)
- [20] N. Prasad, D. Furniss, H. L. Rowe, C. A. Miller, D. H. Gregory and A. B. Seddon, *J. Non-Cryst. Solids*, 356, 2134 (2010)
- [21] P. Bavafa and M. Rezvani, *Results in Physics*, 10, 777 (2018)
- [22] N. F. Mott, *Philos. Mag.* 19, 835 (1969)
- [23] G. N. Greaves, *J. Non-Cryst. Solids*, 11, 427 (1973)
- [24] A. Kumar and A. Kumar, *J. Non-Cryst. Solids*, 386, 51, (2014)
- [25] S. R. Elliott, *Adv. Phys.* 36, 135 (1987)
- [26] D. P. Almond, G. K. Duncan and A. R. West, *Solid State Ion* 8, 159 (1983)
- [27] A. Januszka and R. Nowosielski, *J. Achievements in Materials and Manufacturing Engineering*, 52, 2 (2012)
- [28] H. M. Xiong, X. Zhao and J. S. Chen, *J. Phys. Chem, B*, 105, 10169 (2001)
- [29] J. I. Langford, *J. Appl. Crystallogr*, 11, 10 (1978)

- [30] M. Abdel-Baki, F. A. Abdel-Wahab, Fouad El-Diasty, *J. Appl. Phys.*, 111, 073506 (2012)
- [31] S. Y. Marzouk, N. A. Elalaily, F. M. Ezz-Eldin and W. M. Abd-Allah, *Physica B*, 382, 340 (2006)
- [32] P. Chand, A. Gaur and A. Kumar, *J. Alloys and Compounds*, 539, 174 (2012)
- [33] J. Tauc, *Amorphous and Liquid Semiconductors*, Plenum, New York, 159 (1974)
- [34] N. F. Mott and E. A. Davis, *Electronic Processes in Non-Crystalline Materials*, Clarendon Press, Oxford, (1978)
- [35] E. J. Grant and E. A. Davis, *Solid State Comm.* 15, 563 (1974)
- [36] S. K Dwivedi, M. Dixit and A. Kumar, *J. Mater. Sci. Lett.* 17, 233 (1998)
- [37] D. Kumar and S. Kumar, *Bull. Mater. Sci.* 27, 441 (2004)
- [38] M. M. El-Nahass, H. M. Zeyada, M. M. El-Samanoudy and E. M. El-Menyawy, *J. Phys. Codens. Matter*, 18, 5163 (2006)
- [39] A. Ghosh, *Phys. Rev. B*, 41, 1479 (1990)
- [40] R. Long, *Adv. Phys.* 31, 553 (1982)
- [41] L. Murowski and R. J. Barczynski, *J. Non-Cryst. Solids*, 185, 84 (1995)
- [42] P. H. C. Camargo, K. G. Satyanarayana and F. Wypych, *Mat. Res.* 12, 1 (2009)
- [43] R. A. Bitar and D. E. Arafah, *Sol. Energy Mater. Sol. Cells*, 51, 83 (1998)
- [44] A. Hunt, *J. Non Cryst. Solids*, 144, 21 (1992)
- [45] A. Hunt, *J. Non Cryst. Solids*, 160, 183 (1993)
- [46] L. Murawski and R. J. Barczynski, *J. Non Cryst. Solids*, 196, 275, (1996)
- [47] M. Dult, R. S. Kundu, J. Hooda, S. Murugavel, R. Punia and N. Kishore, *J. Non Cryst. Solids*, 423, 1 (2015)
- [48] A. B. Karmakar, K. Rademann Andrey and L. Stepanov, *Glass Nanocomposites, Synthesis, Properties and Applications*, , Elsevier Inc. (2016)
- [49] S. Ojha, M. Roy, A. Chamuah, K. Bhattacharya and S. Bhattacharya, *Materials Letters* 258, 126792 (2020)
- [50] S. Bhattacharya and A. Ghosh, *J. Am. Cer. Soc.*, 91, 753 (2008)

Chapter 3

STUDY OF ELECTRICAL CHARACTERIZATION AND MICROSTRUCTURE OF Ag₂S DOPED S-Te CHALCOGENIDE SYSTEM

3.1. INTRODUCTION

Chalcogenide glass, a class of amorphous semiconductors, is a very interesting subject of research due to its unique properties and potential applications in solid state devices. It possesses many unique optical, electrical, mechanical and electronics properties. The ability of tailoring these properties by adding impurities in the Chalcogenide glasses makes these glasses different from other available glasses. These glasses exhibit high refractive indices, large optical nonlinearity, phase change capability, wide IR transparency and excellent photo sensitivity [1, 2] which make them suitable in different applications like optical fibres, thermal imaging, remote chemical sensors etc [3-13].

In this chapter, the effect of doping of Ag₂S on the structural and electrical properties of Sulphur - Tellurium based Chalcogenide system having composition $x\text{Ag}_2\text{S} - (1 - x) (0.5 \text{S} - 0.5 \text{Te})$ where, $x = 0.35$ and 0.45 . The addition of Ag₂S to the system changes its structure and hence its electrical properties. Among chalcogen Tellurium shows strong metallic character due to which its glass formation ability is weak. Also, thermal stability of Te based glasses is poor because of the lower glass transition temperature. To overcome these drawbacks, Te is doped with other suitable elements to improve its ability to be usable in various applications. To improve the glass formation ability Te can be doped with S.

In this research work Ag₂S doped S-Te glassy system has been prepared and its structural characterization and study of its electrical properties have been carried out to see its possible usage in various academic and industrial applications. For structural characterization, different techniques like - XRD, TEM, FT-IR spectroscopy, density and molar volume studies have been used.

For the preparation of the present system, the conventional melt quenching method has been used. With the help of XRD technique, crystallite size of different phases present in the system, strain, dislocation density, crystalline volume fraction, etc have been determined. With the help of TEM, analysis of distribution of nanoparticles embedded in the system has

been carried out. FT-IR spectroscopy technique has been used to get information regarding different functional groups and molecules present in the system.

DC and AC conductivity measurements of the system were carried out for studying electrical properties. To carry out DC conductivity measurements, two-probe method has been used using 'Metravi' Digital Multimeter (model no. 450 DMM) and for measurements of AC conductivity in the wide range of frequency 42 Hz – 5 MHz at various temperatures (433K-523K), Hioki made LCR Hi – Tester (Model no. 3532-50) was used. The DC conductivity data was analysed with Mott's VRH Model and Greaves's Model at low and high temperature regions respectively. For analysis of AC conductivity of these glassy systems, different models or methods have been used like: Almond West formalism, MN Rule, AC conductivity scaling, dielectric relaxation studies etc. To know the information regarding the conduction mechanism of these glasses, the AC conductivity data have been tried to fit with various models like CBH, NSPT, OLPT etc.

3.2. PREPARATION OF THE GLASSY SYSTEM

Melt-quenching method was used for preparing Chalcogenide glassy alloys of $x\text{Ag}_2\text{S} - (1-x)$ (0.5 S - 0.5 Te), with $x = 0.35$ and 0.45 . At high temperature Chalcogenide glassy systems are having tendency to react with oxygen. All the required chemicals i.e. Silver Sulphide, Sulphur and Tellurium of high purity (Aldrich 99.9%) were weighted as per the atomic percentages and then mixed in a mortar. In order to reduce the tendency of its reaction with oxygen, the mixture was sealed in quartz ampoules under a vacuum of 10^{-4} Torr. The ampoules were then put into furnace, temperature of which was increased to 200°C at a rate of $3^\circ\text{C}/\text{min}$. The furnace was set at that temperature for 1 hour. After that the ampoules containing the melted mixture of the elements were taken out of the furnace and dropped immediately into ice cold water for rapid cooling of the melt. The obtained glassy materials were then ground to fine powder using a mortar for XRD studies. XRD technique has been used to confirm the glassy and partially crystalline nature of the materials. For AC and DC measurements, pellets of the as prepared samples were formed using pelletizer in which the powdered samples were kept under a pressure of $80\text{Kg}/\text{cm}^2$ for about for about 1 hr 30 min. Coating of Silver paste on both the opposite sides of the formed pellets was done to make sure good electrical contact between electrode and the pellet.

3.3. RESULTS AND ANALYSIS

3.3.1. XRD

3.3.1.1. Crystallite size, dislocation density and lattice strain

In Fig-2.2(a) and (b) of Chapter 2, XRD patterns of Ag_2S doped S-Te system having $x = 0.35$ and 0.45 are shown respectively. The sharp peaks in the pattern show the polycrystalline nature of system. Due to the formation of different nano-crystallites several peaks having the $[h k l]$ values: $[1 1 0]$, $[1 1 1]$, $[1 2 -1]$, $[0 2 2]$, $[0 1 3]$, $[0 3 1]$, $[3 1 1]$ for Ag_2S ; $[1 1 -2]$, $[2 1 -1]$, $[1 1 2]$, $[3 0 -4]$ for Ag_2Te ; and $[0 2 1]$ for AgTe_3 can be seen from the XRD pattern [14-16]. On the increase of the value of x in the composition of the system, its polycrystalline nature is found to increase. The crystalline size, dislocation density and lattice strain of the prepared glassy systems have been calculated using Eqns. (2.4), (2.5) and (2.6) of Chapter 2. In Table-3.1 the crystallite sizes of different phases with their Miller indices formed in the glassy system for $x = 0.35$ and 0.45 is shown. Dislocation density and lattice strain of the system are also shown in Table-3.1.

Table-3.1: Crystallite Size, Dislocation Density and Lattice Strain of system $x\text{Ag}_2\text{S} - (1-x)(0.5\text{S} - 0.5\text{Te})$

x	Phases	Crystallite Size (nm)	h k l	Average Crystallite Size (nm)	Dislocation Density (cm^{-2})	Lattice Strain
0.45	Ag_2S	23.06	1 1 0 1 1 1 1 2 -1 0 2 2 0 1 3 0 3 1 3 1 1	18.08	83×10^{-4}	0.273
	Ag_2Te	13.09	1 1 -2 2 1 -1 1 1 2 3 0 -4			
0.35	Ag_2S	25.98	1 1 0 1 1 1 1 2 -1 0 2 2 0 1 3 0 3 1 0 2 3 3 1 1	36.17	15×10^{-4}	0.505
	Ag_2Te	40.85	1 1 -2 2 1 -1 1 1 2 3 0 -4			
	AgTe_3	41.69	0 2 1			

From Table-3.1 it can be observed that the crystallite size of different nano-crystallites decreases and the dislocation density increases on increasing values of x in composition. Due to the increase of dislocation density, the system's disorder also get increased which increases chances of collision of polarons in this system. This results in decrease in the mobility and hence its electrical conductivity of the system having $x = 0.45$.

3.3.1.2. Crystalline Volume Fraction

To find the crystalline volume fraction of the glassy samples the following equation [17] has been used:

$$X_{XRD} = \frac{I_{hkl}}{I_a + K_{hkl} \times I_{hkl}} \quad (3.1)$$

where, I_{hkl} is the area of a diffraction peak for a phase having a particular hkl value, I_a is the maximum area of peak of the considered XRD diffraction pattern and K_{hkl} is the calibration constant value of which has been obtained by using the equation [17]:

$$K_{hkl} = \frac{I_{hkl}}{I_a} \quad (3.2)$$

Table-3.2: Crystalline volume fraction of system $xAg_2S - (1-x) (0.5 S - 0.5 Te)$ where, $x = 0.35$ and 0.45

x	h k l	Phase	Area (I_{hkl})	K_{hkl}	Crystalline volume fraction
0.35	1 1 0	Ag ₂ S	26.044	0.45498	0.37695
	1 1 -2	Ag ₂ Te	57.242	1	0.5
	0 2 1	AgTe ₃	16.713	0.29197	0.26904
	2 1 -1	Ag ₂ Te	23.788	0.41557	0.35437
	1 1 1	Ag ₂ S	13.787	0.24085	0.22765
	1 2 -1	Ag ₂ S	40.291	0.70387	0.47068
	0 2 2	Ag ₂ S	16.049	0.28037	0.25994
	0 1 3	Ag ₂ S	28.071	0.49039	0.39532
	1 1 2	Ag ₂ Te	15.388	0.26882	0.25071
	0 3 1	Ag ₂ S	15.672	0.27378	0.25469
	3 0 -4	Ag ₂ Te	6.5957	0.11522	0.11372
	0 2 3	Ag ₂ S	8.4635	0.14785	0.14469
0.45	3 1 1	Ag ₂ S	29.333	0.51244	0.40586
	1 1 0	Ag ₂ S	21.528	0.96262	0.49964
	1 1 -2	Ag ₂ Te	22.364	1	0.5
	2 1 -1	Ag ₂ Te	6.4898	0.29019	0.26765
	1 1 1	Ag ₂ S	10	0.44715	0.37264
	1 2 -1	Ag ₂ S	17.461	0.78076	0.48507
	0 2 2	Ag ₂ S	5.8571	0.2619	0.24509
	0 1 3	Ag ₂ S	19.340	0.86478	0.49477
	1 1 2	Ag ₂ Te	6.5351	0.29222	0.26923
	0 3 1	Ag ₂ S	7.9340	0.35477	0.31511
	3 1 1	Ag ₂ S	10.906	0.48766	0.39397

The crystalline volume fractions of the samples having $x = 0.35$ is shown in Table-3.2 and have been obtained as: 0.37, 0.22, 0.47, 0.25, 0.39, 0.25 and 0.40 - corresponding to the phase Ag_2S having [h k l] values [1 1 0], [1 1 1], [1 2 -1], [0 2 2], [0 1 3], [0 3 1] and [3 1 1] respectively; 0.5, 0.35, 0.25 and 0.11 - corresponding to the phase Ag_2Te having [h k l] values [1 1 -2], [2 1 -1], [1 1 2] and [3 0 -4] respectively; and 0.27 for the phase AgTe_3 with [h k l] values [0 2 1]. For the sample with $x = 0.45$ the crystalline volume fraction has been obtained as 0.49, 0.37, 0.48, 0.24, 0.49, 0.32 and 0.39 - corresponding to the phase Ag_2S having [h k l] values [1 1 0], [1 1 1], [1 2 -1], [0 2 2], [0 1 3], [0 3 1] and [3 1 1] respectively; and 0.5, 0.27 and 0.27 - corresponding to the phase Ag_2Te having [h k l] values [1 1 -2], [2 1 -1] and [1 1 2] respectively.

The crystalline volume fraction percentage is found to be increased from 30.95% to 38.43% on increasing the value of x from 0.35 to 0.45 in the glass composition as indicated in Table-3.3.

Table-3.3: Crystalline Volume Fraction percentage of system $x\text{Ag}_2\text{S} - (1-x)(0.5\text{S} - 0.5\text{Te})$ where, $x = 0.35$ and 0.45

Values of x	Crystalline Volume fraction (%)
0.35	30.95
0.45	38.43

3.3.2. TEM

TEM images in which distribution of nanoparticles embedded in the glassy system having composition $x\text{Ag}_2\text{S} - (1-x)(0.5\text{S} - 0.5\text{Te})$ where, $x = 0.35$ and 0.45 are exposed in Fig-3.1(a) and (d) respectively. In Fig-3.1(b) and (e) high resolution TEM images of the same samples have been shown. Using ImageJ software the area of the nanoparticles have been calculated and is shown in Table-3.4 and it is found that the average area of nanoparticles is 1353 nm^2 , area of the smallest nanoparticle is 358.677 nm^2 and that of the largest nanoparticle is 3593.812 nm^2 in the system with $x = 0.35$. In Fig-3.1(c) and (f), SAED patterns for this glassy system having $x = 0.35$ and 0.45 respectively are shown.

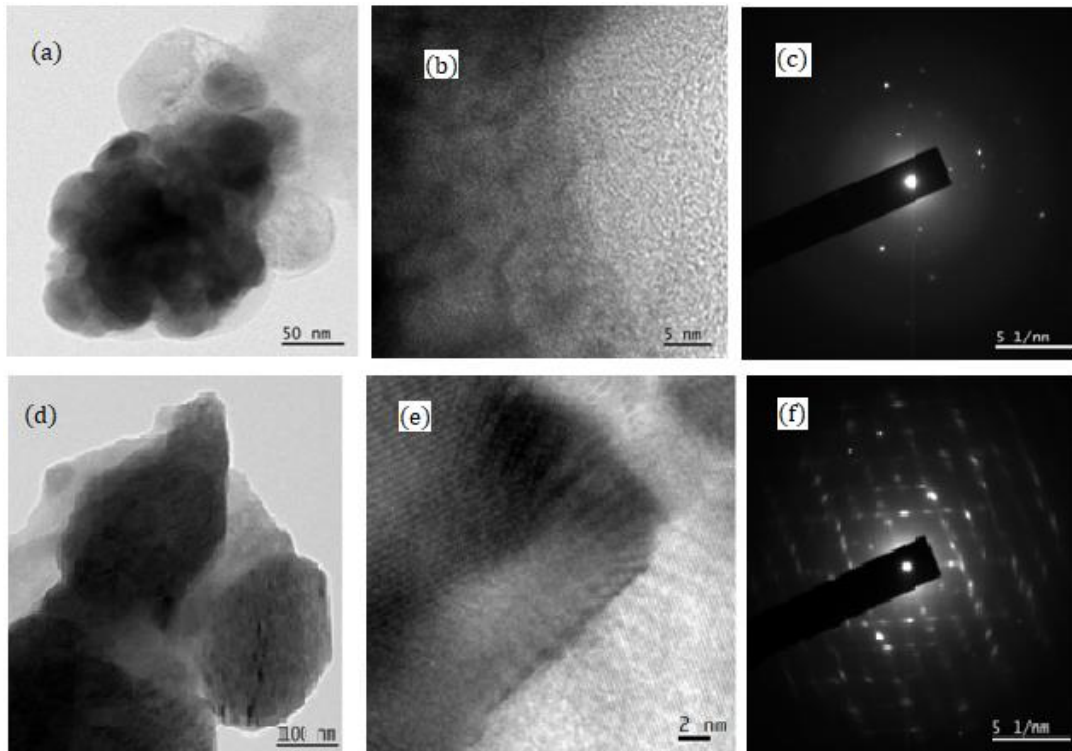


Fig-3.1: TEM images of system $x\text{Ag}_2\text{S} - (1-x) (0.5 \text{ S} - 0.5 \text{ Te})$: (a), (b), (c) – for $x = 0.35$; (d), (e), (f) – for $x = 0.45$

Table-3.4: Area of nanoparticles for the system $x\text{Ag}_2\text{S} - (1-x) (0.5\text{S} - 0.5\text{Te})$ with $x = 0.35$

S. No.	Label	Area (nm^2)
1		1671.538
2		1649.732
3		1649.732
4		366.804
5		2715.367
6		3593.812
7		1137.442
8		844.430
9		1551.139
10		793.073
11		358.677
12		605.121
13		653.540
14	Mean	1353.108
15	SD	949.674
16	Min	358.677
17	Max	3593.812

From this SAED pattern the interplanar spacings (D) between different crystalline phases have been calculated. The D values with corresponding angles (2θ) are presented in Table-3.5

from where we can see that the average interplanar distance of the different nanoparticles in the system is 0.22nm.

Table-3.5: Interplanar distance (from SAED) for the system $x\text{Ag}_2\text{S} - (1-x)(0.5\text{S} - 0.5\text{Te})$ with $x = 0.35$

S. No.	Angle	Length	D = Lattice Plane Distance (nm)
1	-76.161	5.843	0.34228992
2	98.799	6.76	0.295857988
3	65.93	4.467	0.447727782
4	66.265	9.002	0.22217285
5	-75.694	11.73	0.170502984
6	-42.684	7.971	0.250909547
7	-13.764	16.882	0.118469376
8	-90	9.224	0.216825672

3.3.3. FT-IR

FT-IR transmittance spectra of the present glassy system with $x = 0.35$ and 0.45 in the mid infrared region (spectral range $4000\text{cm}^{-1} - 400\text{cm}^{-1}$) is shown in Fig-3.2. Since vibrational bands associated with the basic chemical bonds of the composition of the system are below the wave number 400cm^{-1} , hence they could not be detected.

Chalcogenide glassy systems containing Sulphur are having greater affinity to absorb water related particles. Appearance of bands near wave number 1640cm^{-1} and in the range $3700-3300\text{cm}^{-1}$ are associated with vibrations related to stretching and bending of hydroxyl group in the system [18-20]. Some moisture may be absorbed by the glassy system from atmosphere during its preparation which may be the cause for appearance of absorption bands related to O-H and H_2O groups [21]. The appearance of absorption bands in the spectral range at $500-650\text{cm}^{-1}$ is for the characteristic vibration of Ag-S in the system [22].

The absorption band appeared in the range $1160-1115\text{cm}^{-1}$ are associated with the stretching vibration of sulphoxides S=O [19]. The intermolecular vibration of Te-O bonds are responsible for the absorption bands in the spectral range $780\text{cm}^{-1} - 720\text{cm}^{-1}$ [23].

Thus, in FTIR spectra, the vibrations of chemical bondings of oxygen atoms with the constituent elements of the system are the main cause of the absorption bands. All these bands appeared in the IR spectra are very weak. Hence the FTIR spectra of the system show a good transparency over the mid-infrared region.

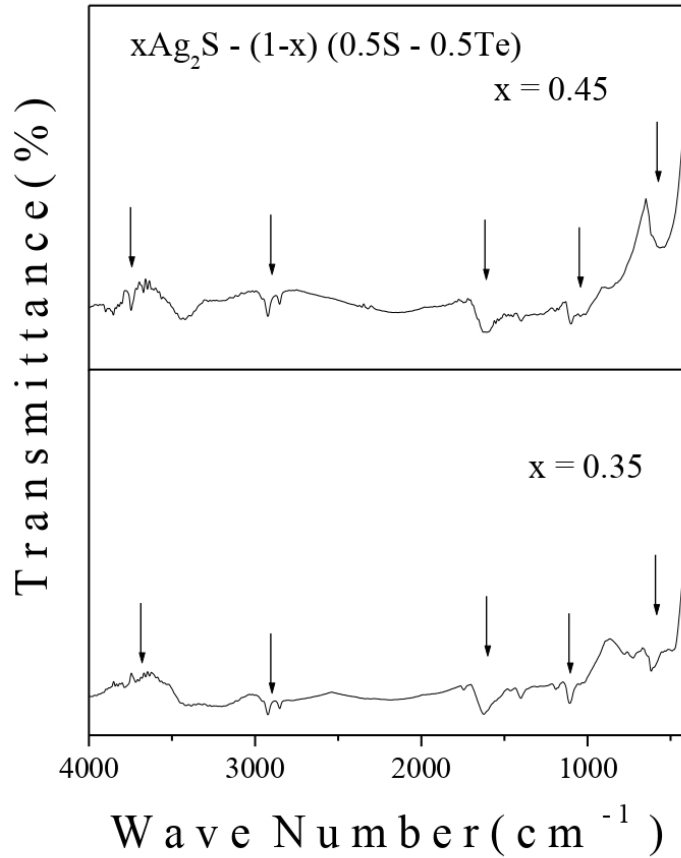


Fig-3.2: FT-IR spectra of system $x\text{Ag}_2\text{S} - (1-x) (0.5\text{S} - 0.5\text{Te})$ where, $x = 0.35$ and 0.45

3.3.4. Density and Molar Volume

To calculate density (ρ) of the system, Archimedes principle was used, which is expressed as [24];

$$\rho = W_a \rho_b / (W_a - W_b) \quad (3.3)$$

where, W_a and W_b represent the weight of the glassy sample in air and in buoyant liquid respectively, ρ_b is the buoyant liquid density and $W_a - W_b$ indicates the buoyancy. In order to find molar volume (V_M) of this system following expression has been used [25]:

$$V_M = \sum \frac{x_i M_i}{\rho} \quad (3.4)$$

where, x_i and M_i represent the molar fraction and the molecular weight respectively of the sample. Table-3.6 shows the calculated ρ and V_M values of the Ag_2S doped S-Te Chalcogenide glassy system.

Table-3.6: ρ and V_M of Chalcogenide system $x\text{Ag}_2\text{S} - (1-x) (0.5 \text{ S} - 0.5 \text{ Te})$ where, $x = 0.35$ and 0.45

x	ρ (gm/cm ³)	V_M (cm ³ /mol)
0.35	4.85	28.56
0.45	3.08	50.38

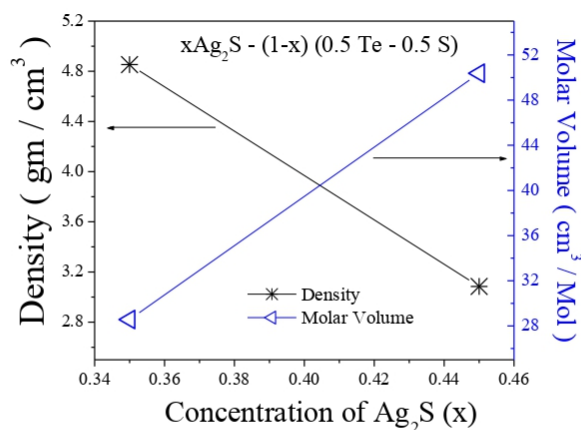


Fig-3.3: Variation of density and molar volume with different values of x for system $x\text{Ag}_2\text{S} - (1-x) (0.5 \text{ S} - 0.5 \text{ Te})$ with $x = 0.35$ and 0.45

In Fig-3.3, the variation of ρ and V_M with different values of x in the system is shown. The decrease of ρ and increase of V_M with the value of x can be observed from Fig-3.3. Higher value of density of a glass is the indication of closely packed particles in the structure.

3.3.5. DC Conductivity

DC electrical conductivity of present system was measured by finding the area, length and resistances at different temperatures of the samples. The change in DC conductivity with temperature of $x\text{Ag}_2\text{S} - (1-x) (0.5 \text{ S} - 0.5 \text{ Te})$ system is shown in Fig-3.4(b). From the figure we found that with the increase of the value of x i.e., the content of Ag_2S in the system, the DC conductivity decreases. From Fig-3.4(b) DC conductivity is found to increase on increasing temperature. This signifies semiconducting nature of the glassy system. From this figure, information regarding defects in structure and density of localized states in system can be obtained. The decrease in resistance with the increase in x is confirmed from Fig-3.4(a), which shows the Cole-Cole plot of the present system with $x = 0.35$ and 0.45 at 170°C .

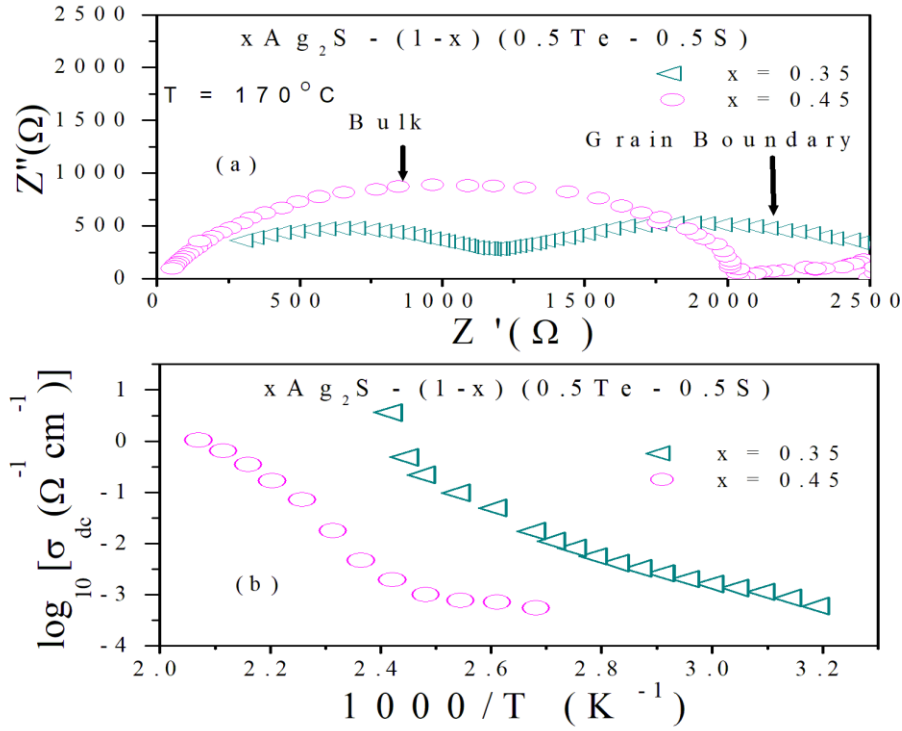


Fig-3.4: (a) Cole-Cole plot at 170°C and (b) DC Conductivity versus 1000/T plot of system $x\text{Ag}_2\text{S} - (1-x)(0.5\text{S} - 0.5\text{Te})$

At lower temperature region, a slight increase of DC conductivity is found when temperature rises. This conductivity is pretentious by impurities and defects in the system's structure. This is an indication of the occurrence of conduction in this region through variable range hopping of polarons in the localized states, which was predicted by Mott's VRH Model [26-28]. The polarons hopping leads to the reaction of neighbouring molecules on the agitation with structural alternations, which causes atomic polarization. [26-28]. At the higher temperature region, the rapid increase of DC conductivity is found with the increase of temperature. It has been analysed with Greaves's Model, according to which the electrical conduction in the system takes place because of the tunnelling of polarons in extended states due to the rise in temperature.

For analysing the thermal activated DC conductivity data at lower (below Debye) temperature, Mott's model [26-28] has been used, according to which DC conductivity σ can be expressed as

$$\sigma = A \exp\left[-\frac{T_0}{T}\right]^{0.25} \quad (3.5)$$

where, both A and T_0 are constants and T_0 can be expressed by

$$T_0 = \frac{16\alpha^3}{K_B N(E_F)} \quad (3.6)$$

here, $N(E_F)$ represents density of localized states near Fermi level, K_B is Boltzmann constant and α^{-1} is degree of localization. The value of $\alpha^{-1} = 10\text{\AA}$.

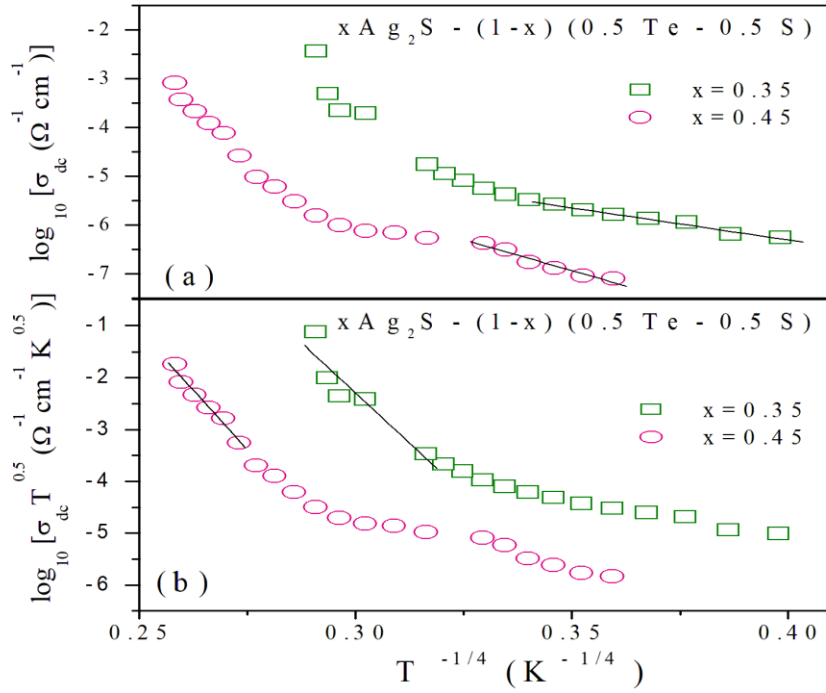


Fig-3.5: Variation of DC Conductivity with temperature of the system $x\text{Ag}_2\text{S} - (1-x)(0.5\text{S} - 0.5\text{Te})$ fitted with (a) Mott's Model (b) Greaves's Model

Fig-3.5(a) shows the variation of DC conductivity with respect to $T^{-0.25}$ (Mott's Model). $N(E_F)$ was calculated from the slopes obtained from linear fitting of the data in Fig-3.5(a) with Eqn. (3.5). Table-3.7 shows the values of $N(E_F)$ for different values of x in the system. The table indicates that the increase of Ag_2S in this system decreases the density of states $N(E_F)$.

At higher temperature regime i.e., above half of Debye temperature, for analyzing DC conductivity data Greaves's Model was used [29]. As per Greaves's Model [29], the DC conductivity of a glass can be expressed by the following equation:

$$\sigma_{DC} T^{1/2} = A' \exp \left[-\frac{T_0'}{T} \right]^{1/4} \quad (3.7)$$

where, both A' and T_0' are constants and T_0' can be expressed by

$$T_0 / = \frac{19.4\alpha^3}{K_B N(E_F)} \quad (3.8)$$

In Fig-3.5(b), $\log(\sigma_{DC}T^{1/2})$ is plotted against $T^{-0.25}$. To calculate $N(E_F)$ at high-temperature region, data of Fig-3.5(b) have been linearly fitted with Eqn. (3.7). $N(E_F)$ values are shown in Table-3.7.

From Table-3.7 it can be observed that $N(E_F)$ increases on increasing Ag_2S content in the system. With more values of $N(E_F)$ in the glassy system with $x = 0.45$, the possibility of collision among polarons may increase, which can decrease the conductivity due to polarons' hopping in the system.

Table-3.7: $N(E_F)$ calculated from Mott's and Greaves models and MN energy of system $xAg_2S - (1-x)(0.5S - 0.5Te)$

Values of x	$N(E_F)$ – Mott's Model ($eV^{-1} cm^{-3}$)	$N(E_F)$ – Greaves's Model ($eV^{-1} cm^{-3}$)	ΔE_{MN} (eV)
0.35	6.94×10^{34}	2.87×10^{31}	10.048
0.45	2.98×10^{35}	3.05×10^{33}	11.865

3.3.6. AC Conductivity

3.3.6.1. Power Law

To express the frequency dependent AC conductivity in glassy semiconductors, Jonscher's power law equation can be used which is given by [30]:

$$\sigma(\omega) = \sigma_0 + A\omega^S \quad (3.9)$$

where, σ_0 denotes conductivity at low frequency region i.e., DC conductivity which is found to be thermally activated, A is pre factor and S represents frequency exponent. The AC conductivity spectra at higher frequencies and different temperatures of this system with $x = 0.35$ and 0.45 are exposed in Fig-3.6(a) and (b) respectively. AC conductivity data is fitted with least square straight line using Eqn. (3.9) which are indicated by the solid lines in the figure. S can be obtained from slopes of the lines. In Fig-3.7(a) and (b) temperature dependency of S for this system having $x = 0.35$ and 0.45 respectively are shown.

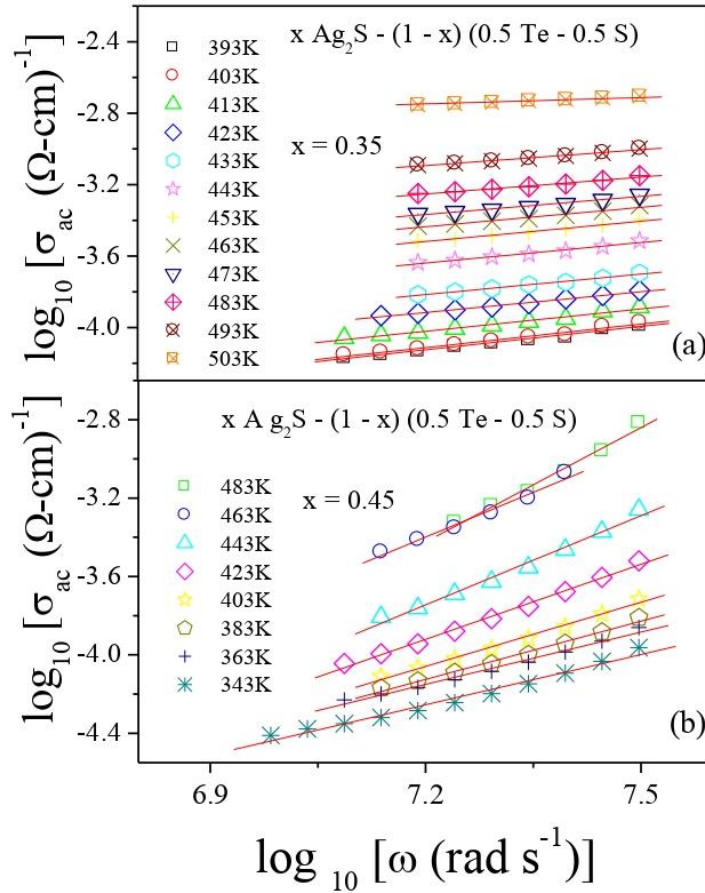


Fig-3.6: High frequency conductivity spectra of system $x\text{Ag}_2\text{S} - (1-x)(0.5\text{S} - 0.5\text{Te})$ with $x =$ (a) 0.35, (b) 0.45. Solid lines indicate best-fitted straight lines, slopes indicate 'S'

For the analysis of conduction mechanisms in glassy systems, different models like Quantum Mechanical Tunnelling (QMT), Correlated Barrier hopping (CBH), Hopping Over a Barrier (HOB), Non-overlapping Small Polaron Tunnelling (NSPT) etc have been proposed by many researchers [31-33].

The experimental data have been attempted to be fitted with the above mentioned models to know the actual conduction mechanism in this system. From the Fig-3.7(a) and (b) it was found that on increasing temperature the values of S increases when $x = 0.45$ and decreases when $x = 0.35$ respectively. From the behavior of S with temperature for the system with $x = 0.35$, it has been revealed that CBH model is the main conduction mechanism, according to which the conduction occurs because of charge carriers' hopping in pairs over potential barrier between two charged defect states.

As per CBH Model [34-36], S can be expressed as

$$S = 1 - \frac{6K_B T}{W_m + K_B T \times \ln(\omega \tau_0)} \quad (3.10)$$

where, W_m denotes maximum barrier height and τ_0 relaxation time. The values W_m and τ_0 have been obtained by non-linear fitting of the data in Fig-3.7(b) with Eqn. (3.10) and the values are shown in Table-3.8.

As per CBH Model [34-36], AC conductivity is expressed as

$$\sigma_{ac} = \frac{n\pi^3 [N(E_F)]^2 \epsilon \epsilon_0 R_{H\omega}^6}{24} \quad (3.11)$$

where, $N(E_F)$ is the concentration of pair states, $R_{H\omega}$ is the hopping distance at frequency ω and n is the number of carriers involved in process of hopping. For the present system with $x = 0.35$ bipolar hopping process may be anticipated the dominant conduction mechanism.

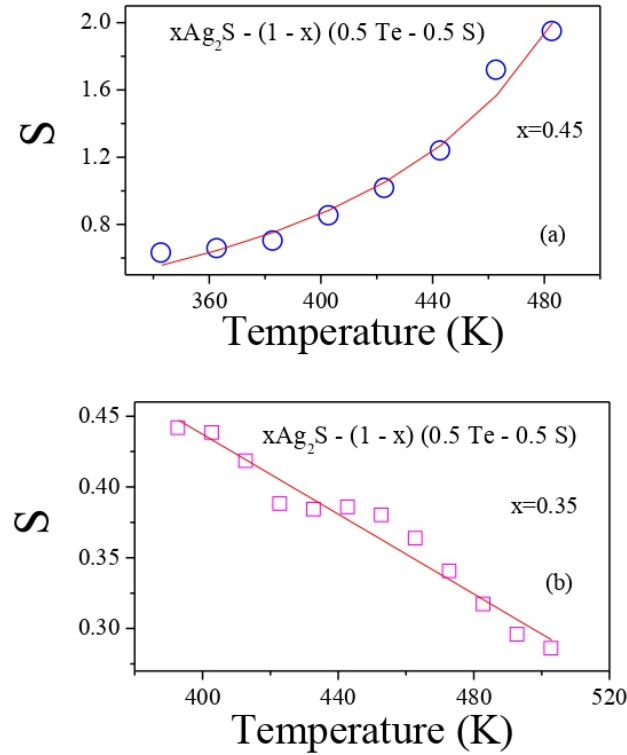


Fig-3.7: S-T plots of $x\text{Ag}_2\text{S} - (1-x)(0.5 \text{S} - 0.5 \text{Te})$ system for $x =$ (a) 0.35 and (b) 0.45. Solid lines indicate the fitting of plots with CBH Model for $x = 0.35$ and with modified NSPT Model for $x = 0.45$

For the AC conductivity mechanism analysis in the present system with $x = 0.45$, the experimental data of Fig-3.7(a) (where S increases with the increase of temperature) have been tried to be fitted with NSPT Model [37]. As per the NSPT Model [37],

$$S = 1 - \frac{4}{\ln\left(\frac{1}{\omega\tau_0}\right) - (W_H/K_B T)} \quad (3.12)$$

where, τ_H is a constant characteristic relaxation time and W_H is the activation energy for polaron transfer. But this attempt was found as unsuccessful due to the poor fitting to the experimental data in Fig-3.7(b). So, in order to get a perfect fitted curve, the NSPT model [37] has been modified a little. The modified NSPT model can be expressed as:

$$S = 1 - \frac{4}{\ln\left(\frac{1}{\omega\tau_H}\right) - (W_H/K_B (T_0 - T))} \quad (3.13)$$

where, T_0 is the temperature at which S becomes unity. In Table-3.8 the values of W_H , τ_H and T_0 are shown which have been obtained from the fitting of Fig-3.7(b) with Eqn. (3.13).

As per NSPT modified model AC conductivity is equal to

$$\sigma_{ac} = \frac{e^2 \pi^4 K_B T [N(E_F)]^2 \omega R_{T\omega}^4}{24\alpha} \quad (3.14)$$

where, e is the charge of an electron, ω represents angular frequency, $N(E_F)$ denotes of defect states, α^{-1} represents wave function localization length for a small polaron and $R_{T\omega}^4$ indicates the tunneling distance at frequency ω . The modified NSPT Model fitting indicates the occurrence of conduction in this glassy system, having $x = 0.45$, due to polarons' tunneling through grain boundary.

Table-3.8: Different parameters obtained from CBH, NSPT (MODIFIED) and ALMOND –WEST formalism for system $x\text{Ag}_2\text{S} - (1-x) (0.5 \text{ S} - 0.5 \text{ Te})$ where $x = 0.35$ and 0.45

x	CBH		NSPT (MODIFIED)			ALMOND –WEST	
	W_m (eV)	τ_0 (s)	W_H (eV)	τ_H (s)	T_0 (K)	E_H (eV)	n
0.35	0.36851	0.00016	---	----	-----	0.0589	1.06
0.45	---	----	0.03918	8.611E-6	417.27	0.1069	1.32

3.3.6.2. Almond West Formalism

The AC conductivity variation with frequency (42 Hz – 5 MHz) at various temperature of the present glassy system with $x = 0.35$ and 0.45 are exposed in Fig-3.8(a) and (b) respectively. AC conductivity has been found to be increased with the increase of temperature and independent on frequency at lower frequency region. The hopping of polarons may be the cause of the frequency independent AC conductivity in the glasses [38, 39]. At higher frequency region, above crossover or hopping frequency, AC conductivity was found to start increasing with frequency which is an indication of correlated motion of polarons [38, 39].

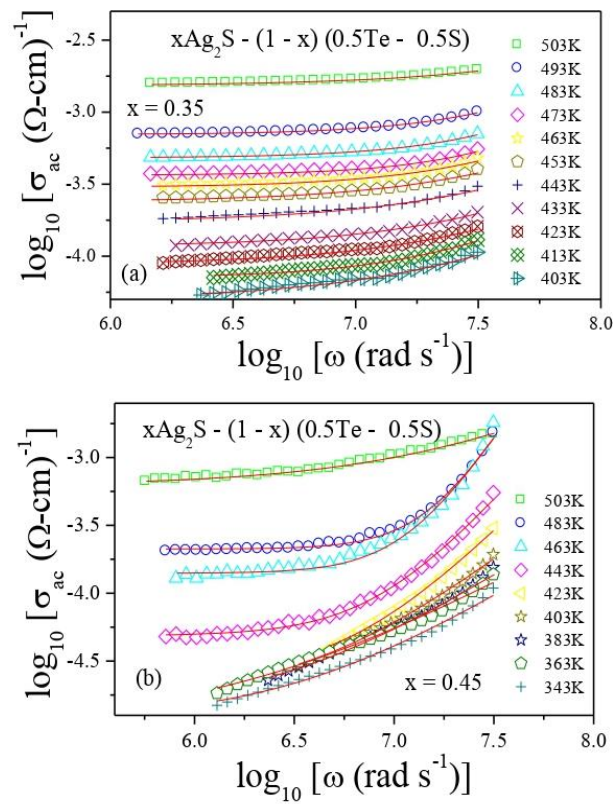


Fig-3.8: AC conductivity spectra, fitted with Almond West formalism, of the system $x\text{Ag}_2\text{S} - (1-x)(0.5\text{S} - 0.5\text{Te})$ with $x =$ (a) 0.35 and (b) 0.45 at different temperatures

To analyse of the AC conductivity of the system, Almond West formalism [38, 39] has been used according to which AC conductivity, which is dependent on frequency, can be represented as:

$$\sigma(\omega) = \sigma_{dc} \left[1 + \left(\frac{\omega}{\omega_H} \right)^n \right] \quad (3.15)$$

where, σ_{DC} represents AC conductivity at lower frequencies, n denotes fractional power law exponent, ω_H is polarons' hopping frequency, and ω represents angular frequency of applied field.

AC conductivity spectra were fitted with Almond West formalism in order to get sufficient information linked to the conduction in the system. In Fig-3.8(a) and (b), the solid lines represent the fitting of AC conductivity data of the system with Eqn. (3.15). The parameters – σ_{DC} , ω_H and n , which were obtained by fitting Fig-3.8 with Eqn. (3.15), are shown in Table-3.9. The AC conductivity spectra of this system with values of $x=0.35$ and 0.45 at $483K$ are shown in Fig-3.9 in which the AC conductivity is found to be increased on increasing the quantity of Ag_2S in the system which validates DC conductivity plots shown in Fig-3.4(b).

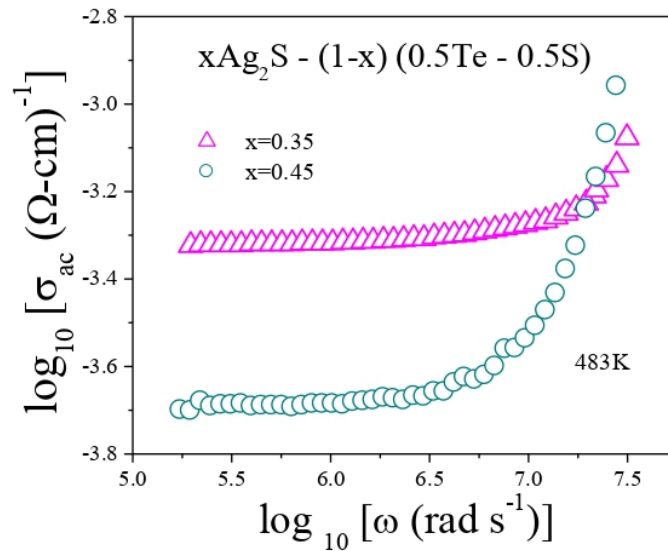


Fig-3.9: Variation of AC conductivity with frequency of system $xAg_2S - (1-x) (0.5 S - 0.5 Te)$ with $x = 0.35$ and 0.45 at $483K$

The variation of temperature dependent hopping frequency ω_H is shown in Fig-3.10 which can be expressed by Arrhenius equation which is:

$$\omega_H = \omega_\alpha \exp\left(\frac{-E_H}{K_B T}\right) \quad (3.16)$$

where, ω_α represents pre-exponential factor and E_H denotes hopping frequency activation energy.

Activation energy for hopping frequency has been calculated by linear fitting of Fig-3.10 with Eqn. (3.16) and is given in Table-3.8, from where we can see that E_H increases on increasing Ag_2S in the present glassy system. From the values of n , frequency exponent, the percolation type motion of polarons can be predicted [39].

Table-3.9: Parameters obtained from Almond West fitting of AC conductivity plots for $xAg_2S - (1-x)(0.5S - 0.5Te)$ system

x	T (K)	σ_{DC}	Error	ω_H	Error	n	Error
0.35	393	0.00005	2.2431E-6	27383441.8498	2829068.19819	0.8563	0.09717
	403	0.00005	1.821E-6	30906943.0411	2020831.04705	0.93639	0.09805
	413	0.00007	1.3793E-6	37409271.10983	1141881.75149	1.15453	0.09453
	423	0.00009	1.6235E-6	41916023.69085	1476448.64088	0.94878	0.07585
	433	0.00012	1.6785E-6	45604508.69626	1448952.41683	1.01981	0.07259
	443	0.00018	2.3923E-6	48499357.17241	2019022.07613	0.91883	0.06859
	453	0.00024	1.3454E-6	54108240.18953	2285498.92365	1.00136	0.04964
	463	0.00031	9.2161E-7	55719850.1889	1811947.73536	1.14115	0.0407
	473	0.00037	6.3561E-7	55220173.98868	1108492.49679	1.35847	0.0321
	483	0.00048	1.027E-6	59648549.96827	1425879.80628	1.2666	0.03409
	493	0.0007	1.0449E-6	64162512.2701	1383199.78537	1.22769	0.02657
503	0.00156	1.6941E-6	134559329.00404	4331617.32775	0.92153	0.01795	
0.45	343	7.4135E-6	8.8467E-7	1360371.11971	398912.77295	0.77465	0.03896
	363	0.00001	1.748E-6	1821278.76417	657177.86855	0.79287	0.04923
	383	0.00001	1.887E-6	3147561.45872	834331.6242	0.95776	0.05403
	403	0.00002	2.0106E-6	4585780.7929	860785.71236	1.14548	0.05629
	423	0.00002	1.8823E-6	6270268.64077	617171.12862	1.47492	0.04696
	443	0.00004	7.6556E-7	7395586.93403	270505.3885	1.55448	0.04417
	463	0.00014	2.5488E-6	11285614.69296	367006.94033	2.15908	0.08329
	483	0.00021	1.7672E-6	15119833.17678	221583.63968	2.34301	0.05704
	503	0.00062	8.5975E-6	17968449.03137	775496.89289	0.69948	0.02689

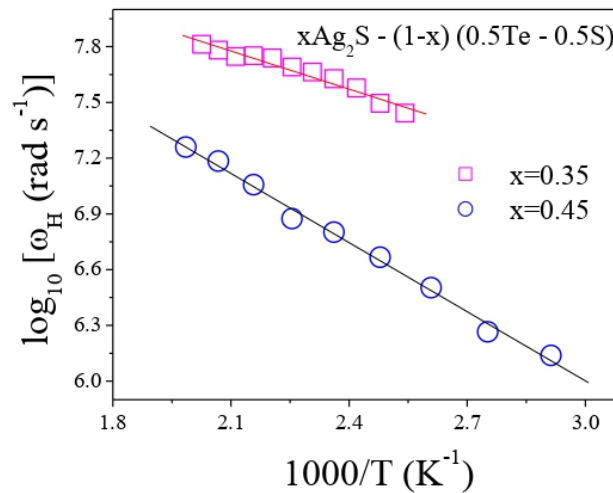


Fig-3.10: Variation of hopping frequency with temperature of system $xAg_2S - (1-x)(0.5S - 0.5Te)$

3.3.6.3. Scaling of AC Conductivity

Scaling of AC conductivity data [36] helps in predicting the dependency of electrical relaxation process of a system on temperature and its composition. In this method, AC conductivity data σ_{AC} is divided by σ_{DC} and frequency axis is divided by ω_H , where both ω_H and σ_{DC} have been obtained from Almont West Formalism fitting. Scaling can be represented by following equation [40]:

$$\frac{\sigma(\omega)}{\sigma_{DC}} = F\left(\frac{\omega}{\omega_H}\right) \quad (3.17)$$

where, F is scaling function. Fig-3.11(a) and (b) show the AC conductivity scaling of the present system with $x = 0.35$ and 0.45 respectively at a variety of temperatures (temperature scaling).

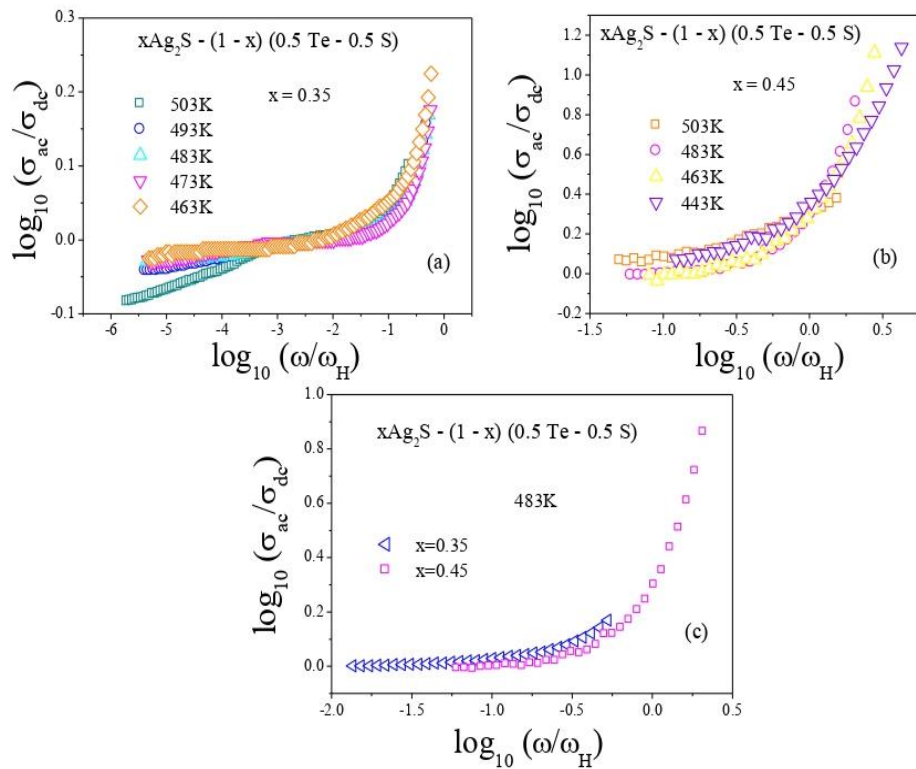


Fig-3.11: AC conductivity scaling of the system $x\text{Ag}_2\text{S} - (1-x) (0.5 \text{ S} - 0.5 \text{ Te})$ with $x =$ (a) 0.35 and (b) 0.45 at different temperatures; (c) Composition scaling at 483K

Fig-3.11(a) and (b) indicates that conductivity spectra of the system at various temperatures merge into a single master curve. This is an indication of the existence of a time temperature superposition [40]. In Fig-3.11(c) the composition scaling i.e., the scaling of AC conductivity data of the system having different values of x (i.e., 0.35 and 0.45) at 483K is shown. In Fig-

3.11(c) the merged conductivity spectra of the given glass into a single master curve is not found. Therefore, the AC conductivity scaling analysis signifies that relaxation mechanism in the system is composition dependent and temperature independent

3.3.6.4. Meyer–Neldel rule

Meyer-Neldel rule can be applied in any situation which involves thermally activated phenomena in crystalline and amorphous semiconductors. In Fig-3.12(a) and (b), change in AC conductivity of present system with temperature at different frequencies are shown for $x = 0.35$ and 0.45 respectively, from which we can notice that with temperature's increase AC conductivity increases.

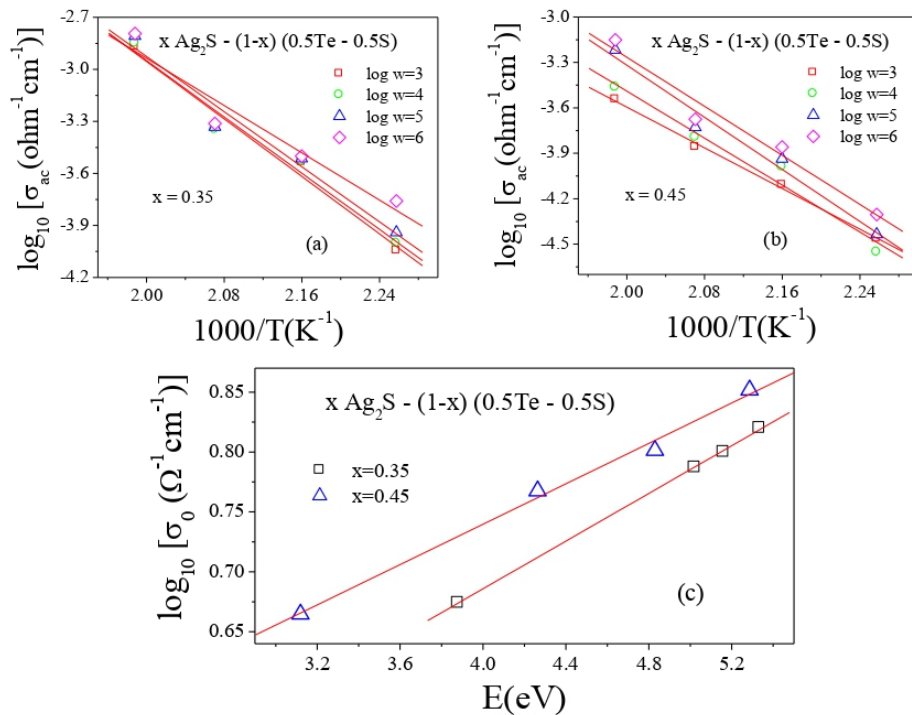


Fig-3.12: (a) $\ln \sigma_{AC}$ versus $1000/T$ plots of the Chalcogenide glassy system $x\text{Ag}_2\text{S} - (1-x) (0.5\text{S} - 0.5\text{Te})$ with $x = 0.35$; (b) $\ln \sigma_{AC}$ versus $1000/T$ plots of the Chalcogenide glassy system $x\text{Ag}_2\text{S} - (1-x) (0.5\text{S} - 0.5\text{Te})$ with $x = 0.45$; (c) $\ln \sigma_0$ versus E (eV) plots of the same system with $x = 0.35$ and 0.45

For semiconducting materials, the relationship of conductivity and temperature is expressed by the following equation [41]:

$$\sigma_{AC} = \sigma_0 \exp\left(-\frac{\Delta E}{K_B T}\right) \quad (3.18)$$

here, ΔE denotes AC conduction activation energy and σ_0 represents pre-exponential factor. The σ_0 and ΔE can be obtained from Fig-3.12(a) and (b). The experimental data of Fig-3.12(a) and (b) have been linearly fitted with Eqn. (3.18). Solid lines in the figures indicate the fitting. From the slopes and intercepts of the solid straight lines, ΔE and σ_0 can be measured respectively. Fig-3.12(a) and (b) indicate the exponential variation of σ_{AC} with temperature, since plots of $\ln \sigma_{AC}$ versus $1000/T$ are found linear.

Fig-3.12(c) is showing variations of σ_0 with ΔE of the present glassy system having $x = 0.35$ and 0.45 , which show linear nature. To explicate σ_0 and ΔE dependence, Meyer-Neldel rule [42-44] has been applied because of the thermally activated nature of the glass system. According to this rule,

$$\sigma_0 = \sigma_{00} \exp\left(\frac{\Delta E}{\Delta E_{MN}}\right) \quad (3.19)$$

where, σ_{00} is a constant and ΔE_{MN} is MN energy. The experimental data of Fig-3.12(c) is fitted with Eqn. (3.19), fitting is indicated by solid lines in the figure. From the slopes of these solid lines, ΔE_{MN} has been calculated, which is shown in Table-3.7. From Table-3.7 the increase of ΔE_{MN} on increasing the value of x from 0.35 to 0.45 in the system has been observed.

3.3.6.5. Mobility and Carrier Density

To find the carrier mobility and density DC polarization technique has been used. In this technique, when a glassy sample having thickness T is placed in between two blocking electrodes and an external fixed DC voltage V is applied to it for an enough long time, then the charge carriers get polarized at the electrode-electrolyte interface. When a state of complete polarization is reached in the sample, the polarity of the DC voltage V is reversed due to which the polarized charge carriers begin to move towards the opposite end within the glassy samples. The mobility of charge carriers can be determined by using the formula:

$$\mu = \frac{T^2}{V\tau} \quad (3.20)$$

where, T is the sample thickness, V is applied voltage and τ denotes time taken by the charge carriers to cross the thickness T of the glassy sample. Carrier density N in the glassy sample can be determined with the help of the following formula:

$$N = \frac{\sigma}{\mu q} \quad (3.21)$$

where, σ , μ and q are conductivity, mobility of charge carriers and charge of an electron respectively.

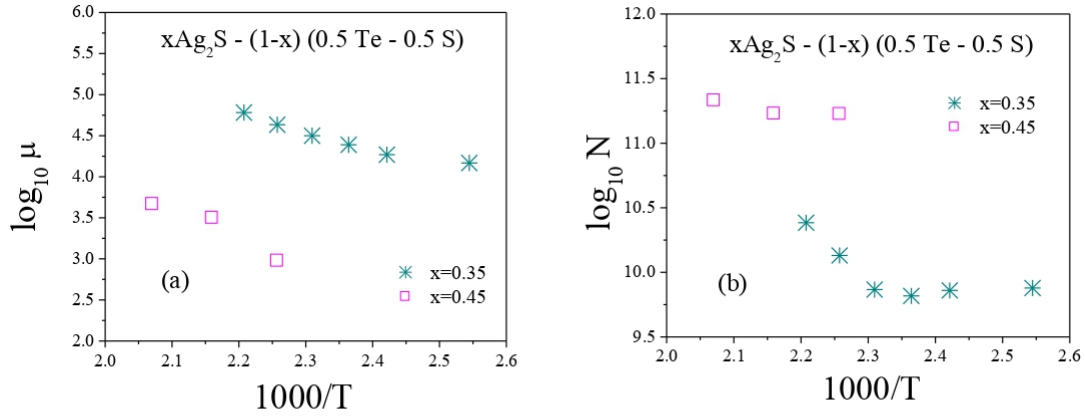


Fig-3.13: (a) $\log_{10} \mu$ versus $1000/T$, (b) $\log_{10} N$ versus $1000/T$ plots for the Chalcogenide glassy system $xAg_2S - (1-x) (0.5 Te - 0.5 S)$ where $x = 0.35$ and 0.45

Fig-3.13(a) shows variation of mobility with temperature for this system with $x = 0.35$ and 0.45 . The mobility is found to decrease on increasing x in composition. Also it is found to be increased with the rise in temperature.

In Fig-3.13(b) $\log_{10} N$ versus $1000/T$ is shown for the same system. From the plot it can be seen that the carrier density N is less in the system which is having lower value of x in the composition i.e. $x = 0.35$ and with the increase of temperature it is found to be increased. In Table-3.10 the average mobility and carrier density data is shown for this system having $x = 0.35$ and 0.45 .

Table-3.10: Average mobility and carrier density of system $xAg_2S - (1-x) (0.5 S - 0.5 Te)$

x	Carrier Mobility, μ ($\Omega^{-1}cm^2C^{-1}$)	Carrier density, N (cm^{-3})
0.35	39902.78	1.29E+10
0.45	2915.86	1.84E+11

3.3.7. Dielectric Properties

3.3.7.1. Permittivity

The studies of dielectric constant ϵ' and dielectric loss ϵ'' of the system $xAg_2S - (1-x) (0.5 S - 0.5 Te)$ having $x = 0.35$ and 0.45 at temperatures $423K - 523K$ and frequency range $42Hz - 5MHz$ have been carried out.

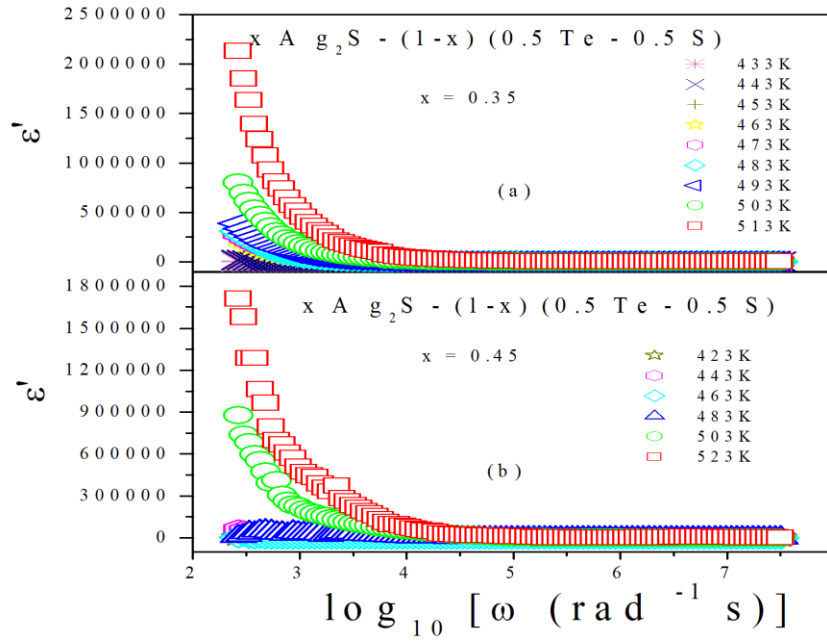


Fig-3.14: Spectra of dielectric constant ϵ' of the system $x\text{Ag}_2\text{S} - (1-x)(0.5\text{Te} - 0.5\text{S})$ at various temperatures for $x =$ (a) 0.35 and (b) 0.45

Fig-3.14(a) and (b) present the plots of ϵ' of the sample with $x = 0.35$ and 0.45 respectively against frequency at diverse temperatures. Fig-3.15(a) and (b) present plots of ϵ'' against frequency of this system with $x = 0.35$ and 0.45 respectively. Exponential decrease of both ϵ' and ϵ'' on increasing the frequency at various temperatures has been observed in Fig-3.14 and Fig-3.15. The accumulation of space charges at glass-electrode interface produces electrode polarization due to which dielectric constant is more at lower frequencies [45]. The effect of polarization decreases with the increase of frequency as the molecular dipoles in the system could not track the rapid variation of electric field. Hence, on increasing frequency in the system both ϵ' and ϵ'' start to decrease and show frequency independent nature.

The increase of both ϵ' and ϵ'' on temperature rise can be observed from Fig-3.14 and Fig-3.15. This occurs mainly due to the increase in polarization effect in the system because of decrease in bond energies as the intermolecular forces get weakened by the rise in temperature, which results in enhancing the orientational vibrations and increasing polarization. Fig-3.14 and Fig-3.15 also show the increase of both ϵ' and ϵ'' with decrease of x in the composition of the present system. This is a clear indication of higher conductivity in the present system having value of $x = 0.35$ as compared to 0.45 .

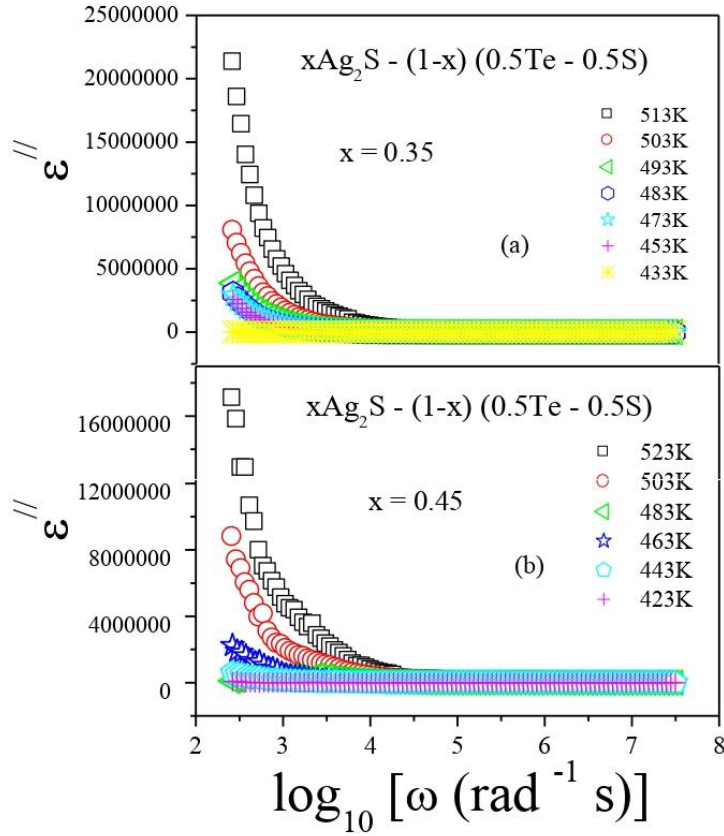


Fig-3.15: Spectra of dielectric loss ϵ'' of the system $x\text{Ag}_2\text{S} - (1-x) (0.5\text{Te} - 0.5\text{S})$ at various temperatures for $x =$ (a) 0.35 and (b) 0.45

The characteristics frequency ω_m of the dielectric loss for a glassy system can be obtained from the peaks of dielectric loss versus frequency plot. But in the present system ω_m couldn't be obtained because of the absence of any peak in the plot, as shown in Fig-3.15.

According to many available reports [46-48], the temperature dependent peak or characteristics frequency ω_m can be expressed by Arrhenius equation:

$$\omega_m = \omega_0 \exp\left(\frac{-W_f}{K_B T}\right) \quad (3.22)$$

where, W_f is the activation energy related with dielectric loss process.

Fig-3.16 shows variations of the angular frequency, ω , with reciprocal of temperature for the system with $x = 0.35$ and 0.45 at a fixed dielectric loss, $\epsilon'' = 50000$. To obtain activation energy related to dielectric loss process, W_f , linear fitting of Fig-3.16 with Eqn. (3.22) have been done.

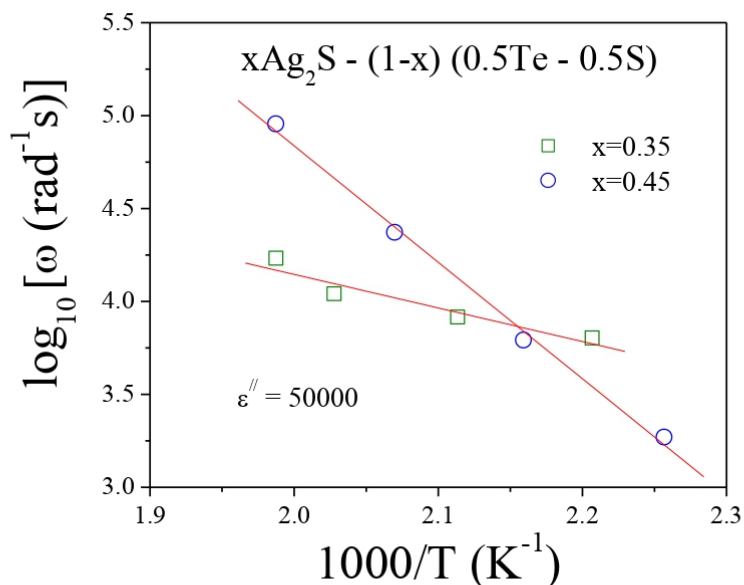


Fig-3.16: Plot of angular frequency, ω , with reciprocal of temperature for system $x\text{Ag}_2\text{S} - (1-x) (0.5\text{S} - 0.5\text{Te})$ with $x = 0.35$ and 0.45 at a fixed dielectric loss, $\epsilon'' = 50000$

From the slopes of the linear fitted lines W_f has been calculated and shown in Table-3.11. The increase of activation energy, related with dielectric loss process, on increasing amount of Ag_2S in the present glassy system is clearly indicated in Table-3.11.

Table-3.11: Activation energies of system $x\text{Ag}_2\text{S} - (1-x) (0.5\text{S} - 0.5\text{Te})$ obtained from Dielectric loss & Electric Modulus plots:

x	Activation Energy from Dielectric loss plots, W_f (eV)	Activation Energy from Electric Modulus, E_m (eV)
0.35	0.36	0.4344
0.45	1.24	0.6149

3.3.7.2. Electric Modulus

The electrical relaxation properties of these glasses have been studied using electrical modulus formalism, details of which are discussed in the section 2.4.3.2 of Chapter 2. The complex electric modulus suppresses the effects of polarization at the electrode - electrolyte interface of a glass [49-50]. In Fig-3.17(a) and (b) plots of real M' and imaginary M'' parts of electric modulus against frequency are shown respectively for the present glassy system with $x = 0.35$. In Fig-3.18(a) and (b) the plots of M' and M'' against frequency are shown respectively of the system with $x = 0.45$.

In Fig-3.17(a) and Fig-3.18(a), M' is found to approach zero at all the mentioned temperatures in low frequency region which mainly occurs because of the suppression of electrode polarization because of unavailability of restoring forces of charge carriers (polarons) [49-50]. But at higher frequencies, dispersion in M' has been found and M' exhibits a maximum value which is: $(M_\infty) = (\epsilon_\infty)^{-1}$ because of the electrical relaxation of polarons [49-50]. In Fig-3.17(a) and Fig-3.18(a), a gradual decrease of M' with rise of temperature is found which may imply the involvement of polarons' mobility in small range in the conduction mechanism of the system.

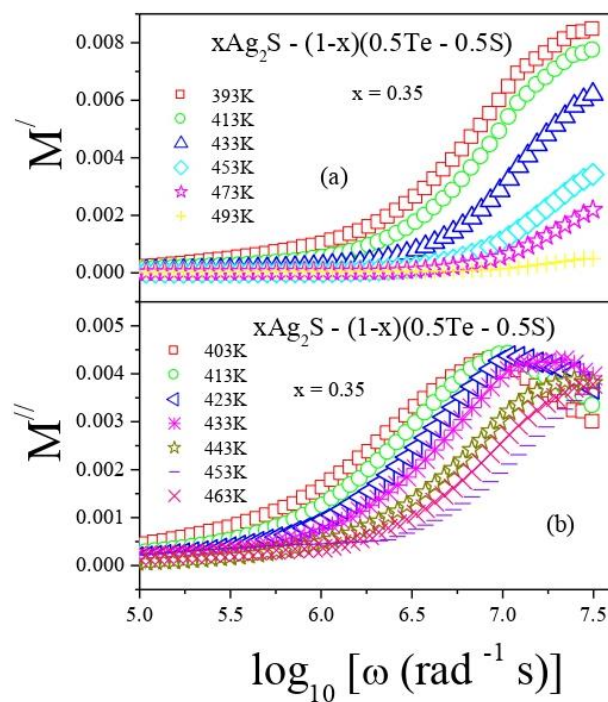


Fig-3.17: Spectra of (a) M' and (b) M'' of $x\text{Ag}_2\text{S} - (1-x)(0.5\text{S} - 0.5\text{Te})$ system for $x = 0.35$

The shifting of M'' peaks towards higher frequencies on increasing temperature, as shown in Fig-3.17(b) and Fig-3.18(b), is a sign of temperature dependent relaxation process in system. The movement of thermally activated charge carriers may reduce relaxation time and increase relaxation frequency. Polarons' hopping over long distances may be the cause for the conduction in these glasses below the peak relaxation frequency ω_{max} . Above ω_{max} reason of conduction mechanism may be the localized motion of charge carriers over short distances [32, 50]. The M'' peak shifting indicates the stabilization of the system in a short time for an external force at eminent temperature.

Fig-3.19 represents the variation of peak frequencies ω_m , frequencies at which M'' peaks occurred, with temperature for the system with $x = 0.35$ and 0.45 . Because of the temperature dependent behaviour observed from Fig-3.19, Arrhenius equation has been applied to find the activation energy E_m for relaxation process associated with electric modulus of the system which can be expressed by:

$$\omega_m = \omega_0 \exp\left(\frac{-E_m}{K_B T}\right) \quad (3.23)$$

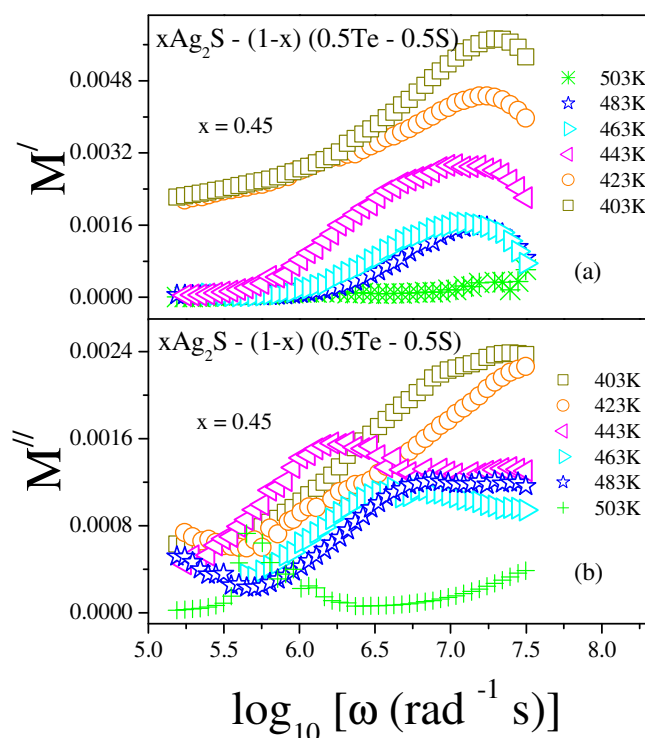


Fig-3.18: Plots of (a) M' and (b) M'' against frequency of $x\text{Ag}_2\text{S} - (1-x)(0.5\text{S} - 0.5\text{Te})$ system for $x = 0.45$

where, ω_0 is pre exponential factor, E_m denotes activation energy from complex modulus plot. Activation energy E_m of the present system with $x = 0.35$ and 0.45 was measured from slopes of the lines obtained from linearly fitting of Fig-3.19 with Eqn. (3.23) and is shown in Table-3.11. The temperature dependency of ω_m , reciprocal of which indicates the relaxation time τ_m (i.e. $\tau_m = 1/\omega_m$), is shown in Fig-3.19. The increase of ω_m and hence the decrease of τ_m with the increase of temperature can be observed from Fig-3.19. The figure also indicates the increase of ω_m and hence the decrease of τ_m with the decrease of x value i.e. content of

Ag₂S in the system. Lower values of relaxation time directly indicate the higher conductivity due polaron hopping in the system.

The increase of activation energy, associated with complex modulus plots, on increasing Ag₂S in the system can be observed from the Table-3.11. This is a clear indication of the decrease of conductivity on increasing Ag₂S in the system. The activation energies calculated from permittivity (dielectric loss) and electric modulus (complex) were found in close agreement.

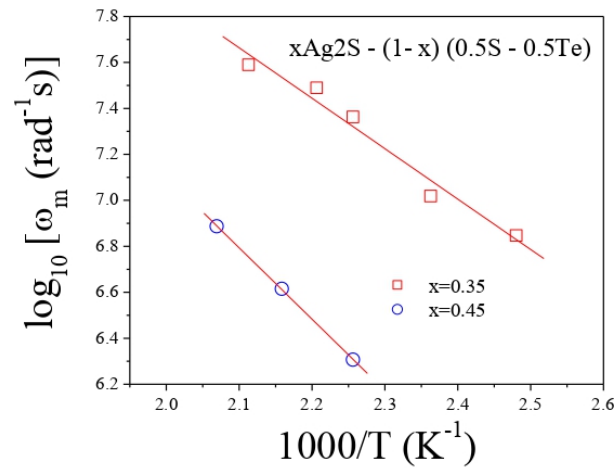


Fig-3.19: Plot of $\log_{10} \omega_m$ versus $1000/T$ of system $x\text{Ag}_2\text{S} - (1-x) (0.5\text{S} - 0.5\text{Te})$ where, $x = 0.35$ and 0.45

3.3.7.3. Electric Modulus Scaling

The scaling of dielectric modulus data M'' of the glass have been carried out for analyzing the relaxation process in the present system. To do the scaling, the x-axis of Fig-3.17(b) and Fig-3.18(b) i.e., M'' values have been divided by M''_{\max} (maximum value of imaginary modulus) and y-axis i.e., ω values, by ω_{\max} (the frequency at which M'' peak occurs). Fig-3.20(a) and (b) represent the temperature scaling of electric modulus M'' plots of the present system having $x = 0.35$ and 0.45 respectively at diverse temperatures (range is 443K – 503K). In Fig-3.20(a) and (b) overlapping of all the scaled data has been found which is an indication of temperature independent relaxation process in the glassy system.

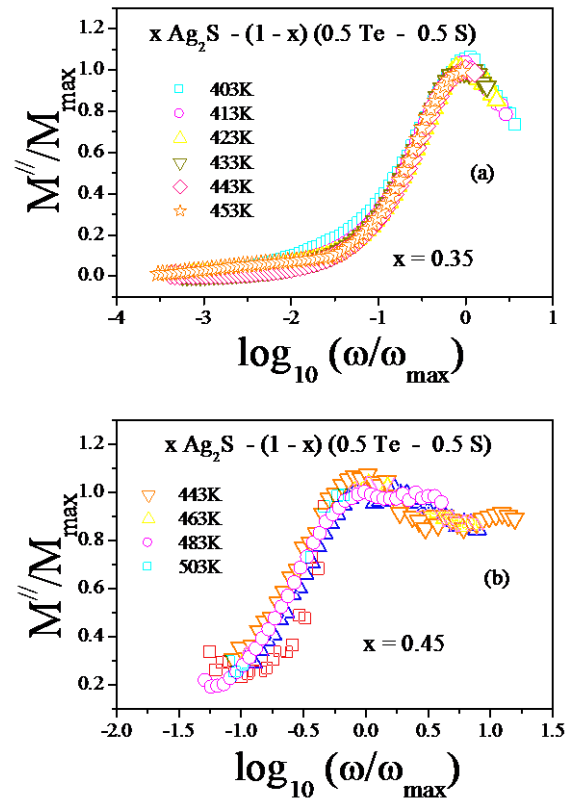


Fig-3.20: Temperature scaling of M'' at various temperatures of glassy system $x\text{Ag}_2\text{S} - (1-x)(0.5\text{Te} - 0.5\text{S})$ with $x =$ (a) 0.35 and (b) 0.45

In Fig-3.21 the composition scaling in which electric modulus M'' plots of the present system having $x = 0.35$ and 0.45 at a fixed temperature (463K) is shown. The non-overlapping of the plots in Fig-3.21 is a clear indication of composition dependent relaxation process in the system. So, the system's composition dependent and temperature independent nature of relaxation process can be observed from the electric modulus scaling process of the present glassy system.

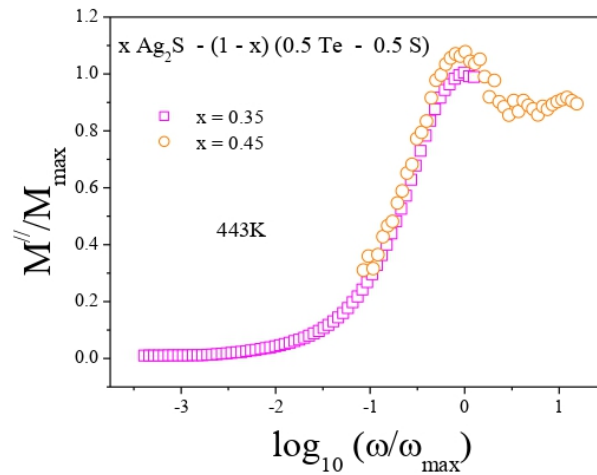


Fig-3.21: Composition scaling of M'' of $x\text{Ag}_2\text{S} - (1-x)(0.5\text{Te} - 0.5\text{S})$ system at 443K

3.4. CONCLUSION

In this chapter, the preparation of Ag_2S doped S-Te based Chalcogenide glassy system having composition $x\text{Ag}_2\text{S} - (1-x)(0.5\text{S} - 0.5\text{Te})$, where $x = 0.35$ and 0.45 , using Melt-quenching method has been discussed. The use of different techniques like XRD, TEM, FT-IR spectroscopy, density and molar volume studies for physical characterization of the system has been reported. From the XRD analysis, the size of the different phases present in the system with their $[h,k,l]$ values and dislocation density have been calculated. The average crystallite size in the system is found to decrease and dislocation density is found to increase with the increase of value of x i.e., content of Ag_2S in the system. The increase of dislocation density increases disorder in the system due to which possibility of collision of charge carriers in the system increases. This may results in decrease in the mobility and hence electrical conductivity in the system.

From the TEM analysis the distribution of nanoparticles embedded in the present glassy system has been observed. Using this technique the area of nanoparticles in the system has been calculated. The average area of nanoparticles in the system with $x = 0.35$ is 1353 nm^2 . From SAED pattern, obtained using TEM, interplanar spacings (D) between different crystalline phases in the system have been calculated.

From the analysis of FT-IR spectroscopy spectra of the present glassy system, a good transparency in the spectral range $4000\text{cm}^{-1} - 400\text{cm}^{-1}$ can be observed and most of the

absorption bands can be assigned to vibrational bands of oxides and hydrides bonds which arises due to the presence of extrinsic impurities in the system introduced during its preparation. FT-IR spectra indicate the presences of different functional groups and molecules like O-H, C-H and H₂O in the glassy system.

For structural characterization, molar volume and density measurements of the system have also been carried out. The density decreases and molar volume increases on increasing x in composition of the glassy system. Therefore, the system having less values of x (i.e., Ag₂S content) is having closely packed particles in the structure.

Study of electrical properties of the present system in frequency range: 42Hz - 5MHz and at diverse temperatures (433K-523K) is also reported here. To analysis the DC conductivity data, Mott's model and Greaves's model have been used at higher and lower temperature regions respectively. With the help of these models, density of localized states in the system has been calculated which is found to increase with the value of x in the composition. With more density of localized states in the system having x = 0.45, the possibility of collision among polarons may increase which can decrease the conductivity due to polarons' hopping in the system. Here, DC conductivity is found to increase on increasing temperature and decreasing Ag₂S content.

For analysing AC conductivity data of the system, Power Law, Almond West formalism and MN Rule were used. CBH model was found to be the appropriate conduction mechanism in the system with x = 0.35 in which the conduction occurs due to charge carriers' hopping in pairs over the potential barrier between two charged defect states. Whereas, NSPT (modified) model is found to be suitable for analyzing AC conductivity data of the system having x = 0.45. From AC conductivity scaling, nature of the relaxation process in the system was found to be temperature independent and composition dependent.

The AC conductivity was found to increase on increasing temperature but independent on frequency at lower frequencies. At higher frequencies, above crossover or hopping frequency, it increases with frequency. With the help of Almond West formalism, activation energy E_H for hopping frequency has been calculated, which is found to increase on increasing amount of Ag₂S in the system.

Study of dielectric relaxation of the system at various temperatures (range: 423K – 523K) and in frequency range 42Hz – 5MHz has been carried out from which the decrease of ϵ' and ϵ''

with increase of frequency and decrease of temperature have been observed. Activation energy related to the relaxation process in the system was calculated from the analysis of the permittivity and electric modulus plots which is found to increase on increasing Ag₂S in present system. The merging of imaginary electric modulus spectra on a single master curve in electric modulus scaling process at different temperatures, i.e., temperature scaling, point towards the independent nature of dielectric relaxation process on temperature. But the merging of imaginary electric modulus spectra on a single master curve is not found in composition scaling. Therefore, the dielectric relaxation of this system is temperature independent and composition dependent.

REFERENCES

- [1] V. Kokorina, CRC Press, Boca Raton, Fla (1996)
- [2] E. M. Vogel, M. J. Weber, and DMon Krol. *Physics and Chemistry of glasses* 32, 6, 231 (1991)
- [3] A. B. Seddon, *J. Non-Cryst. Solids* 184, 44 (1995)
- [4] A. Zakery and S. R. Elliott, *J. Non-Cryst. Solids* 330, 1 (2003)
- [5] B. J. Eggleton, B. Luther-Davies, and K. Richardson, *Nat. Photonics*, 5, 141 (2011)
- [6] H. G. Dantanarayana, N. Abdel-Moneim, Z. Tang, L. Sojka, S. Sujecki, D. Furniss, A. B. Seddon, I. Kubat, O. Bang, and T. M. Benson, *Opt. Mater. Express* 4, 1444 (2014)
- [7] J. D. Musgraves, K. Richardson, and H. Jain, *Opt. Mater. Express* 1, 921 (2011)
- [8] L. Li, H. Lin, S. Qiao, Y. Zou, S. Danto, K. Richardson, J. D. Musgraves, N. Lu, and J. Hu, *Nat. Photonics* 8, 643 (2014)
- [9] Z. Tang, V. S. Shiryaev, D. Furniss, L. Sojka, S. Sujecki, T. M. Benson, A. B. Seddon, and M. F. Churbanov, *Opt. Mater. Express* 5, 1722 (2015)
- [10] A. F. Kosolapov, A. D. Pryamikov, A. S. Biriukov, V. S. Shiryaev, M. S. Astapovich, G. E. Snopatin, V. G. Plotnichenko, M. F. Churbanov, and E. M. Dianov, *Opt. Express* 19, 25723 (2011)
- [11] C. Plesa, D. Turcanu, C. Todirica, and I. Nicola, *Chalcogenide Lett.* 12, 633 (2015)
- [12] D. H. Cha, H.-J. Kim, Y. Hwang, J. C. Jeong, and J.-H. Kim, *Appl. Opt.* 51, 5649 (2012)

- [13] Sato, K. Igarashi, M. Taniwaki, K. Tanimoto, and Y. Kikuchi, *J. Appl. Phys. Lett.* 62, 669 (1993)
- [14] R.B. Shafizade, F.I. Aliev, I.V. Ivanova, M.M. Kazinets, I.R. Nuriev and R.M. Sultanov, *Inorg. Mater.* 9, 975 (1973)
- [15] A. Van Der Lee and J.L. De Boer, *Acta Crystallogr. C* 49, 1444 (1993)
- [16] A. J. J. Frueh, *Am. Mineral.* 46, 654 (1961)
- [17] M. Luysberg, *J. Philos. Mag. A*, 75, 31 (1997)
- [18] T.S. Kavetskiy, A. P. Kovalskiy, V. D. Pamukchieva and O. I. Shpotyuk, *Infrared Phys. Tech.*, 41, 41 (2000)
- [19] G. Socrates, “Infrared and Raman Characteristic Group Frequencies”, 3rd Edition, John Wiley & Sons Ltd, 2004
- [20] M. Efimov and V. G. Pogareva, *J. Non-Cryst. Solids*, 275, 189 (2000)
- [21] V. Pamukchieva, K. Todorova, O. C. Mocioin, M. Zaharescu, A. Szekeres and M. Gartner, *J. Physics*, 356, 012047 (2012)
- [22] Y. Y. Kim and D. Walsh, *Nanoscale* 2, 240 (2010)
- [23] B. Frumarova, J. Oswald, P. Krecmer, M. Frumar, V. Cerny and V. Smrcka, *Opt. Mater.*, 6, 217 (1996)
- [24] A. Januszka, R. Nowosielski, *J. Achievements in Mat. and Manufacturing Engg.*, 52, 2 (2012)
- [25] H. M. Xiong, X. Zhao, J. S. Chen, *J. Phys. Chem. B*, 105, 10169 (2001)
- [26] N.F. Mott, E.A. Davis, *Electronic Processes in Non-Crystalline Materials* (Clarendon Press, Oxford) (1979)
- [27] M. Abdel-Baki, F.A. Abdel-Wahab, Fouad El-Diasty, *J. Appl. Phys.*, 111, 073506 (2012)
- [28] N.F. Mott, *Philos. Mag.* 19, 835 (1969)
- [29] G.N. Greaves, *J. Non-Cryst. Solids*, 11, 427 (1973)
- [30] A. K. Jonscher, *Nature* 267, 673 (1977)
- [31] A. B. Karmakar, K. Rademann Andrey, L. Stepanov, *Glass Nanocomposites, Synthesis, Properties and Applications*, Elsevier Inc., (2016)
- [32] S. Ojha, M. Roy, A. Chamuah, K. Bhattacharya and S. Bhattacharya, *Materials Letters*, 258, 126792 (2020)
- [33] J. Z. Weiss, *Anorg. Allg. Chem.*, 435, 113 (1977)
- [34] N. F. Mott, *J. Non-Cryst. Solids*, 1,1 (1968)

- [35] R. Murugaraj, *J Mater Sci* 42, 10065 (2007)
- [36] A. Ghosh, *Phys. Rev. B*, 42, 5665 (1990)
- [37] S. Karmakar and D. Behera, *J. Physics: Condensed Matter*, 31, 245701 (2019)
- [38] D. P. Almond, G. K. Duncan and A. R. West, *Solid State Ionics*, 8, 159 (1983)
- [39] B. Roling, A. Happe, F. Funke and M. D. Ingram, *Phy. Rev. Lett.*, 78, 2160 (1997)
- [40] A. Ghosh and A. Pan, *Phy. Rev. Lett.*, 84, 2188 (2000)
- [41] K. Shimakawa and F. Abdel-Wahab, *Appl. Phys. Lett.*, 70, 5 (1997)
- [42] R. Arora and A. Kumar, *Phys. Status Solidi A*, 125, 273 (1991)
- [43] S. K. Dwivedi, M. Dixit and A. Kumar, *J. Mater. Sci. Lett.* 17, 233 (1998)
- [44] D. Kumar and S. Kumar, *Bull. Mater. Sci.* 27, 441 (2004)
- [45] R. A. Bitar and D. E. Arafah, *Sol. Energy Mater. Sol. Cells*, 51, 83 (1998)
- [46] A. Hunt, *J. Non Cryst. Solids*, 160, 183, (1993)
- [47] L. Murawski and R. J. Barczynski, *J. Non Cryst. Solids*, 196, 275, (1996)
- [48] J. Ross Macdonald, "Impedance Spectroscopy", John Wiley & Sons, New York (1987)
- [49] A. B. Karmakar, K. Rademann Andrey and L. Stepanov, "Glass Nanocomposites, Synthesis, Properties and Applications", Elsevier Inc., (2016)
- [50] S. Bhattacharya and A. Ghosh, *J. Am. Cer Soc.*, 91, 753 (2008)

Chapter 4

STUDY OF STRUCTURAL BEHAVIOUR AND ELECTRICAL CONDUCTIVITY OF Cu DOPED S-Te GLASSY SYSTEM

4.1. INTRODUCTION

In this chapter, the influence of doping of Cu (which is a Transition Metal Ion, TMI) on the structural and electrical properties of Sulphur - Tellurium based Chalcogenide system having composition $x\text{Cu} - (1 - x) (0.5 \text{ S} - 0.5 \text{ Te})$ where, $x = 0.0, 0.1, 0.2$ and 0.3 has been discussed. TMIs contain partially filled d sub-shell and belong to Group 3 to 12 of the periodic table. In TMI doped glassy systems, the propensity of generation of small polarons is relatively high and conductivity of these glasses depends on temperature as well as frequency. In these glassy systems the electrical conduction is usually occurred due to the hopping of polarons among different localized states [1]. TMI doping in a glassy system can change its structure and thus its conduction mechanisms which enhances its usefulness in many applications.

Study of structural characterization and electrical properties of Copper doped Sulphur-Tellurium glassy systems having composition $x\text{Cu} - (1 - x) (0.5 \text{ S} - 0.5 \text{ Te})$, where $x=0.0, 0.1, 0.2$ and 0.3 , have been reported to see its possible usage in various academic and industrial applications.

Among chalcogen, Tellurium shows strong metallic character due to which its glass formation ability is weak. Also, thermal stability of Te based glasses is poor because of the lower glass transition temperature. To overcome these drawbacks, Te is doped with other suitable elements to improve its ability to be usable in various applications. To improve the glass formation ability Te can be doped with S. Copper, a TMI, has a tendency to form variety of compounds due to its several oxidation states i.e., -2, +1, +2, +3 and +4. So, doping of Copper in a Chalcogenide system can change the structure of the system and hence its electrical properties. Many reports by several researchers are available on study of various properties of Copper doped Chalcogenide glasses [2-7].

In this work, the structural analysis of Cu based S-Te system has been carried out with the help of different structural characterization techniques like XRD, TEM, FT-IR spectroscopy, molar volume and density calculations. The system was prepared by melt quenching process. With the help of XRD technique, the crystallite size of different phases present in the system, strain, dislocation density, crystalline volume fraction, etc have been determined. With the help of TEM, information (like area, interatomic distance etc.) about the nanoparticles present in the glassy system has been obtained. FT-IR spectroscopy technique has been used to get information regarding different functional groups and molecules present in the system.

The measurements of DC and AC conductivity were carried out for getting the information in relation to the localized states in this glassy system. To carry out DC conductivity measurements of the system, two-probe method has been used using ‘Metravi’ Digital Multimeter (model no. 450 DMM). The DC conductivity data was analysed with the help of Mott’s VRH Model and Greaves’s Model at lower and higher temperatures respectively. Measurements of AC conductivity of the system were accomplished in the wide range of frequency 42 Hz – 5 MHz at various temperatures (333K-463K). For the analysis of these data, different models or methods have been used like: Almond West formalism, MN Rule, AC conductivity scaling, dielectric relaxation studies etc. To know the information regarding the conduction mechanism of these glasses the AC conductivity data have been tried to fit with various models like CBH, NSPT, OLPT etc.

4.2. PREPARATION OF THE GLASSY SYSTEM

Melt-quenching method was used to prepare glassy alloys of $x\text{Cu} - (1 - x)$ ($0.5\text{S} - 0.5\text{Te}$) where, $x=0.0, 0.1, 0.2$ and 0.3 . All the requisite chemicals i.e. Copper, Sulphur and Tellurium of high purity (Aldrich 99.9%) were weighted as per the atomic percentages and then mixed and crushed to a very fine powder. These glasses are having tendency to react with oxygen at high temperature. In order to reduce the tendency of its reaction with oxygen, the sealing of powdered mixture in quartz ampoules was accomplished under 10^{-4} Torr vacuum. Those ampoules were then put into a furnace and furnace temperature was increased to 500°C at a rate of $3^{\circ}\text{C}/\text{min}$. After 2 hrs the temperature was increased with the same rate to 700°C and the ampoules were kept there for about 30 min. After that, the ampoules were brought out from the furnace and dropped immediately in ice cold water for rapid cooling of the melt. The obtained glassy materials were then ground to fine powder using a mortar for XRD

studies. XRD technique has been used to confirm the glassy and partially crystalline nature of the materials. The composition of the chemicals in the alloy was verified by Energy Dispersive X-Ray (EDX) Spectroscopy which confirms absence of oxygen in glassy samples.

For measuring DC and AC conductivities, pellets of the prepared systems were formed with the help of pelletizer in which the powdered samples were kept under a pressure of 80Kg/cm^2 for about 1 hr 30 min. Coating of Silver paste on both the opposite sides of the formed pellets was done to make sure good electrical contact between electrode and the pellet.

4.3. RESULTS AND ANALYSIS

4.3.1. XRD

4.3.1.1. Calculations of crystallite size, dislocation density and lattice strain

In Fig-4.1 XRD patterns of Cu doped S-Te system having $x = 0.0, 0.1, 0.2$ and 0.3 are shown. The peaks in the XRD pattern point to the polycrystalline nature of this system. Due to the formation of different nano-crystallites, several peaks having the $[h\ k\ l]$ values: $[1\ 0\ 0]$, $[1\ 0\ 2]$, $[1\ 1\ 1]$, $[2\ 0\ 1]$, $[0\ 2\ 2]$ – for Te; $[2\ 0\ 0]$, $[4\ 0\ 0]$ - for TeS; $[2\ 0\ -2]$, $[2\ 1\ -3]$ – for $\text{Te}_{0.5}\text{S}_{3.5}$; $[2\ 0\ 0]$ – for TeS; $[1\ 0\ 1]$, $[1\ 0\ 3]$ – for Cu Te_2 ; $[1\ 1\ 1]$, $[2\ 2\ 0]$ – for CuS_2 ; $[0\ 2\ 2]$, $[1\ 3\ 1]$, $[2\ 0\ 6]$ – for CuS ; and $[2\ 0\ 3]$ – for $\text{Cu}_{1.43}\text{Te}$ can be seen from the XRD pattern [8-19]. On increasing the value of x in the system's composition, its polycrystalline nature has found to be increased. The crystallite size, dislocation density and lattice strain of this system have been calculated using Eqns. (2.4), (2.5) and (2.6) respectively of Chapter 2. In Table-4.1 the various phases formed in the system having $x = 0.0, 0.1, 0.2$ and 0.3 along with their crystallite sizes and Miller indices are shown. Table-4.1 also shows the calculated dislocation density and lattice strain of the system.

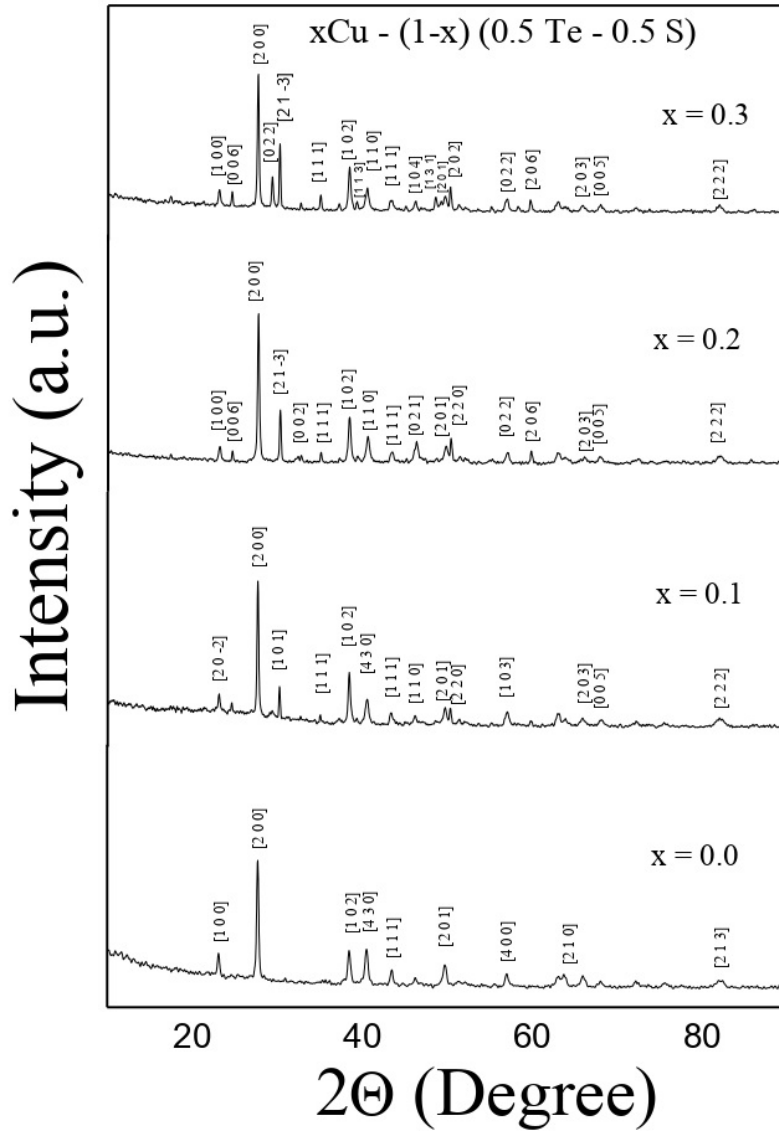


Fig-4.1: XRD patterns of Chalcogenide glassy system $x\text{Cu} - (1-x) (0.5 \text{ S} - 0.5 \text{ Te})$ where, $x = 0.0, 0.1, 0.2$ and 0.3

From Table-4.1 it is found that average crystallite size of various nano-crystallites increases and dislocation density decreases on increasing the content of Cu in the composition. Reduction of dislocation density on the increase of Cu reduces the system's disorder, which decreases the possibility of collision of polarons. This can increase the mobility of carriers which increases electrical conductivity in the system.

Table-4.I: Calculated values of crystallite size, lattice strain and dislocation density of system xCu – (1-x)(0.5S – 0.5Te)

x	Phases	Crystallite size (nm)	h k l	Average crystallite size (nm)	Dislocation density (nm ⁻²)	Lattice strain
0.0	Te	23.56	1 0 0 1 0 2 1 1 1 2 0 1 2 1 0	23.77	0.00177	0.35167 6
	TeS	29.37	2 0 0 4 0 0			
	TeS ₇	18.38	4 3 0 4 0 0			
0.1	Te	38.02	1 0 2 2 0 1	34.25	0.000852	0.36734 1
	Te _{0.5} S _{3.5}	41.17	2 0 -2			
	TeS	49.82	2 0 0			
	CuTe ₂	39.93	1 0 1 1 0 3			
	CuS ₂	55.13	1 1 1 2 2 0			
	Cu	26.03	1 1 1			
	Cu ₉ S ₅	21.91	1 1 0			
	CuTe	18.25	0 0 5			
Cu _{1.43} Te	18.02	2 0 3				
0.2	Te	27.65	1 0 0 1 0 2 1 1 0 1 1 1 2 0 1 0 2 2	43.27	0.000534	0.14379 1
	Cu _{1.75} Te	61.91	0 0 6			
	TeS	49.83	2 0 0			
	Te _{0.5} S _{3.5}	62.66	2 1 -3			
	Cu Te ₂	10.50	0 0 2			
	CuS ₂	75.71	1 1 1 2 2 0			
	Cu S	93.04	2 0 6			
	Cu _{1.43} Te	12.02	2 0 3			
	Cu ₉ S ₅	18.23	0 2 4			
	Cu Te	21.16	0 2 1 0 0 5			
0.3	Te	28.47	1 0 0 1 0 2 1 1 0 1 1 1 2 0 1 1 1 2 0 2 2	44.96	0.000495	0.04631
	Cu _{1.75} Te	85.85	0 0 6			
	TeS	49.83	2 0 0			
	CuS	47.41	0 2 2 1 3 1 2 0 6			
	Te _{0.5} S _{3.5}	62.66	2 1 -3			
	CuS ₂	63.43	1 1 1			
	Cu 1.96 S	42.83	1 1 3			
	Cu ₉ S ₅	32.88	1 0 4			
	Cu _{1.43} Te	18.02	2 0 3			
	Cu Te	18.25	0 0 5			

4.3.1.2. Crystalline Volume Fraction (CVF)

Table-4.2: Crystalline volume fraction of system $x\text{Cu} - (1-x) (0.5 \text{ S} - 0.5 \text{ Te})$

x	h k l	Phase	Area (I_{hkl})	K_{hkl}	Crystalline volume fraction
0.0	1 0 0	Te	11.703	0.17939	0.1738
	2 0 0	TeS	65.238	1	0.5
	1 0 2	Te	21.610	0.33125	0.2985
	4 3 0	TeS ₇	26.699	0.40926	0.35054
	1 1 1	Te	10.305	0.15796	0.15411
	2 0 1	Te	17.706	0.27141	0.25279
	4 0 0	TeS	9.6843	0.14845	0.14525
0.1	2 1 3	Te	23.896	0.36629	0.32296
	2 0 -2	Te _{0.5} S _{3.5}	13.423	0.11566	0.11413
	2 0 0	TeS	116.06	1	0.5
	1 0 1	CuTe ₂	21.905	0.18874	0.18225
	1 1 1	CuS ₂	5.1529	0.0444	0.04431
	1 0 2	Te	54.127	0.46637	0.38306
	4 3 0	TeS ₇	37.862	0.32623	0.29485
	1 1 1	Cu	15.524	0.13376	0.13141
	1 1 0	Cu ₉ S ₅	9.3578	0.08063	0.08011
	2 0 1	Te	18.031	0.15536	0.1517
	2 2 0	CuS ₂	14.693	0.1266	0.1246
	1 0 3	CuTe ₂	25.081	0.2161	0.20646
	2 0 3	Cu _{1.43} Te	14.214	0.12247	0.12066
	0.2	0 0 5	CuTe	11.838	0.102
2 2 2		CuTe	36.388	0.31353	0.28547
1 0 0		Te	25.398	0.11943	0.11775
0 0 6		Cu _{1.75} Te	10.405	0.04893	0.04881
1 0 1		Te	212.66	1	0.5
2 1 -3		Te _{0.5} S _{3.5}	58.713	0.27609	0.25653
1 1 1		CuS ₂	11.269	0.05299	0.05284
1 0 2		Te	82.579	0.38831	0.33743
1 1 0		Te	59.952	0.28191	0.26116
1 1 1		Te	37.214	0.17499	0.16979
0 2 1		CuTe ₂	52.711	0.24787	0.23352
0 2 2		Te	29.446	0.13847	0.13586
0.3	2 0 6	CuS	16.794	0.07897	0.07848
	0 0 5	Cu ₉ S ₅	17.152	0.08065	0.08013
	2 2 2	CuTe	34.489	0.16218	0.15802
	1 0 0	Te	22.639	0.13973	0.13705
	0 0 6	Cu _{1.75} Te	13.966	0.0862	0.08556
	1 0 1	Te	162.02	1	0.5
	0 2 2	CuS	33.052	0.204	0.19585
	2 1 -3	Te _{0.5} S _{3.5}	61.443	0.37923	0.33155
	1 1 1	CuS ₂	16.257	0.10034	0.09934
	1 0 2	Te	67.383	0.41589	0.35457
	1 1 3	Cu _{1.96} S	8.1084	0.05005	0.04992
	1 1 0	Te	42.511	0.26238	0.24548
	1 1 1	Te	23.405	0.14446	0.1415
	1 0 4	Cu ₉ S ₅	15.028	0.09275	0.09196
	1 3 1	CuS	17.287	0.1067	0.1055
	2 0 1	Te	17.323	0.10692	0.10571
	2 0 2	Cu _{1.75} Te	28.007	0.17286	0.16785
0 2 2	Te	27.345	0.16878	0.1641	
2 0 6	CuS	15.271	0.09425	0.09342	
2 0 3	Cu _{1.43} Te	17.253	0.10649	0.10529	
0 0 5	CuTe	20.647	0.12743	0.1254	
2 2 2	CuTe	27.376	0.16897	0.16428	

The crystalline volume fraction (CVF) of the system was calculated using Eqn. (3.1) of Chapter 3. The CVF of the system having $x = 0.0$ have been obtained as: 0.17, 0.30, 0.15, 0.25 and 0.32 corresponding to the phase Te having [h k l] values [1 0 0], [1 0 2], [1 1 1], [2 0 1] and [2 1 3] respectively; 0.5 and 0.14 for the phase TeS with [h k l] values [2 0 0] and [4 0 0] respectively; and 0.35 corresponds to the phase TeS₇ having [h k l] values [4 3 0]. Similarly CVF of the present system having $x = 0.1, 0.2$ and 0.3 have also been calculated, the details of which is given in Table-4.2. In Table-4.3 the CVF percentage of the system is shown from which decrease of CVF percentage on increasing Cu in the system is found.

Table-4.3: Crystalline Volume Fraction (%) of system $x\text{Cu} - (1-x)(0.5\text{S} - 0.5\text{Te})$ where, $x=0.0, 0.1, 0.2, 0.3$

Values of x	Crystalline Volume Fraction (%)
0.0	27
0.1	20
0.2	19
0.3	17

4.3.2. TEM

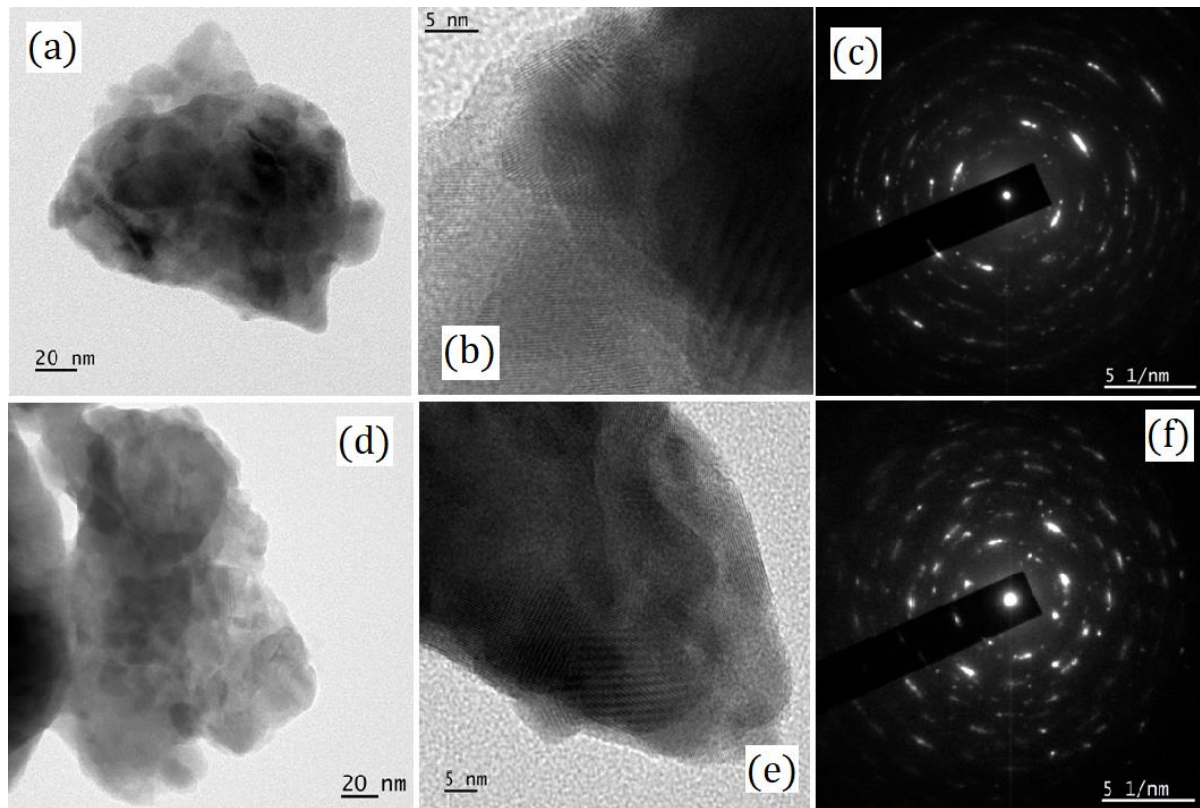


Fig-4.2: TEM Images of glassy system $x\text{Cu} - (1-x)(0.5\text{S} - 0.5\text{Te})$ (a), (b), (c) – for $x = 0.2$; (d), (e), (f) – for $x = 0.3$

In Fig-4.2 (a) and (d) TEM images in which distribution of nanoparticles embedded in system $x\text{Cu} - (1-x)(0.5\text{S} - 0.5\text{Te})$ with $x = 0.2$ and 0.3 respectively are shown. In Fig-4.2(b) and (e) high resolution TEM images of the same samples have been shown. Using ImageJ software the area of the nanoparticles have been calculated and is shown in Table-4.4 and it has been found that the average area of nanoparticles is 269.7 nm^2 , area of the smallest nanoparticle is 84.17 nm^2 and that of the largest nanoparticle is 845.68 nm^2 in the system.

Table-4.4: Area of nanoparticles of $x\text{Cu} - (1-x)(0.5\text{S} - 0.5\text{Te})$ system having $x = 0.3$

S.No.	Label	Area
1		266.502
2		148.302
3		845.681
4		329.174
5		84.175
6		108.814
7		156.842
8		84.555
9		642.300
10		188.026
11		290.583
12		92.182
13	Mean	269.761
14	SD	240.229
15	Min	84.175
16	Max	845.681

In Fig-4.2(c) and (f) shows the SAED patterns of this glassy system for $x = 0.3$ and 0.4 respectively. From this SAED pattern the interplanar spacings (D) between different crystalline phases have been calculated. The D values with corresponding angles (2θ) are listed in Table-4.5. It has been found that the average interplanar distance of the different nanoparticles in the system is 0.104 nm .

Table-4.5: Interplanar distance (from SAED) of $x\text{Cu} - (1-x)(0.5\text{S} - 0.5\text{Te})$ where, $x=0.3$

S. No.	Angle	Length	D, Lattice Plane Distance (nm)
1	-111.801	8.122	0.123122384
2	-105.268	8.163	0.122503981
3	-10.33	8.296	0.120540019
4	-18.54	10.722	0.093266182
5	-8.206	13.172	0.075918615
6	10.147	14.073	0.071058054
7	-6.503	6.02	0.166112957
8	54.948	16.998	0.058830451
9	-0.492	15.623	0.064008193

4.3.3. FT-IR

FT-IR transmittance spectra of this system are shown in Fig-4.3 which indicates very good transparency in the spectral range $4000\text{cm}^{-1} - 400\text{cm}^{-1}$. It can be observed from Fig-4.3 that most of the absorption bands appeared in the present glassy system can be assigned to vibrational bands of oxides and hydrides bonds as Chalcogenide glassy systems containing Sulphur are having greater affinity to absorb water related particles. The chemical bonds formed due to the presence of extrinsic impurities in the glassy system may be the cause for the appearance of these bands in the spectra of Fig-4.3.

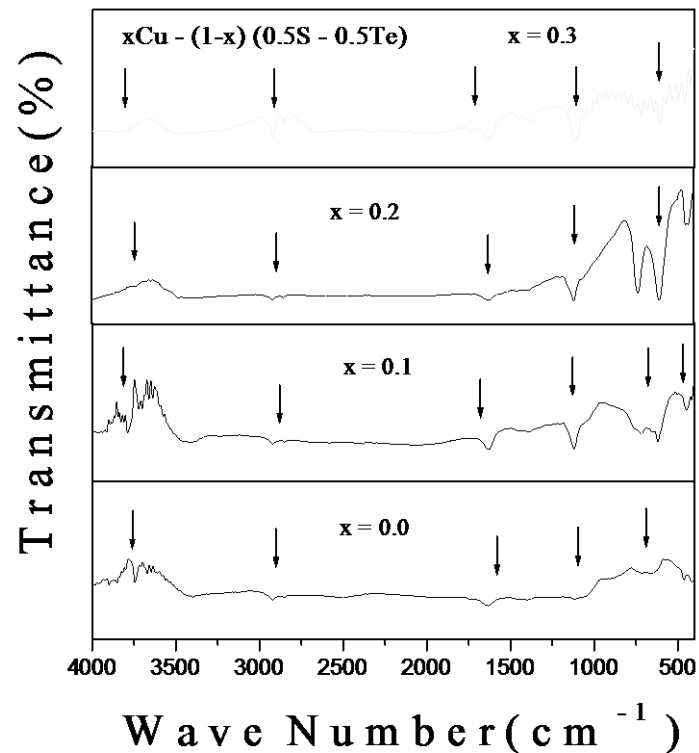


Fig-4.3: FT-IR spectra of system $x\text{Cu} - (1-x) (0.5\text{S} - 0.5\text{Te})$

Appearance of bands near wave number 1640 cm^{-1} and in the range $3700-3300\text{cm}^{-1}$ are associated with vibrations occur due to stretching and bending of hydroxyl groups in the system [20-22]. Absorption of moisture by the glassy system from atmosphere during its preparation may be the cause for appearance of absorption bands related to O – H and H_2O groups [23].

The absorption band appeared in the range $1160\text{-}1115\text{cm}^{-1}$ are associated with the stretching vibration of sulphoxides $\text{S}=\text{O}$ [21]. In Fig-4.3 two strong absorption bands can be observed at 735cm^{-1} and 602cm^{-1} in the present glassy system having value of $x = 0.2$ in its composition. The intermolecular vibration of Te-O bonds may be responsible for the appearance of absorption bands in the spectral ranges $720\text{cm}^{-1} - 780\text{cm}^{-1}$ & $668\text{cm}^{-1} - 529\text{cm}^{-1}$ [24, 25].

4.3.4. Density and Molar Volume

Archimedes principle has been applied to calculate the Density (ρ) of the present glassy system which can be expressed as Eqn. (3.3) of Chapter 3. To calculate molar volume (V_M) of this system Eqn. (3.4) of Chapter 3 has been used. Table-4.6 presents the calculated values of ρ and V_M of the Cu doped S - Te Chalcogenide glassy system for different values of x .

Table-4.6: Density and molar volume of system $x\text{Cu} - (1-x)(0.5\text{S} - 0.5\text{Te})$ where, $x = 0.0$ and 0.1

x	ρ (gm/cm^3)	V_M (cm^3/mol)
0.0	3.75	21.29
0.1	0.34	230.01

In Fig-4.4, the variation of ρ and V_M with different values of x in the system is shown. It can be observed from Fig-4.4 that the density decreases and the molar volume increases with the value of x . High value of density in a glass is the indication of closely packed particles in the structure.

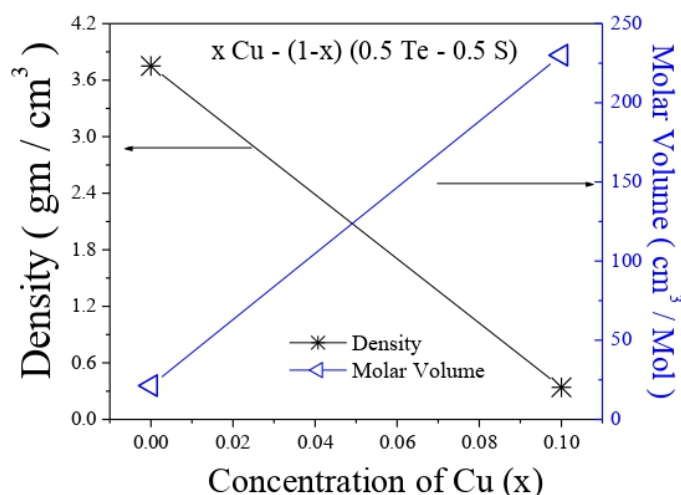


Fig-4.4: Variation of density and molar volume with different values of x for Chalcogenide glassy system $x\text{Cu} - (1-x)(0.5\text{S} - 0.5\text{Te})$

4.3.5. Analysis of DC Conductivity

DC conductivity at different temperatures of this system was measured. The DC conductivity variation of the system with temperature is shown in Fig-4.5. The figure indicates that when x (content of Cu in the system) increases, DC conductivity increases. From Fig-4.5, information regarding defects in structure and density of localized states in the system was obtained. Increase of DC conductivity on increasing temperature is found in Fig-4.5. This signifies semiconducting nature of the glassy system. The decrease in resistance on increasing temperature as well as content of Cu is confirmed from Fig-4.6(a), (b), (c) and (d) which show Cole-Cole plots of present system with $x = 0.0, 0.1, 0.2$ and 0.3 respectively.

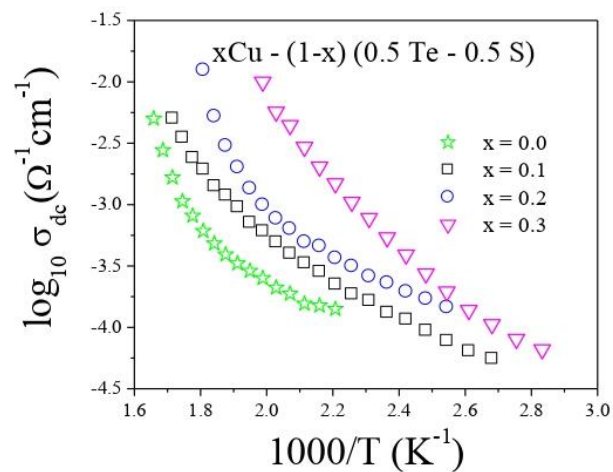


Fig-4.5: DC conductivity versus temperature plots of Chalcogenide system $x\text{Cu} - (1-x) (0.5 \text{ S} - 0.5 \text{ Te})$ where, $x = 0.0, 0.1, 0.2$ and 0.3

There is a slight increase of DC conductivity is seen on rising of temperature, as shown in Fig-4.5, and the conductivity is pretentious by impurities and defects in structure of the system at lower temperature region This is an indication of the occurrence of conduction in this region through variable range hopping of polarons in the localized states, which was predicted by Mott's VRH Model. At the higher temperature region, DC conductivity is found to increase rapidly with rise of temperature which has been analysed with Greaves's Model, according to which the electrical conduction in the system takes place because of the tunnelling of polarons in extended states due to the rise in temperature. The details of both models have been discussed in Section 3.3.5 of Chapter 3.

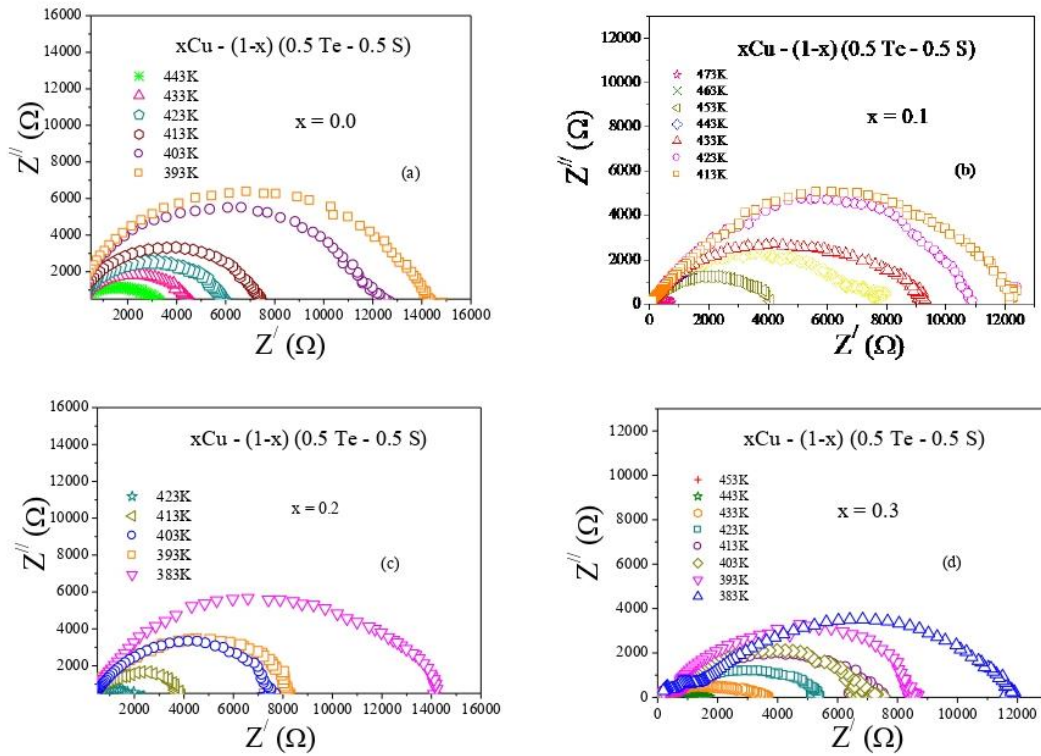


Fig-4.6: Cole-Cole plots of $x\text{Cu} - (1-x)(0.5\text{Te} - 0.5\text{S})$ where, $x =$ (a) 0.0 (b) 0.1 (c) 0.2 and (d) 0.3

Fig-4.7(a) shows the change in DC conductivity with respect to $T^{-0.25}$. Density of states $N(E_F)$ was calculated from slopes of the linear fitting of the data in Fig-4.7(a) at lower temperature region with Eqn. (3.5) of Chapter 3. The calculated values of $N(E_F)$ for various values of x in the present glassy system is given in Table-4.7. The table indicates that the increase of Cu in this system decreases the density of states $N(E_F)$.

In Fig-4.7(b), $\log_{10}(\sigma_{DC}T^{1/2})$ is plotted against $T^{-0.25}$. To calculate $N(E_F)$, data in Fig-4.7(b) have been linearly fitted with Eqn. (3.7) of Chapter 3 at high temperature region (Greaves' model) and values of $N(E_F)$ are presented in Table-4.7. From Table-4.7 $N(E_F)$ is found to decrease with the increase of Cu in the glassy system. With more density of localized states in the glassy sample with $x = 0.0$, the possibility of collision among polarons may increase which can decrease the conductivity due to charge carriers hopping in the system. The values of $N(E_F)$ calculated from Mott's & Greaves' models are not same because these models work on dissimilar temperature ranges.

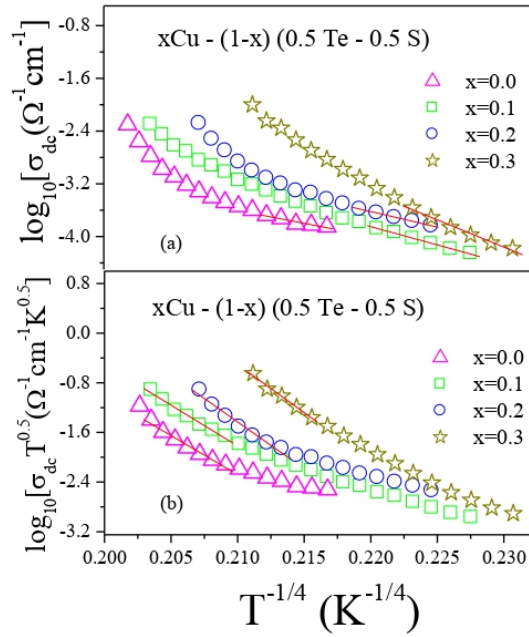


Fig-4.7: DC conductivity versus temperature plots of system $x\text{Cu} - (1-x) (0.5 \text{ Te} - 0.5 \text{ S})$ fitted with (a) Mott's model (b) Greaves's model

Table-4.7: Values of $N(E_F)$ calculated from Mott's and Greaves models and MN energy of system $x\text{Cu} - (1-x) (0.5 \text{ S} - 0.5 \text{ Te})$

x	$N(E_F)$ -Mott's Model ($\text{eV}^{-1} \text{cm}^{-3}$)	$N(E_F)$ -Greaves's Model ($\text{eV}^{-1} \text{cm}^{-3}$)	ΔE_{MN} (eV)
0.0	1.70468E+20	1.91359E+28	0.102
0.1	4.18877E+19	1.60419E+28	0.094
0.2	8.02162E+19	9.17461E+27	0.049
0.3	8.4487E+18	8.29888E+27	0.045

4.3.6. AC Conductivity Analysis

4.3.6.1. Power Law

Jonscher's Power Law equation, which has been discussed in Section 3.3.6.1 of Chapter 3, is used for expressing AC conductivity of amorphous semiconductors. Fig-4.8(a), (b), (c) and (d) show the plots of AC conductivity data with respect to frequency at higher frequency region and at various temperatures for this system with $x = 0.0, 0.1, 0.2$ and 0.3 respectively. The plots of Fig-4.8 are linearly fitted with Eqn. (3.9) of Chapter 3 which are shown by the solid lines in the figure. From the slopes of these lines, values of S have been obtained.

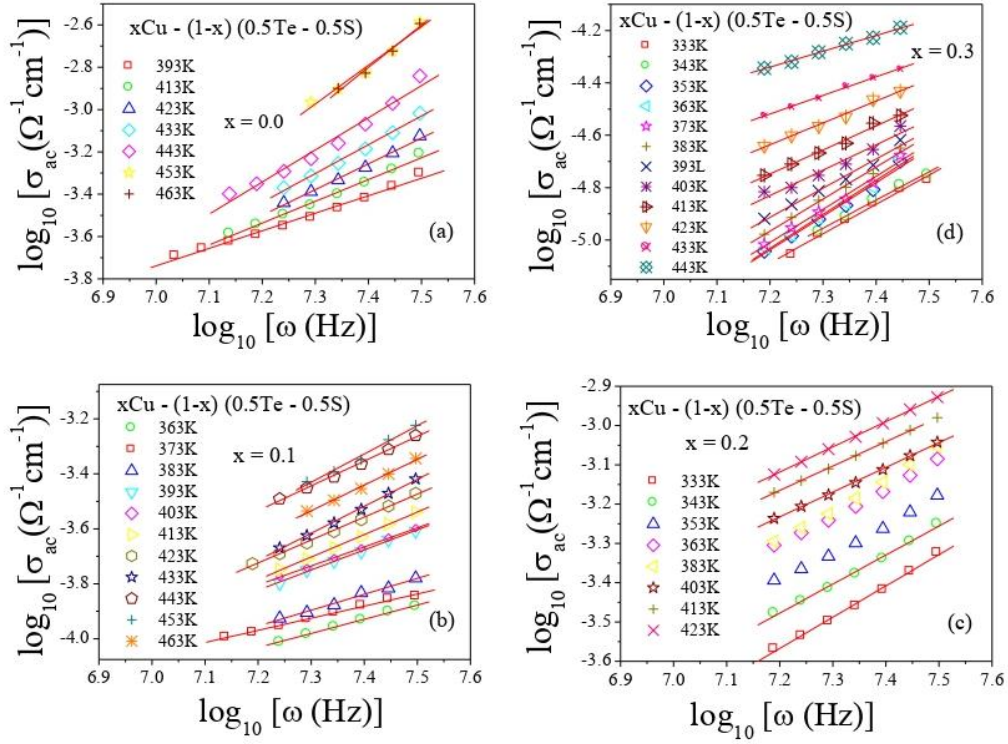


Fig-4.8: Plots of AC conductivity versus frequency plots of system $x\text{Cu} - (1-x)(0.5\text{S} - 0.5\text{Te})$ for $x =$ (a) 0.0 (b) 0.1 (c) 0.2 and 0.3

The temperature dependency of S for the present system with $x = 0.0, 0.1, 0.2$ and 0.3 is shown in Fig-4.9(a), (b), (c) and (d) respectively. The availability of many models for the analysis of AC conduction mechanisms in amorphous semiconductors have been discussed in Section 3.3.6.1 of Chapter 3. To know the actual conduction mechanism in the present system, Fig-4.9(a), (b), (c) and (d) have been tried to fit with those models. It is found that in Fig-4.9(a) and (c), where $x = 0.0$ and 0.2 , the value of S increases with temperature T . Fig-4.9(a) and (c) are found to be fitted with Modified NSPT model (the detail of which is given in Section 3.3.6.1 of Chapter 3). Fig-4.9(b) and (d), in which S is found to be decreased with temperature, are successfully fitted with CBH Model. Details of this model are also given in Section 3.3.6.1 of Chapter 3. All the fitting parameters i.e., τ_0 , τ_H , W_H , W_m and T_o , obtained from the fittings of Fig-4.9(a) and (c) with Eqn. (3.13) and Fig-4.9(b) and (d) with Eqn. (3.10) of Chapter 3, are shown in Table-4.8.

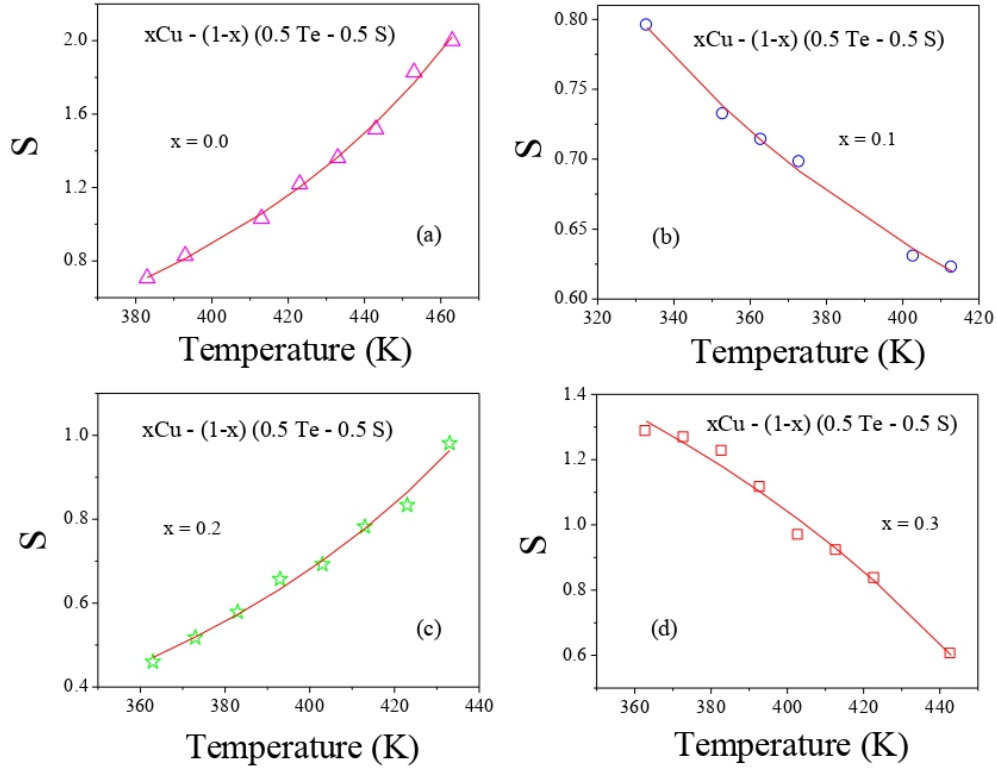


Fig-4.9: S versus T plots of system $x\text{Cu} - (1-x) (0.5 \text{ Te} - 0.5 \text{ S})$ for $x =$ (a) 0.0 (b) 0.1 (c) 0.2 (d) 0.3
Fitting of the plots for $x = 0.1$ and 0.3 with CBH model and for $x = 0.0$ and 0.2 with NSPT (modified) model are indicated by solid lines

Table-4.8: Fitting parameters of CBH model, NSPT (modified) model and Almond West formalism of system $x\text{Cu} - (1-x)(0.5\text{S} - 0.5\text{Te})$

Values of x	CBH			NSPT (MODIFIED)			ALMOND WEST	
	W_m (eV)	τ_0 (s)	T_O (K)	W_H (eV)	τ_H (s)	T_O (K)	E_H (eV)	n
0.0	---	----	-----	0.02659	0.00003	408.72776	0.290	1.46282
0.1	0.08916	0.3569	284.70387	---	----	-----	0.069	0.81788
0.2	----	-----	-----	0.03071	0.00001	436.30923	0.060	1.08118
0.3	0.05829	0.00001	404.87336	---	----	-----	0.038	1.99969

We can therefore conclude that for the present glassy system in which value of x is 0.0 and 0.2 the NSPT modified model has been applied to find mechanism of conduction, according to which charge carriers tunneling through grain boundaries is main cause of conduction. CBH model was observed as most appropriate for this system with $x=0.1$ and 0.3 , according to which the conduction occurs because of charge carriers' hopping in pairs over potential barrier between two defect states.

4.3.6.2. Almond West Formalism

Fig-4.10(a), (b), (c) and (d) show the AC conductivity spectra in range 42 Hz – 5 MHz at temperatures in the range of 333K-463K of the present glassy system with $x=0.0, 0.1, 0.2$ and 0.3 respectively. AC conductivity has been found to be increased with the temperature and independent on frequency at lower frequency region. The hopping of polarons may be the cause of the frequency independent AC conductivity in such glasses [26, 27]. At high frequencies, above hopping or crossover frequency, increase of AC conductivity is found with frequency which occurs due to correlated motion of polarons [26, 27].

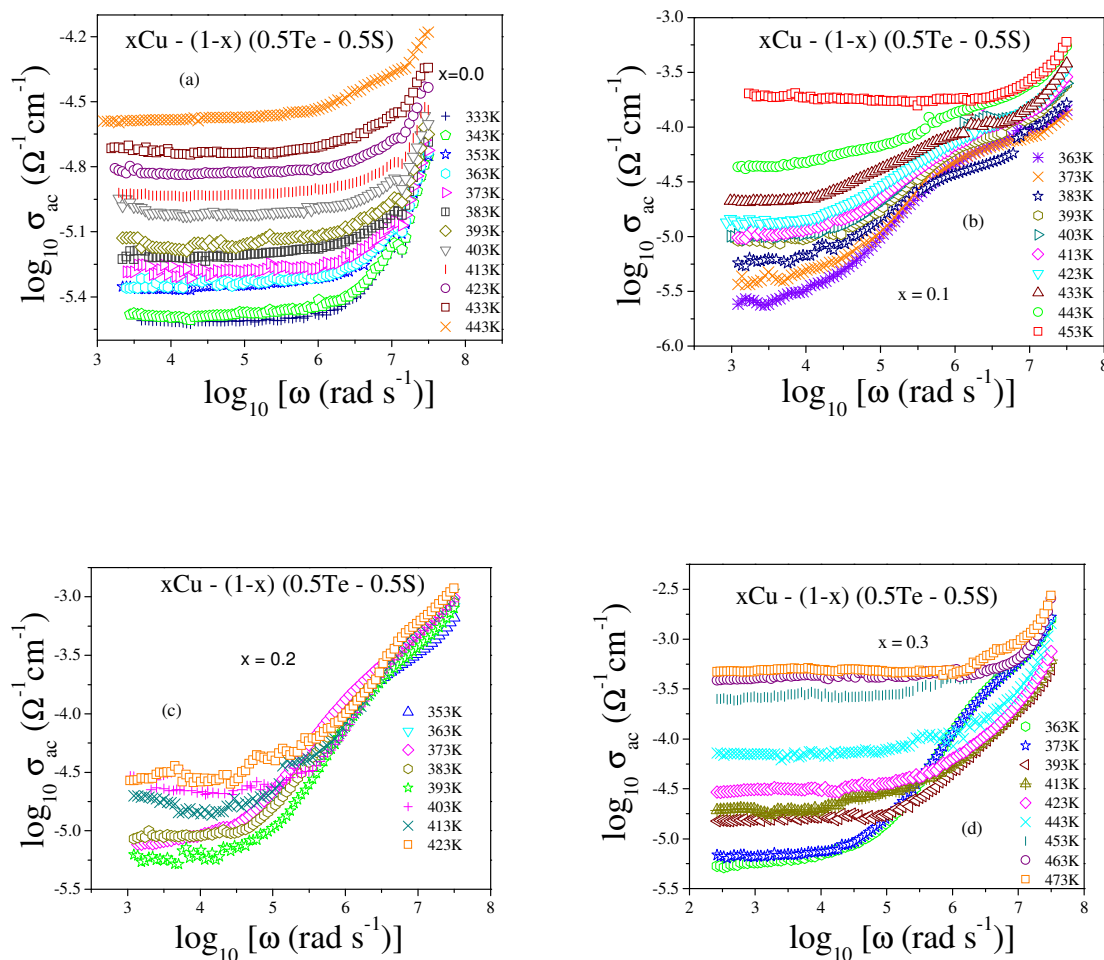


Fig-4.10: Variation of AC conductivity of $x\text{Cu} - (1-x) (0.5\text{S} - 0.5\text{Te})$ where, $x =$ (a) 0.0, (b) 0.1, (c) 0.2 and (d) 0.3 at different temperatures

For the analysis of the AC conductivity spectra Almond West formalism has been applied, details of which is given in Section 3.3.6.2 of Chapter 3. Fig-4.11(a), (b), (c) and (d) show the

AC conductivity spectra of present glassy system for $x = 0.0, 0.1, 0.2$ and 0.3 respectively fitted with Almond West formalism i.e. Eqn. (3.15) of Chapter 3. Fittings are indicated by solid lines in the plots.

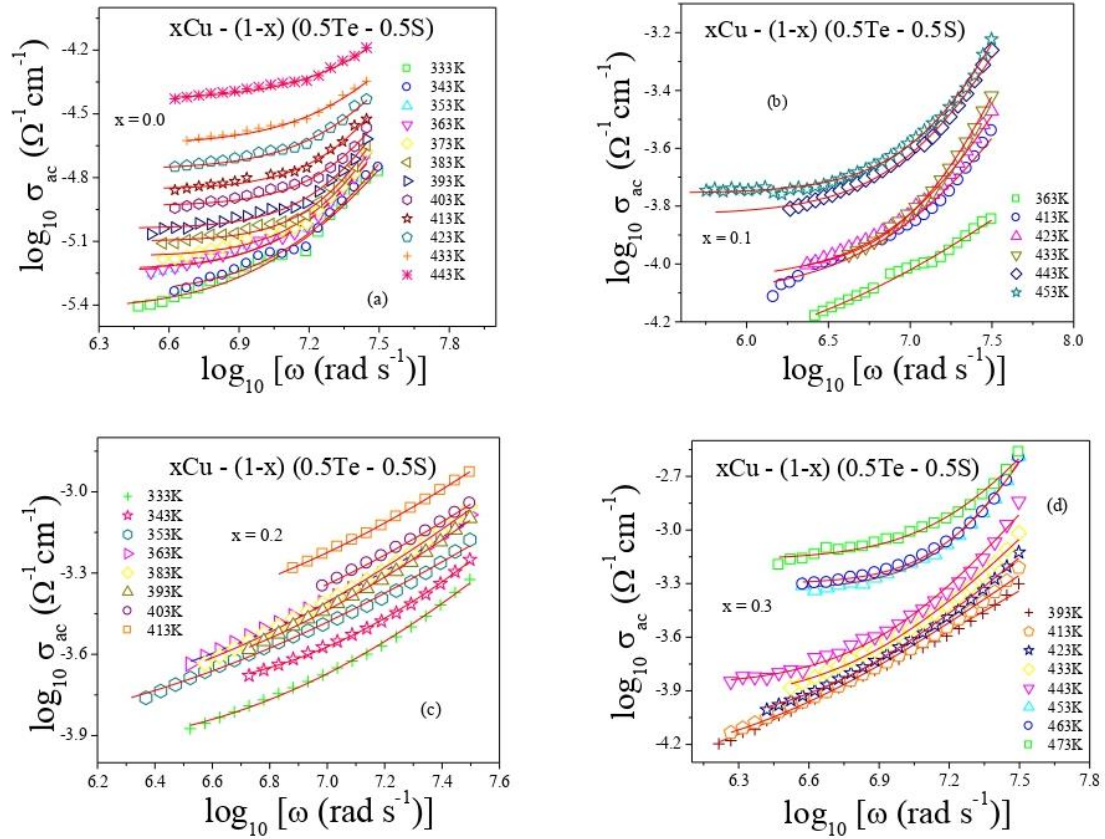


Fig-4.11: AC conductivity spectra, fitted with Almond West formalism, of the system $x\text{Cu} - (1-x) (0.5\text{S} - 0.5\text{Te})$ where, $x =$ (a) 0.0, (b) 0.1, (c) 0.2 and (d) 0.3 at different temperatures

Different parameters like $-\sigma_{DC}$, ω_H and n have been obtained by fitting Fig-4.11 with Eqn. (3.15) of Chapter 3. The conductivity spectra of all the samples of the present system at 423K are shown in Fig-4.12 in which the AC conductivity is found to increase on the increase of amount of Cu in the system's composition which validates DC conductivity plots shown in Fig-4.5.

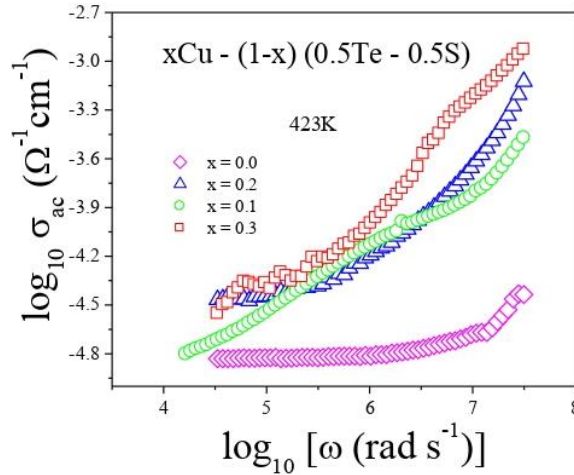


Fig-4.12: Variation of AC conductivity with frequency of Chalcogenide system $x\text{Cu} - (1-x) (0.5\text{S} - 0.5\text{Te})$ system at 423K

The temperature dependency of hopping frequency ω_H of the present system is shown in Fig-4.13 which can be represented by the Arrhenius equation, Eqn. (3.16) of Chapter 3, explanation of which is given in Section 3.3.6.2 of Chapter 3.

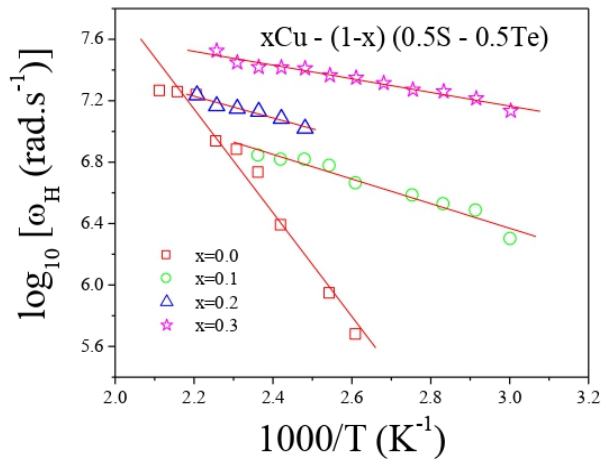


Fig-4.13: Variation of hopping frequency with temperature of Chalcogenide system $x\text{Cu} - (1-x) (0.5\text{S} - 0.5\text{Te})$ where, $x = 0.0, 0.1, 0.2$ and 0.3

To calculate the activation energy for hopping frequency E_H Fig-4.13 has been linearly fitted with Eqn. (3.16) of Chapter 3. The values of E_H and n of the system for $x = 0.0, 0.1, 0.2$ and 0.3 is shown in Table-4.8. It can be seen in Table-4.8 that activation energy for hopping frequency E_H lessens on increasing the amount of Cu in the present system. From the values of n , frequency exponent, the percolation type movement of polarons can be expected [27].

4.3.6.3. AC Conductivity Scaling

AC conductivity scaling process helps in predicting the dependency of electrical relaxation process on composition and temperature of glasses. The detail of AC conductivity scaling is discussed in Section 3.3.6.3 of Chapter 3. Fig-4.14(a), (b), (c) and (d) present AC conductivity scaling of this system having $x = 0.0, 0.1, 0.2$ and 0.3 respectively at different temperatures (temperature scaling). Overlapping of conductivity spectra at all the temperatures in a single curve is found in Fig-4.14(a), (b), (c) and (d), which suggests temperature independent relaxation process in the system [28].

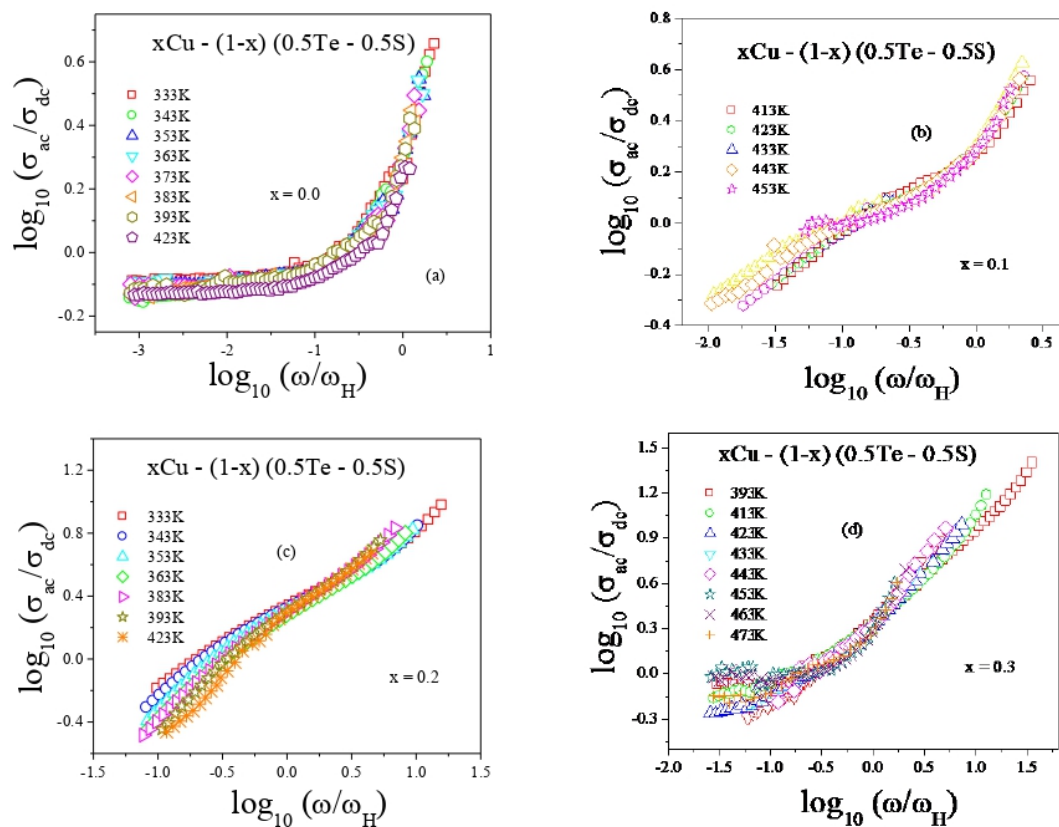


Fig-4.14: AC conductivity temperature scaling of the system $x\text{Cu} - (1-x)(0.5\text{S} - 0.5\text{Te})$ where, $x =$ (a) 0.0, (b) 0.1, (c) 0.2 and (d) 0.3

In Fig-4.15 the composition scaling i.e., the scaling of AC conductivity data of the system having values of x equal to 0.0, 0.1, 0.2 and 0.3 at 423K is shown. In Fig-4.15 the non-overlapping of ac conductivity data is found. From the analysis of AC conductivity scaling, composition dependent and temperature independent relaxation mechanism in the system has been found.

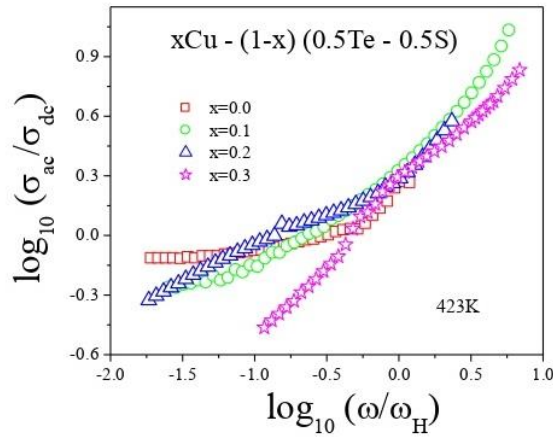


Fig-4.15: AC conductivity composition scaling of Chalcogenide system $x\text{Cu} - (1-x) (0.5\text{S} - 0.5\text{Te})$ where $x = 0.0, 0.1, 0.2$ and 0.3 at 423K

4.3.6.4. Meyer–Neldel rule

Meyer-Neldel rule has been applied for analysing mechanism of electrical conduction in the present system, details of which have already been discussed in Section 3.3.6.4 of Chapter 3. The change in AC conductivity of this system, having $x = 0.0, 0.1, 0.2$ and 0.3 , with respect to temperature at four different frequencies are shown in Fig-4.16(a), (b), (c) and (d) respectively. It was observed from Fig-4.16 that when temperature increases, the AC conductivity increases. The variations of AC conductivity of these semiconducting materials above the room temperature can be expressed by Eqn. (3.18) of Chapter 3. The experimental data of Fig-4.16(a), (b), (c) and (d) were linearly fitted with Eqn. (3.18) of Chapter 3 to obtain the values of σ_0 and ΔE of the present system with different values of x from intercepts and slopes respectively of the fitted lines.

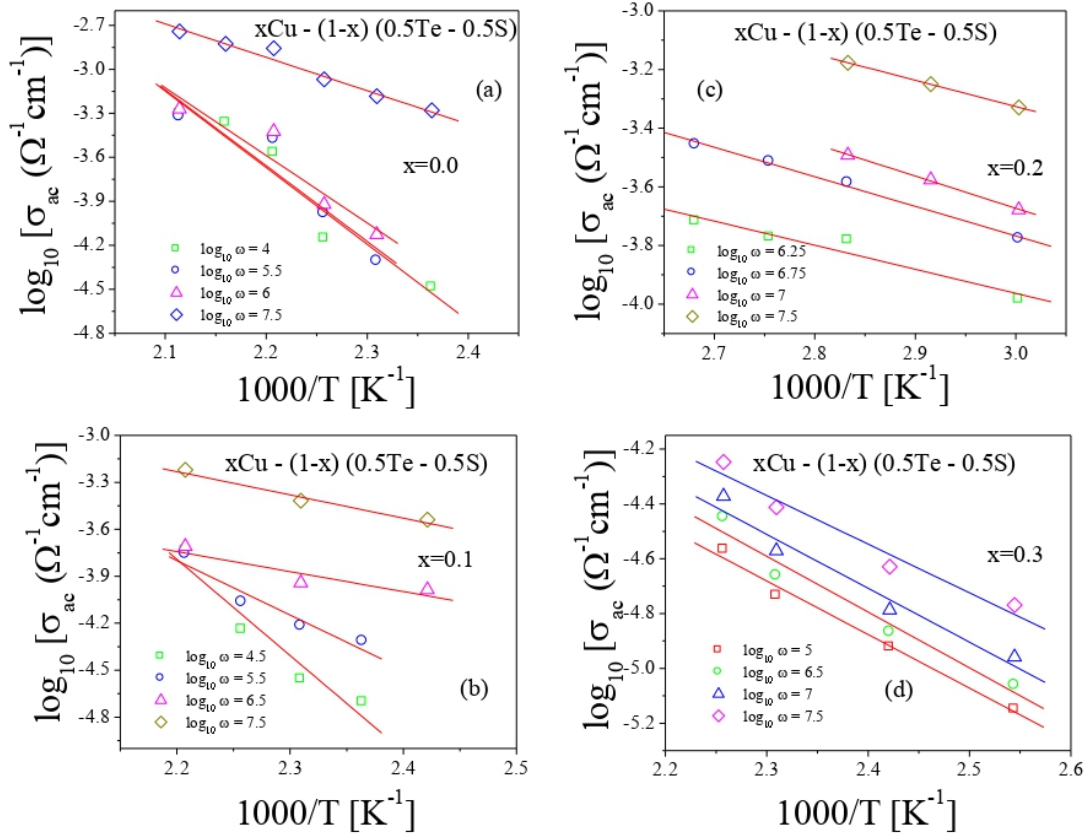


Fig-4.16: Variation of AC conductivity versus temperature of system $x\text{Cu} - (1-x)(0.5\text{S} - 0.5\text{Te})$ where, $x =$ (a) 0.0 (b) 0.1 (c) 0.2 and (d) 0.3

Fig-4.17(a), (b), (c) and (d) show the variations of σ_0 with ΔE of this system having $x = 0.0, 0.1, 0.2,$ and 0.3 respectively, which show linear nature. To explicate σ_0 and its ΔE dependence, MN Rule has been applied because of the temperature dependent behavior of this system. The MN activation energy for this system with $x = 0.0, 0.1, 0.2$ and 0.3 were obtained from slopes of straight lines obtained from linearly fitting of Fig-4.17(a), (b), (c) and (d) with Eqn. (3.19) of Chapter 3 and is shown in Table-4.7. The decrease in MN activation energy on increase of x in the system can be seen from Table-4.7 which is a clear indication of increase of conductivity on the increase of amount of Cu in the system.

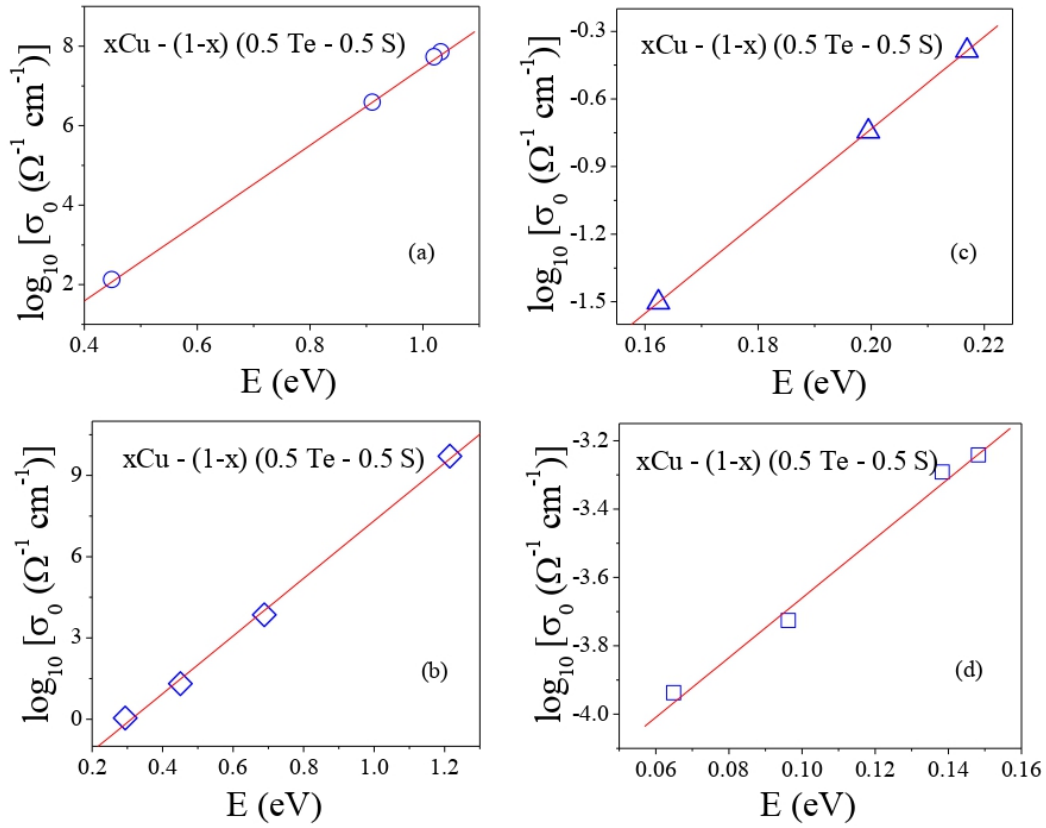


Fig-4.17: Variation of $\ln \sigma_0$ with E of system $x\text{Cu} - (1-x)(0.5\text{S} - 0.5\text{Te})$ where, $x =$ (a) 0.0 (b) 0.1 (c) 0.2 and (d) 0.3

4.3.6.5. Mobility and Carrier Density

To find the mobility μ and carrier density N of the system DC polarization technique has been used, details of which have been discussed in Section 3.3.6.5 of Chapter 3. The mobility of charge carriers has been determined using Eqn. (3.20) of Chapter 3. To determine the carrier density 'N' Eqn. (3.21) of Chapter 3 has been used.

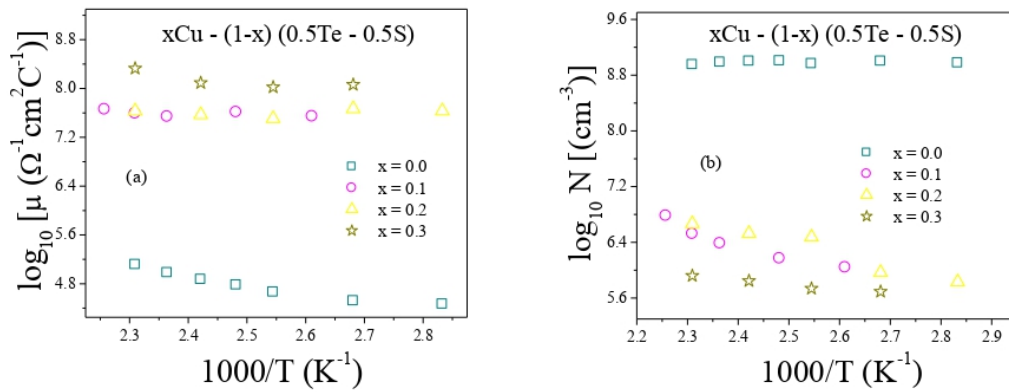


Fig-4.18: Plots of (a) $\log_{10} \mu$ versus $1000/T$ and (b) $\log_{10} N$ versus $1000/T$ for system $x\text{Cu} - (1-x)(0.5 \text{S} - 0.5 \text{Te})$ system where, $x = 0.0, 0.1, 0.2$ and 0.3

Fig-4.18(a) shows the plot of $\log_{10} \mu$ versus $1000/T$, where T indicates temperature in Kelvin, for the system. The mobility is found to be increased with the increase of x in the composition. Also, it has been found to be increased on the increase of temperature. In Fig-4.18(b) $\log_{10} N$ versus $1000/T$ of present glassy system is shown. From Fig-4.18(b) it is clearly observed that the value of carrier density 'N' is less in the system which is having more value of x in the composition i.e. $x = 0.3$ and with the increase of temperature it is found to be increased. In Table-4.9 the mobility and the carrier density data of the system is shown.

Table-4.9: Average mobility and carrier density of $x\text{Cu} - (1-x) (0.5\text{S} - 0.5\text{Te})$ system where, $x = 0.0, 0.1, 0.2$ and 0.3

x	Carrier Mobility μ ($\Omega^{-1}\text{cm}^2\text{C}^{-1}$)	Carrier density N (cm^{-3})
0.0	67014.92	9.51281E8
0.1	32562423	3.1478E6
0.2	4.03E+07	2.45037E6
0.3	1.39E+08	647482.01439

4.3.7. Dielectric Properties Analysis

4.3.7.1. Permittivity

The dependency of dielectric constant ϵ' and dielectric loss ϵ'' of the present system on frequency (range: 42Hz – 5MHz) and temperature (range: 333K – 453K) have been studied. Fig-4.19(a), (b), (c) and (d) show plots of ϵ' of the sample with $x = 0.0, 0.1, 0.2$ and 0.3 respectively against frequency at a range of temperatures. The plots of ϵ'' against frequency at different temperatures of the present system having $x = 0.0, 0.1, 0.2$ and 0.3 are shown in Fig-4.20(a), (b), (c) and (d) respectively. Exponential decrease of both ϵ' and ϵ'' on increasing the frequency at various temperatures has been observed from Fig-4.19 and Fig-4.20. The more value of ϵ' in lower frequencies is mainly due to occurrence of electrode polarization because of the accumulation of space charges at glass-electrode interface.

The effect of polarization decreases with the increase of frequency as the molecular dipoles in the system cannot follow the fast variation of the electric field. Hence, on increasing frequency in the system both ϵ' and ϵ'' start to decrease and show frequency independent nature.

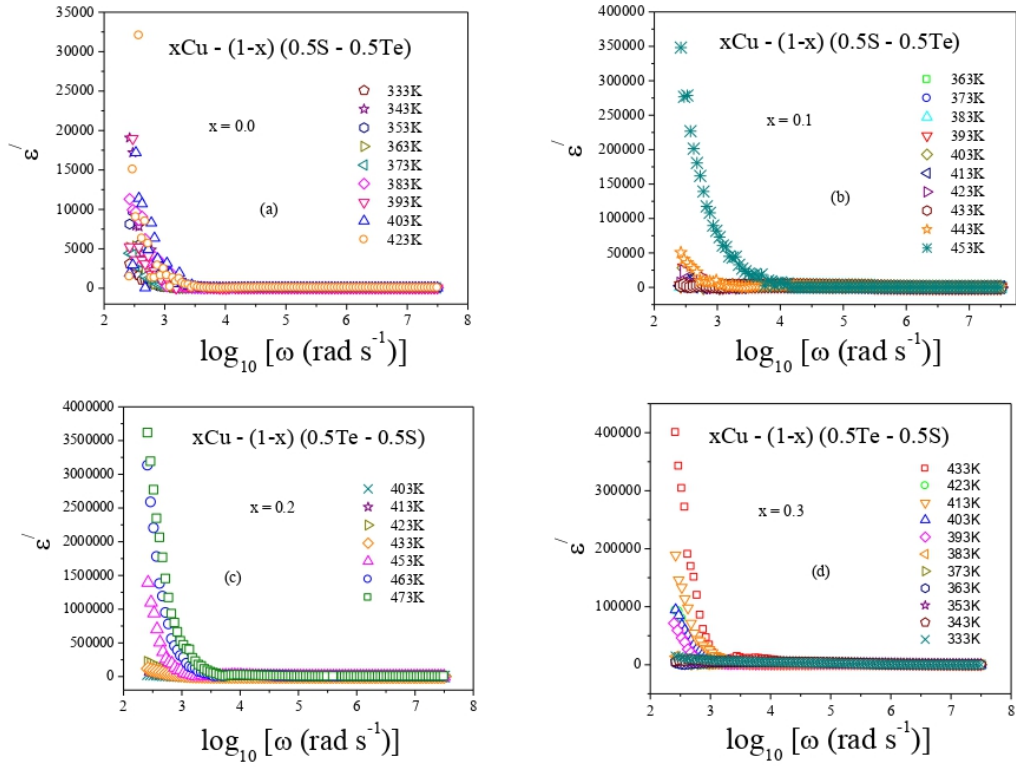


Fig-4.19: Spectra of dielectric constant ϵ' of Chalcogenide system $x\text{Cu} - (1-x) (0.5\text{S} - 0.5\text{Te})$ for $x =$ (a) 0.0 (b) 0.1 (c) 0.2 and (d) 0.3 at various temperatures

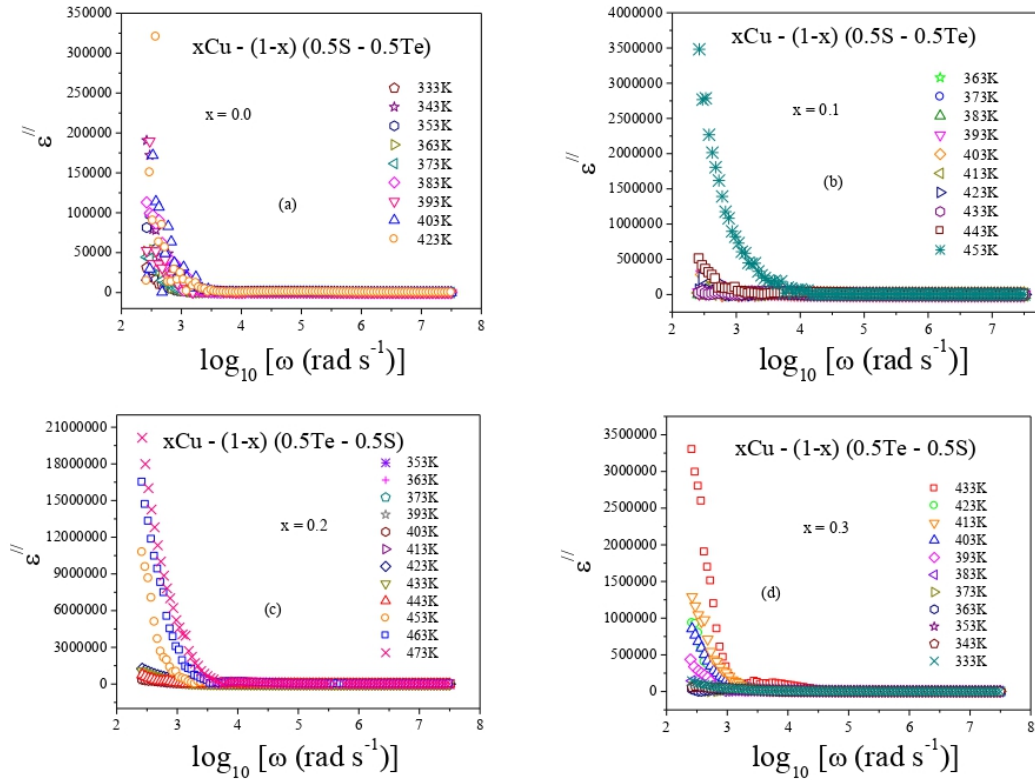


Fig-4.20: Variation of dielectric loss ϵ'' with frequency of the system $x\text{Cu} - (1-x) (0.5\text{S} - 0.5\text{Te})$ for $x =$ (a) 0.0 (b) 0.1 (c) 0.2 and (d) 0.3 at various temperatures

The increase of both ϵ' and ϵ'' on the increase of temperature can be observed from Fig-4.19 and Fig-4.20. This occurs mainly due the increase in polarization effect in the system because of decrease in bond energies as the intermolecular forces get weakened by the rise in temperature, which results in enhancing the orientational vibrations and increasing polarization. Fig-4.19 and Fig-4.20 also show the increase of both ϵ' and ϵ'' on increasing the value of x in the composition of the present system. This is a clear indication of higher conductivity in the present system having more value of x i.e., content of Cu.

4.3.7.2. Electric Modulus

The electrical relaxation properties of these glasses have been studied using electrical modulus formalism details of which has already been discussed in the section 2.4.3.2 of Chapter 2.

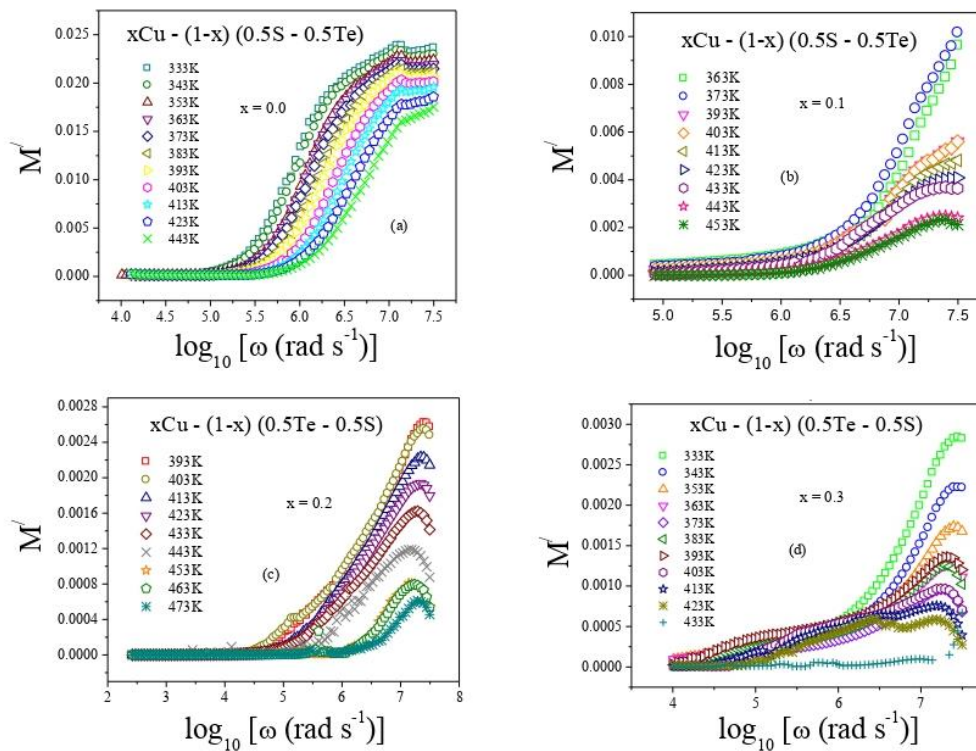


Fig-4.21: Variation of real electric modulus M' with frequency of Chalcogenide system $x\text{Cu} - (1-x) (0.5\text{S} - 0.5\text{Te})$ for $x =$ (a) 0.0 (b) 0.1 (c) 0.2 and (d) 0.3 at various temperatures

In Fig-4.21(a), (b), (c) and (d) the variation of real part of electric modulus M' with frequency is shown for the system having $x = 0.0, 0.1, 0.2$ and 0.3 respectively. In Fig-4.21 (a), (b) (c) and (d), M' is found to approach zero at all the mentioned temperatures and low frequency region which mainly occurs because of the suppression of electrode polarization because of unavailability of restoring forces of charge carriers [29-31]. But at higher frequencies,

dispersion in M' has been found and M' exhibits a maximum value which is: $(M_\infty) = (\epsilon_\infty)^{-1}$ because of the electrical relaxation of polarons [29-31]. In Fig-4.21 (a), (b) (c) and (d), a gradual decrease in M' with the rise of temperature is found which may implies the involvement of movement of polarons, within small range, in the conduction mechanism of the glassy system.

Fig-4.22(a), (b), (c) and (d) show the plots of imaginary electric modulus M'' against frequency of the system in which $x = 0.0, 0.1, 0.2$ and 0.3 respectively. The shifting of M'' peaks towards higher frequencies on increasing temperature, which can be observed in Fig-4.22, is a sign of temperature dependency of electrical relaxation in this glassy system. The movement of thermally activated charge carriers may reduce the relaxation time and increase the relaxation frequency. The hopping of polarons over long distances may be the cause of conduction in these glasses below the peak relaxation frequency ω_{\max} . Above ω_{\max} the cause of conduction mechanism may be the localized motion of charge carriers over short distances [30, 31]. The M'' peak shifting indicates the system stabilization in a small time at eminent temperature.

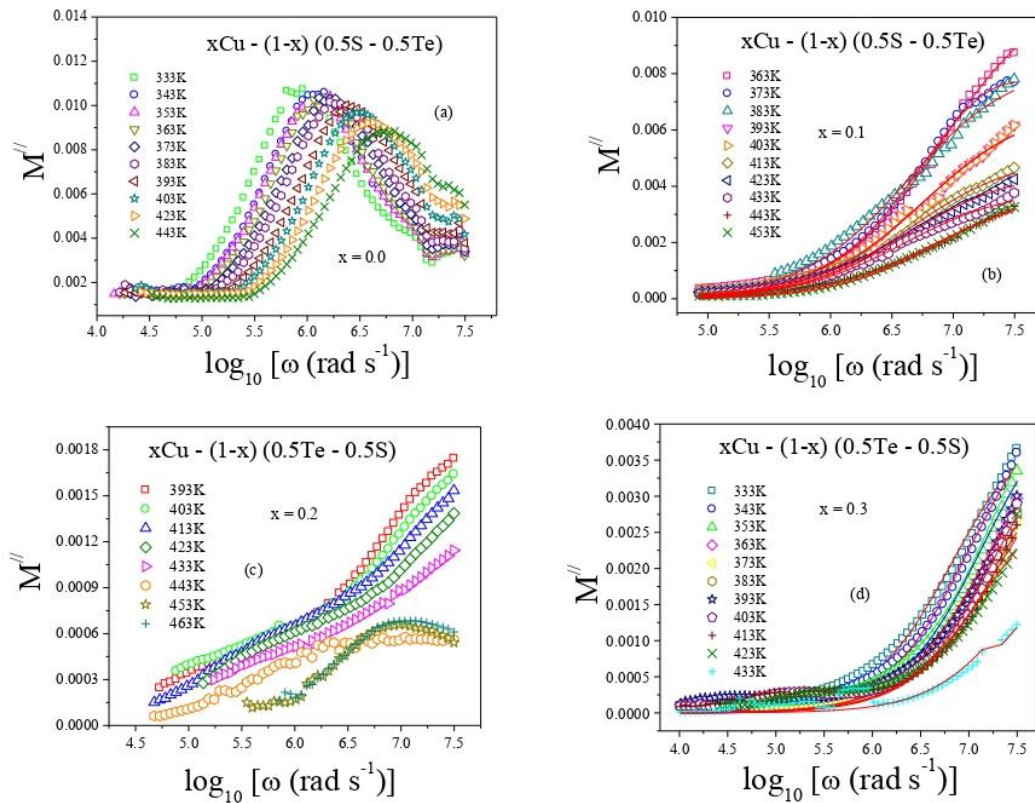


Fig-4.22: Variation of imaginary electric modulus M'' of Chalcogenide system $x\text{Cu} - (1-x) (0.5\text{S} - 0.5\text{Te})$ for $x =$ (a) 0.0 (b) 0.1 (c) 0.2 and (d) 0.3 at various temperatures

Fig-4.23 represents the variation of peak frequencies f_{\max} , frequencies at which M'' peaks occurred, with temperature for the system with $x = 0.0, 0.1, 0.2$ and 0.3 . Since temperature dependent behaviour can be observed from Fig-4.23, so Arrhenius equation has been applied to find the activation energy E_m for relaxation process associated with electric modulus of the system which can be expressed by:

$$f_{\max} = f_0 \exp\left(\frac{-E_m}{K_B T}\right) \quad (4.1)$$

where, f_0 is pre exponential factor. Electric modulus activation energy E_m of this system was measured from slopes of the straight lines obtained from linearly fitting of Fig-4.23 with Eqn. (4.1) and is shown in Table-4.10. The temperature dependency of f_{\max} (where, $\omega_m = 2\pi f_{\max}$, reciprocal of which indicates the relaxation time τ_m i.e. $\tau_m = 1/\omega_m$), is shown in Fig-4.23. The increase of f_{\max} and hence the decrease of relaxation time τ_m with increase of temperature could be observed from the Fig-4.23. It also indicates the increase of ω_m with increase of x value i.e. content of Cu in the system. Lower values of relaxation time directly indicate the higher conductivity due polaron hopping in the system.

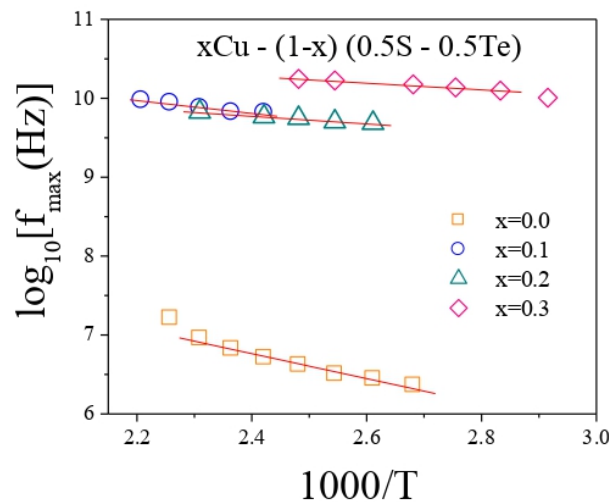


Fig-4.23: Variation of f_{\max} with temperature of system $x\text{Cu} - (1-x) (0.5\text{S} - 0.5\text{Te})$ system where, $x = 0.0, 0.1, 0.2,$ and 0.3

The decrease of activation energy on increasing amount of Cu in this system can be seen from Table-4.10. This is a clear indication of the increase of conductivity on increasing content of Cu in the system.

Table-4.10: Calculated values of E_m , associated with dielectric relaxation for $x\text{Cu} - (1-x)(0.5\text{S} - 0.5\text{Te})$ system

x	E_m (eV)
0.0	0.313339
0.1	0.160932
0.2	0.095573
0.3	0.083285

4.6.7.3. Electric Modulus Scaling

To analyze the relaxation process of this system dielectric modulus M'' scaling have been carried out. For this, the x-axis i.e., M'' values of Fig-4.22(a), (b), (c) and (d) have been divided by M''_{\max} (maximum value of imaginary modulus) and y-axis i.e., ω values, by ω_{\max} (the frequency at which M'' peak occurs). Fig-4.24(a), (b), (c) and (d) represent the temperature scaling of electric modulus M'' plots of the present system having $x = 0.0, 0.1, 0.2$ and 0.3 respectively at different temperatures in the range from 343K to 453K. In Fig-4.24(a), (b), (c) and (d) overlapping of all the scaled data has been found which proves that the relaxation process in this system is not dependent on temperature.

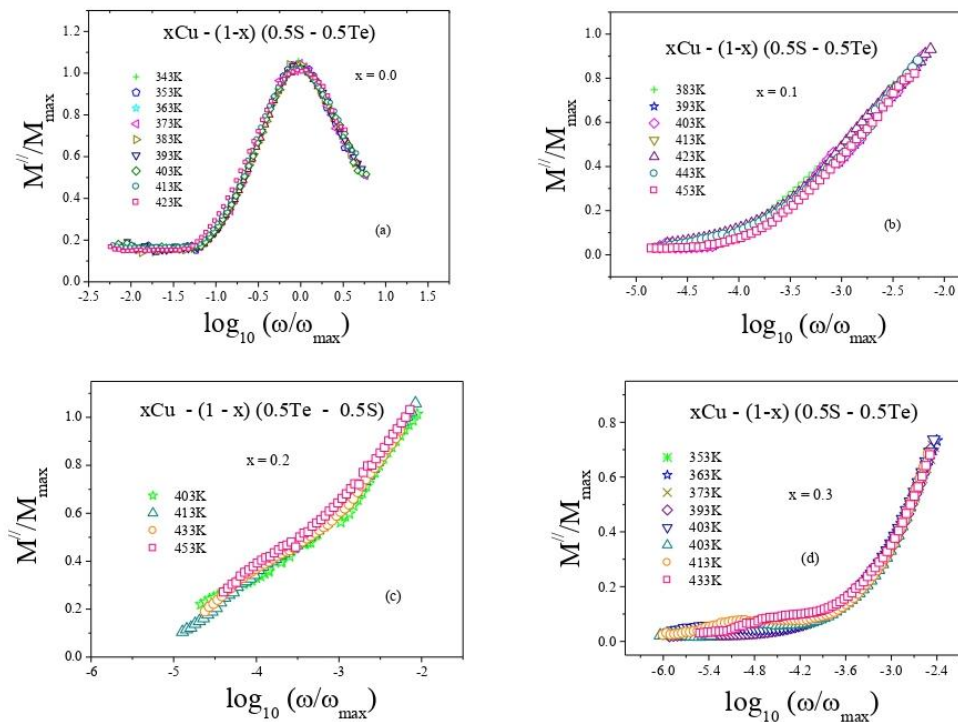


Fig-4.24: Temperature scaling of M'' for the system $x\text{Cu} - (1-x)(0.5\text{S} - 0.5\text{Te})$ having $x =$ (a) 0.0 (b) 0.1 (c) 0.2 and (d) 0.3

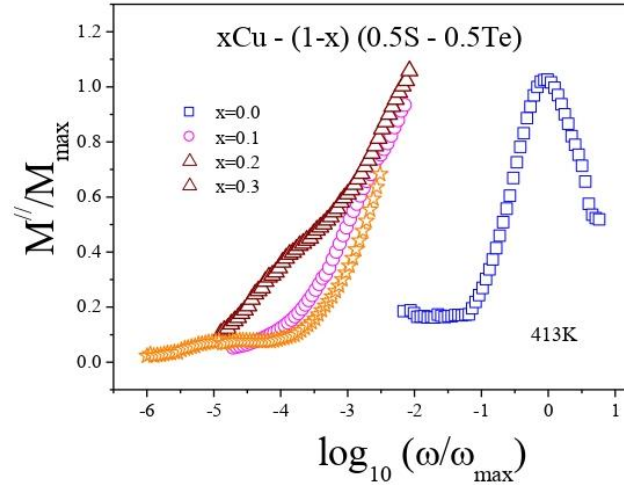


Fig-4.25: Composition scaling of M'' of Chalcogenide glassy system $x\text{Cu} - (1-x) (0.5\text{S} - 0.5\text{Te})$ where $x = 0.0, 0.1, 0.2$ and 0.3 at 413K

In Fig-4.25 the composition scaling in which electric modulus M'' plots of the present system having $x = 0.0, 0.1, 0.2$ and 0.3 at a fixed temperature (413K) is shown. The non-overlapping of the plots in Fig-4.25 clearly signifies that the electric relaxation of this system is dependent on composition of the glassy system. So, the temperature independent and composition dependent nature of relaxation process can be observed from the electric modulus scaling process of the present glassy system.

4.4.CONCLUSION

The preparation of Chalcogenide glassy system having composition $x\text{Cu} - (1-x)(0.5\text{S} - 0.5\text{Te})$, where $x = 0.0, 0.1, 0.2$ and 0.3 was carried out with the help of melt-quenching process. With the help of XRD analysis, the structural information of the system was obtained. From the XRD analysis, the size of the different phases present in the system with their $[h,k,l]$ values, dislocation density and CVF have been calculated. The crystallite size was found to increase and dislocation density was found to decrease when the amount of Cu is increased in the system.

From TEM analysis, the presence of various nanoparticles in the system has been found. Using TEM, area of nanoparticles in the system has been calculated. The average area of nanoparticles in the system is 269.7 nm^2 . The interplanar spacings (D) between different crystalline phases in the system have been calculated from SAED pattern obtained from TEM technique. From the analysis of FT-IR Spectroscopy technique, a good transparency of this

system in the spectral range $4000\text{cm}^{-1} - 400\text{cm}^{-1}$ can be observed and most of the absorption bands can be assigned to vibrational bands of oxides and hydrides bonds which arise due to the presence of extrinsic impurities in the system introduced during its preparation. FT-IR spectra indicate the presence of different functional groups and molecules like O-H, C-H, C-O, Te-O and H₂O in the system.

To study the electrical properties of the present system, DC and AC conductivity measurements at different temperatures (range: 333K – 463K) and frequencies (range: 42 Hz – 5 MHz) and have been carried out. The increase of DC conductivity on increasing x or content of Cu in the system has been seen. For the analysis of DC conductivity data at lower temperatures, Mott's VRH model and at higher temperatures Greaves model was used. From the analysis, the decrease of density of localized states with the increase of Cu content in system has been observed. With less density of localized states in the sample with $x = 0.3$, the possibility of collision among polarons get decreased which can increase the conductivity due to hopping of polarons in the system.

Temperature dependent DC conductivity points to the semiconductor type nature of this system. The Cole-Cole plots confirm the decrease of system's resistance on increasing amount of Cu in the system. The decrease of density and increase of molar volume was observed on increasing the content of Cu.

For analysing AC conductivity data of the system, Power Law, Almond West formalism and MN Rule have been used. For interpreting the conduction mechanism in the system, CBH Model is found as the most appropriate model for the system having values of $x = 0.1$ and 0.3 and for $x = 0.0$ and 0.2 the NSPT (modified) model is found as the most suitable. AC conductivity scaling signifies that the system's relaxation process is not dependent on temperature but is dependent on its composition. The increase in mobility of charge carriers and decrease in carrier density were observed with enhancement of amount of Cu in this system

Almond West model has been applied for the analysis of AC conductivity data from which E_H of this system has been calculated. E_H is found to reduce with amount of Cu in the system. Study of dielectric relaxation has been carried out from which the decrease of ϵ' and ϵ'' with the increase of frequency and decrease of temperature has been seen. Activation energy associated with the relaxation process in the glass has been calculated from the analysis of the electric modulus plots which is found to be reduced on increasing the values of x. From the

temperature scaling of M'' spectra, the overlapping of imaginary electric modulus spectra at different temperatures points towards non dependency of system's dielectric relaxation on temperature. In composition scaling, the non-overlapping of imaginary electric modulus spectra on a single master curve at a particular temperature for different compositions has been found. It points towards the system's relaxation process dependency on its composition. Hence the dielectric relaxation of this system is temperature independent and composition dependent.

REFERENCES

- [1] A. Mansingh, J. K. Vaid and R. P. Tondon, *J. Physics. C Solid State Physics*, 10, 4061 (1977)
- [2] F. Skuban, S. R. Lukić-Petrović, M. V. Šiljegović, D. M. Petrović and M. Slankamenac, *Chalcogenide Letters*, 15,7 (2018)
- [3] A. V. Danilov and R. L. Myuller, *Zh. Prikl. Khim.*, 35, 2012 (1962)
- [4] A. V. Danilov and El Mosli, *Fiz. Tverd. Tela.*, 5, 2105 (1963) [*Sov. Phys.-Solid State*. 5 1472 (1963)]
- [5] R. Andreichin, *Jnl. Non Cryst. Solids*, 4, 73 (1970)
- [6] B. T. Kolomiets, Y. V. Rukhladev, and V. P. Shilo, *J. Non Cryst. Solids*, 5, 402 (1971)
- [7] Juejun Hu, Xiaochen Sun, A. M. Agarwal, Jean-Francois Viens, Lionel C. Kimerling, L. Petit, N. Carlie, K. C. Richardson, T. Anderson, J. Choi and M. Richardson, *Journal of Applied Physics* 101, 063520 (2007)
- [8] S. Jobic, R. Brec and J. Rouxel, *Solid State Chemistry*, 96, 169 (1992)
- [9] A. L. N. Stevels and G. A. Wiegers, *Recl. Trav. Chim. Pays-Bas.*, 90, 352 (1971)
- [10] Y. G. Asadov, G. B. Gasymov, K. M. Dzhafarov and L. V. Rustamova, *Sov. Phys. Crystallogr*, 36, 84 (1991)
- [11] M. Pupp, J. Weiss and Z. Anorg. Allg. Chem., 440, 31 (1978)
- [12] H. Fjellvag, F. Gronvold, S. Stolen, A. F. Andresen, R. Mueller-Kaefer, A. Simon. *Z. Kristallogr.*, 184, 111 (1988)
- [13] A. Kjekshus and T. Rakke, *Acta Chem. A Scand*, 33, 617 (1979)
- [14] M. Leon, N. Terao and F. Rueda, *Phys. A Solidi Status*, 67, 11 (1981)
- [15] S. Kashida and K. Yamamoto, *J. Phys. Condens. Matter*, 3, 6559 (1991)

- [16] A. Janosi, *Acta Crystallogr.* 17, 311 (1964)
- [17] E. J. Mittemeijer, R. H. J. Fastenau and R. P. Van Ingen, *J. Applied Physics*, 76, 1871 (1994)
- [18] Y. Ohmasa, I. Yamamoto, M. Yao and H. Endo, *J. Phys. Soc. Jpn.*, 64, 4766 (1995)
- [19] R. Steudel, O. Schumann, J. Buschmann and P. Luger, *Angew. Chem.* 110, 2502 (1998)
- [20] T. S. Kavetskiy, A. P. Kovalskiy, V. D. Pamukchieva and O. I. Shpotyuk, *Infrared Phys. Tech.*, 41, 41 (2000)
- [21] G. Socrates, “Infrared and Raman Characteristic Group Frequencies”, 3rd Edition, John Wiley & Sons Ltd. (2004)
- [22] M. Efimov and V. G. Pogareva, *J. Non-Cryst. Solids*, 275, 189 (2000)
- [23] V. Pamukchieva, K. Todorova, O. C. Mocioin, M. Zaharescu, A. Szekeres and M. Gartner, *J. Physics*, 356, 012047 (2012)
- [24] D. Munoz-Martin, M. A. Villegas, J. Gonzala and J. M. Fernandez-Navarro, *J. Eur. Ceram. Soc.*, 29, 2903 (2009)
- [25] B. Frumarova, J. Oswald, P. Krecmer, M. Frumar, V. Cerny and V. Smrcka, *Opt. Mater.*, 6, 217 (1996)
- [26] D. P. Almond, G. K. Duncan and A. R. West, *Solid State Ionics*, 8, 159 (1983)
- [27] B. Roling, A. Happe, F. Funke and M. D. Ingram, *Phy. Rev. Lett.*, 78, 2160 (1997)
- [28] S. K. Dwivedi, M. Dixit and A. Kumar, *J. Mater. Sci. Lett.* 17, 233 (1998)
- [29] A. B. Karmakar, K. Rademann Andrey and L. Stepanov, *Glass Nanocomposites, Synthesis, Properties and Applications*, Elsevier Inc. (2016)
- [30] S. Ojha, M. Roy, A. Chamuah, K. Bhattacharya and S. Bhattacharya, *Materials Letters* 258, 126792 (2020)
- [31] S. Bhattacharya and A. Ghosh, *J. Am. Cer Soc.* 91, 753 (2008)

Chapter 5

STUDY OF ELECTRICAL CONDUCTIVITY AND DIELECTRIC RELAXATION OF $\text{Ag}_2\text{S} - \text{Se} - \text{Ge}$ GLASSY SYSTEM

5.1. INTRODUCTION

In this chapter, the effect of Ag_2S doping on electrical properties of Selenium - Germanium based Chalcogenide system having composition $x\text{Ag}_2\text{S} - (1-x) (0.5\text{Se} - 0.5\text{Ge})$ where, $x = 0.1$ and 0.2 , has been discussed. Selenium possesses reversible phase transformation property [1] because of which it can be used in many applications like rectifiers, photocells, switching, memory devices etc. But it has some drawbacks also like small life span and low photo sensitivity. To conquer this problem, it is doped with elements having high sensitivity, crystallization temperature and smaller ageing effects [2]. The glass transition temperature of Se based glassy systems can be increased by addition of Ge to the system [3]. Ge also helps in improving the corrosion resistance [4]. However, Se-Ge based systems are not thermally stable leading to crystallization. To improve the stability, addition of Ag_2S to this system has been attempted. Ag_2S possesses many attractive properties like narrow band gap, low cost, good chemical stability, and optical properties which make it usable in various applications such as photovoltaic cells, infrared detectors, superionic conductors, photoelectric switches, gas sensors etc [5].

In this chapter, preparation of Ag_2S doped Se-Ge glassy system with the help of melt-quenching method is discussed. For carrying out structural analysis of this system, different structural characterization techniques like XRD, UV-Vis, FT-IR, molar volume and density calculations etc have been used. XRD is a very powerful tool used for characterization of a material. Here, calculation of crystallite size, dislocation density, lattice strain and crystalline volume fraction of the prepared glassy system is reported. UV-Vis spectroscopy is another practice which is used for the structural analysis of a system. In this chapter the calculation of optical band gap energy of this system using UV-Vis method is reported. Here, FT-IR Spectroscopic study of the prepared glassy system is also reported which is a structural characterization technique used to obtain information about the presence of impurities and

their chemical bonding in a material. Measurement of density and molar volume of a glassy system also play a very important role for its structural analysis.

The DC and AC conductivity measurements of the present system have been undertaken to obtain the information regarding electrical properties. The DC conductivity of the system was interpreted with the help of Mott's VRH Model at low temperature region. For higher temperature DC conductivity, Greaves's Model was used. With the help of these two models, the density of localized states $N(E_F)$ in this system can be determined. For the analysis of AC conductivity of these glasses, different models and methods have been used like: Power Law, Almond West Formalism, MN Rule, AC conductivity scaling, dielectric relaxation studies etc. To know the information regarding the conduction mechanism of these glasses, the AC conductivity data have been tried to fit with various models like CBH, NSPT, OLPT etc. Scaling of AC conductivity is useful to find the temperature and composition dependency of charge carriers' relaxation dynamics in the system. Measurements of carrier mobility and carrier density in the system have also been reported here. To study electrical relaxation properties of this glassy system, its permittivity and electrical modulus measurements and their analysis have also been carried out.

5.2. PREPARATION OF THE GLASSY SYSTEM

Glassy alloys of $x\text{Ag}_2\text{S} - (1-x)(0.5\text{Se} - 0.5\text{Ge})$ where, $x = 0.1$ and 0.2 were prepared using melt quenching process. All the necessary chemicals i.e. Silver-Sulphide, Selenium and Germanium of high purity (Aldrich 99.9%) were weighted as per the atomic percentages and then mixed and crushed to a very fine powder in a mortar. As Chalcogenide glasses are having tendency to react with oxygen at high temperature, so the mixture was sealed in quartz ampoules under a vacuum of 10^{-4} Torr to reduce this tendency. The ampoules were then kept into a furnace where the temperature was raised at a rate of 3°C per minute to 250°C . After two hours the temperature of furnace was increased with the same rate to 750°C and the ampoules were kept at that temperature for about two hours. Temperature of the furnace was then raised to 900°C . After one hour the ampoules containing the melted mixture of the elements were taken out of the furnace and kept immediately in a bowl containing crushed ice for rapid cooling of the melt. The obtained glassy materials were then ground to fine powder using a mortar for structural characterization. For confirming glassy and partially crystalline nature of the materials, XRD technique has been used. For DC and AC

measurements, pellets of the as prepared samples were formed using pelletizer in which the powdered samples were kept under a pressure of 80Kg/cm^2 for about 1 hour 30 minutes. Coating of Silver paste on both the opposite sides of the formed pellets was done to make sure good electrical contact between electrode and the pellet. To carry out DC conductivity measurements of the system, two-probe method has been used using ‘Metravi’ Digital Multimeter (model no. 450 DMM). For AC conductivity measurements at different temperatures (333K - 533K) and in the frequency range from 42Hz to 5MHz, Hioki made LCR Hi-Tester has been used.

5.3. RESULTS AND ANALYSIS

5.3.1. XRD

5.3.1.1. Calculations of Crystallite Size, Dislocation Density and Lattice Strain

XRD patterns of the samples of the $x\text{Ag}_2\text{S} - (1-x) (0.5\text{Se} - 0.5\text{Ge})$ system with $x = 0.1$ and 0.2 are shown in Fig-5.1. The presence of peaks in the pattern points to the polycrystalline nature of the system.

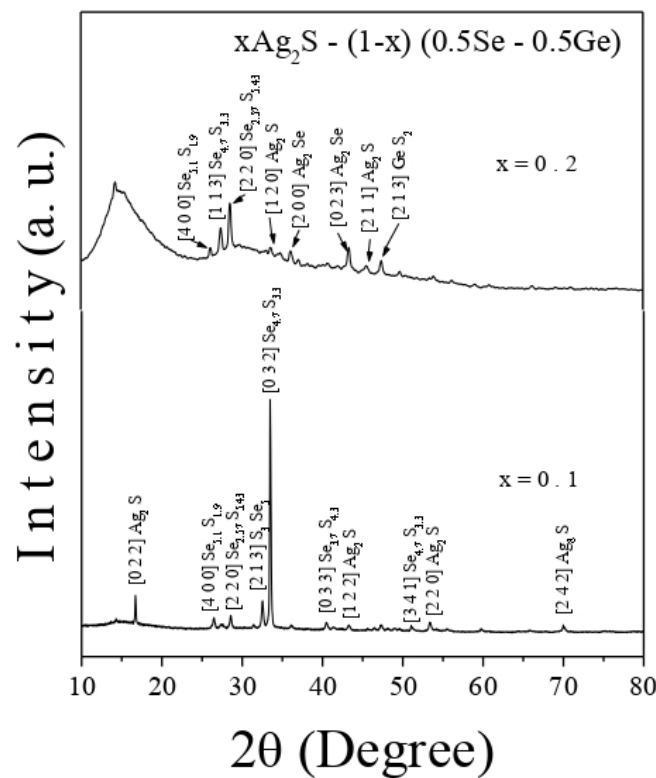


Fig-5.1: XRD diffractograms of Chalcogenide system $x\text{Ag}_2\text{S} - (1-x) (0.5\text{Se} - 0.5\text{Ge})$ with $x = 0.1$ and 0.2

Due to the formation of different nano-crystallites, several peaks having the [h k l] values: [0 2 2], [1 2 2], [2 2 0], [1 2 0]– for Ag₂S (JCPDS No. 03-0844); [4 0 0] – for Se_{5.1}S_{1.9} (JCPDS No. 78-0266); [2 2 0] – for Se_{2.57}S_{5.43} (JCPDS No. 73-2267); [0 3 2], [3 4 1], [1 1 3] – for Se_{4.7}S_{3.3} (JCPDS No. 71-0248); [2 4 2] – for Ag₈S (JCPDS No. 83-0674); and [2 0 0], [0 2 3] – for Ag₂Se (JCPDS No. 71-2410) can be observed in the XRD pattern.

In Table-5.1 the crystallite sizes of different phases with their Miller indices formed in the glassy system for x = 0.1 and 0.2 is shown. On the increase of the value of x i.e. the Ag₂S content in the composition of the system, its polycrystalline nature has been found to decrease. Crystallite size, dislocation density and lattice strain of the prepared glass samples have been calculated using Eqns. (2.4), (2.5) and (2.6) respectively of Chapter 2. Table-5.1 also shows the values of dislocation density and lattice strain of this system.

From Table-5.1 it can be observed that the average crystallite size of different nano-crystallites decreases and dislocation density increases on increasing the values of x in the composition. The increase in dislocation density with the increase of Ag₂S increases the disorder in the system.

Table-5.1: Crystallite Size, Dislocation Density and Lattice Strain of xAg₂S - (1 - x) (0.5Se – 0.5Ge) glassy system with x = 0.1 and 0.2

x	Crystallite Size (in nm)		[h k l]	Dislocation Density (nm ⁻²)	Lattice Strain
0.1	Ag ₂ S	40.97	[0 2 2] [1 2 2] [2 2 0]	0.000943	0.028979
	Se _{5.1} S _{1.9}	31.91	[4 0 0]		
	Se _{2.57} S _{5.43}	35.84	[2 2 0]		
	S ₃ Se ₅	38.38	[2 1 3]		
	Se _{4.7} S _{3.3}	42.10	[0 3 2] [3 4 1]		
	Se _{3.7} S _{4.3}	27.63	[0 3 3]		
	Ag ₈ S	25.83	[2 4 2]		
0.2	Ag ₂ S	20.95	[1 2 0] [2 1 1]	0.001681	0.02584
	Se _{5.1} S _{1.9}	31.11	[4 0 0]		
	Se _{2.57} S _{5.43}	29.19	[2 2 0]		
	Ag ₂ Se	26.25	[2 0 0] [0 2 3]		
	Se _{4.7} S _{3.3}	28.18	[1 1 3]		
	GeS ₂	24.78	[2 1 3]		

5.3.1.2. Crystalline Volume Fraction

The crystalline volume fraction of the glassy samples has been calculated using Eqn. (3.1) of Chapter 3.

Table-5.2: Crystalline volume fraction calculation of $x\text{Ag}_2\text{S} - (1 - x) (0.5\text{Se} - 0.5\text{Ge})$ system

x	h k l	Phase	Area (I_{hkl})	$K_{hkl} = I_{hkl} / I_a$	Crystalline volume fraction, X_{XRD} $= I_{hkl} / (I_a + K_{hkl} * I_{hkl})$
0.1	0 2 2	Ag_2S	177.31	0.09126	0.0905
	4 0 0	$\text{Se}_{5.1}\text{S}_{1.9}$	126.91	0.06532	0.06504
	2 2 0	$\text{Se}_{2.57}\text{S}_{5.43}$	139.54	0.07182	0.07145
	2 1 3	S_3Se_5	326.24	0.16791	0.1633
	0 3 2	$\text{Se}_{4.7}\text{S}_{3.3}$	1943.0	1	0.5
	0 3 3	$\text{Se}_{3.7}\text{S}_{4.3}$	97.901	0.05039	0.05026
	1 1 2	Ag_2S	73.445	0.0378	0.03775
	3 4 1	$\text{Se}_{4.7}\text{S}_{3.3}$	62.606	0.03222	0.03219
	2 2 0	Ag_2S	131.75	0.06781	0.0675
	2 4 2	Ag_8S	80.684	0.04153	0.04145
0.2	4 0 0	$\text{Se}_{5.1}\text{S}_{1.9}$	24.365	0.1961	0.18884
	1 1 3	$\text{Se}_{4.7}\text{S}_{3.3}$	72.706	0.58516	0.4359
	2 2 0	$\text{Se}_{2.57}\text{S}_{5.43}$	124.25	1	0.5
	2 0 0	Ag_2Se	40.302	0.32436	0.29348
	0 2 3	Ag_2Se	57.049	0.45915	0.3792
	2 1 1	Ag_2S	30.104	0.24229	0.22885
	2 1 3	GeS_2	40.482	0.32581	0.29454

The crystalline volume fractions of the present glassy system having $x = 0.1$ have been obtained as: 0.09, 0.038 and 0.068 corresponding to the phase Ag_2S having [h k l] values [0 2 2], [1 1 2] and [2 2 0] respectively; 0.068 for the phase $\text{Se}_{5.1}\text{S}_{1.9}$ having [h k l] values [4 0 0]; 0.071 for the phase $\text{Se}_{2.57}\text{S}_{5.43}$ with [h k l] values [2 2 0]; 0.163 for the phase S_3Se_5 having [h k l] values [2 1 3]; 0.5 and 0.032 for the phase $\text{Se}_{4.7}\text{S}_{3.3}$ with [h k l] values [0 3 2] and [3 4 1] respectively; 0.05 for the phase $\text{Se}_{3.7}\text{S}_{4.3}$ with [h k l] values [0 3 3]; and 0.04153 corresponds to the phase Ag_8S with [h k l] values [2 4 2]. Similarly crystalline volume fractions of the present system with $x = 0.2$ have also been calculated, the details of which is shown in Table-5.2. The crystalline volume fraction percentage is found to be increased from 11% to 33% on increasing the value of x from 0.1 to 0.2 in the glass composition as indicated in Table-5.3.

Table-5.3: Crystalline Volume fraction (%) of $x\text{Ag}_2\text{S} - (1 - x) (0.5\text{Se} - 0.5\text{Ge})$ system

Values of x	Crystalline Volume fraction (%)
0.1	11.19
0.2	33.15

5.3.2. UV-Vis Spectroscopy

UV-Vis spectroscopy has been used for structural analysis of present glassy system. This technique has already been explained in Section 2.3.4 of Chapter 2. Absorption coefficient $\alpha(\nu)$ i.e., the degree of absorption of light by the glassy sample at distinct wavelengths has been measured with the help of Eqn. (2.8) of Chapter 2. Using this technique, optical band gap energy of this system was calculated by using Eqn. (2.9) of Chapter 2.

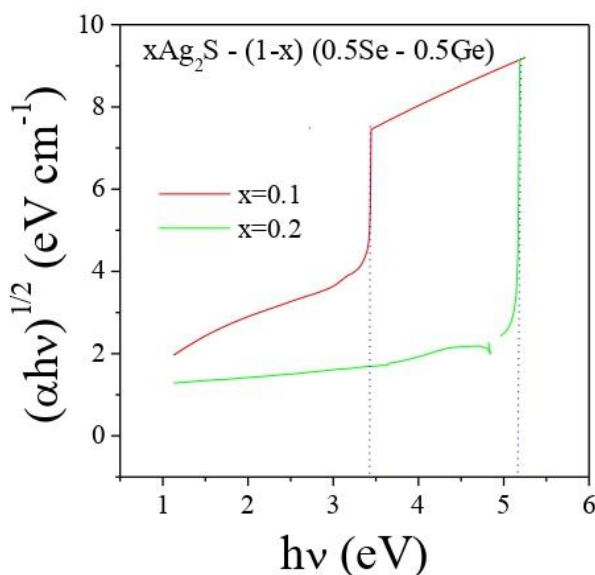


Fig-5.2: Tauc's plots of Chalcogenide glassy alloys of $x\text{Ag}_2\text{S} - (1-x) (0.5\text{Se} - 0.5\text{Ge})$ where, $x = 0.1$ and 0.2

In Fig-5.2 Tauc's plot of the present system is shown in which $(\alpha h\nu)^{1/2}$ is plotted against $h\nu$ for values of x equal to 0.1 and 0.2. From the Tauc's plot the optical band gap energy E_{opt} has been calculated and is shown in Table-5.4. E_{opt} is found to increase on increasing the amount of Ag_2S in the present system.

Table-5.4: Optical band gap energy of $x\text{Ag}_2\text{S} - (1-x) (0.5\text{Se} - 0.5\text{Ge})$ system

x	E_{opt} (eV)
0.1	3.42
0.2	5.16

5.3.3. FT-IR

FT-IR transmittance spectra of present glassy system in the spectral range $4000\text{cm}^{-1} - 400\text{cm}^{-1}$ are shown in Fig-5.3. Appearance of bands near wave number 1640cm^{-1} and in the range $3700 - 3300\text{cm}^{-1}$ is associated with stretching and bending vibrations of hydroxyl group in

the system [6-8]. A strong absorption band is appeared in the range $900 - 730 \text{ cm}^{-1}$ which may be related to the stretching vibration of the bond Ge – O [7].

Most of the absorption bands in the spectra of the present glassy system are related to the oxides and hydrides impurities which may be introduced in the system from the environment or from precursors and quartz ampoules during its preparation [9] as Chalcogenide glassy systems containing Sulphur are having greater affinity to absorb water related particles. The appearance of band at $500\text{--}650\text{cm}^{-1}$ is due to the characteristic vibration of Ag–S in the system [10].

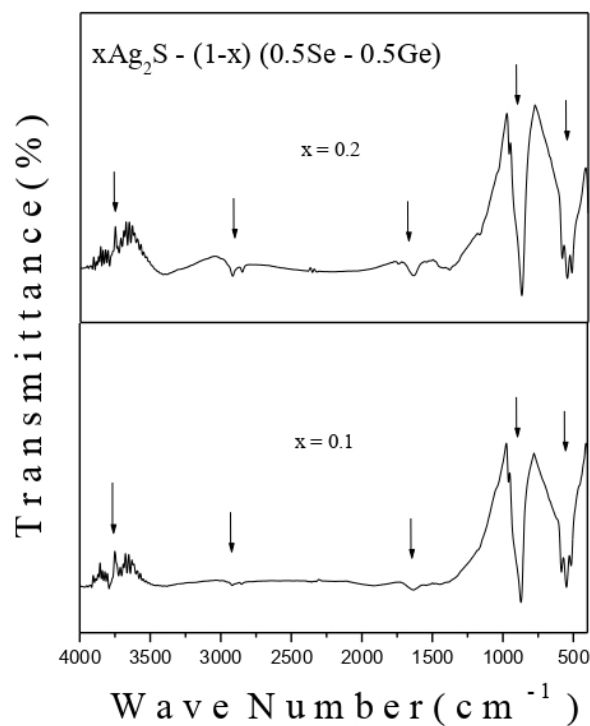


Fig-5.3: FT-IR transmittance spectra of the Chalcogenide system $x\text{Ag}_2\text{S} - (1-x) (0.5 \text{ Se} - 0.5 \text{ Ge})$ where, $x = 0.1$ and 0.2

5.3.4. Density and Molar Volume

Density ρ and molar volume V_M measurements of a system play very important role to analysis its structure. To calculate the Density (ρ) of the present glassy system, Archimedes principle has been applied which has been expressed as Eqn. (3.3) of Chapter 3. To calculate the molar volume of the present glassy system Eqn. (3.4) of Chapter 3 has been used. Table-5.5 shows the measured ρ and V_M values of this system for different values of x .

Table-5.5: Values of ρ and V_M of system $xAg_2S - (1-x) (0.5Se - 0.5Ge)$ where $x=0.1$ and 0.2

x	ρ (gm/cm ³)	V_M (cm ³ /mol)
0.1	6.39	14.55
0.2	5.88	18.74

In Fig-5.4, the variation of ρ and V_M with different values of x in the system is shown.

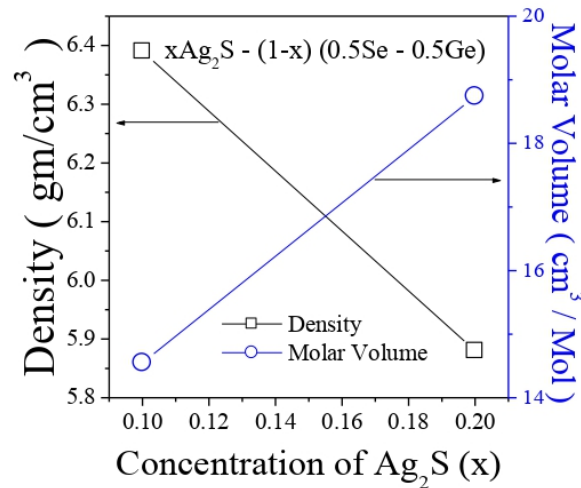


Fig-5.4: Variation of density and molar volume with different values of x of Chalcogenide glassy system $xAg_2S - (1-x) (0.5 Se - 0.5 Ge)$

The decrease of ρ and increase of V_M with the increase of the value of x can be observed from Fig-5.4. High value of density in a glass is an indication of closely packed particles in the structure.

5.3.5. DC Conductivity

From the electrical conductivity study of a material, information regarding nature of the defect centres can be obtained which assist to determine the type of conduction mechanisms in the material [11]. Density of defect states in mobility gaps - control the electrical properties in Chalcogenide glasses [11].

DC conductivity of the present glassy system has been measured at diverse temperatures. The DC conductivity variation of the system, having values of $x = 0.1$ and 0.2 , with temperature is shown in Fig-5.5. The figure indicates that with the increase of x i.e., content of Ag_2S in this system, DC conductivity increases. From Fig-5.5 information regarding structural defects and density of localized states in system has been obtained. Fig-5.5 indicates the

semiconducting behaviour of the present glassy system as the DC conductivity is found to enhance with rising of temperature.

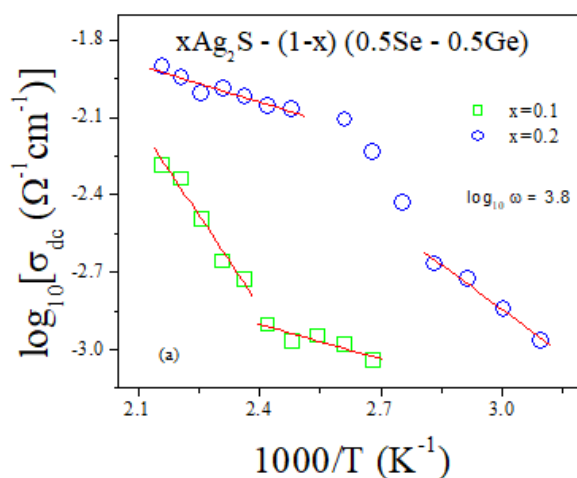


Fig-5.5: Variation of DC Conductivity with temperature of Chalcogenide system $x\text{Ag}_2\text{S} - (1-x) (0.5\text{Se} - 0.5\text{Ge})$ where, $x = 0.1$ and 0.2

Activation energies of the system correspond to DC conductivity for $x = 0.1$ and 0.2 were calculated from slopes of the straight lines obtained from linear fitting of the plots of Fig-5.5 at lower and higher temperature regions and are shown in Table-5.6. The reduction of activation energy on increasing x i.e., Ag_2S content, at higher temperature region can be observed from Table-5.6. But at the lower temperature region, enhancement of activation energy on increasing x in the composition of the glassy system is found. The presence of grain boundary effect may be the cause of this discrepancy at lower temperature region.

Table-5.6: Activation energy calculated from linear fitting of DC conductivity plots at lower and higher temperature region

x	Activation Energy at low temperature (eV)	Activation Energy at high temperature (eV)
0.1	0.088	0.47
0.2	0.23	0.095

There is a slight increase in DC conductivity with temperature, as shown in Fig-5.5, which is affected by the presence of defects in structure and impurities in the system at lower temperature region. This is an indication of the occurrence of conduction in this region through variable range hopping of polarons in the localized states, which was predicted by

Mott's VRH Model. At higher temperatures, DC conductivity increases rapidly, as shown in Fig-5.5, with the increase of temperature which has been analysed with Greaves's Model, according to which the electrical conduction in the system takes place because of the tunnelling of polarons in extended states due to the rise in temperature. The details of Mott's and Greaves's Models have been discussed in Section 3.3.5 of Chapter 3.

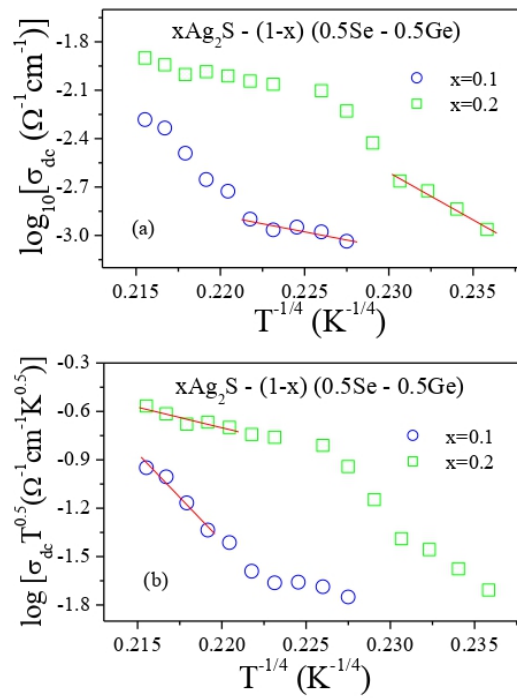


Fig-5.6: DC Conductivity plots of system $x\text{Ag}_2\text{S} - (1-x) (0.5\text{Se} - 0.5\text{Ge})$ fitted with (a) Mott's Model and (b) Greaves's Model

Fig-5.6(a) shows variation of DC conductivity with respect to $T^{-0.25}$. The density of states at Fermi level $N(E_F)$ was obtained from the slopes of linear fitting of the data in Fig-5.6(a) at lower temperature region with Eqn. (3.5) of Chapter 3. Table-5.7 shows the values of $N(E_F)$ for different values of x in the present glassy system. From Table-5.7 the decreases of $N(E_F)$, calculated from Mott's model, can be observed on increasing the content of Ag_2S in the system which is because of the presence of grain boundary effects at the lower temperature region [12].

In Fig-5.6(b), $\log(\sigma_{DC}T^{1/2})$ is plotted against $T^{-0.25}$. To calculate $N(E_F)$, data in Fig-5.6(b) have been linearly fitted with Eqn. (3.7) of Chapter 3 at high temperature region (Greaves' model) and values of $N(E_F)$ were calculated from slopes of the fitted straight lines and are shown in Table-5.7. From Table-5.7 it can be seen that $N(E_F)$, calculated from Greaves's

model, increases on increasing x in the system which indicates the development of more localised states for hopping of polarons.

Thus it can be concluded from Table-5.7 that in lower temperature region the decrease of $N(E_F)$, obtained from Mott's model, with increase of Ag_2S in the system may lowers the conductivity because of less polaron hopping among the states. Whereas, the increase of $N(E_F)$ with the increase of Ag_2S at higher temperature region (obtained from Greaves's model) enhances the probability of hopping of polarons among the localized states and thus increases the conductivity in the system. This analysis is in accord with the results shown in Table-5.6, i.e., increase in activation energy or decrease in conductivity in lower temperature region and decrease in activation energy or increase in conductivity in higher temperature region.

Table-5.7: Values of $N(E_F)$ obtained using Mott's and Greaves's models and MN energy of system $xAg_2S - (1-x)(0.5Se - 0.5Ge)$

Values of x	$N(E_F)$ (Mott's Model) ($eV^{-1}cm^{-3}$)	$N(E_F)$ (Greaves's Model) ($eV^{-1}cm^{-3}$)	ΔE_{MN} (eV)
0.1	2.3968E+21	3.41717E+28	0.14
0.2	3.33671E+19	1.13565E+31	0.11

5.3.6. AC Conductivity

5.3.6.1. Power Law

Jonscher's power law equation, which has been discussed in Section 3.3.6.1 of Chapter 3, has been used for expressing frequency dependent AC conductivity of the system. The plots of AC conductivity data with respect to frequency at higher frequency region and at various temperatures are shown in Fig-5.7(a) and (b) for the present system with $x = 0.1$ and 0.2 respectively. The AC conductivity data is fitted with least square straight line using Eqn. (3.9) of Chapter 3. The solid lines in Fig-5.7 indicate the fitting. Values of S were calculated from the slopes of the solid lines.

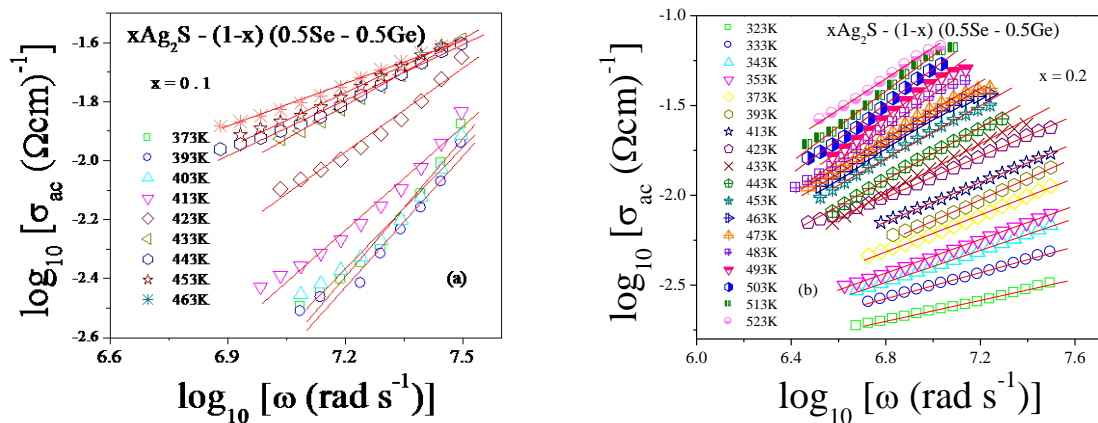


Fig-5.7: High frequency conductivity spectra of Chalcogenide glassy system $x\text{Ag}_2\text{S} - (1-x) (0.5\text{Se} - 0.5\text{Ge})$ for (a) $x = 0.1$ and (b) $x = 0.2$. Solid lines indicate best-fitted straight lines, slopes indicate ‘S’

Fig-5.8(a) and (b) show the variation of S with temperature for this system with $x = 0.1$ and 0.2 respectively. The availability of different models for the analysis of AC conduction mechanisms in amorphous semiconductors have been discussed in Section 3.3.6.1 of Chapter 3.

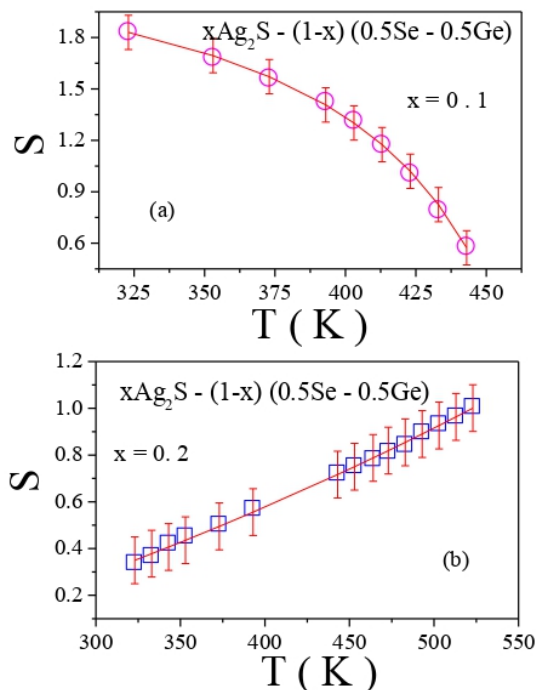


Fig-5.8: S-T plot of Chalcogenide glassy system $x\text{Ag}_2\text{S} - (1-x) (0.5\text{Se} - 0.5\text{Ge})$ for (a) $x = 0.1$ and (b) $x = 0.2$. Solid lines indicate the fitting of plots with CBH Model for $x = 0.1$ and with modified NSPT Model for $x = 0.2$

To know the actual conduction mechanism in the present system, Fig-5.8(a) and (b) have been tried to fit with those models. It is found that in Fig-5.8(a) where $x = 0.1$, the value of S decreases with temperature T . Fig-5.8(a) is found to be fitted with CBH model (the detail of which is given in Section 3.3.6.1 of Chapter 3). Fig-5.8(b), in which S is found to increase on increasing temperature, is successfully fitted with Modified NSPT Model. Detail of this model is also given in Section 3.3.6.1 of Chapter 3. All the fitting parameters i.e., τ_0 , τ_H , W_H , W_m and T_0 , obtained from the fitting of Fig-5.8(a) with Eqn. (3.10) of Chapter 3 and Fig-5.8(b) with Eqn. (3.13) of Chapter 3, are presented in Table-5.8.

Table-5.8: Fitting parameters of CBH model, NSPT (Modified) model and Almond West formalism of Chalcogenide glassy system $xAg_2S - (1-x) (0.5Se - 0.5Ge)$ with $x = 0.1$ and 0.2

x	CBH			NSPT (MODIFIED)			ALMOND - WEST	
	W_m (eV)	τ_0 (s)	T_0 (K)	W_H (eV)	τ_H (s)	T_0 (K)	E_H (eV)	n
0.1	0.02918	3.2836E-6	424.12717				0.01346	1.76
0.2				0.09115	0.00007	522.78282	0.0310	1.12

This can therefore be concluded that for the present glassy system in which value of x is 0.2 the NSPT modified model is propitious to find the conduction mechanism according to which tunneling of polarons through grain boundary is the main cause for conduction. Whereas, CBH model is found to be most appropriate for the present system with $x = 0.1$, according to which the conduction occurs because of charge carriers' hopping in pairs over potential barrier between two charged defect states.

5.3.6.2. Almond West Formalism

The AC conductivity variation with frequency in low and high frequency regions at various temperatures (range: 333K - 533K) of the present glassy system with $x = 0.2$ is shown in Fig-5.9(a) and (b) respectively. The increase of AC conductivity on increasing temperature can be observed in Fig-5.9(a). At lower frequencies the conductivity was found to be independent on frequency, which corresponds to DC conductivity of system. The hopping of polarons may be the cause of the frequency independent AC conductivity in such glasses [13-15]. At high frequencies, above hopping or crossover frequency, the AC conductivity starts increasing with frequency, as shown in Fig-5.9(b), which may take place due to correlated motion of polarons [8-10]. In Fig-5.9(c), the conductivity spectra of the present system with $x = 0.1$ and 0.2 at 353K is shown.

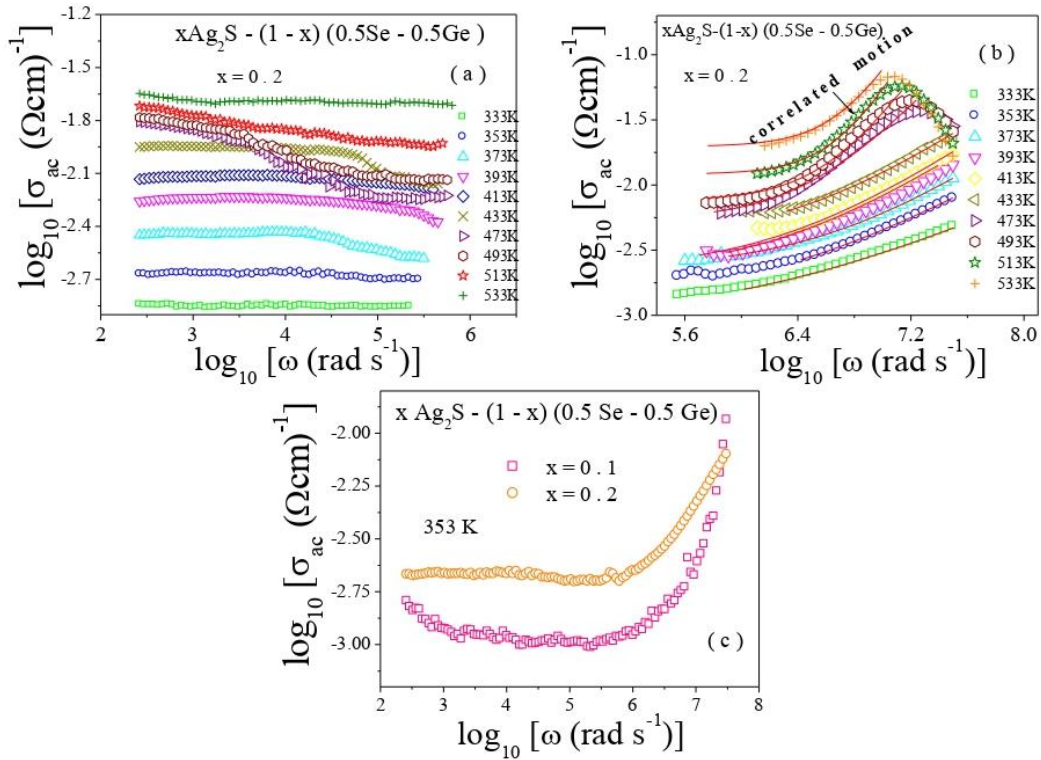


Fig-5.9: Conductivity spectra of system $x\text{Ag}_2\text{S} - (1-x) (0.5\text{Se} - 0.5\text{Ge})$ for $x = 0.2$ at various temperatures in (a) low frequency and (b) high frequency zones. Solid lines indicate best fitted curves using Almond West formalism in the limited frequency zone (correlated motion); (c) Conductivity spectra of the system for $x = 0.1$ and 0.2 at a 353K

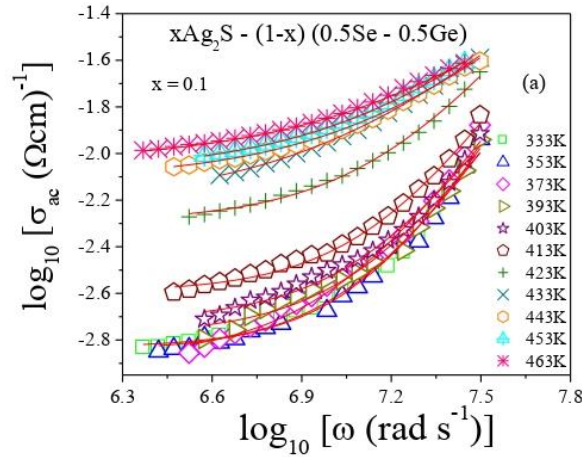


Fig-5.10: Conductivity spectra of system $x\text{Ag}_2\text{S} - (1-x) (0.5\text{Se} - 0.5\text{Ge})$ for $x = 0.1$ at various temperatures in higher frequency region. Solid lines indicate best fitted curves using Almond West formalism

Fig-5.10 shows variation of AC conductivity with frequency of the present glassy system having $x = 0.1$ at various temperatures (333K – 463K) in higher frequency region. For the analysis of the AC conductivity spectra of this system, Almond West formalism has been

applied, details of which have been given in Section 3.3.6.2 of Chapter 3. Solid lines in Fig-5.9(b) and Fig-5.10 show the fitting of AC conductivity spectra with Almond West formalism i.e. Eqn. (3.15) of Chapter 3, for the present system having $x = 0.2$ and 0.1 respectively.

Different parameters like σ_{DC} , ω_H and n have been obtained by fitting Fig-5.9(b) and Fig-5.10 with Eqn. (3.15) of Chapter 3. In Fig-5.9(c), the conductivity spectra of the present system with $x = 0.1$ and 0.2 at $353K$ is shown, from which the conductivity is found to increase on increasing x i.e., the content of Ag_2S in the glass composition which validates DC conductivity plots shown in Fig-5.5.

The variation of hopping frequency ω_H with temperature of the present system is shown in Fig-5.11 which can be represented by the Arrhenius equation, Eqn. (3.16) of Chapter 3, explanation of which is given in Section 3.3.6.2 of Chapter 3. To calculate the activation energy for hopping frequency E_H Fig-5.11 has been linearly fitted with Eqn. (3.16) of Chapter 3. The values of E_H and n of the present glassy system having $x = 0.1$ and 0.2 is shown in Table-5.8 from which increase in activation energy for hopping frequency E_H on increasing the amount of Ag_2S in the system can be observed. From the values of n (since $n > 1$), the percolation type motion of polarons can be predicted [15].

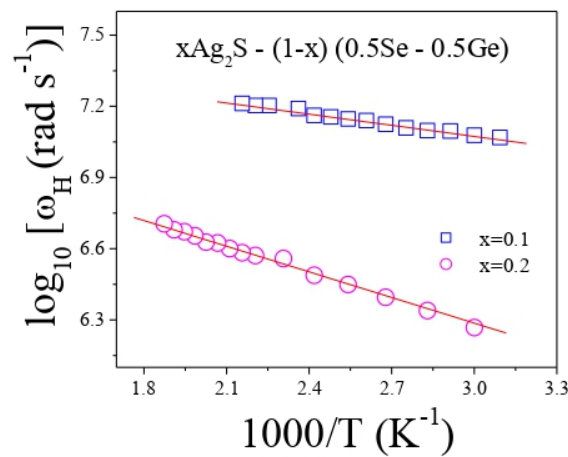


Fig-5.11: Plot of $\log_{10} \omega_H$ versus $1000/T$ of the Chalcogenide system $xAg_2S - (1-x) (0.5 Se - 0.5 Ge)$ where, $x = 0.1$ and 0.2

5.3.6.3. AC Conductivity Scaling

AC conductivity scaling process helps in predicting the dependency of electrical relaxation process on composition and temperature of glasses. The detail of AC conductivity scaling is discussed in Section 3.3.6.3 of Chapter 3.

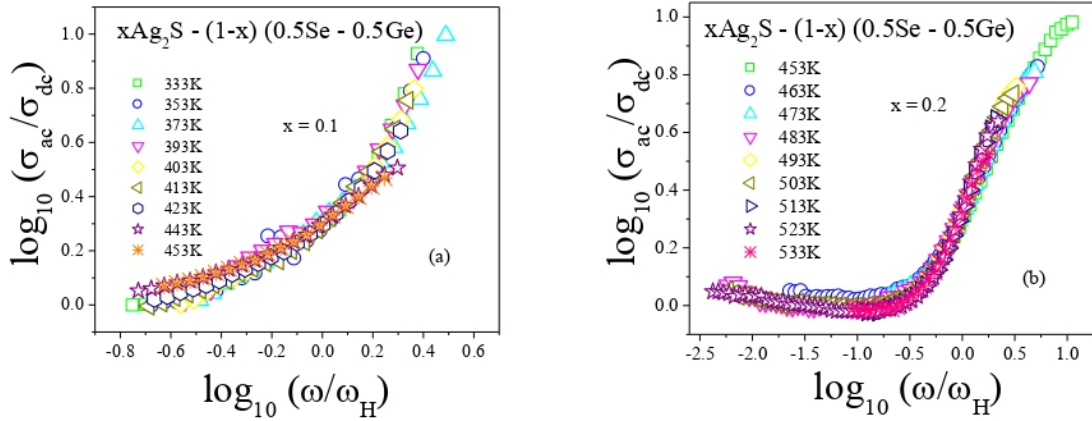


Fig-5.12: AC conductivity scaling of the system $x\text{Ag}_2\text{S} - (1-x) (0.5\text{Se} - 0.5\text{Ge})$ where, $x =$ (a) 0.1 and (b) 0.2 at different temperatures

Fig-5.12(a) and (b) show the AC conductivity scaling of the present system with $x = 0.1$ and 0.2 respectively at diverse temperatures (temperature scaling). It is observed from Fig-5.12(a) and (b) that the conductivity spectra of the system at diverse temperatures overlap in a single curve which is an indication of the existence of a time temperature superposition [16].

In Fig-5.13 the composition scaling i.e., the scaling of AC conductivity data of the system having different values of x (i.e., 0.1 and 0.2) at 373K is shown. In Fig-5.13 the non-overlapping of ac conductivity data is found. From the analysis of AC conductivity scaling, composition dependent and temperature independent relaxation mechanism in the system has been found.

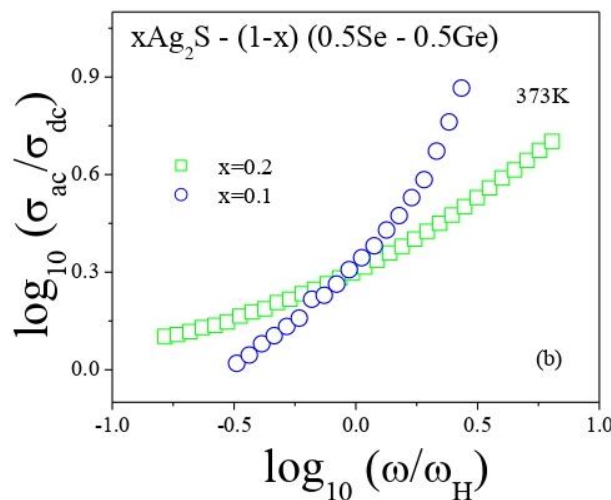


Fig-5.13: AC conductivity scaling of Chalcogenide system $x\text{Ag}_2\text{S} - (1-x) (0.5\text{Se} - 0.5\text{Ge})$ where, $x = 0.1$ and 0.2 at 373K

5.3.6.4. Meyer–Neldel (MN) rule

Meyer-Neldel rule has been applied for analyzing conduction mechanism in the present system, details of which have already been discussed in Section 3.3.6.4 of Chapter 3. The change in AC conductivity of this system, having $x = 0.1$ and 0.2 , with temperature at four different frequencies are shown in Fig-5.14(a) and (b) respectively. It is seen from Fig-5.14(a) and (b) that AC conductivity increases on increasing temperature. The variations of AC conductivity of these semiconducting materials above the room temperature can be expressed by Eqn. (3.18) of Chapter 3. The plots of Fig-5.14(a) and (b) have been linearly fitted with Eqn. (3.18) of Chapter 3 to get the values of ΔE and σ_0 . The values of ΔE were calculated from the slopes of these fitted lines and from the intercepts of the fitted lines, the values of σ_0 of the present system have been obtained.

Fig-5.15(a) and (b) show the variations of σ_0 with ΔE of the present glassy system for $x = 0.1$ and 0.2 respectively, which show linear nature. To explicate σ_0 and its ΔE dependence, MN rule has been applied because of the thermally activated nature of the present glassy system.

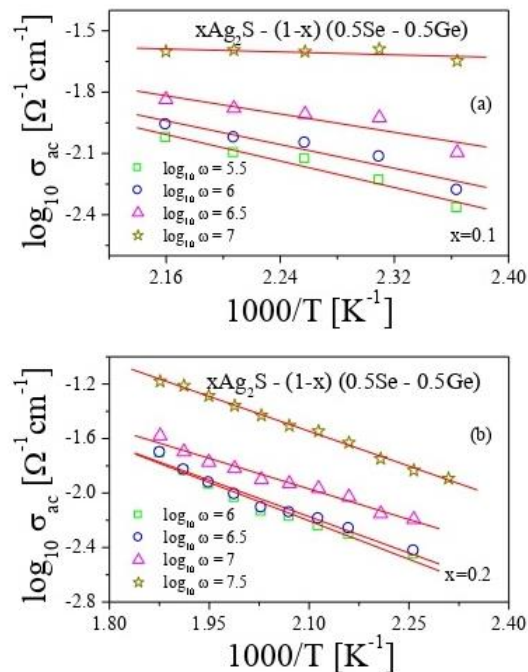


Fig-5.14: $\ln \sigma_{AC}$ versus $1000/T$ plots of system $xAg_2S - (1-x) (0.5 Se - 0.5 Ge)$ where, $x =$ (a) 0.1 and (b) 0.2

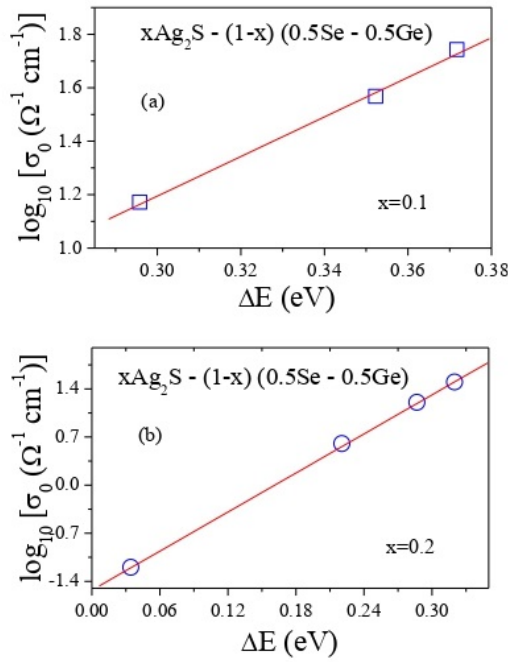


Fig-5.15: $\ln \sigma_0$ versus ΔE (eV) plots of system $x\text{Ag}_2\text{S} - (1-x)(0.5\text{Se} - 0.5\text{Ge})$ where, $x =$ (a) 0.1 and (b) 0.2.

The MN activation energy of the system with $x = 0.1$ and 0.2 have been obtained from slopes of the linearly fitted plots of Fig-5.15(a) and (b) with Eqn. (3.19) of Chapter 3 and is shown in Table-5.7. The decrease in MN activation energy on increasing the value of x in the present glassy system could be observed from Table-5.7 which is a clear indication of increase of conductivity with the increase of content of Ag_2S in the system.

5.3.6.5. Mobility and Carrier Density

To find the carrier mobility (μ) and carrier density (N) of the present glassy system DC polarization technique has been used, details of which have been discussed in Section 3.3.6.5 of Chapter 3. The mobility of charge carriers has been determined by Eqn. (3.20) of Chapter 3. To determine the carrier density 'N', Eqn. (3.21) of Chapter 3 has been used.

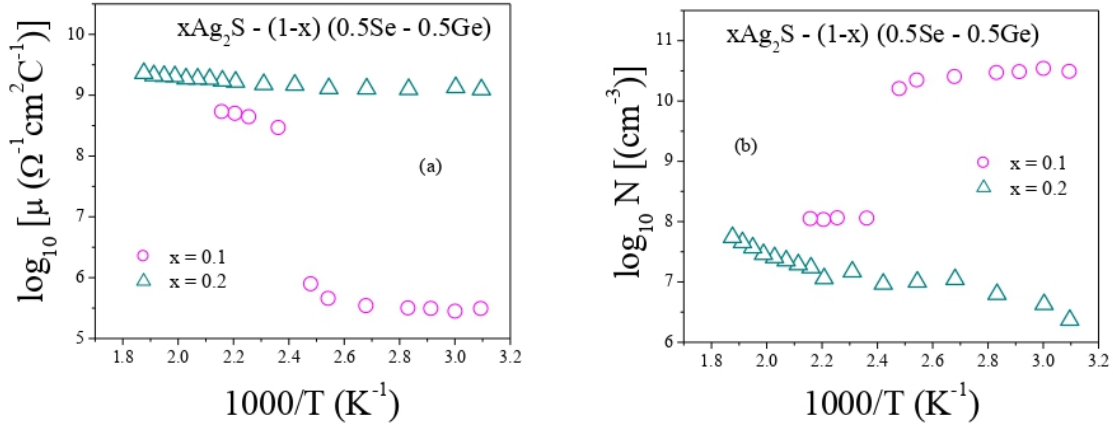


Fig-5.16: Plots of (a) $\log_{10} \mu$ versus $1000/T$, (b) $\log_{10} N$ versus $1000/T$ for the Chalcogenide glassy system $x\text{Ag}_2\text{S} - (1-x) (0.5\text{Se} - 0.5\text{Ge})$ with $x = 0.1$ and 0.2

Fig-5.16(a) shows the plot of $\log_{10} \mu$ versus $1000/T$, where T is the temperature, of the system with $x = 0.1$ and 0.2 . The mobility is found to increase with the increase of x in the composition. Also it has been found to be increased with the rise in temperature of the system. In Fig-5.16(b) $\log_{10} N$ versus $1000/T$ of the present system is shown. From Fig-5.16(b) it can be seen that the value of carrier density is less in the system in which the value of x is more in the composition i.e. $x = 0.2$. In Table-5.9 the average mobility and carrier density data is shown for the system with $x = 0.1$ and 0.2 .

Table-5.9: Average mobility and carrier density of system $x\text{Ag}_2\text{S} - (1-x) (0.5\text{Se} - 0.5\text{Ge})$ with $x = 0.1$ and 0.2

x	Carrier Mobility, μ ($\Omega^{-1}\text{cm}^2\text{C}^{-1}$)	Carrier density, N (cm^{-3})
0.1	1.58E8	1.69E10
0.2	1.67E9	2E7

5.3.7. Dielectric Properties Analysis

5.3.7.1. Permittivity

The dependency of ϵ' and ϵ'' of the present glassy system i.e., $x\text{Ag}_2\text{S} - (1-x) (0.5\text{Se} - 0.5\text{Ge})$ with $x =$ (a) 0.1 and (b) 0.2 on temperature (range: $323\text{K}-4633\text{K}$) and frequency (range: $42\text{Hz} - 5\text{MHz}$) have been studied.

Fig-5.17(a) and (b) show the plots of dielectric constant ϵ' of this system with $x = 0.1$ and 0.2 respectively against frequency at various temperatures. Fig-5.18(a) and (b) show the plots of dielectric loss ϵ'' against frequency at different temperatures of the present system with $x = 0.1$ and 0.2 respectively. Exponential decrease of both ϵ' and ϵ'' on increasing frequency at

various temperatures can be seen from Fig-5.17 and Fig-5.18. The more value of dielectric constant at lower frequencies is primarily because of the occurrence of electrode polarization due to accumulation of space charges at glass-electrode interface.

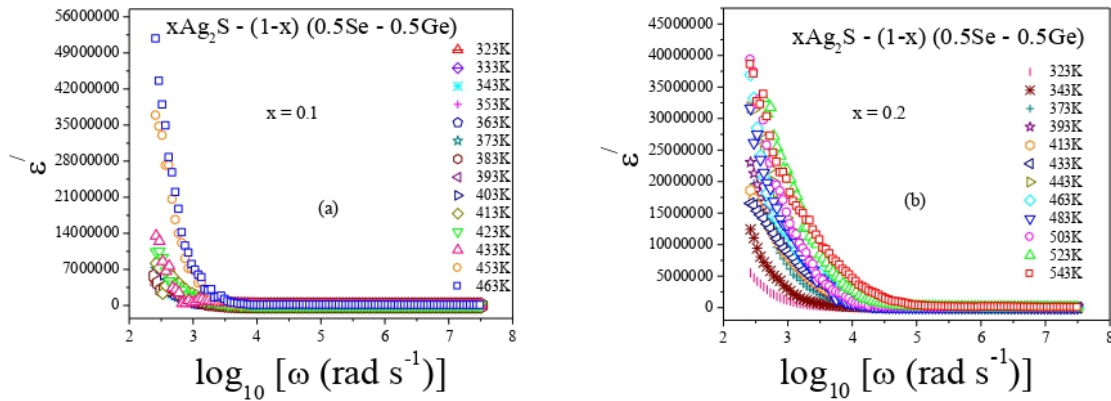


Fig-5.17: Variation of dielectric constant ϵ' with frequency of the system $x\text{Ag}_2\text{S} - (1-x) (0.5\text{Se} - 0.5\text{Ge})$ at various temperatures for $x =$ (a) 0.1 and (b) 0.2

The effect of polarization decreases with the increase of frequency as the molecular dipoles in the system cannot follow the fast variation of the electric field. Hence, on increasing frequency in the system both ϵ' and ϵ'' start to decrease and show frequency independent nature.

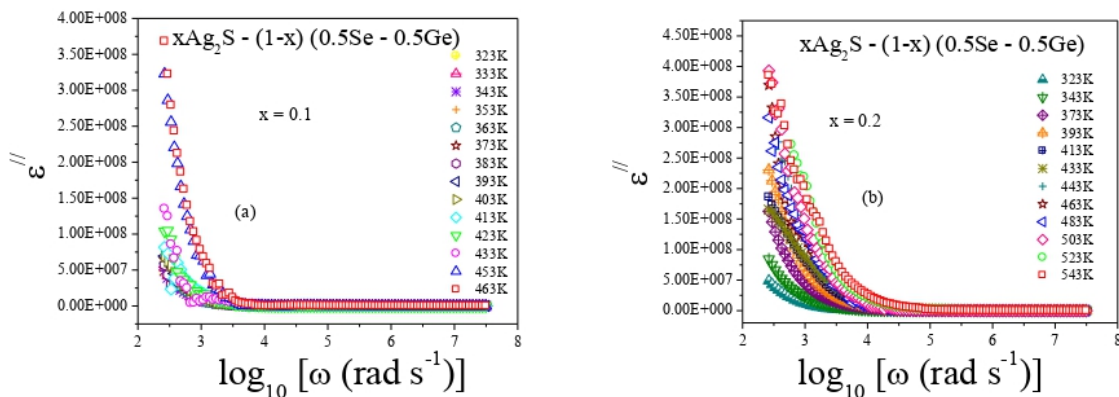


Fig-5.18: Variation of dielectric loss ϵ'' with frequency of the system $x\text{Ag}_2\text{S} - (1-x) (0.5\text{Se} - 0.5\text{Ge})$ at various temperatures for $x =$ (a) 0.1 and (b) 0.2

The increase of both ϵ' and ϵ'' on the increase of temperature can be seen in Fig-5.17 and Fig-5.18. This occurs mainly due the increase in polarization effect in the system because of decrease in bond energies as the intermolecular forces get weakened by the rise in temperature, which results in enhancing the orientational vibrations and increasing polarization. Fig-5.17 and Fig-5.18 also show the increase of both ϵ' and ϵ'' on increase of x

in the composition of the present system. This is a clear indication of higher conductivity in the present system having more value of x i.e., content of Ag_2S .

5.3.7.2. Electric Modulus

The electrical relaxation properties of these glasses have been studied with the use of electric modulus formalism, details of which has already been discussed in the section 2.4.3.2 of Chapter 2. Fig-5.19(a) and (b) show the plots of the real part of electric modulus M' versus frequency of the present glassy system with $x = 0.1$ and 0.2 respectively. In Fig-5.19(a) and (b), M' is found to approach zero at all the mentioned temperatures and in low frequency region which mainly occurs because of the suppression of electrode polarization because of unavailability of restoring forces of charge carriers [17-19]. But at higher frequencies, dispersion in M' has been found and M' exhibits a maximum value which is: $(M_\infty) = (\epsilon_\infty)^{-1}$ because of the electrical relaxation of polarons [17-19]. In Fig-5.19(a) and (b) a gradual decrease in M' with the rise of temperature is found which may imply the involvement of movement of polarons, within a small range, in the conduction mechanism of this glassy system.

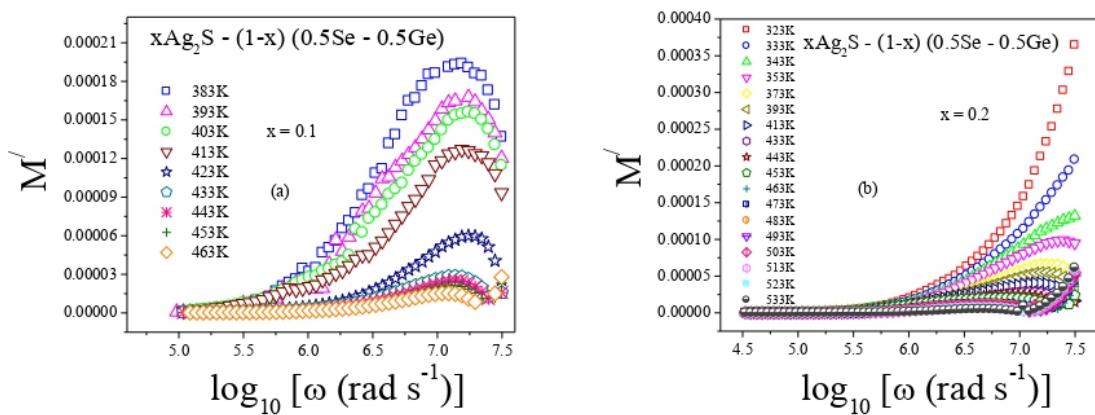


Fig-5.19: Variation of real electric modulus M' with frequency of Chalcogenide system $x\text{Ag}_2\text{S} - (1-x) (0.5 \text{ Se} - 0.5 \text{ Ge})$ at various temperatures for $x =$ (a) 0.1 and (b) 0.2

Fig-5.20(a) and (b) show imaginary electric modulus M'' against frequency graph of the system with $x = 0.1$ and 0.2 respectively. With the increase of temperature, the shifting of M'' peaks towards higher frequencies, as shown in Fig-5.20(a) and (b), is found which is an indication of temperature dependent relaxation process in this glassy system. The movement of thermally activated charge carriers may reduce the relaxation time and increase the relaxation frequency.

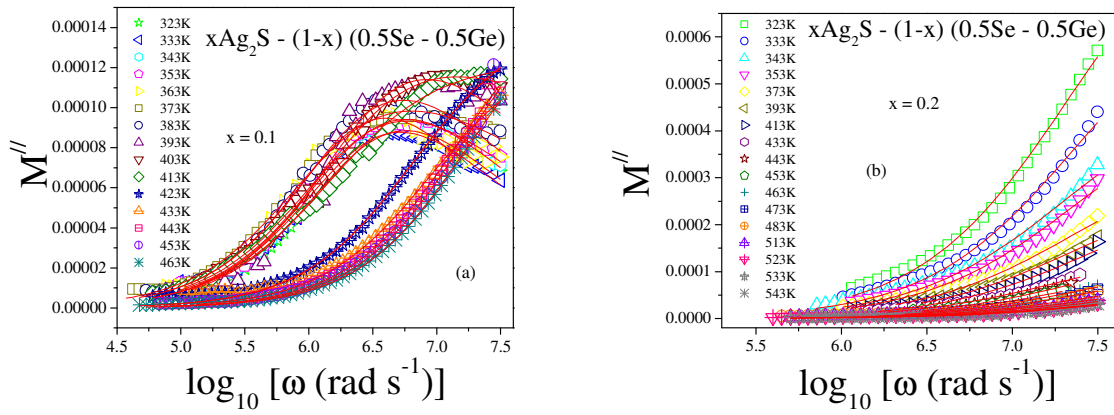


Fig-5.20: Variation of imaginary electric modulus M'' with frequency of Chalcogenide system $xAg_2S - (1-x) (0.5Se - 0.5Ge)$ at various temperatures for $x =$ (a) 0.1 and (b) 0.2

The hopping of charge carriers/polarons over long distances may be the cause for the conduction in these glasses below the peak relaxation frequency ω_{max} . Above ω_{max} the cause of conduction mechanism may be the localized motion of charge carriers over short distances [18, 19]. The M'' peak shifting indicates the stabilization of the system in a short time for an external force at eminent temperature.

Fig-5.21(a) shows M'' spectra of the system with $x = 0.1$ and 0.2 at $463K$ from which the decrease in M'' values with the increase in x (i.e., content of Ag_2S) is found. M'' can be defined by the equation [15]:

$$M'' = \frac{M''_{max}}{(1-\beta) + \frac{\beta}{1+\beta} [\beta(\omega_{max}/\omega) + (\omega/\omega_{max})^\beta]} \quad (5.1)$$

where, $0 < \beta < 1$, M''_{max} is the peak value of imaginary electric modulus, ω_{max} is angular frequency corresponds to M''_{max} , and β is Kohlrausch-Williams-Watts (KWW) stretched coefficient [20]. M'' versus $\log \omega$ plots (Fig-5.20) of this system with $x = 0.1$ and 0.2 have been fitted with Eqn. (5.1), which is indicated by solid lines in Fig-5.20(a) and (b) respectively, to obtain the values of M''_{max} , ω_{max} and β . β is found to decrease on increasing x in composition of the present system and is shown in Table-5.10.

To determine the activation energy (E_τ) related to the relaxation time τ , Eqn. (2.27) of Chapter 2 has been used. Fig-5.21(b) shows the change in relaxation time τ with temperature of the system with $x = 0.1$ and 0.2 . Solid lines in Fig-5.21(b) indicate the linear fitting of $\log_{10} \tau$ versus $1000/T$ plots with Eqn. (2.27) of Chapter 2. Values of E_τ have been calculated

from slopes of fitted lines and are presented in Table-5.10. From Fig-5.21(b), the decrease of relaxation time τ on increasing temperature can be observed. From this figure the decrease of relaxation time τ with the increase of x i.e. the content of Ag_2S in the system can also be observed. Lower values of relaxation time directly indicate the higher conductivity due to polaron hopping in the system.

Table-5.10: Structural parameter (β), and activation energy corresponding to relaxation time (E_τ) of system $x\text{Ag}_2\text{S} - (1-x)(0.5\text{Se} - 0.5\text{Ge})$ with $x = 0.1$ and 0.2

x	β	E_τ (eV)
0.1	0.30	0.26
0.2	0.042	0.07

The decrease of E_τ on increasing amount of Ag_2S in the present system can be seen from Table-5.10. This is a clear indication of the increase of conductivity on increasing content of Ag_2S in the system.

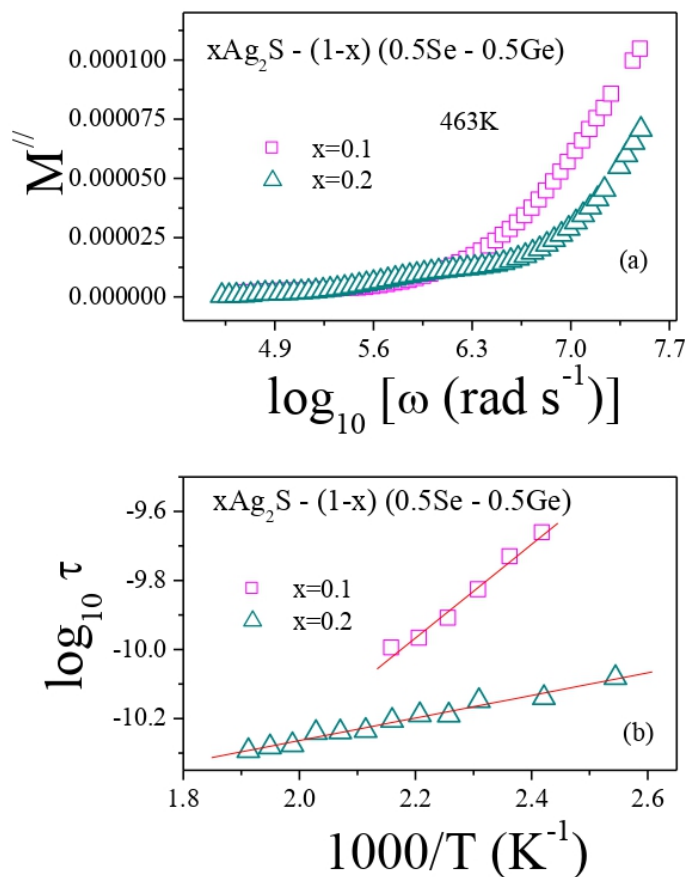


Fig-5.21: (a) Variation of M'' with frequency of Chalcogenide system $x\text{Ag}_2\text{S} - (1-x)(0.5\text{Se} - 0.5\text{Ge})$ with $x = 0.1$ and 0.2 at $T = 463\text{K}$, (b) Plot of $\log_{10} \tau$ versus $1000/T$ for the system $x\text{Ag}_2\text{S} - (1-x)(0.5\text{Se} - 0.5\text{Ge})$

5.3.7.3. Electric Modulus Scaling

For the analysis of relaxation process in the system, electric modulus scaling has been carried out. For this, the x-axis i.e., M'' values of Fig-5.20(a) and (b) have been divided by M''_{\max} (maximum value of imaginary modulus) and y-axis i.e., ω values, by ω_{\max} (the frequency at which M'' peak occurs). Temperature scaling of the M'' plots of the present system having $x = 0.1$ and 0.2 are shown in Fig-5.22(a) and (b) respectively at different temperatures in the range from 333K to 463K. In Fig-5.22(a) and (b) overlapping of all the scaled data has been found, which is an indication of temperature independent relaxation process in the glass.

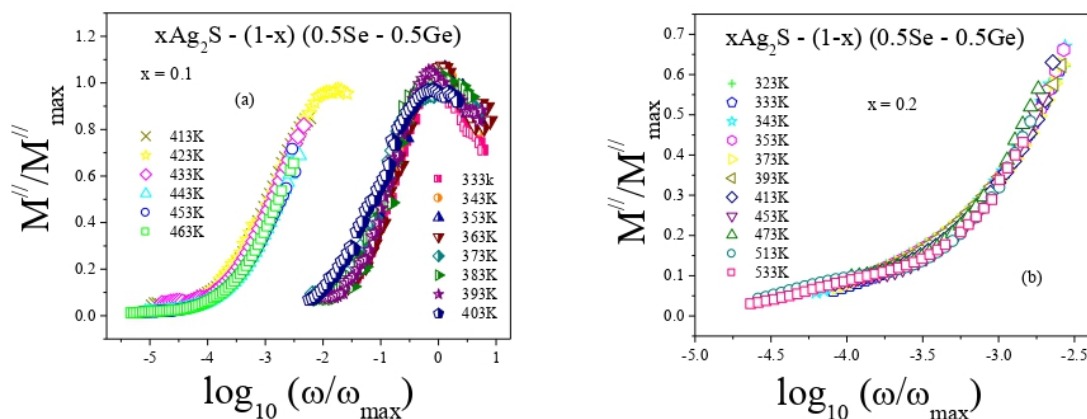


Fig-5.22: Temperature scaling of M'' at various temperatures of glassy system $x\text{Ag}_2\text{S} - (1-x) (0.5\text{Se} - 0.5\text{Ge})$ where, $x =$ (a) 0.1 and (b) 0.2

In Fig-5.23 the composition scaling in which electric modulus M'' plots of the present system having $x = 0.1$ and 0.2 at a fixed temperature (433K) is shown. The overlapping of the plots in Fig-5.23 is a clear indication of composition independent relaxation process in the system at 433K. But at lower temperature region (333K – 403K) overlapping of plots in composition scaling cannot be possible.

Therefore, at higher temperature region (413K – 463K) the electrical relaxation process is found to be independent on temperature as well as composition. But in low temperature region (333K – 403K), it is composition dependent and temperature independent.

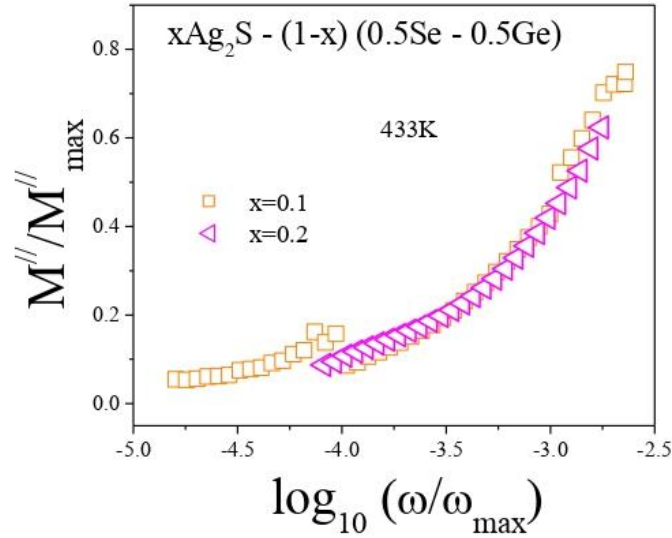


Fig-5.23: Composition scaling of M'' of Chalcogenide glassy system $x\text{Ag}_2\text{S} - (1-x) (0.5\text{Se} - 0.5\text{Ge})$ at 433 K

5.4. CONCLUSION

The Chalcogenide glassy system of composition $x\text{Ag}_2\text{S} - (1-x) (0.5\text{Se} - 0.5\text{Ge})$, where $x = 0.1$ and 0.2 using melt-quenching method has been prepared. With the help of XRD technique, polycrystalline nature of the system has been observed. The crystalline volume fraction percentage is found to increase with the increase of x in the system. From the XRD analysis, the sizes of the different phases present in the system with their $[h, k, l]$ values and dislocation density have been calculated. The decrease of crystallite size and increase of dislocation density on increasing Ag_2S in the system have been found. The increase in dislocation density on increasing Ag_2S increases disorder in the system, which may results in the decrease in conductivity due to possibility of collisions in the glassy system.

For the structural analysis of the system, Ultraviolet-visible (UV-Vis) spectroscopy has also been used. The optical band gap energy, calculated from this method, is found to increase from 3.42 eV to 5.16 eV on increasing value of x from 0.1 to 0.2 in the composition of the glass. From the analysis of FT-IR spectroscopy spectra of the present glassy system, a good transparency in the spectral range $4000\text{cm}^{-1} - 400\text{cm}^{-1}$ can be observed and most of the absorption bands can be assigned to vibrational bands of oxides and hydrides bonds which arises due to the presence of extrinsic impurities in the system introduced during its

preparation. FT-IR spectra indicate the presences of different functional groups and molecules like O-H, C-H, Ge-O-Ge, Sulphones and H₂O in the system.

For studying the electrical properties of this glassy system, DC and AC conductivity measurements at different temperatures (333K-463K) have been carried out. The increase in DC conductivity on increasing Ag₂S in the composition of the glass was found. DC conductivity's increase with temperature indicates semiconducting behaviour of the system. Mott's Model and Greaves's Model have been used for the analysis of DC conductivity data at lower and higher temperature regions respectively. Almond West model has been applied for the analysis of AC conductivity spectra at diverse temperatures and frequencies (range: 42 Hz – 5 MHz), from which hopping frequency of the present system has been calculated. The activation energy related to hopping frequency is found to increase on increasing the amount of Ag₂S in the system.

For interpreting conduction mechanism in the system, CBH Model is found as the most suitable model for the system having value of $x = 0.1$, according to which the conduction occurs due to polarons's hopping over the potential barrier among defect states. For $x = 0.2$, the modified NSPT model is found as the most suitable, according to which tunneling of polarons through grain boundary is the main cause for conduction. AC conductivity scaling signifies that the system's relaxation process is not dependent on temperature but is dependent on its composition. The carrier mobility and density in the present system have been calculated. Carrier mobility is found to increase and carrier density is found to reduce on increasing x i.e., Ag₂S content in the system.

From the dielectric permittivity studies, the decrease of ϵ' and ϵ'' on increasing frequency and decreasing temperature has been observed. Activation energy linked to the relaxation process in system has been calculated from the analysis of the electric modulus plots which is found to decrease on increasing the amount of Ag₂S in the system. The electric modulus studies confirm the temperature dependent relaxation process in the present system. The temperature and composition scaling of M'' spectra at higher temperature region (413K – 463K) indicate that the electrical relaxation process is not dependent on temperature as well as composition, but in low temperature region (333K – 403K), it is dependent on composition but independent on temperature.

REFERENCES

- [1] S. A. Khan, M. Zulfequar and M. Husain, *Solid State Communication* 123, 463 (2002)
- [2] N. Suri, K. S. Bindra, P. Kumar and R. Thangaraj, *J. Non Cryst. Solids* 353, 1264 (2007)
- [3] R. Mathur and A. Kumar, *Rev. Phys. Appl.* 21, 579 (1986)
- [4] R. Chiba and N. Funakoshi, *J. Non Cryst. Solids* 105, 149 (1988)
- [5] Chunyan Cui, Xiaoru Li, Jixian Liu, Yongchao Hou, Yuqing Zhao and Guocheng Zhong, *Nanoscale Research Letters*, 10, 431 (2015)
- [6] T. S. Kavetskiy, A. P. Kovalskiy, V. D. Pamukchieva and O. I. Shpotyuk, *Infrared Phys. Tech.*, 41, 41 (2000)
- [7] G. Socrates, “Infrared and Raman Characteristic Group Frequencies”, 3rd Edition, John Wiley and Sons Ltd (2004)
- [8] M. Efimov and V. G. Pogareva, *J. Non-Cryst, Solids*, 275, 189 (2000)
- [9] V. Pamukchieva, K. Todorova, O. C. Mocioin, M. Zaharescu, A. Szekeres and M. Gartner, *J. Physics*, 356, 012047 (2012)
- [10] Y. Y. Kim and D. Walsh, *Nanoscale* 2, 240 (2010)
- [11] J. Singh, *J. Mater. Sci.: Mater. Electron.*, 14, 171 (2003)
- [12] N. F. Mott, E. A. Davis, “Electronic Processes in Non-Crystalline Materials”, Clarendon Press, Oxford, (1979)
- [13] A. Mansingh, J. K. Vaid and R. P. Tondon, *J. Phys. (C) Solid State Physics*, 10, 4061 (1977)
- [14] D. P. Almond, G. K. Duncan and A. R. West, *Solid State Ionics*, 8, 159 (1983)
- [15] B. Roling, A. Happe, F. Funke and M. D. Ingram, *Phy. Rev. Lett.*, 78, 2160 (1997)
- [16] A. Ghosh and A. Pan, *Phy. Rev. Lett.*, 84, 2188 (2000)
- [17] A. B. Karmakar, K. Rademann Andrey, L. Stepanov, “Glass Nanocomposites, Synthesis, Properties and Applications”, Elsevier Inc., (2016)
- [18] S. Ojha, M. Roy, A. Chamuah, K. Bhattacharya and S. Bhattacharya, *Materials Letters* 258, 126792 (2020)
- [19] S. Bhattacharya and A. Ghosh, *J. Am. Cer Soc.* 91, 753 (2008)
- [20] R. Bergman, *J. Appl. Phys.*, 88, 1356 (2000)

Chapter 6

STUDY OF ELECTRICAL SPECTRA OF $\text{Ag}_2\text{S} - \text{Se} - \text{Te}$ CHALCOGENIDE GLASSY SYSTEM

6.1. INTRODUCTION

In this chapter the structural and electrical properties of Ag_2S doped Se-Te Chalcogenide glassy system having composition $x\text{Ag}_2\text{S} - (1-x) (0.5 \text{ Se} - 0.5 \text{ Te})$, where, $x = 0.05, 0.1$ and 0.2 , are discussed. The unique and extraordinary electrical, mechanical, thermal, optical and physical properties of Chalcogenide glasses, a class of amorphous semiconductors or non oxide glasses, have shown their usefulness at technological level [1-5]. Selenium has been drawing attention of researchers for many years due to its several possible applications like xerography, rectifiers, photocells, memory devices etc [6]. However, short life time, low photosensitivity and fragile like properties of Selenium barred it from being used in many other applications. To overcome this problem, Selenium is added with some suitable elements, like group II – VI, of periodic table which helps it to become useful in some applications like optical switching. Alloys of Se-Te have shown many advantageous properties such as high photosensitivity, high crystallization temperature, small ageing effect, and more hardness [7-10] which enhance the possibility of their uses in many solid state devices.

The purpose of this investigation is to study the electrical properties of Ag_2S -Se-Te glassy system which are mainly dependent on temperature, frequency and composition. Ag_2S exhibits several attractive properties like narrow band gap, low cost, good chemical stability, and optical properties [11]. It is a semiconductor having band gap of about 1.5eV. Some of the applications of Ag_2S are photovoltaic cells, infrared detectors, superionic conductors, photoelectric switches, gas sensors etc. Although Ag_2S possesses many attractive properties yet it has some limitations because of its requirement of complex preparation process and very low yield [11]. To overcome its limitations, Ag_2S can be composite with other suitable elements.

The chapter starts with the preparation of the present system using melt quenching method followed by studies of its structural and electrical properties. XRD and FT-IR techniques

were used for its structural analysis. Using XRD technique, crystallite size of different phases, strain, dislocation density, crystalline volume fraction, etc can be determined. FT-IR is used to get information regarding different functional groups and molecules present in the system.

For studying electrical properties of the system, DC and AC measurements have been carried out. To carry out DC conductivity measurements, two-probe method has been used using 'MetraVi' Digital Multimeter (model no. 450 DMM) and for measuring AC conductivity in the frequency range from 42Hz to 5MHz at diverse temperatures (303K – 423K), Hioki made LCR Hi-Tester (Model No. 3532-50) was used. To analyse AC conductivity of these glasses, different models or methods have been used like: Almond West Formalism, MN Rule, AC conductivity scaling, dielectric relaxation studies etc. To know the information regarding the conduction mechanism of these glasses the AC conductivity data have been tried to fit with various models like CBH, NSPT, OLPT etc. Permittivity and electrical modulus calculations have been used for the study of electrical relaxation properties of these glassy systems.

6.2. PREPARATION OF THE GLASSY SYSTEM

Chalcogenide glassy system, $x\text{Ag}_2\text{S} - (1-x) (0.5\text{Se} - 0.5\text{Te})$ where, $x = 0.05, 0.1$ and 0.2 was prepared with the help of melt-quenching method. For this, high purity (Aldrich 99.9%) Ag_2S , Se and Te in powdered form, were taken in suitable atomic weight percentage (as per the composition) and mixed in a mortar. The mixture was sealed in quartz ampoules in a high vacuum (10^{-4} Torr) in order to avoid oxidation in the present glassy system at high temperature. The ampoules were then placed inside furnace at 250°C . The temperature of the furnace was set to rise at the rate of $3^\circ\text{C}/\text{min}$. The ampoules containing mixtures were kept at that temperature for one hour. Then the temperature of furnace was increased to 500°C and the ampoules were heated at that temperature for two hours. The temperature of the furnace was then raised to 850°C and the ampoules were kept there for two hours. After that the mixture inside the ampoules were found in melted form. The ampoules were then taken out from the furnace and immediately kept on ice to get the system in glassy form. Pellets of the as prepared samples are formed to carry out AC and DC measurements. To get good electrical contact between electrode and the glassy sample, silver paste is coated on both the sides of the pellets.

6.3. RESULTS AND ANALYSIS

6.3.1. XRD

6.3.1.1. Crystallite Size, Dislocation Density and Lattice Strain

XRD patterns of Ag_2S doped Se-Te glassy system with $x = 0.05, 0.1$ and 0.2 are shown in Fig-6.1. The sharp peaks in the patterns point to the polycrystalline nature of this system. Due to the formation of different nano-crystallites, several peaks having different $[h\ k\ l]$ values like $[1\ 0\ 0]$ and $[2\ 0\ 1]$ for $\text{Te}_{0.5}\text{Se}_{0.5}$ [12], $[2\ 2\ 0]$ for $\text{Te}_{0.5}\text{Se}_{3.5}$ [13], $[1\ 1\ 0]$ for Ag_2S (JCPDS Card no. 75-1061), $[1\ 4\ 1]$ for S_3Se_5 (JCPDS Card no. 71-1118), $[5\ 1\ 0]$ for $\text{Ag}_{4.53}\text{Te}_3$ (JCPDS Card no. 86-1953), $[4\ 4\ 0]$ for Ag_5Te_3 (JCPDS Card no. 86-1168) and $[4\ 2\ 2]$ for TeS (JCPDS Card no.78-1062), can be observed in the XRD pattern.

The crystallite size, dislocation density and lattice strain of the prepared glassy samples have been calculated using Eqns. (2.4), (2.5) and (2.6) respectively of Chapter 2. In Table-6.1 the crystallite sizes of different phases with their Miller indices formed in the system for $x = 0.05, 0.1$ and 0.2 is shown. The values of dislocation density and lattice strain of the present system are also shown in Table-6.1.

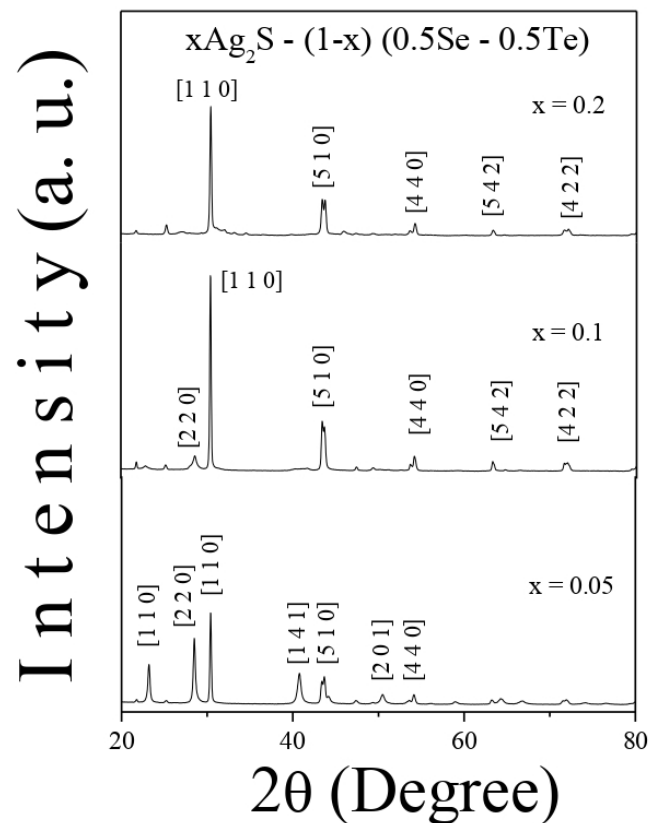


Fig-6.1: XRD diffractograms of Chalcogenide system $x\text{Ag}_2\text{S} - (1-x)(0.5\text{Se} - 0.5\text{Te})$ where, $x = 0.05, 0.1$ and 0.2

Table-6.2 indicates the variation of crystallite size of different phases with the values of x in the system. The phases which formed with Se (i.e., $\text{Te}_{0.5}\text{Se}_{0.5}$, S_3Se_5 and $\text{Te}_{0.5}\text{Se}_{3.5}$) are found to disappear with the increase of x. The crystallite sizes of Ag containing phases (i.e., Ag_2S , $\text{Ag}_{4.53}\text{Te}_3$ and Ag_5Te_3) are found to first increase and then decrease with x. Hence dislocation density of the system due to the presence of these phases first decrease and then increase with increase of x. Hence the system having x = 0.1 shows the utmost crystallite size and least dislocation density. Low value of dislocation density decreases the disorder in the system. This decreases the possibility of collision of charge carriers/polarons which increases their mobility and hence the electrical conductivity.

Table-6.1: Crystallite size, dislocation density and lattice strain of Chalcogenide system $x\text{Ag}_2\text{S} - (1-x) (0.5 \text{ Se} - 0.5 \text{ Te})$ for x = 0.05, 0.1, 0.2

x	Pos. [°2Th.]	FWHM [°2Th.]	Crystallite Size, in nm (particle name)	Phases	h	k	l	Strain	Dislocation Density
0.05	23.23	0.2303	34.8286	$\text{Te}_{0.5}\text{Se}_{0.5}$	1	0	0	-0.04106	0.0008244
	28.49	0.2047	39.5993	$\text{Te}_{0.5}\text{Se}_{3.5}$	2	2	0	-0.00563	0.0006377
	30.39	0.1498	54.3481	Ag_2S	1	1	0	-0.06676	0.0003386
	40.74	0.307	27.2980	S_3Se_5	1	4	1	0.003868	0.001342
	43.58	0.4546	18.6119	$\text{Ag}_{4.53}\text{Te}_3$	5	1	0	-0.56312	0.0028868
	50.48	0.42063	20.6488	$\text{Te}_{0.5}\text{Se}_{0.5}$	2	0	1	0.949866	0.0023454
	54.14	0.27938	31.5790	Ag_5Te_3	4	4	0	-0.02689	0.0010028
0.1	25.21	0.21454	37.5260	$\text{Ag}_{4.53}\text{Te}_3$	3	0	2	1.335834	0.0007101
	28.58	0.46792	17.3270	$\text{Te}_{0.5}\text{Se}_{3.5}$	2	2	0	-0.01844	0.0033308
	30.42	0.1407	57.8673	Ag_2S	1	1	0	-0.06501	0.0002986
	43.56	0.42257	20.0210	$\text{Ag}_{4.53}\text{Te}_3$	5	1	0	-0.49287	0.0024948
	54.17	0.24173	36.5027	Ag_5Te_3	4	4	0	-0.02438	0.0007505
	63.31	0.28751	32.0985	Ag_5Te_3	5	4	2	0.294261	0.0009706
	71.86	0.6449	15.0429	TeS	4	2	2	0.03198	0.0044191
0.2	25.30	0.21981	36.6332	$\text{Ag}_{4.53}\text{Te}_3$	3	0	2	0.621928	0.0007452
	30.45	0.1623	50.1701	Ag_2S	1	1	0	-0.07823	0.0003973
	43.59	0.5283	16.0163	$\text{Ag}_{4.53}\text{Te}_3$	5	1	0	-0.68069	0.0038983
	54.16	0.2558	34.4941	Ag_5Te_3	4	4	0	-0.0256	0.0008404
	63.33	0.29981	30.7857	Ag_5Te_3	5	4	2	0.291019	0.0010551
	71.89	0.84126	11.5338	TeS	4	2	2	0.038557	0.0075171

Table-6.2: Variation of Crystallite size of different phases present in the system $x\text{Ag}_2\text{S} - (1-x)(0.5\text{Se} - 0.5\text{Te})$ for $x = 0.05, 0.1, 0.2$

x	$\text{Te}_{0.5}\text{Se}_{3.5}$	Ag_2S	S_3Se_5	$\text{Ag}_{4.53}\text{Te}_3$	$\text{Te}_{0.5}\text{Se}_{0.5}$	Ag_5Te_3	TeS
0.05	39.60	54.35	27.30	18.61	20.65 and 34.83	31.58	-
0.1	17.33	57.87	-	20.02	-	36.50	15.04
0.2	-	50.17	-	16.02	-	34.49	11.53

6.3.1.2. Crystalline Volume Fraction

The crystalline volume fraction of the glassy samples has been calculated using Eqn. (3.1) of Chapter 3. The crystalline volume fractions of the present glassy system with $x = 0.05, 0.1$ and 0.2 containing different phases having different $[h\ k\ l]$ values is shown in Table-6.3.

Table-6.3: Crystalline volume fraction of different phases present in Chalcogenide glassy system $x\text{Ag}_2\text{S} - (1-x)(0.5\text{Se} - 0.5\text{Te})$ for $x = 0.05, 0.1, 0.2$

x	Phases	h	k	l	Area (I_{hkl})	$K_{hkl} = I_{hkl} / I_a$	Crystalline volume fraction
0.05	$\text{Te}_{0.5}\text{Se}_{0.5}$	1	0	0	872.39	0.57943	0.43379
	$\text{Te}_{0.5}\text{Se}_{3.5}$	2	2	0	1457.1	0.96779	0.49973
	Ag_2S	1	1	0	1505.6	1	0.5
	S_3Se_5	1	4	1	1121.8	0.74509	0.47911
	$\text{Ag}_{4.53}\text{Te}_3$	5	1	0	1141.8	0.75837	0.48147
	$\text{Te}_{0.5}\text{Se}_{0.5}$	2	0	1	362.20	0.24057	0.22741
	Ag_5Te_3	4	4	0	212.36	0.14105	0.1383
0.1	$\text{Te}_{0.5}\text{Se}_{3.5}$	2	2	0	532.12	0.17451	0.16935
	Ag_2S	1	1	0	3049.3	1	0.5
	$\text{Ag}_{4.53}\text{Te}_3$	5	1	0	1963.9	0.64405	0.45522
	Ag_5Te_3	4	4	0	363.38	0.11917	0.1175
	Ag_5Te_3	5	4	2	234.53	0.07691	0.07646
	TeS	4	2	2	507.07	0.16629	0.16182
0.2	Ag_2S	1	1	0	2320.8	1	0.5
	$\text{Ag}_{4.53}\text{Te}_3$	5	1	0	1735.3	0.74772	0.47959
	Ag_5Te_3	4	4	0	271.47	0.11697	0.11539
	Ag_5Te_3	5	4	2	155.10	0.06683	0.06653
	TeS	4	2	2	496.93	0.21412	0.20473

Table-6.4 shows the Crystalline Volume Fraction (%) of the present glassy system. Table-6.4 indicates that when value of x increases from 0.05 to 0.1 in the glass composition, the

crystalline volume fraction percentage decreases from 39.4% to 24.7% and at $x = 0.2$ it is found to increase to 27.3%.

Table-6.4: Crystalline Volume Fraction (%) of Chalcogenide system $x\text{Ag}_2\text{S} - (1-x)(0.5\text{Se} - 0.5\text{Te})$ for $x = 0.05, 0.1, 0.2$

Values of x	Crystalline Volume Fraction (%)
0.05	39.4
0.1	24.7
0.2	27.3

6.3.2. FT-IR

The present glassy system showed a good transparency in the spectral range $4000\text{cm}^{-1} - 400\text{cm}^{-1}$. In Fig-6.2, FT-IR spectra of the present glassy system having $x = 0.05, 0.1$ and 0.2 is shown. Since vibrational bands associated with the basic chemical bonds of the composition of the system are below the wave number 400 cm^{-1} , hence they could not be detected. Very few absorption bands can be observed in Fig-6.2 which occurred due to the chemical bonds of impurities present in the system. The percentage of intensity of absorption bands is very small.

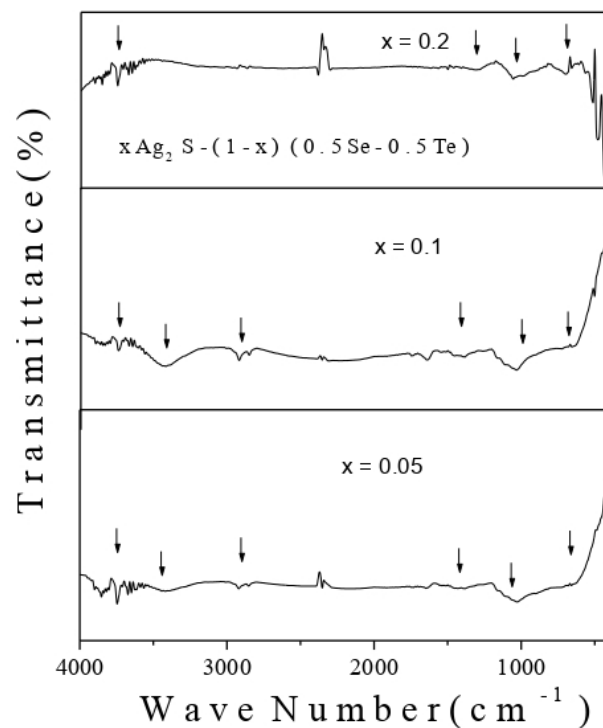


Fig-6.2: FT-IR transmittance spectra of Chalcogenide system $x\text{Ag}_2\text{S} - (1-x)(0.5\text{Se} - 0.5\text{Te})$ where, $x = 0.05, 0.1$ and 0.2

Chalcogenide glassy systems containing Sulphur are having greater affinity to absorb water related particles. Appearance of bands near wave number 1640 cm^{-1} and in the range $3700\text{--}3300\text{ cm}^{-1}$ are associated with stretching and bending vibrations of hydroxyl group in system [14-15]. Some moisture may be absorbed by the glassy system from atmosphere during its preparation which may be the cause for appearance of absorption bands related to O-H and H_2O groups [15]. The appearance of band at $500\text{--}650\text{ cm}^{-1}$ is due to the characteristic vibration of Ag – S in the system [16].

All these bands appeared in the IR spectra are very weak and independent on the composition of the glassy system. The band appeared around 2351 cm^{-1} may be associated with H_2S molecules which occurs in the spectral range $2340\text{ cm}^{-1} - 2365\text{ cm}^{-1}$ [15]. The appearance of band at $1000 - 800\text{ cm}^{-1}$ is due to vibration of $\text{Se} = \text{O}$ in the system [14]. The intermolecular vibration of $\text{Te} - \text{O}$ bonds are responsible for the absorption bands in the spectral range $780\text{ cm}^{-1} - 720\text{ cm}^{-1}$ [17].

6.3.3. DC Conductivity

The measurement of DC conductivity of the present glassy system was carried out at various temperatures. The plot represents change of DC conductivity σ_{DC} with temperature of the system having values of $x = 0.05, 0.1$ and 0.2 is shown in Fig-6.3. The increase of DC conductivity on increasing value of x from 0.05 to 0.1 in the system can be seen from Fig-6.3. On the further increase of x i.e., from 0.1 to 0.2 the DC conductivity is found to decrease. Fig-6.3 indicates the semiconducting behaviour of this system as the DC conductivity is found to increase on increasing temperature.

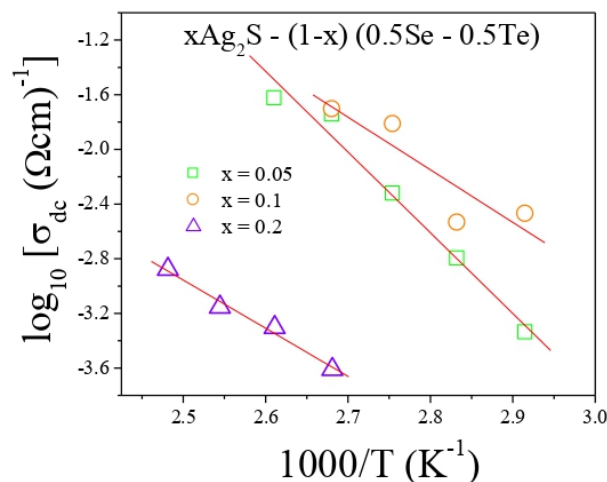


Fig-6.3: Variation of DC Conductivity with temperature of Chalcogenide system $x\text{Ag}_2\text{S} - (1-x)(0.5\text{Se} - 0.5\text{Te})$ where, $x = 0.05, 0.1, 0.2$

Activation energies correspond to DC conductivity for $x = 0.05, 0.1$ and 0.2 of the system have been calculated from the slopes of linear fittings of the plots of Fig-6.3 and are shown in Table-6.5. Decrease in activation energy on increase of x from 0.05 to 0.1 is found. On the further increase of x in the composition of the glassy system, an increase in activation energy is found. In Fig-6.4 Cole-Cole plot of the present system with $x = 0.05, 0.1$ and 0.2 at 343K is shown. From Fig-6.4 the decrease in resistance with the increase of x from 0.05 to 0.1 and its increase on further increase of x from 0.1 to 0.2 is confirmed. This zigzag nature of activation energy can be correlated with the structure of this system.

Table-6.5: Activation energy calculated from linear fitting of DC conductivity plots of system $x\text{Ag}_2\text{S} - (1-x) (0.5\text{Se} - 0.5\text{Te})$ for $x = 0.05, 0.1, 0.2$

x	Activation Energy (eV)
0.05	1.17
0.1	0.67
0.2	0.70

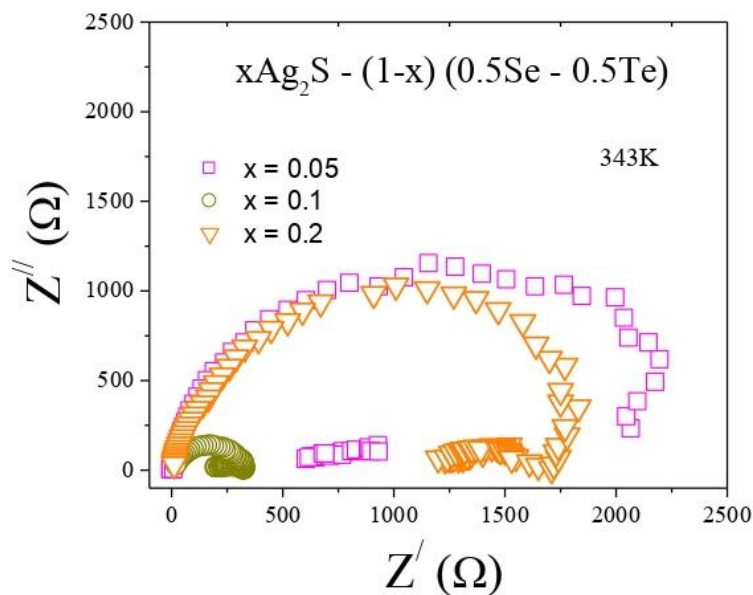


Fig-6.4: Cole-Cole plots of Chalcogenide system $x\text{Ag}_2\text{S} - (1-x) (0.5\text{Se} - 0.5\text{Te})$ where, $x = 0.05, 0.1, 0.2$ at 343K

6.3.4. AC Conductivity

6.3.4.1. Power Law

Jonscher's power law equation, which has already been discussed in Section 3.3.6.1 of Chapter 3, was used for expressing AC conductivity of this system.. The plots of AC conductivity data with respect to frequency at the frequency region $235\text{Hz} - 1.5\text{MHz}$ and at a

range of temperatures are shown in Fig-6.5(a), (b) and (c) for the present system with $x = 0.05, 0.1$ and 0.2 respectively. It can be observed from the figure that AC conductivity of the system increases linearly on increasing frequency. The increase of conductivity with the increase of temperature can also be observed from Fig-6.5, which confirms the thermally activated nature of the system.

The AC conductivity data of Fig-6.5 are fitted with least square straight lines using Eqn. (3.9) of Chapter 3 which is indicated by the solid lines in Fig-6.5. The values of frequency exponent S were calculated from slopes of the solid lines. In Fig-6.6(a), (b) and (c), the plots of variation of S with temperature of this system with $x = 0.05, 0.1$ and 0.2 respectively are shown. To know the conduction mechanism in the present system, Fig-6.6(a), (b) and (c) were analyzed by trying to fit with different available models. Details of these models have already been discussed in Section 3.3.6.1 of Chapter 3.

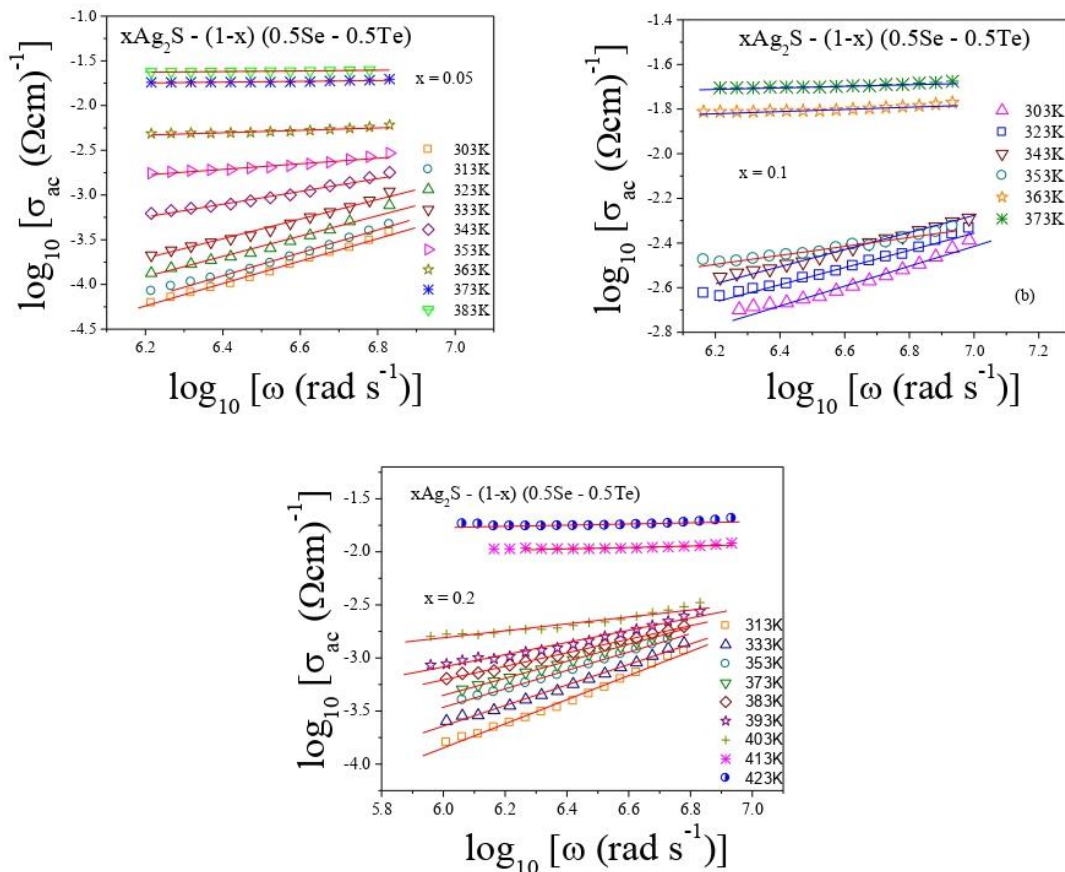


Fig-6.5: Conductivity spectra of glassy alloy $x\text{Ag}_2\text{S} - (1-x)(0.5\text{Se} - 0.5\text{Te})$ where, $x =$ (a) 0.05, (b) 0.1 and (c) 0.2 in frequency region 235Hz – 1.5MHz. Solid lines indicate best-fitted straight lines, slopes indicate ‘S’

Fig-6.6(a), (b) and (c) are found to be best fitted with correlated barrier hopping (CBH) modified model. Details of CBH model are given in Section 3.3.6.1 of Chapter 3. In CBH modified model S can be expressed as

$$S = 1 - \frac{6K_B T}{W_m + K_B(T - T_0) \times \ln(\omega \tau_0)} \quad (6.1)$$

where, T_0 represents the temperature at which S becomes unity and W_m is the maximum barrier height and τ_0 represents relaxation time. All the fitting parameters i.e., τ_0 , W_H and T_0 obtained from the fittings of Fig-6.6(a), (b) and (c) with Eqn. (6.1) are shown in Table-6.6. Solid lines in Fig-6.6 show the best fitted curve with Eqn. (6.1).

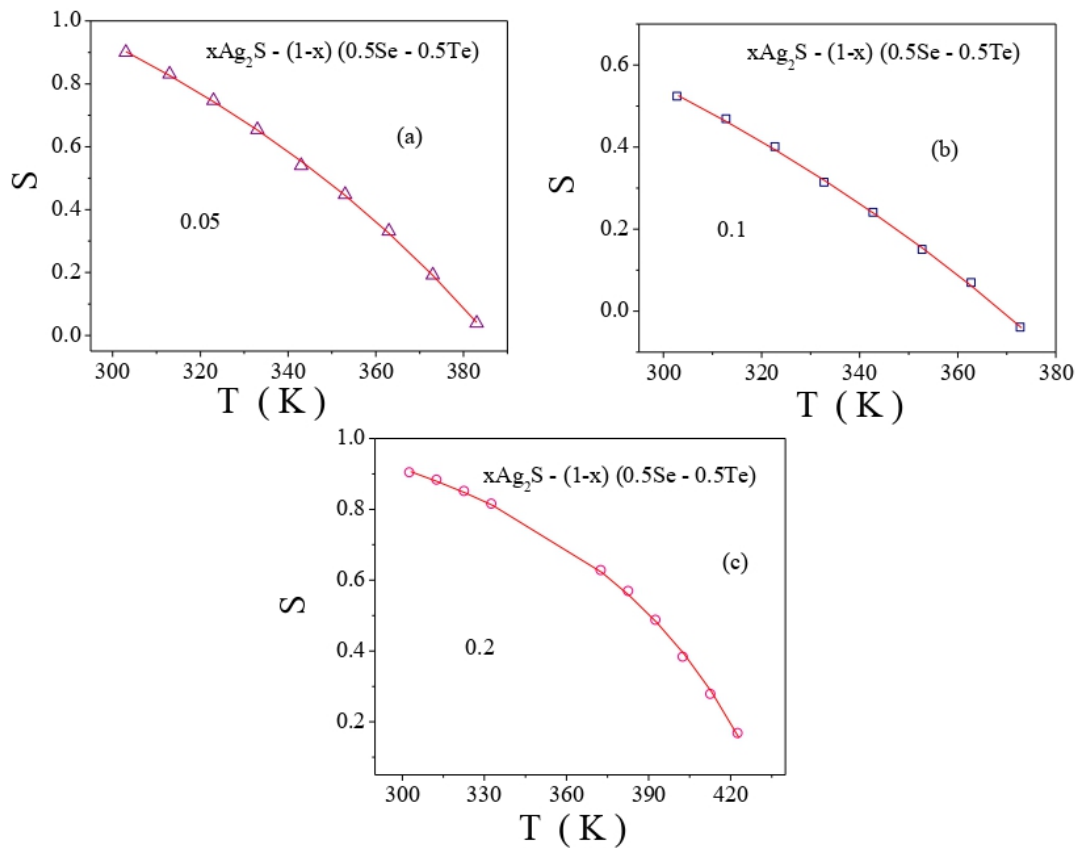


Fig-6.6: S versus T plots of Chalcogenide glassy alloy $xAg_2S - (1-x) (0.5Se - 0.5Te)$ where, $x =$ (a) 0.05, (b) 0.1 and (c) 0.2. Solid lines indicate the fitting of plots with CBH (modified) model

We therefore found that for the present glassy system CBH (modified) model is most suitable for conduction mechanism, according to which the conduction occurs because of charge carriers' hopping in pairs over potential barrier between two charged defect states.

Table-6.6: Different parameters obtained from CBH (modified) model fitting and Almond West formalism of system $x\text{Ag}_2\text{S} - (1-x) (0.5 \text{ Se} - 0.5 \text{ Te})$ for $x = 0.05, 0.1, 0.2$

x	CBH (modified form)			ALMOND -WEST	
	W_m (eV) (± 0.01)	τ_0 (s) $\times 10^{-6}$ (± 0.001)	T_0 (K) (± 1.0)	E_H (eV) (± 0.01)	n (± 0.01)
0.05	0.07874	5.0091	279.42	0.498	2.46
0.10	0.11433	2.7909	265.70	0.3824	1.80
0.20	0.09874	7.6066	321.78	0.900	1.68

6.3.4.2. Almond West Formalism

The variation of AC conductivity of the system having $x = 0.05, 0.1$ and 0.2 with frequency at various temperatures (range: 303K-423K) is shown in Fig-6.7(a), (b) and (c) respectively which have been analysed for exploring the crossover or hopping frequency and conduction pathways of polarons in the system. On increasing temperature, the AC conductivity is found to increase and it is independent on frequency at lower frequency region. It point towards that the AC conductivity at low frequency region of the system is thermally activated. The hopping of polarons may be the cause of the frequency independent AC conductivity in such glasses [18, 19]. At higher frequency region, above crossover or hopping frequency, AC conductivity starts increasing with frequency which occurs due to correlated motion of polarons [18, 19] which is ruled by Jonscher power law (which has already been discussed in Section 3.3.6.1 of Chapter 3).

For the analysis of the AC conductivity spectra, for getting various information regarding conduction process in the system, Almond West formalism is applied, details of which have been given in Section 3.3.6.2 of Chapter 3. Solid lines in Fig-6.7(a), (b) and (c) show the Almond West formalism fitted AC conductivity spectra of the present system. Different parameters like - σ_{DC} , ω_H and n have been obtained by fitting Fig-6.7 with Eqn. (3.15) of Chapter 3. The values of fractional power law exponent n of the system with $x = 0.05, 0.1$ and 0.2 are shown in Table-6.6 which is found to be greater than one for all values of x. The value of n is strongly linked to the dimensions of conduction pathways in the system. The $n > 1$ values indicated that the motion of polarons in the system is of percolation type [20].

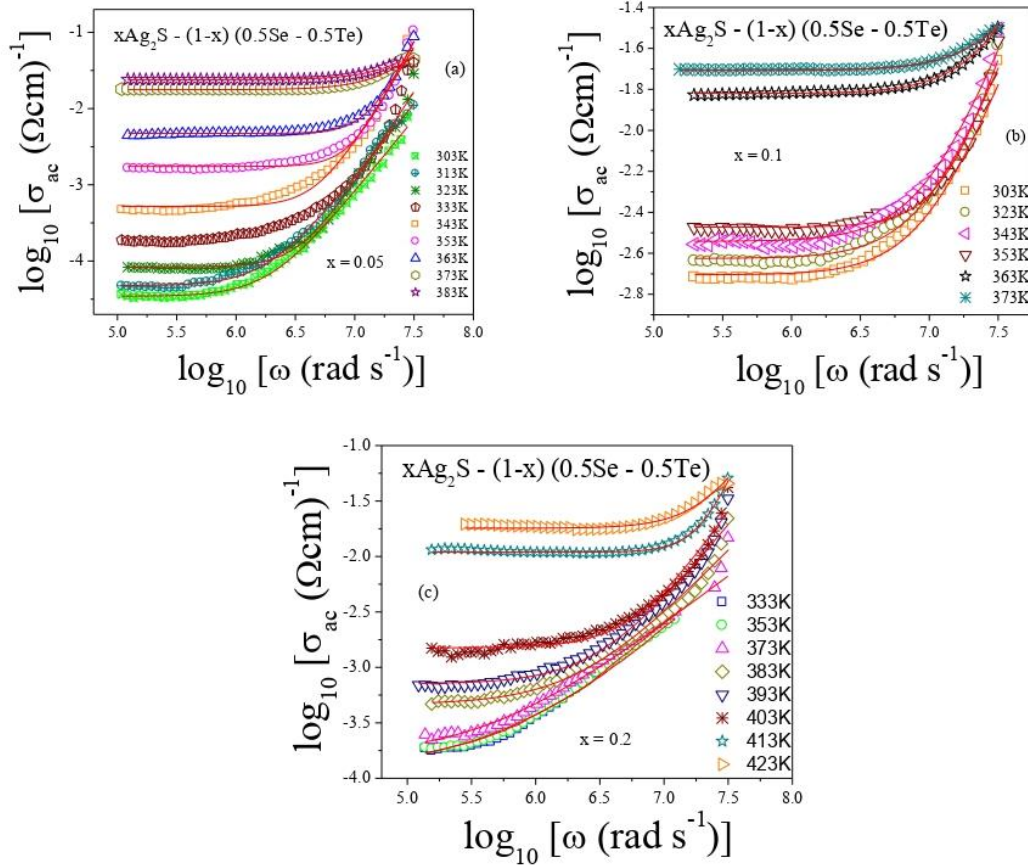


Fig-6.7: AC conductivity spectra of the system $x\text{Ag}_2\text{S} - (1-x)(0.5\text{Se} - 0.5\text{Te})$ where, $x =$ (a) 0.05, (b) 0.1 and (c) 0.2 at different temperatures

Conductivity spectra of this system having values of $x = 0.05, 0.1$ and 0.2 at 363K are shown in Fig-6.8 in which the AC conductivity is found to increase first and then decrease with the increase in x i.e., the content of Ag_2S in the glass composition which validates DC conductivity plots shown in Fig-6.3. The maximum ac conductivity is exhibited by the system having value of $x = 0.1$. The decrease of conductivity at $x = 0.2$ is an indication of decrease of the rate of polaron hopping. The increase of Crystalline Volume Fraction (%) with the increase of x from 0.1 to 0.2 (as shown in Table-6.4) indicates the limitation in open structure which reduces the amount of free volume in the system for the hopping of polarons. This results in the decrease of AC conductivity in the system with $x=0.2$.

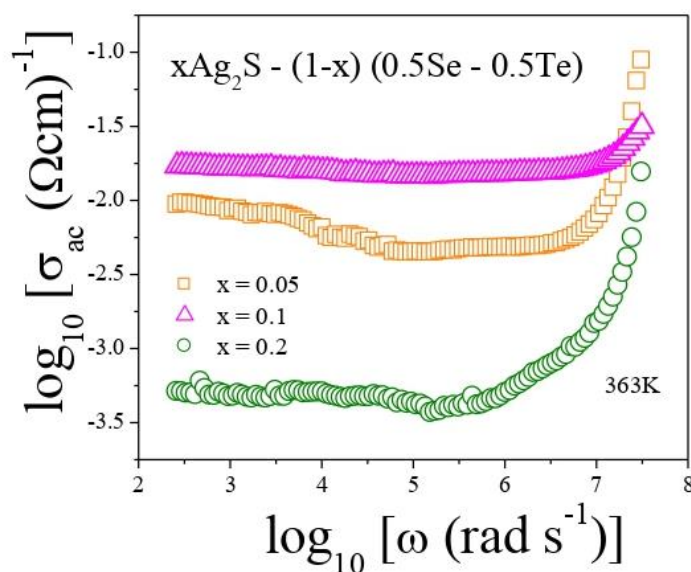


Fig-6.8: AC conductivity spectra of the system $x\text{Ag}_2\text{S} - (1-x) (0.5\text{Se} - 0.5\text{Te})$ where, $x = 0.05, 0.1$ and 0.2 at 363K

The variation of hopping frequency ω_H with temperature of the present system is shown in Fig-6.9(a), which can be represented by the Arrhenius equation, Eqn. (3.16) of Chapter 3 (explanation of which is given in Section 3.3.6.2 of Chapter 3). Fig-6.9(a) shows the thermally activated nature of hopping frequency ω_H which is found to increase on increasing temperature. ω_H value is found maximum in the system having $x = 0.1$.

To calculate the activation energy for hopping frequency E_H , plots of Fig-6.9(a) has been linearly fitted with Eqn. (3.16) of Chapter 3. From the slopes of fitted straight lines, E_H of the present glassy system having $x = 0.05, 0.1$ and 0.2 have been calculated and are shown in Table-6.6.

The variation of E_H with x is shown in Fig-6.9(b). The figure indicates that E_H decreases initially and then increases on increasing the amount of Ag_2S in the system. E_H is found to be minimum in the system having $x = 0.1$. The decrease of activation energy E_H indicates the increase of hopping frequency of polarons and hence the electrical conductivity in the system as the dislocation nature of the system approves the conduction due to hopping of polarons.

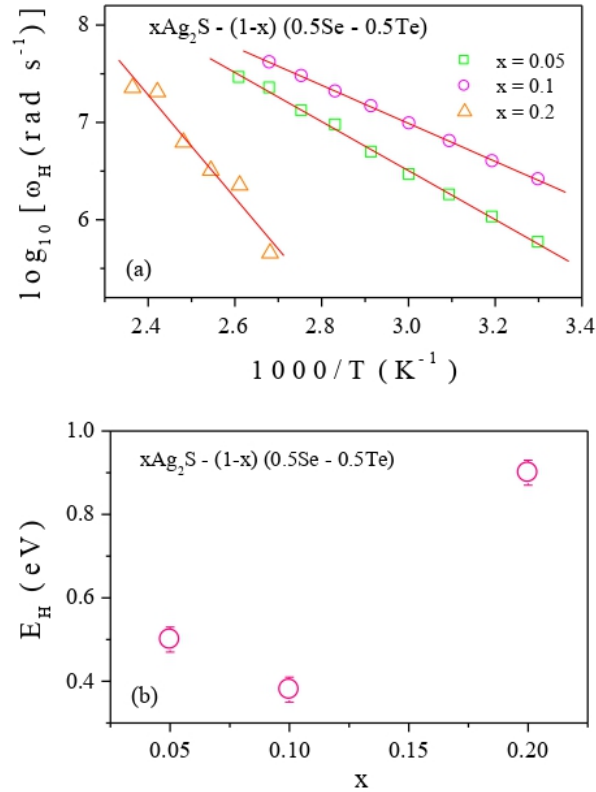


Fig-6.9: (a) Plot of ω_H versus $1000/T$ of Chalcogenide system $x\text{Ag}_2\text{S} - (1-x)(0.5\text{Se} - 0.5\text{Te})$ where, $x = 0.05, 0.1, 0.2$
(b) Plot of E_H versus x of the same system

6.3.4.3. AC Conductivity Scaling

AC conductivity scaling process helps in predicting the dependency of electrical relaxation process on composition and temperature of glasses.. The detail of AC conductivity scaling has been discussed in Section 3.3.6.3 of Chapter 3.

Fig-6.10(a), (b) and (c) show the AC conductivity scaling of the present system with $x = 0.05, 0.1$ and 0.2 respectively at different temperatures. It can be seen from Fig-6.10(a), (b) and (c) that conductivity spectra of the system at different temperatures overlaps in a single curve which suggests the temperature independent relaxation process in the system. In Fig-6.11, the composition scaling i.e., the scaling of AC conductivity data of the system having different values of x (i.e., $0.05, 0.1$ and 0.2) at a fixed temperature (373K) is shown. In Fig-6.11 the non-overlapping of conductivity spectra of the system into a single master curve is found, which is an indication of composition dependent relaxation process in the system since the structure of the system must change with the content of Ag_2S in the system.

From the analysis of AC conductivity scaling, composition dependent and temperature independent relaxation mechanism in the system has been found.

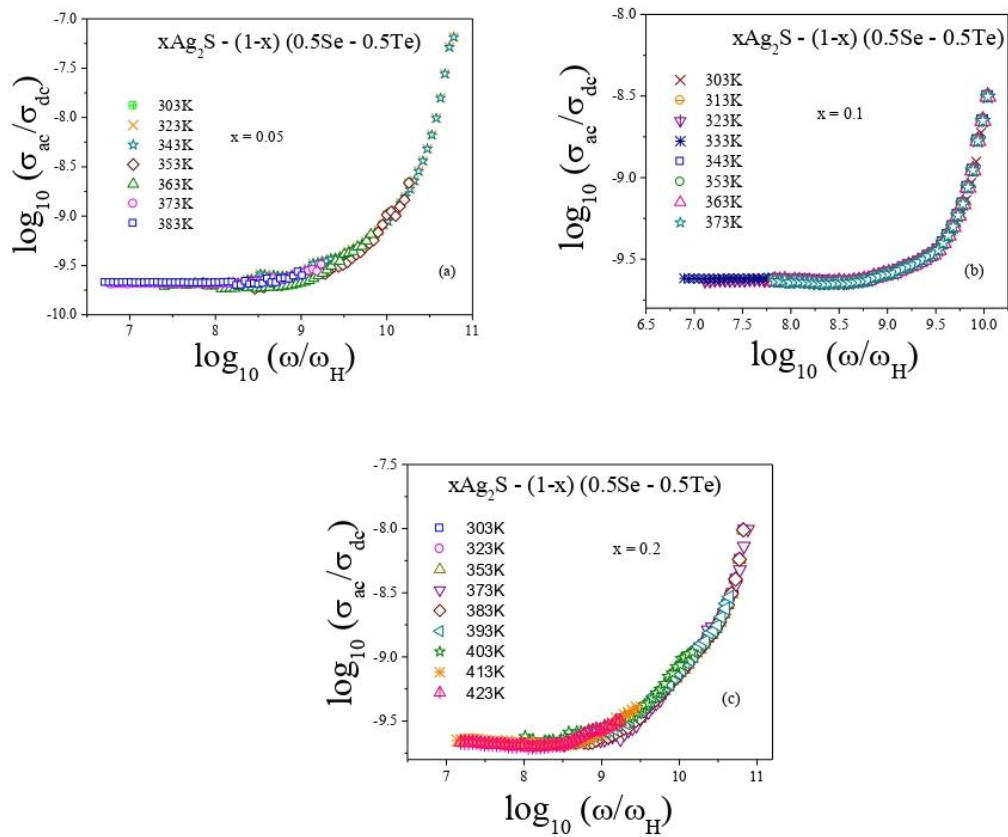


Fig-6.10: AC conductivity scaling of Chalcogenide system $x\text{Ag}_2\text{S} - (1-x)(0.5\text{Se} - 0.5\text{Te})$ where, $x =$ (a) 0.05, (b) 0.1 and (c) 0.2 at different temperatures

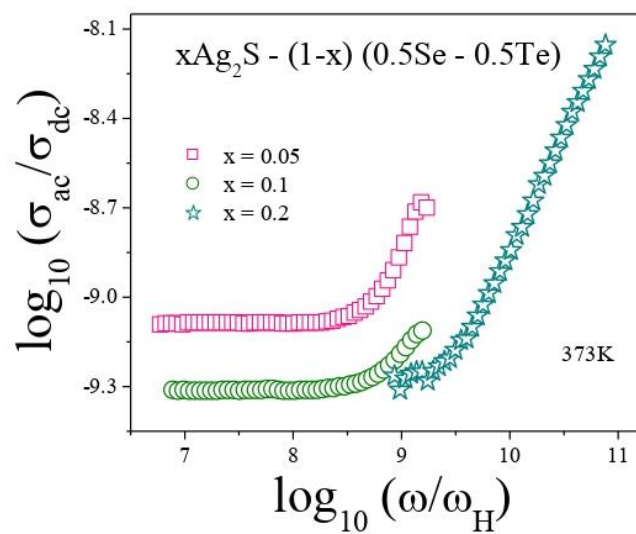


Fig-6.11: AC conductivity scaling of the system $x\text{Ag}_2\text{S} - (1-x)(0.5\text{Se} - 0.5\text{Te})$ for $x = 0.05, 0.1$ and 0.2 at 373K

6.3.4.4 Mobility and Carrier Density

To find the carrier mobility (μ) and carrier density (N) of the present glassy system DC polarization technique has been used, details of which have already been discussed in Section 3.3.6.5 of Chapter 3. The mobility of charge carriers has been determined by Eqn. (3.20) of Chapter 3. To determine the carrier density ‘ N ’ Eqn. (3.21) of Chapter 3 has been used.

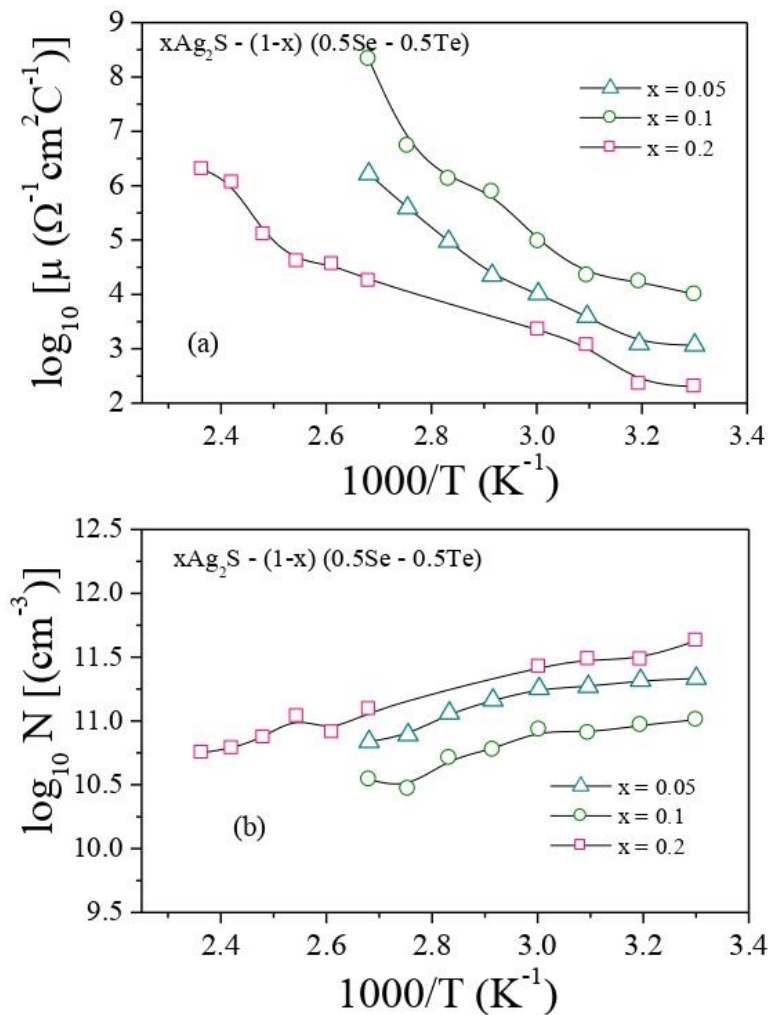


Fig- 6.12: (a) $\log_{10} \mu$ versus $1000/T$, (b) $\log_{10} N$ versus $1000/T$ for the Chalcogenide glassy system $x\text{Ag}_2\text{S} - (1-x)(0.5\text{Se} - 0.5\text{Te})$ where, $x = 0.05, 0.1$ and 0.2

Fig-6.12(a) shows the plot of $\log_{10} \mu$ versus $1000/T$, where T is the temperature in Kelvin, of the system with $x = 0.05, 0.1$ and 0.2 . The mobility is found to increase first and then decrease with the increase of x in the composition. It is found maximum in the system which is having $x = 0.1$. It is found to increase on temperature rising in the system.

In Fig-6.12(b) $\log_{10} N$ versus $1000/T$ of the present system is shown. From Fig-6.13(b) it can be seen that the value of carrier density is maximum in the system which is having the value of $x = 0.1$ in the composition. In Table-6.7 the average mobility and carrier density data is shown for the system with $x = 0.05, 0.1$ and 0.2 .

Table-6.7: Average mobility and carrier density of system $x\text{Ag}_2\text{S} - (1-x) (0.5 \text{ Se} - 0.5 \text{ Te})$ for $x = 0.05, 0.1, 0.2$

x	Carrier Mobility, μ ($\Omega^{-1}\text{cm}^2\text{C}^{-1}$)	Carrier density, N (cm^{-3})
0.05	536453.911	1.02E+11
0.1	55222758.85	1.47E+10
0.2	563593.6	7.30E+10

6.3.5. Study of Dielectric Properties

6.3.5.1. Permittivity

The temperature and frequency dependent ϵ' and ϵ'' of the present glassy system i.e., $x\text{Ag}_2\text{S} - (1-x) (0.5 \text{ Se} - 0.5 \text{ Te})$ in frequency range 42Hz – 5MHz at various temperatures (range: 303K-423K) and have been calculated. Fig-6.13(a), (b) and (c) show the variation of ϵ' of the system with $x = 0.05, 0.1$ and 0.2 respectively with frequency at various temperatures.

It can be observed from Fig-6.13 and Fig-6.14 that both ϵ' and ϵ'' decrease on the increase of frequency at various temperatures. The more values of ϵ' at lower frequencies are e mainly due to the occurrence of electrode polarization because of the accumulation of space charges at glass-electrode interface, which mainly occurs at the frequency range between 1 and 10^3 Hz. With the increase of frequency the effect of polarization decreases because the molecular dipoles in the system cannot follow the fast variation of the electric field. Hence, on increasing frequency in the system, ϵ' starts decreasing and show frequency independent nature. So, absence of electronic polarization (which occurs at $\sim 10^{16}$ Hz) and ionic polarization (which occurs at $\sim 10^{13}$ Hz) can be observed in the system.

Fig-6.14(a), (b) and (c) show the plots of ϵ'' against frequency at different temperatures of the present system having $x = 0.05, 0.1$ and 0.2 respectively. ϵ'' occurs due to the loss of thermal energy in the lattice of the system when polarons move over long distances. The dielectric loss indicates the contributions of conduction loss, ionic vibrational loss and dipole relaxation loss in the system.

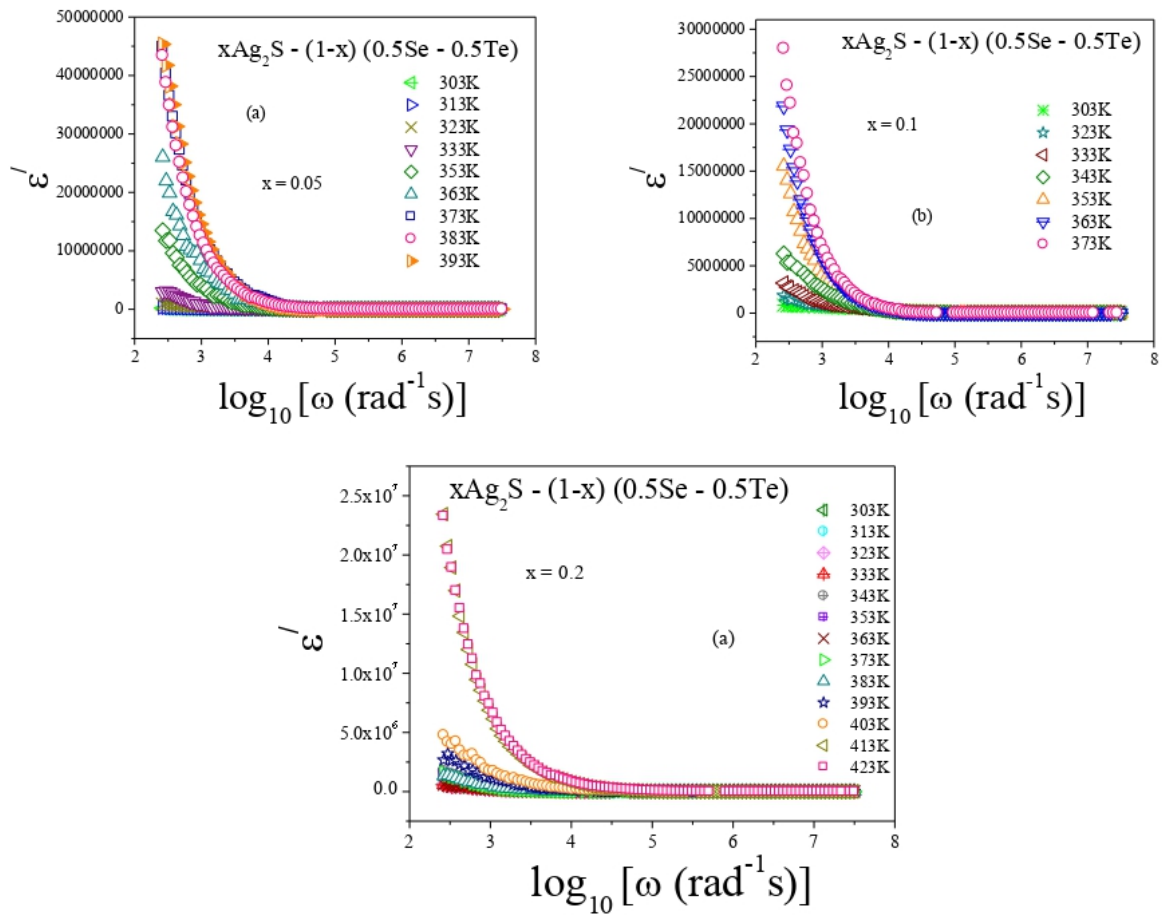


Fig-6.13: Variation of dielectric constant ϵ' with frequency of Chalcogenide system $x\text{Ag}_2\text{S} - (1-x) (0.5\text{Se} - 0.5\text{Te})$ at various temperatures for $x =$ (a) 0.05, (b) 0.1 and (c) 0.2

The increase of ϵ' and ϵ'' on the increase of temperature can be observed from Fig-6.13 and Fig-6.14 respectively. The reason behind this is the increase of polarization effect in the system due to decrease in bond energies as the intermolecular forces get weakened by the temperature rise, which results in enhancing the orientational vibrations and hence increases the polarization. At higher temperatures, the contribution of all the losses to ϵ'' of the system is the reason of higher ϵ'' .

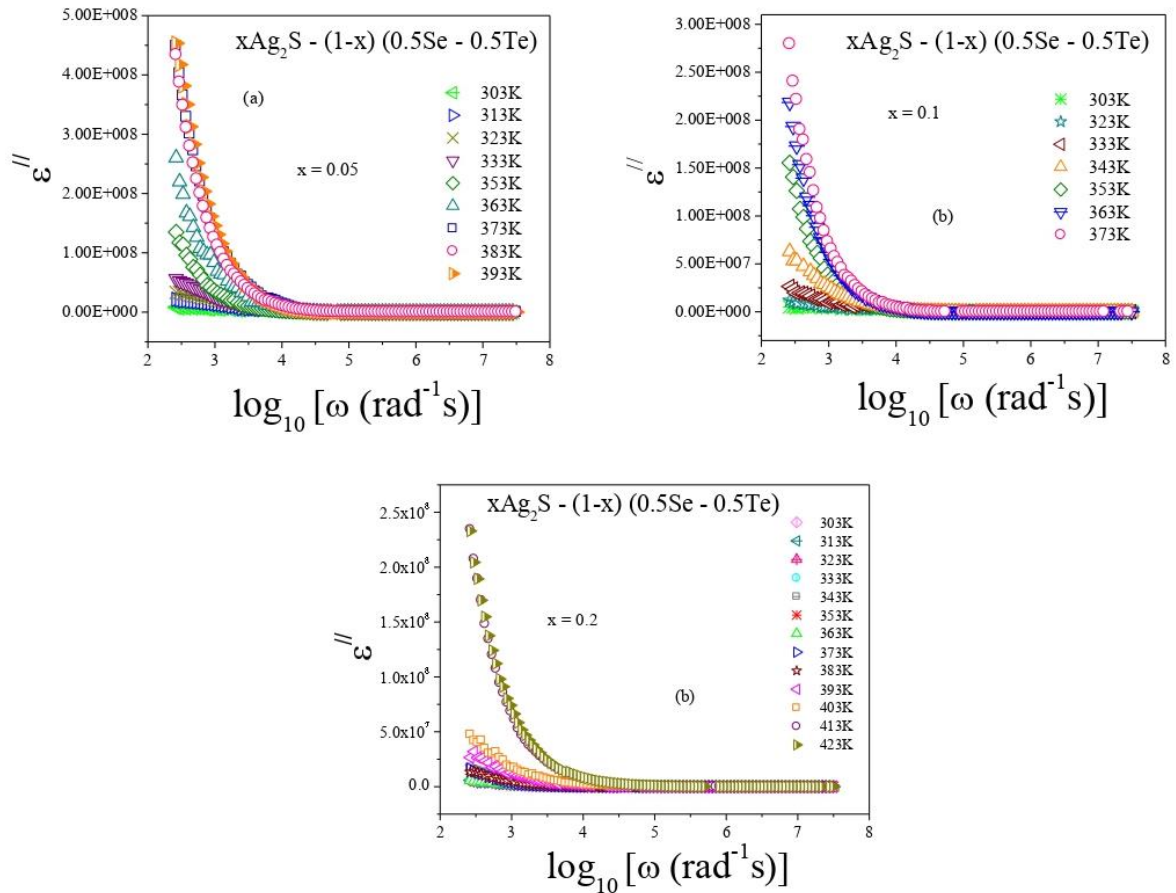


Fig-6.14: Variation of dielectric loss ϵ'' with frequency of Chalcogenide system $x\text{Ag}_2\text{S} - (1-x) (0.5\text{Se} - 0.5\text{Te})$ at various temperatures where, $x =$ (a) 0.05, (b) 0.1 and (c) 0.2

6.3.5.2. Electric Modulus

The electrical relaxation properties of these glasses is studied using electrical modulus formalism details of which has already been discussed in the in the Section 2.4.3.2 of Chapter 2. In Fig-6.15(a), (b) and (c) the variation of real part of electric modulus M' with frequency is shown for the system having $x = 0.0, 0.1, 0.2$ and 0.3 respectively. In Fig-6.15(a), (b) and (c), M' is found to approach zero at all the mentioned temperatures and low frequency region which mainly occurs because of the suppression of electrode polarization because of unavailability of restoring forces of charge carriers [21-23]. But at higher frequencies, dispersion in M' is found and M' exhibits a maximum value which is: $(M_\infty) = (\epsilon_\infty)^{-1}$ because of the electrical relaxation of polarons [21-23]. In Fig-6.15(a), (b) and (c) a gradual decrease in M' with the rise of temperature is found which may implies the of movement of polarons, within small range, in the conduction mechanism of the glassy system.

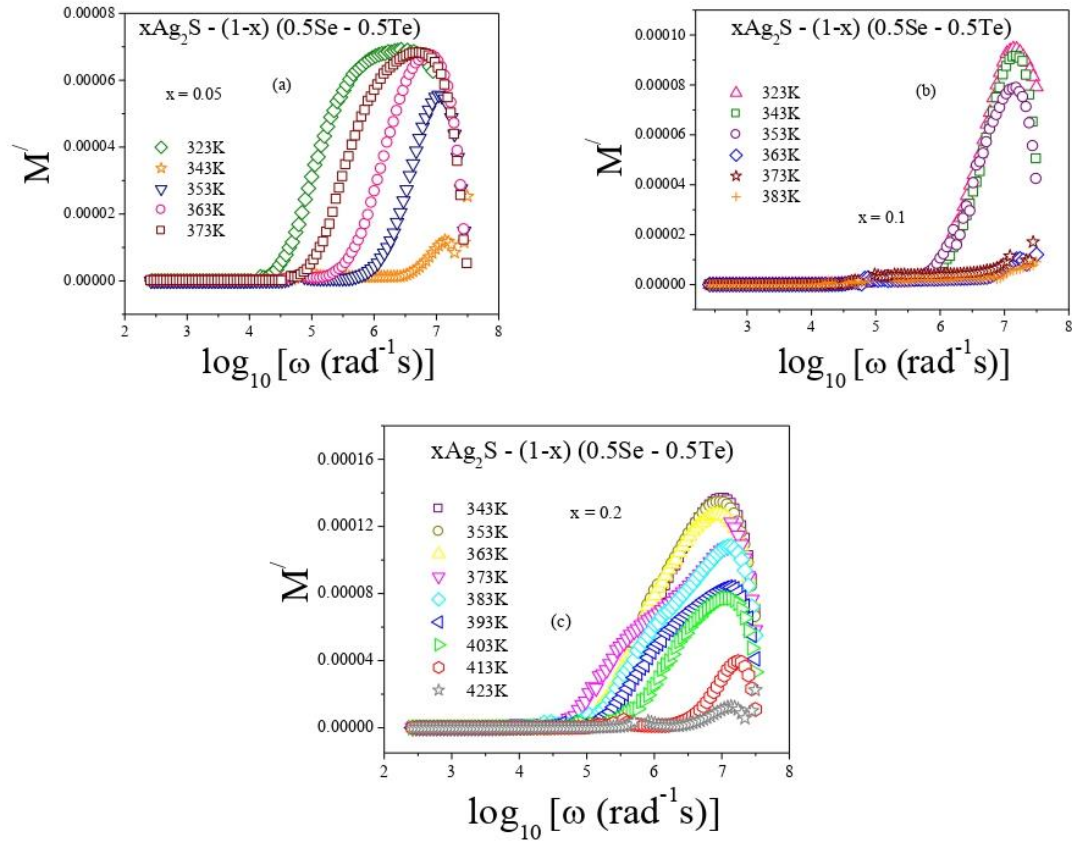


Fig-6.15: Variation of real electric modulus M' with frequency of Chalcogenide system $x\text{Ag}_2\text{S} - (1-x)(0.5\text{Se} - 0.5\text{Te})$ at various temperatures with $x =$ (a) 0.05, (b) 0.1 and (c) 0.2

Fig-6.16(a), (b) and (c) show the variation of imaginary electric modulus M'' with frequency of the system with $x = 0.05, 0.1$ and 0.2 respectively. The shifting of M'' peaks towards higher frequencies with the increase of temperature, as shown in Fig-6.16, signifies that the relaxation process of the glassy system is dependent on temperature. The movement of thermally activated charge carriers may reduce the relaxation time and increase the relaxation frequency. Polarons' hopping over long distances may be the cause for the conduction in these glasses below the peak relaxation frequency ω_{\max} . Above ω_{\max} the cause of conduction mechanism may be the localized motion of charge carriers over short distances [22, 23]. The M'' peak shifting indicates the stabilization of the system in a short time for an external force at eminent temperature.

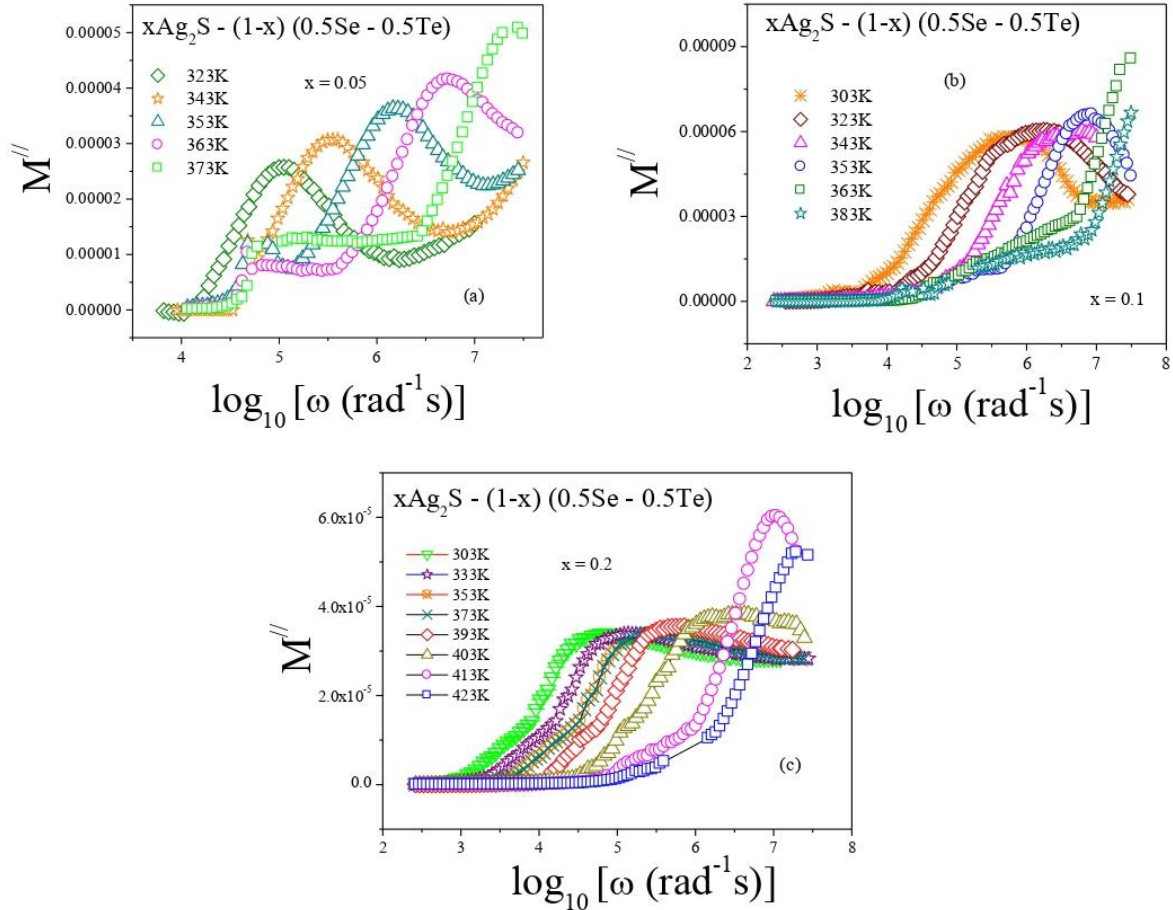


Fig-6.16: Variation of imaginary electric modulus M'' with frequency of Chalcogenide system $x\text{Ag}_2\text{S} - (1-x) (0.5\text{Se} - 0.5\text{Te})$ at various temperatures with $x =$ (a) 0.05, (b) 0.1 and (c) 0.2

To obtain values of M''_{\max} (maximum value of M''), ω_{\max} (angular frequency corresponds to M''_{\max}), and β (Kohlrausch-Williams-Watts stretched coefficient), imaginary electric modulus M'' spectra of the system having $x = 0.05, 0.1$ and 0.2 (i.e., Fig-6.16) have been fitted with Eqn. (5.1) of Chapter 5. The variation of relaxation time τ (where, $\tau = 1/\omega_{\max}$) with temperature for the present system with $x = 0.05, 0.1$ and 0.2 is shown in Fig-6.17. The decrease of relaxation time with the rise of temperature points towards the semiconducting behaviour of this system.

To determine the activation energy (E_{τ}) related to the relaxation time τ , Eqn. (27) of Chapter 2 is used. Solid lines in Fig-6.17 indicate the linear fitting of $\log_{10} \tau$ versus $1000/T$ plots with Eqn. (27) of Chapter 2. E_{τ} has been measured from slopes of the solid lines and is shown in Table-6.8. The relaxation time τ is found to first decrease and then increase with the increase of x i.e. the content of Ag_2S in the system, as shown in Fig-6.17. Lower values of relaxation time directly indicate the higher conductivity due polaron hopping in the system. Table-6.8

shows the variation of activation energy E_τ related to the dielectric relaxation process with x , in which the decrease of activation energy with the increase of x and then its increase on further increase of x is indicated.

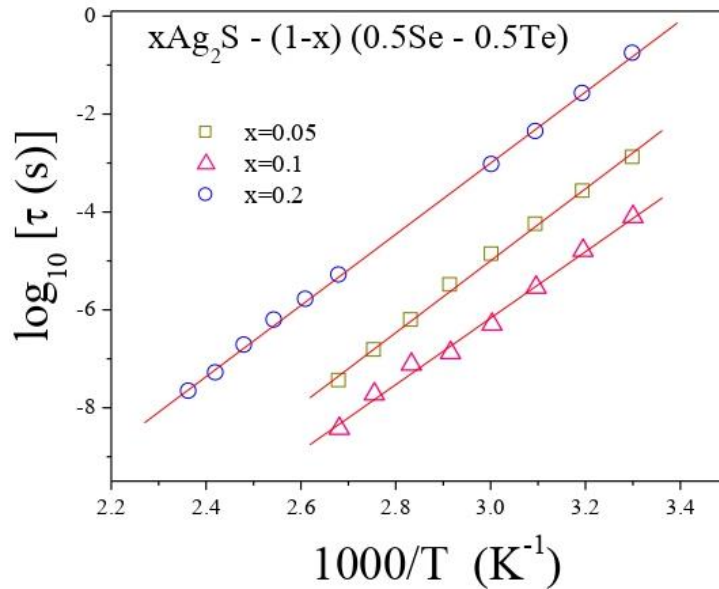


Fig-6.17: Variation of τ with temperature of Chalcogenide system $x\text{Ag}_2\text{S} - (1-x) (0.5 \text{ Se} - 0.5 \text{ Te})$ where, $x = 0.05, 0.1$ and 0.2

Table-6.8: Variation of activation energy related to dielectric relaxation process of system $x\text{Ag}_2\text{S} - (1-x) (0.5 \text{ Se} - 0.5 \text{ Te})$ with x

x	E_τ (eV)
0.05	1.48
0.1	1.20
0.2	1.52

6.3.5.3. Electric Modulus Scaling

To analyze the relaxation process in the present system dielectric modulus M'' scaling is carried out. For this, the y-axis i.e., M'' values of Fig-6.16(a), (b) and (c) are divided by M''_{\max} (maximum value of imaginary modulus) and x-axis i.e., ω values, by ω_{\max} (the frequency at which M'' peak occurs). Fig-6.18(a), (b) and (c) show the temperature scaling of the electric modulus M'' plots of the present system having $x = 0.05, 0.1$ and 0.2 respectively at various temperatures in the range from 303K to 423K. In Fig-6.18(a), (b) and (c) the overlapping of scaled data is found, which is an indication of temperature independent relaxation process of the system.

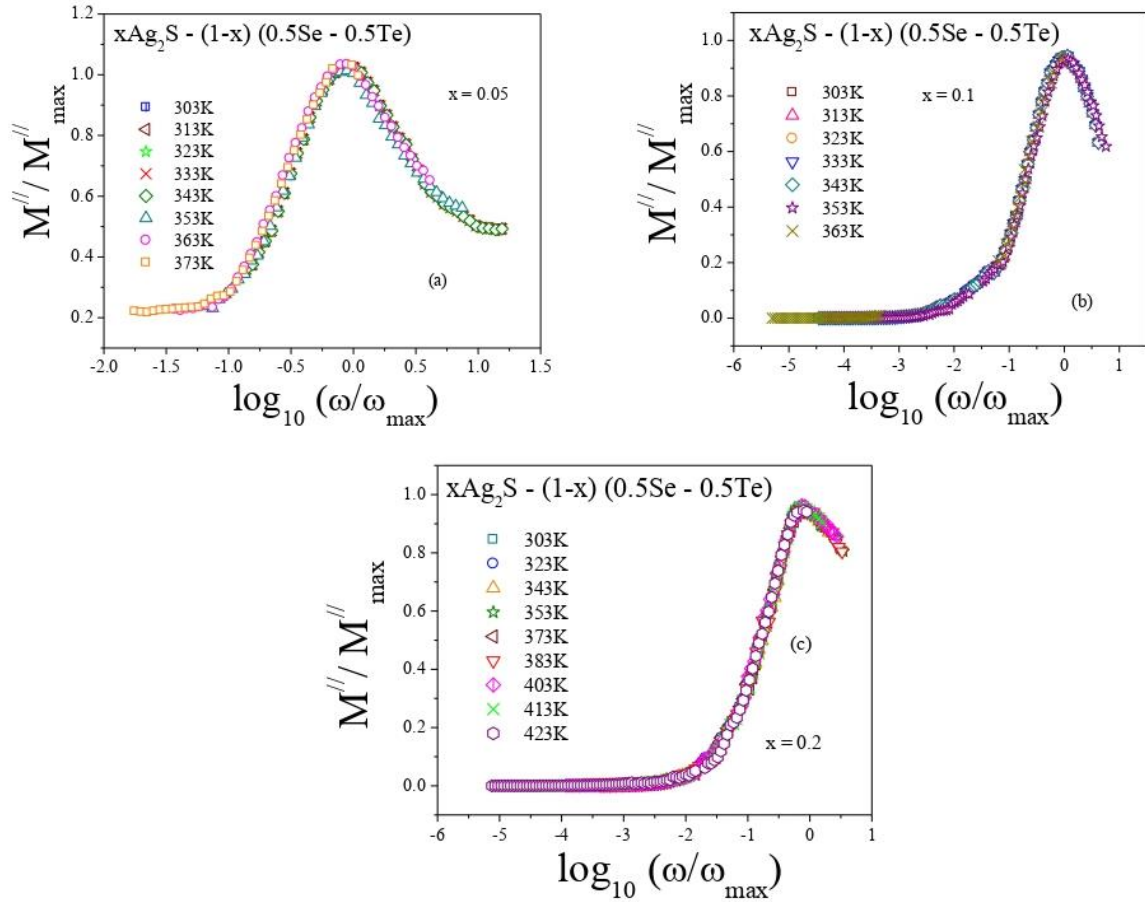


Fig-6.18: Temperature scaling of M'' of Chalcogenide system $xAg_2S - (1-x) (0.5 Se - 0.5 Te)$ with $x =$ (a) 0.05, (b) 0.1 and (c) 0.2

In Fig-6.19, composition scaling in which electric modulus M'' scaling plots of the present system having $x = 0.05, 0.1$ and 0.2 at a fixed temperature ($343K$) is shown. The non-overlapping of the plots in Fig-6.19 is a clear indication of composition dependent relaxation process in the system. So, the temperature independent and composition dependent nature of relaxation process can be observed from the electric modulus scaling process of the present glassy system.

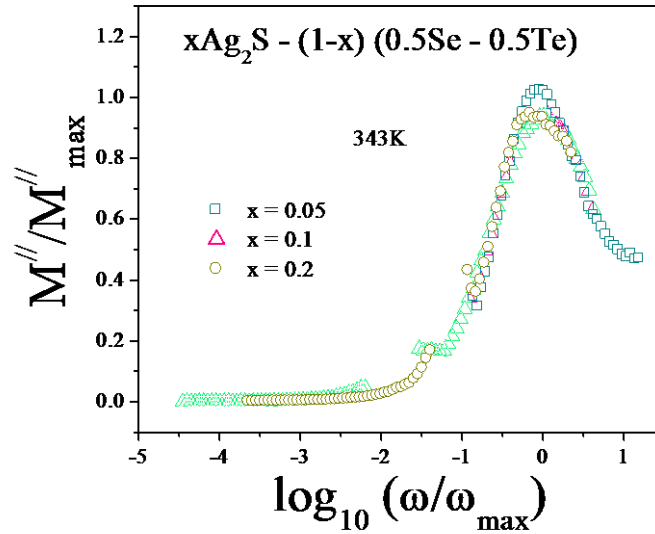


Fig-6.19: Composition scaling of M'' of Chalcogenide system $x\text{Ag}_2\text{S} - (1-x)(0.5\text{Se} - 0.5\text{Te})$ for $x = 0.05, 0.1$ and 0.2 at 343K

6.4. CONCLUSION:

Chalcogenide glassy system having composition $x\text{Ag}_2\text{S} - (1-x)(0.5\text{Se} - 0.5\text{Te})$, in which $x = 0.05, 0.1$ and 0.2 , was prepared using melt quenching method. With the help of XRD technique polycrystalline nature of the system has been observed. From the XRD analysis, the size of the different phases present in the system with their $[h,k,l]$ values and dislocation density have been calculated. The system having $x = 0.1$ shows the maximum crystallite size and minimum dislocation density. The crystalline volume fraction is found minimum in the system having value of $x = 0.1$.

From the analysis of FT-IR spectroscopy spectra of the present glassy system, a good transparency in the spectral range $4000\text{cm}^{-1} - 400\text{cm}^{-1}$ can be observed and most of the absorption bands can be assigned to vibrational bands of oxides and hydrides bonds which may be arisen due to the presence of extrinsic impurities in the system introduced during its preparation. FT-IR spectra indicate the presence of different functional groups and molecules like O-H, Ag - S, H_2S and H_2O in the glassy system.

To study the electrical properties of the present system, DC and AC conductivity measurements at various frequencies (range: $42\text{Hz} - 5\text{MHz}$) and temperatures (range: $303\text{K}-$

423K) have been carried out. From the plots of DC conductivity versus temperature, activation energies of the system have been calculated. The activation energy is found to decrease first and then increase with the increase of x . From Cole-Cole plot, the resistance of the system is found to decrease on the increase of x from 0.05 to 0.1 and then increase on the increase of x from 0.1 to 0.2. The maximum DC conductivity is observed in the system having value of $x = 0.1$. Increase of DC conductivity with temperature confirms the semiconducting nature of this system.

Almond West model has been applied for the analysis of AC conductivity data from which E_H of this system has been calculated. The decrease of activation energy related to hopping frequency is found with the increase of Ag_2S content i.e., x in the system from 0.05 to 0.1. The activation energy E_H is then found to increase when x increases from 0.1 to 0.2. The minimum E_H is found in the system with $x = 0.1$ which confirms the maximum conductivity in the system. It validates the observations of DC conductivity analysis.

For interpreting the conduction mechanism in the system, CBH (modified) Model is found as the most appropriate model for the system according to which conduction occurs because of hopping of polarons in pairs over potential barrier between two charged defect states. AC conductivity scaling signifies that the system's relaxation process is not dependent on temperature but is dependent on its composition. The carrier mobility and density in the present system is calculated. Carrier mobility is found to increase first and then decrease with the increase of x i.e., Ag_2S content in the system. The maximum carrier mobility is found in the system having $x = 0.1$ in the composition.

From the dielectric permittivity studies, the decrease of both ϵ' and ϵ'' on increasing frequency and decreasing temperature is observed. Activation energy associated with the relaxation process in the glass E_τ is calculated from the analysis of the electric modulus plots. E_τ is found to decrease first and then increase with the increase of Ag_2S content in the present system and it is found minimum in the sample of the system having value of $x = 0.1$. The electric modulus studies confirm the temperature dependent relaxation process in the present system. The temperature and composition scaling of M'' spectra in temperature region 303K – 423K indicate that the electrical relaxation process is independent on temperature but dependent on composition of the system.

REFERENCES

- [1] V. Pamukchieva, A. Szekeres, K. Todorova, E. Svab and M. Fabian, *Opt. Mater.*, 32, 45 (2009)
- [2] J. Sharma and S. Kumar, *J. Alloys Compd.*, 506, 710 (2010)
- [3] S. R. Gunti and S. Asokan, *J. Non-Cryst. Solids*, 356, 1637 (2010)
- [4] A. K. Singh, *J. Non-Oxide Glasses*, 3, 1 (2012)
- [5] N. Sharma, S. Shukla, J. Sharma and S. Kumar, *J. Non-Oxide Glasses*, 3, 121 (2011)
- [6] Ambika and P. B. Burman, *Physica B*, 405, 822 (2010)
- [7] Asobe, Masaki. *Optical Fiber Technology*, 3, 2, 142 (1997)
- [8] A. Zakery, and S. R. Elliott, *J. Non-Crystalline Solids*, 330, 1 (2003)
- [9] A. B. Seddon, *J. Non-Crystalline Solids*, 184, 44 (1995)
- [10] S. O. Kasap, T. Wagner, V. Aiyah, O. Krylouk, A. Bekirov, and L. Tichy. *J. Mat.Sci.*, 34, 3779 (1999)
- [11] Chunyan Cui, Xiaoru Li, Jixian Liu, Yongchao Hou, Yuqing Zhao and Guocheng Zhong, *Nanoscale Research Letters*, 10, 431 (2015)
- [12] Y. Ohmasa, I. Yamamoto, M. Yao and H. Endo, *J. Phys. Soc. Jpn.* 64, 4766 (1995)
- [13] M. Pupp, J. Weiss and Z. Anorg, *Allg. Chem.* 440 31 (1978)
- [14] G. Socrates, “Infrared and Raman Characteristic Group Frequencies”, 3rd Edition, John Wiley and Sons Ltd (2004)
- [15] T. S. Kavetsky, A. P. Kovalskiy, V. D. Pamukchieva and O. I. Shpotyuk, *Infrared Phys. Tech.*, 41, 41 (2000)
- [16] Y. Y. Kim and D. Walsh, *Nanoscale* 2, 240 (2010)
- [17] B. Frumarova, J. Oswald, P. Krecmer, M. Frumar, V. Cerny and V. Smrcka, *Opt. Mater.*, 6, 217 (1996)
- [18] A. Mansingh, J. K. Vaid and R. P. Tondon, *J. Phys. (C) Solid State Physics*, 10, 4061 (1977)
- [19] D. P. Almond, G. K. Duncan and A. R. West, *Solid State Ionics*, 8, 159 (1983)
- [20] B. Roling, A. Happe, F. Funke and M. D. Ingram, *Phy. Rev. Lett.*, 78, 2160 (1997)
- [21] A. B. Karmakar, K. Rademann Andrey and L. Stepanov, “Glass Nanocomposites, Synthesis, Properties and Applications”, Elsevier Inc., (2016)
- [22] S. Ojha, M. Roy, A. Chamuah, K. Bhattacharya and S. Bhattacharya, *Materials Letters* 258, 126792 (2020)
- [23] S. Bhattacharya and A. Ghosh, *J. Am. Cer Soc.* 91, 753 (2008)

Chapter 7

CONCLUSIONS AND FUTURE PROSPECTS

In the present work Transition Metal Ions doped Chalcogenide glassy systems having compositions: $x\text{Ag}_2\text{S} - (1-x) (0.5\text{S} - 0.\text{Te})$ where $x = 0.35$ and 0.45 ; $x\text{Cu} - (1-x) (0.5\text{S} - 0.\text{Te})$ where $x = 0.0, 0.1, 0.2$ and 0.3 ; $x\text{Ag}_2\text{S} - (1-x) (0.5\text{Se} - 0.\text{Ge})$ where $x = 0.1$ and 0.2 ; and $x\text{Ag}_2\text{S} - (1-x) (0.5\text{Se} - 0.\text{Te})$ where $x = 0.05, 0.1$ and 0.2 , have been prepared using melt quenching process [1-6].

The metallic character of Te is stronger than the other chalcogens. But its ability of forming glass is very weak. To improve its ability, Te has been doped with S. Cu is having ability of forming many compounds because of its several oxidation states. Its tendency to form small polarons is very high for electrical conduction. The reversible phase transformation property of Se is exceptional, which makes them suitable for using in applications like rectifiers, memory devices, switches, photocells, etc [7]. But short life time and low photosensitivity are major drawbacks of Se. For overcoming this, Se can be doped with Ge [8]. The thermal stability of chalcogens is very poor. The use of Cu and Ag_2S in the prepared glassy systems helped in improving the stability.

The structural characterization and electrical relaxation studies of all the prepared systems have been carried out using various techniques. Based on the observations obtained from the results and analysis of the various techniques, following conclusions can be made:

- **Structural Characterization**

From XRD analysis, crystalline size and dislocation density of the systems have been determined from where we have observed that with the increase of crystallite size, the dislocation density in the system decreases and the possibility of enhancement of conductivity increases. The decrease of crystalline volume fraction, calculated from XRD, indicates the increase of conductivity in the systems. The polycrystalline nature of the systems has been confirmed by XRD and TEM studies

From TEM images analysis we have observed the texture, shape and size of different nanophases present in the prepared systems. From FT-IR spectrum, good transparency of all the prepared glassy systems in the mid infrared region has been observed which indicates the

suitability of these systems in optical fibre applications. Optical band gap energy has been calculated with the help of UV-Vis Spectroscopy method. From the density and molar volume measurements the information regarding the closeness of particles in the systems has been revealed.

- **DC Conductivity**

From the DC Conductivity measurements, the information regarding the dependency of systems' conductivity on temperature can be obtained. The negative temperature resistance of the systems, observed from DC conductivity measurements, indicates the semiconducting behaviour of the systems

Density of localized states of the prepared glassy systems has been calculated by fitting DC conductivity data with Mott's and Greaves's Models in lower and higher temperature regions respectively. Less conductivity in the lower temperatures is due to hopping of charge carriers in localized states. Rapid increase of conductivity at higher temperatures is due to thermal assisted tunnelling of charge carriers in the extended states

- **AC Conductivity**

Conductivity of the systems is found to be in the order of $10^{-2} - 10^{-3} \Omega^{-1} \text{cm}^{-1}$ which indicates the semiconducting property of the systems. Appropriate conduction mechanisms for all the prepared systems have been determined from the fitting of S-T plots, which were obtained by using power law, with different models like CBH, NSPT etc.

With the use of Almond West Formalism, the activation energies for hopping frequency for all systems have been determined. Meyer- Neldel (MN) rule has been successfully exploited to interpret AC conductivity data. Dielectric constant, dielectric loss and electric modulus (real and imaginary) have been measured for all systems at various temperatures and frequency range 42Hz – 5MHz. The temperature dependent relaxation process in the present system has been confirmed from the study of electric modulus formalism. Mobility and carrier density in all the present systems have been estimated and correlated with conduction process.

Activation energies for relaxation process of all the systems have also been determined from modulus plots. From ac conductivity scaling and electric modulus scaling, the temperature

independent and composition dependent nature of the relaxation process in the glassy systems have been observed.

- **Possible Applications**

Because of the tunable electrical conductivity and controllable concentration of carriers, the prepared Chalcogenide glassy systems can be used in many electronics devices such as photovoltaic solar cells, gas sensors, light emitting diodes, photodetectors, temperature sensors, transparent diodes, photoresistors, laser diodes, electrochromic windows etc.

FUTURE PROSPECTS

- To identify the possible solid state device applications of these semiconducting glass nanocomposites for industry and academic purposes
- To carry out some more structural characterization of these materials using FESEM, DSC etc
- To study the optical properties of these materials
- To check the suitability of these materials in optical device applications
- To prepare some new type of Chalcogenide glassy systems doped with TMIs like Vanadium, Molybdenum and Manganese to study their structural and electrical properties.

REFERENCES

- [1] S. Ojha, M. S.Ali, M. Roy and S. Bhattacharya, *Materials Research Express*, 8, 085203 (2021)
- [2] S. Ojha, M. Roy, A. Chamuah, K. Bhattacharya and S. Bhattacharya, *Phys. Chem. Chem. Phys.*, 22, 42, 24600-24613 (2020)
- [3] S. Ojha, M. Roy, A. Chamuah, K. Bhattacharya and S. Bhattacharya, *S N Applied Sciences*, 2:838 (2020)
- [4] S. Ojha, M. Roy, A. Chamuah, K. Bhattacharya and S. Bhattacharya, *International Journal of Advanced Science and Engineering*, 6, S2 28-34 (2020)

- [5] S. Ojha, M. Roy, A. Chamuah, K. Bhattacharya and S. Bhattacharya, *Materials Letters* 258, 126792 (2020)
- [6] S. Ojha, A. D. Das, M. Roy and S. Bhattacharya, *Physica B: Condensed Matter* 538, 191–198 (2018)
- [7] S. A. Khan, M. Zulfequar and M. Husain, *Solid State Communication* 123, 463 (2002)
- [8] R. Mathur and A. Kumar, *Rev. Phys. Appl.* 21, 579 (1986)